

# UNIVERSITAT POLITÈCNICA DE VALÈNCIA

Departamento de Química



**Engineering catalytic sites for oxidation and  
condensation reactions using metal-organic  
frameworks or graphene-based materials**

**DOCTORAL THESIS**

Submitted by

**Cristina Vallés García**

Supervisors

**Dr. Sergio Navalón Oltra  
Dra. Mercedes Álvaro Rodríguez**

Valencia, July 2021





UNIVERSITAT  
POLITÈCNICA  
DE VALÈNCIA

Sergio Navalón Oltra, PhD in Chemical Engineering and Associate Professor at the *Universitat Politècnica de València* and Mercedes Álvaro Rodríguez, PhD in Chemistry and Professor at the *Universitat Politècnica de València*.

CERTIFY:

That the work “Engineering catalytic sites for oxidation and condensation reactions using metal-organic frameworks or graphene-based materials” has been developed by Cristina Vallés García under their supervision at the Departamento de Química of the Universitat Politècnica de València, as a Thesis Project to obtain the degree of PhD in Sustainable Chemistry at the Universitat Politècnica de València.

Dr. Sergio Navalón Oltra

Dra. Mercedes Álvaro Rodríguez



***A mi familia y pareja***



***“Eres lo que haces,  
no lo que dices que vas hacer”***

*Carl Jung*





## Agradecimientos

Ante todo, debo agradecer a Mercedes Álvaro y Sergio Navalón la oportunidad de poder realizar esta tesis doctoral con ellos. En especial a Sergio por su guía constante en el laboratorio y por enseñarme que siempre se es capaz de llegar a todo en fecha. También a Hermenegildo García porque es un honor haber podido trabajar en su grupo.

Así como a los grupos de Christian Serre y Nathalie Steunou por el conocimiento adquirido en las diversas colaboraciones llevadas a cabo.

Llegado este momento del final de mis más de tres años de tesis doctoral, me viene a la mente no solo este último periodo, sino también el inicio de mi formación académica. Por eso en estos agradecimientos quiero recordar a todos los que han sido importantes durante este largo camino y que con su granito de arena han conseguido que llegue hoy a presentar mi Tesis Doctoral en Química.

En primer lugar, a mis compañeras del Conservatorio de Danza, pues fue en esos años donde aprendimos el verdadero significado del esfuerzo y a “sudar sangre”.

Desde preescolar hasta la Universidad tengo recuerdo de ciertos maestros y profesores de los cuales siempre recordaré esa palabra o frase de motivación o inspiración y si de profesores que me han inspirado se trata, tengo que nombrar a Carlos Gómez, diría que fue mi profesor de química inorgánica, mi director de TFG y TFM, pero fue mucho más que es. Nunca olvidaré cómo creía en sus alumnos, en cómo amaba lo que hacía y cómo lo transmitía, me dedique a lo que me dedique espero ser, aunque sea, la mitad de buena que tú.

A Nuria Villena, mi mejor amiga de la infancia la que me enseñó a diferenciar entre derecha e izquierda y a atarme los cordones de las zapatillas.

A Patricia, Belén, Christian y Cere por lo que aprendí de cada uno de vosotros, por nuestras conversaciones para arreglar la economía mundial, por las cenas, comidas, regalos de cumpleaños y amigos invisibles, en especial a Cere con el que viví todo lo anterior y todo lo posterior, gracias por recordarme quien era en los peores momentos de estos 4 años.

Y cómo no, a cada una de mis amigas de la universidad, por el apoyo incondicional durante la carrera, por haberme aguantado, haber comprendido mi objetivo y haber estado a mi lado durante el camino Andrea Jiménez, Olga, María, Lucía, Navarré, Laura, Ana y en especial a Andrea Martínez, mi rubia, si durante la carrera fuiste un gran apoyo, fuera de ella te has convertido en mi viga maestra.

A todos los miembros del grupo empezando por los doctorandos Ana, Lu, Elena, Rocío, Yong, Manuel, Jiajun, Antón, Alejandra, Xiangze, Horatiu, y a los nuevos Andrés y Alberto, me alegro de haber coincidido en vuestro inicio. Post-doc, profesores y técnicas Ana Primo, Abde, Josep, Pedro, Belén, Amparo y por último a Esther porque trabajar contigo es sinónimo de no rendirse, pocas personas transmiten tanta energía como tú.

Agradecer a todos con los que he compartido el laboratorio, donde hemos pasado momentos malos, pero también muy buenos, primero a nuestros maestros Andrea y Juan Carlos agradecerles la paciencia que tuvieron con nosotras y todos sus consejos. A tí Andrea decirte que tu marcha fue dura y que durante los siguientes años te he echado de menos más veces de las que imagine y hubiese querido, gracias por tu granito de arena en esta Tesis. A los estudiantes

de paso, Josemi, Alberto y Ana, qué manera de alegrarnos los días. Al ahora Doctor Manfredi, pero en su momento doctorando, estuviste poco, pero nos quedó claro lo gran persona e investigador que eras enseguida. A Antón por aguantarnos a todas sin decir ni mu. A nuestra galleguiña Novoa, con la que no puedes quedar ningún jueves porque ya los tiene todos ocupados hasta el 2040, gracias por las risas que me has dado, no cambies nunca. A Celia, que llegó para darnos paz y tranquilidad, ¡o eso creíamos! Por cierto, cuando me vaya te doy mi cajón (y limpio). A Herme Jr. por ser como un hermano mayor para todas. Y con las que empecé este viaje Arianna y María, esto ha sido una montaña rusa en la cual siempre nos hemos tenido y ahora cada una seguirá su camino os deseo mucha suerte a las dos. Arianna admiro tu sangre fría, de pase lo que pase siempre tener una sonrisa en la cara. A tí, María, quiero decirte que compartir los meses de entregar y exponer la tesis contigo ha sido un placer, que recordaré esos días en los que tú me pegabas los nervios, pero eras tú quien se quejaba de mi pierna saltarina, gracias por intentar ser mi psicóloga y animarme cuando me veías llorando y tranquilizarme cuando perdía los nervios.

Pero en especial, a Rubén y a Eva, porque llegasteis en el momento que más lo necesitaba, fuisteis luz, aire fresco y sobre todo me cargasteis las pilas, sinceramente mi futuro ya no me lo imagino sin vosotros. Gracias Rubén, por ser mi mejor compañero de baile, por las horas al teléfono durante la cuarentena y por formar parte de la familia que se elige. A tí, Eva, no dejes que apaguen tu luz, y si nadie pule el diamante que tienes dentro hazlo tú, porque eres capaz de eso y mucho más, que sepas que solo por haberte conocido estos 4 años ya han merecido la pena, por convertirte en mi media pera, gracias por venir con un sofá de regalo.

A Marina, Juan Fran y Bea porque, aunque no compartimos laboratorio fuisteis imprescindibles cada uno de los días, por las comidas que se llevó el coronavirus.

A los chicos del laboratorio del 2.2, Lorena, Jorge, Alex y en especial a Jorge Herrera por salvarme del Word. Os deseo todo lo mejor a los 4.

También a los técnicos del Departamento de Química, Manolo, Susana y a Enrique. Igual que a todos aquellos técnicos del ITQ que me han realizado medidas, Alejandro (EPR), José Miguel (IRCN), Amparo y Maribel (Área), M. Jesús y Fani (ICP), (Análisis elemental), Adelina (RAMAN), Dolo (XPS) y al equipo de microscopía.

Por todos los noes que os he dicho a innumerables planes, y por lo planes a los que dije que sí, porque estar con vosotras sí que es desconectar de todo esto, Raquel por esas cerezas en el parque, Isa y Laura porque pensar en vosotras es recordar comidas llenas de risas, Patri... porque contigo ni sabes cuándo empieza el plan ni cuándo acaba, Marta por ser la persona con la que puedes contar en cualquier momento y Andrea por ser tan igual y diferente a mí al mismo tiempo y por tus clases de Inglés.

Paco y Elena, por darme lo más importante de mi vida y por ayudarnos en todo.

A mi abuelita Carmen, que sin entender qué es todo esto siempre me anima a seguir y dice muy orgullosa que trabajo en la Universidad.

A mi hermano Mimi, mi guerrero, por darme las mejores Noches de Reyes con película y pizza, porque sólo espero que estés igual de orgulloso de mí como yo lo estoy de ti.

A esa gente que sin saberlo dijo o hizo algo que me sirvió para seguir durante estos años, a Oscar García, a mi cuñada Lorena, mis sobrinos Rubén, Hugo, Mya, José y Praia, a Begoña, Jaime, a Raúl Pérez, a Juan Monmeneu y Lola Soler.

A Carlos Pérez, porque eres el que más ha sufrido esto conmigo, has aprendido como yo lo que es investigar. Gracias por saber tranquilizarme, gracias por hacer imposible que mis enfados duren más de 2 segundos después de haberte visto, pero sobre todo gracias por apoyarme en todos los días de mi vida, en el que me levanto queriendo ser química, o en el día que quiero ser agente inmobiliario, o farmacéutica o astronauta, aunque no lo entiendas. Por confiar en mí más que yo misma.

Y, por último y más importante, a vosotros dos, María García y Juan Vicente Vallés, mamá y papá por esos sábados de ir a puzol, por esas noches despiertos mientras estudiaba después de llegar del conservatorio, por esas noches de nervios, por recogerme de la biblioteca a las tantas de la noche, por no enseñarme a tirar la toalla, por aguantar mi mal humor, en resumen, por no dudar nunca de mí, por estar siempre que os he necesitado en todo, por ser vuestra prioridad, por esto y mucho más esta tesis no es sólo mía también es vuestra.



## Style

This Doctoral Thesis is written in a journal article compilation style format constituted by eight chapters in which the main features of the developed work are described. A literature review is detailed in Chapter 1 to synthesize the state of the art of reactions catalyzed by MOFs or graphene-based materials, raising the issues addressed during the course of this doctoral thesis. Chapter 2 collects the objectives of the Thesis. Chapters 3, 4, 5 and 6 compile the research articles where the results of this thesis are published. Chapter 7 summarizes the conclusions of work while Chapter 8 collect the abstract of the Thesis. Annex I collects the publications and participation in conferences.





## ***Abbreviations and Acronyms***



## Abbreviations and Acronyms

<b>4-MeDBT</b>	4-Methyldibenzothiophene
<b>4,6-diMeDBT</b>	4,6-Dimethyldibenzothiophene
<b>ACN</b>	Acetonitrile
<b>AcOH</b>	Acetic acid
<b>ASC</b>	Ascorbic acid
<b>ATR-FTIR</b>	Attenuated total reflection-Infrared spectroscopy fourier transform
<b>BDC</b>	Terephthalic acid or benzenedicarboxylate
<b>BET</b>	Brunauer-Emmett-Taller
<b>BJH</b>	Barret-Joyner-Halenda
<b>BTC</b>	1,3,5-benzenetricarboxylate
<b>CUS</b>	Coordinatively unsaturated sites
<b>DBT</b>	Dibenzothiophene
<b>DBT-O<sub>2</sub></b>	Dibenzothiophene sulfone
<b>DMA</b>	N,N-dimethylaniline
<b>DMF</b>	Dmimethylformamide
<b>DMSO</b>	Dimethylsulfoxide
<b>DTGS</b>	Deuterated triglycine sulfate detector
<b>E-factor</b>	Environmental-factor
<b>E<sub>1/2</sub></b>	Halfwave potential
<b>E<sub>a</sub></b>	Activation energy
<b>EDX</b>	Energy dispersive X-Ray
<b>EtOH</b>	Ethanol
<b>EXAFS</b>	Extended X-Ray absorption fine structure
<b>FID</b>	Flame ionization detector
<b>FT-IR</b>	Infrared spectroscopy fourier transform
<b>GC</b>	Chromatography
<b>GC-MS</b>	Gas Chromatography coupled to Mass Spectrometry
<b>GO</b>	Graphene oxide
<b>H<sub>4</sub>TTFTB</b>	Tetrathiafulvalene tetrabenzoic
<b>HOAc</b>	Acetic acid
<b>HPLC</b>	High performance liquid chromatography
<b>HQ</b>	Hydroquinone
<b>HS</b>	High spin
<b>HZ</b>	Hydrazine
<b>ICP</b>	Inductively coupled plasma
<b>ICP-AES</b>	Inductively coupled plasma-atomic emission

	spectroscopy
<b>ICP-OES</b>	Inductive coupling plasma-optical emission spectrometry
<b>IR</b>	Infrared spectroscopy
<b>IS</b>	Isomer shift
<b>MeOH</b>	Methanol
<b>MIL</b>	Materiaux de l'Institute Lavoiser
<b>MOF</b>	Metal-organic frameworks
<b>NMR</b>	Nuclear magnetic resonance spectroscopy
<b>OAc</b>	Acetate
<b>PXRD</b>	Powder X-Ray diffraction
<b>R<sup>2</sup></b>	Regression coefficient
<b>rGO</b>	Reduced graphene oxide
<b>rGO-T</b>	Thermally reduced graphene oxide
<b>ROS</b>	Reactive oxygen species
<b>SEM</b>	Scanning electron microscopy
<b>SI</b>	Suplementariy information
<b>ST</b>	Supertetrahedra
<b>TEMPO</b>	2,2,6,6-Tetramethyl-1-piperidinyloxy
<b>TGA</b>	Thermogravimetric analysis
<b>TMAOH</b>	Tetramethylammonium hydroxide
<b>TOF</b>	Turnover frequency
<b>TON</b>	Turnover number
<b>TPD</b>	Temperature programmed desorption
<b>TPD-MS</b>	Temperature programmed desorption coupled to a mass-spectrometer
<b>UiO</b>	University of Oslo
<b>XP</b>	X-ray photoelectron
<b>XPS</b>	X-ray photoelectron spectroscopy
<b>XRD</b>	Powder X-ray diffraction

## ***INDEX***



# INDEX

<b>Chapter 1. Introduction .....</b>	<b>1</b>
1.1 Catalysis .....	3
1.2. Heterogeneous catalysis .....	4
1.3. Oxidation reactions .....	7
1.4. Condensation reactions.....	8
1.5 Metal-organic frameworks.....	11
1.6 MOFs as heterogeneous catalysts.....	12
1.7 MOFs for oxidation reactions.....	15
1.8. MOFs as catalysts for condensation reactions.....	20
1.9. Metal-free heterogeneous catalysts .....	23
1.10. Graphene-based materials as metal-free catalysts.....	25
1.11. References.....	31
<b>Chapter 2. Objectives .....</b>	<b>35</b>
<b>Chapter 3. Desing of stable mixed-metal MIL-101(Cr/Fe) materials with enhanced catalytic activity for the Prins reaction .....</b>	<b>39</b>
3.1 Abstract .....	43
3.2 Introduction.....	43
3.3 Results and discussion.....	46
3.3.1 Catalyst preparation.....	46
3.3.2 Catalytic activity .....	53
3.3.3 Characterization of acid sites .....	62
3.4 Conclusions.....	66
3.5 Experimental section.....	66
3.5.1 Materials .....	66
3.5.2 Catalyst preparation.....	66
3.5.3 Characterization .....	67
3.5.4 Catalytic reaction.....	68

3.6 Acknowledgments.....	69
3.7 References.....	71
3.8 Supplementary Material.....	74

**Chapter 4. Nitro functionalized chromium terephthalate metal-organic framework as multifunctional solid acid for the synthesis of benzimidazoles..... 85**

4.1 Abstract .....	89
4.2 Introduction .....	89
4.3 Experimental .....	92
4.3.1 Materials .....	92
4.3.2 Catalyst preparation.....	92
4.3.3 Catalyst characterization.....	93
4.3.4 Reaction procedure.....	94
4.4 Results and discussion.....	95
4.4.1 Structural description of catalysts.....	95
4.4.2 Catalytic activity .....	97
4.4.3 Characterization of the Lewis acid centers .....	107
4.5. Conclusions.....	109
4.6 Acknowledgements .....	110
4.7 References.....	111
4.8 Supporting information.....	114

**Chapter 5. MIL-101(Cr)-NO<sub>2</sub> as efficient catalyts for the aerobic oxidation of thiophenols and the oxidative desulfurization of dibenzothiophenes ..... 133**

5.1 Abstract .....	137
5.2 Introduction.....	137
5.3 Materials and methods .....	140
5.3.1 Materials .....	140
5.3.2 Catalyst characterization.....	140
5.3.3 Catalytic experiments.....	141



5.3.4 Product analysis .....	141
5.4 Results and discussion .....	142
5.4.1 Catalyst properties .....	142
5.4.2 Aerobic oxidation of thiophenols to disulfides .....	143
5.4.3 Aerobic oxidative desulfurization of diesel fractions. Use of DBTs .....	149
5.5 Conclusions.....	156
5.6 Acknowledgements .....	157
5.7 Reference .....	158
5.8 Supplementary Material.....	160
<b>Chapter 6. <i>Tuning the active sites in reduced graphene oxide by hydroquinone functionalization for the aerobic oxidations of thiophenol and indane</i></b> .....	<b>167</b>
6.1 Abstract .....	171
6.2 Introduction.....	171
6.3 Experimental section.....	173
6.3.1 Materials .....	173
6.3.2 Catalyst preparation.....	173
6.3.3 Instrumentation .....	175
6.3.4 Aerobic oxidation of thiophenol .....	175
6.3.5 Aerobic oxidation of indane.....	175
6.4 Results and discussion.....	176
6.4.1 Functionalizations of rGO.....	176
6.4.2 Aerobic oxidation of thiophenol .....	179
6.4.3 Aerobic oxidation of indane .....	183
6.5 Conclusions.....	189
6.6 Acknowledgements .....	190
6.7 References.....	191
6.8 Supplementary information .....	193
<b>Chapter 7. <i>Conclusions</i></b> .....	<b>195</b>
<b>Chapter 8. <i>Abstract of the Thesis</i></b> .....	<b>201</b>

8.1 Abstract .....	203
8.2 Resumen .....	204
8.3 Resum .....	205
<b>Annex I. <i>Publications and conferences</i>.....</b>	<b>207</b>
Publications derived from the present Thesis.....	209
Other Publications.....	210
Conferences.....	211

## **Chapter 1. *Introduction***



## 1.1 Catalysis

Catalysis is vitally important for the world economy.<sup>1</sup> Most chemical processes are catalysed.<sup>2</sup> Catalysis allows the transformation of raw materials into valuable chemicals and fuels.<sup>3</sup> Fig. 1 shows in a simplified form some representative branches of the chemical industry where a catalyst is used.<sup>4</sup>

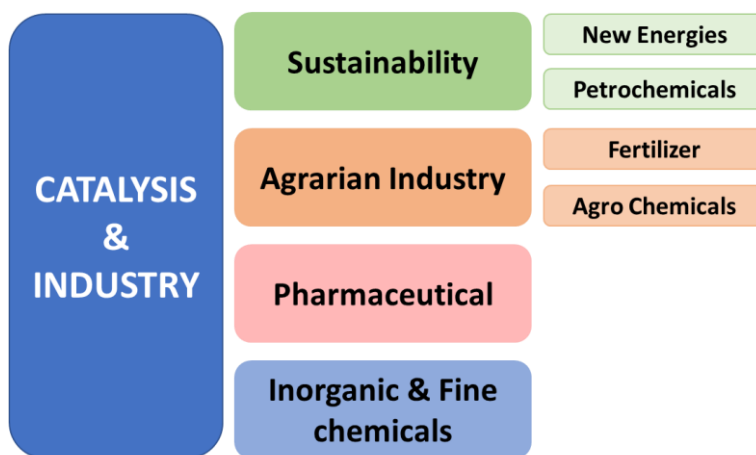


**Fig.1** Simplified illustration of some branches of the chemical industry that use catalysts.

A catalyst can be simply defined as a substance that allows the transformation of reactants into products through a series of elementary steps in which the catalyst participates and at the end of the process the catalyst is regenerated in its original form.<sup>5</sup> The series of elemental steps by which a reaction occurs is called the reaction mechanism. Typically, a catalyst increases the reaction rate of a chemical process by modifying the reaction mechanism and decreasing the activation energy of the process. The catalyst modifies the kinetics of the chemical reaction but does not change the thermodynamics of the process.<sup>6</sup> The sites where the substrate binds to the catalyst are called the active centres of the

catalyst.<sup>7,8</sup> Fig. 2 shows a simplified illustration of how a catalyst modifies the reaction mechanism of a reaction and decreases the activation energy of the process without modifying the thermodynamics.

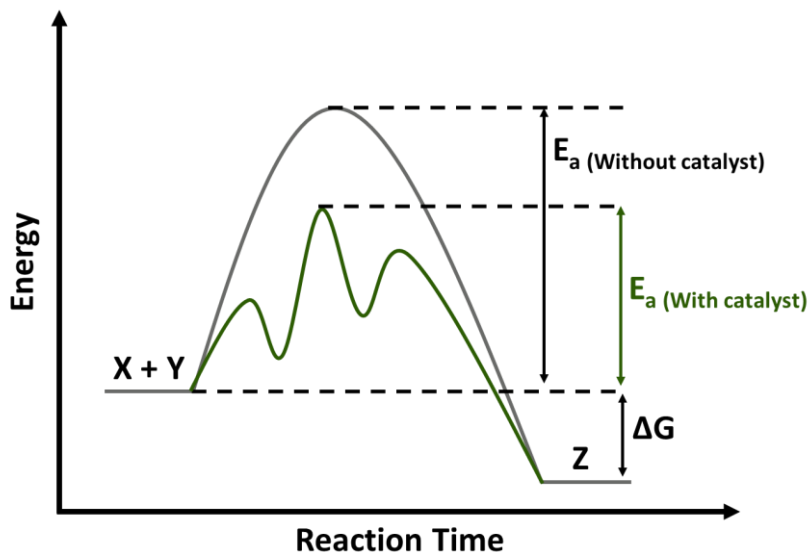


**Fig. 2** Basic illustration of the effect of a catalyst on the energy diagram profile of a reaction ( $X + Y \rightarrow Z$ ).

Most of the catalysts employed worldwide are based on transition metals.<sup>9–11</sup> The transition metal active sites that are present in the catalyst usually act as Lewis or redox centres during the catalytic reaction.<sup>11,12</sup>

## 1.2. Heterogeneous catalysis

Heterogeneous catalysts in a solid form dominate the market of catalysis at an industrial scale.<sup>13</sup> It is estimated that more than 90 % of chemical processes employ a heterogeneous catalyst. One of the major advantages of using solid heterogeneous catalysts in a chemical process is the relatively easy separation from the gas and/or liquid reaction mixture when compared to homogeneous

catalysts.<sup>14</sup> Heterogeneous catalysis facilitates catalyst recovery, reactivation, and recycling and so makes industrial processes technically and economically feasible. In addition, heterogeneous catalysis enables the development of relatively simple industrial processes under continuous flow operations. Fig. 3 illustrates the basic steps that take place in a heterogeneous porous solid catalyst from the bulk phase to the active site of the catalyst where the reaction takes place, and then the desorption and diffusion processes leading to the bulk phase of the reaction.<sup>15</sup>

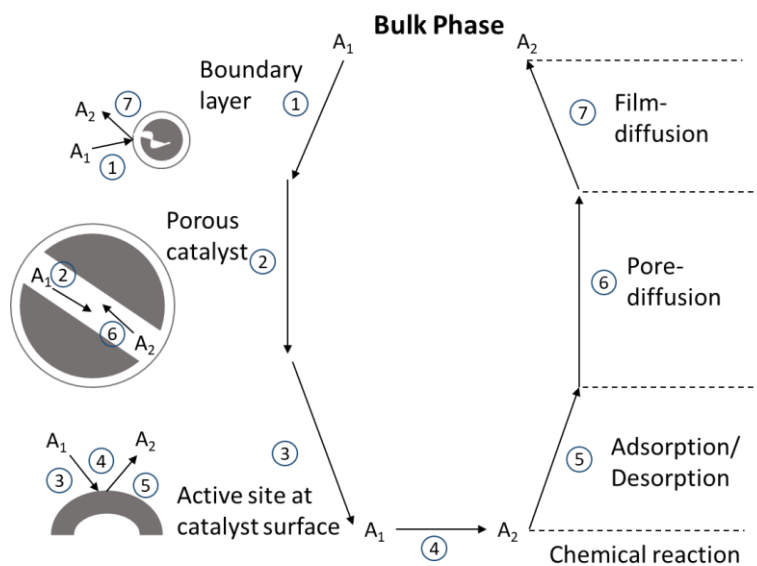


**Fig. 3** Individual steps of a simple, heterogeneous catalytic fluid-solid reaction  $A_1 \rightarrow A_2$  carried out on a porous catalyst. Adapted with permission from<sup>15</sup>

Heterogeneous catalysts are implemented in a wide range of chemical sectors from petrochemistry and fine chemicals to environmental and energetic applications.<sup>16–18</sup> Furthermore, heterogeneous catalysis enables accomplishing many of the 12 principles of green chemistry (Fig. 4). Over the years, the estimation of the greenness of a chemical process has been an important matter of research.<sup>19,20</sup> The environmental-factor (E-factor) and atom efficiency were two of the first procedures developed for this purpose. The E-factor is the weight ratio

of wastes generated relative to the weight of the desired product expressed in kg. The atom efficiency is related with the conversion efficiency in a reaction in terms of atoms involved and the desired product generated. Therefore, it can be easily recognised how, for example, the use of heterogeneous oxidation catalysts that can activate molecular oxygen for the oxidation of organic compounds favours the greenness of a chemical process relative to the use of transition metal salts as oxidants.

**Table 1** Green chemistry and heterogeneous catalysis<sup>21</sup>

S. No.	Green chemistry principles	Heterogeneous catalysis
1	Waster prevention	Minimized waste
2	Atom economy	More atom- and step- economical
3	Less hazardous synthesis	Generally low toxicity
4	Desing for safer products	No relevant (product not process)
5	Safer solvents and auxiliaries	Usually, green solvent are used
6	Energy efficiency	Mild conditions/energy efficient and recycled
7	Renewable feedstocks	Catalysts can prepare from renewable sources
8	Reduced derivatives	Eliminates protection/ de-protection steps
9	Catalysis	Solid materials are catalysts
10	Desing for degradation	Selective catalytic reagments are possible
11	Real-time análisis	Applicability to catalytic processes
12	Inherently safer processes	Mild and safe conditions

Furthermore, as the world moves towards a more sustainable environment, new opportunities for the development of environmentally benign solid catalysts have appeared.<sup>22,23</sup> Over the last 20 years, the possibility of replacing the traditional transition-based catalyst with metal-free catalysts has attracted increasing interest.<sup>24–28</sup> Several demonstrations have shown the possibility of using carbon-based materials as an alternative to metal-based catalysts.<sup>29–31</sup> The area that studies the use of carbon-based materials as metal-free catalysts is called carbocatalysis.



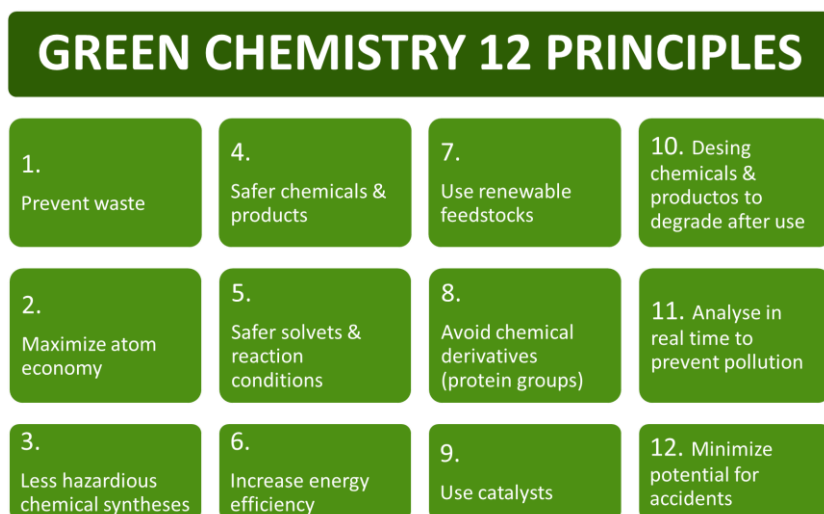


Fig. 4 Catalysis and 12 principles of green chemistry.

### 1.3. Oxidation reactions

Oxidation reactions are one of the most important reactions for the chemical industry.<sup>32–34</sup> Commonly, industrial processes at medium-to-large scale employ a transition metal based-catalyst to perform selective oxidations.<sup>34,35</sup> Homogeneous catalysis frequently employs a soluble metal compound as a catalyst. Heterogeneous oxidation catalysts are often based on high surface area metal and/or metal oxides.<sup>36,37</sup> Some of the common oxidants employed during the catalytic processes include hydrogen peroxide, organic peroxides, hydroperoxides, and molecular oxygen.<sup>38</sup> Sometimes industrial oxidation reactions are non-catalysed processes that employ inorganic metal salts as oxidants (such as potassium permanganate or potassium dichromate) or non-metal oxidants such as chlorine or chlorite.

In general, the active centres of a transition metal-based catalysts act as Lewis acid sites for the activation of oxidation, or as active centres that accelerate the

oxidation reaction through a reversible swing of the metal ions between two oxidation states (Equations 1 and 2, Scheme 1).<sup>39,40</sup> From a sustainable and operational point of view, molecular oxygen is one of the oxygen preferred oxidants and water is its final reaction product. Given these precedents and considering the objectives, Chaption 2 of the thesis will introduce the possibilities of using metal-organic frameworks (MOFs) as heterogeneous catalysts for oxidation reactions.

a) *Lewis acid activation of oxidation*



b) *Electron transfer*



**Scheme 1** (a) Active centres of a transition metal-based catalysts act as Lewis acid sites for the activation of oxidation. (b) Active centres of a transition metal-based catalysts act as active centres that accelerate the oxidation reaction through a reversible swing of the metal ions between two oxidation states. Reprinted with permission from ref<sup>41</sup>

A step forward in the field of oxidations will be the development of active, selective, and cost-effective metal-free carbon catalysts for aerobic oxidations.<sup>26,27</sup> Chaption 6 will illustrate the possibility of using graphene-based materials for the oxidation of organic substrates using molecular O<sub>2</sub> as an oxidant. The revised examples will be taken as precedents for Chapter 6.

## 1.4. Condensation reactions

Condensation reactions represent an important synthetic tool for the preparation of a large variety of organic compounds in the chemical industry.<sup>42,43</sup>



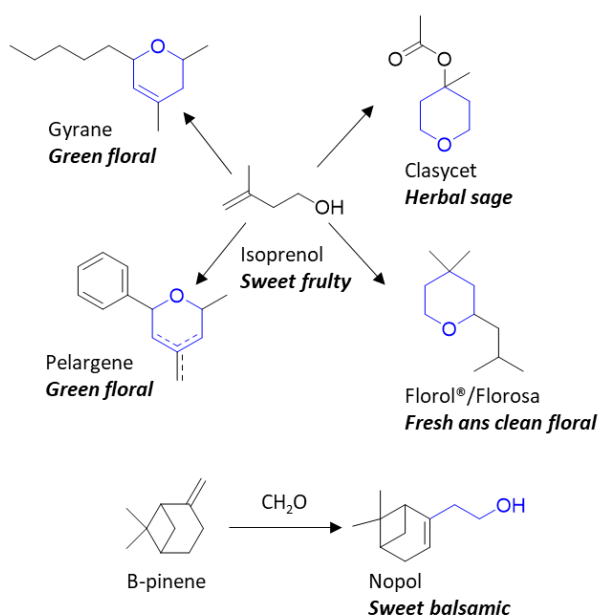


**Fig. 6** Representative examples of the use of isoprenol and β-pinene for producing fragrance ingredients. Reprinted with permission from ref.<sup>44</sup>

Another common class of compounds for the chemical industry where acid-catalysed condensation reactions can be involved are benzimidazoles.<sup>45</sup> Benzimidazoles are present in many important biological compounds including natural products and drug molecules. Fig. 7 shows the chemical structures of some benzimidazole-containing drugs.

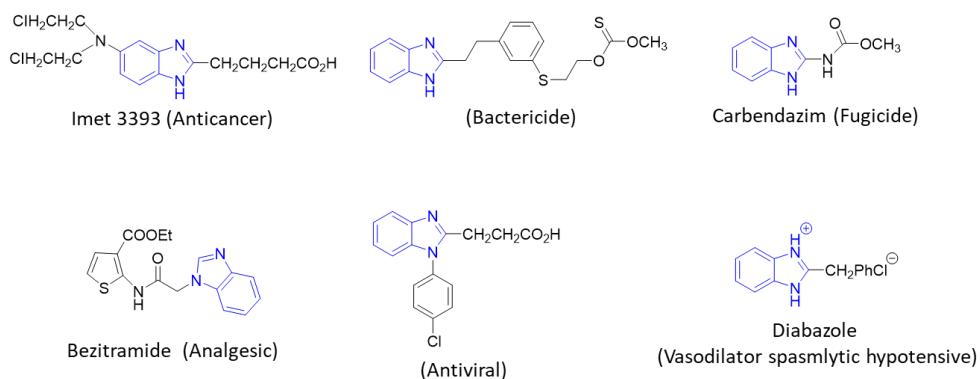


**Fig. 7** Some benzimidazole-containing drugs. Reprinted with permission from ref.<sup>45</sup>

One of the possible routes for the preparation of benzimidazoles involves the acid-catalysed reaction between *o*-phenylenediamines with aldehydes to yield 2-substituted benzimidazoles.<sup>45</sup> The reaction occurs through a condensation mechanism followed by oxidative dehydrogenation. Section 4.1 describes some precedents for Chapter 4 of this thesis on the use of MOFs as heterogeneous catalysts for the synthesis of benzimidazoles through the pathway shown in Fig. 8.

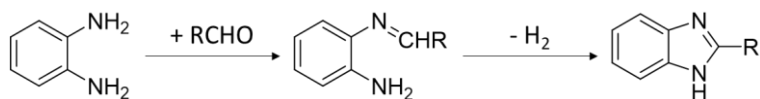


**Fig. 8** General reaction of aldehydes with *o*-phenylenediamines to yield 2-substituted benzimidazoles.

## 1.5 Metal-organic frameworks

MOFs also known as porous coordination polymers are crystalline porous materials constituted by metal ions or metal cluster coordinated to organic ligands (Fig. 9).<sup>46–51</sup> Currently, thousands of MOFs have been prepared using

transition metal ions, as well as alkaline earth metal ions as metal nodes coordinated with a large variety of organic ligands.<sup>50,52–54</sup>

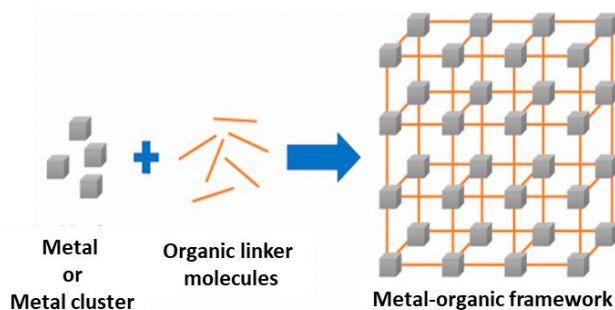


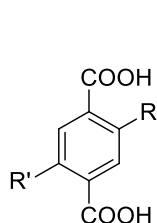
**Fig. 9** Simplified illustration of the MOF structure. Reprinted with permission from ref.<sup>55</sup>

Some of the unique properties of MOFs include a large surface area and significant porosity together with considerable flexibility and tunability of both the metal nodes and the organic ligands render materials with many applications.<sup>50,53,56,57</sup> Applications using MOFs include adsorption and separation of fluids,<sup>56,58</sup> catalysis,<sup>58–62</sup> photocatalysis,<sup>58,63</sup> sensing,<sup>64</sup> water remediation,<sup>65,66</sup> optoelectronics,<sup>67,68</sup> magnetism,<sup>69,70</sup> and biomedicine.<sup>71</sup>

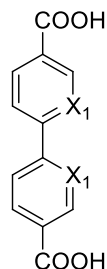
## 1.6 MOFs as heterogeneous catalysts

The number of active and robust MOFs in the area of heterogeneous catalysis is still limited.<sup>59–62</sup> Stable MOFs employed as heterogeneous catalysts are often constituted by tri- or tetravalent transition metal ions such as  $\text{Al}^{3+}$ ,  $\text{Fe}^{3+}$ ,  $\text{Cr}^{3+}$ ,  $\text{Zr}^{4+}$  or  $\text{Ti}^{4+}$  coordinated to di- or tricarboxylic substituted aromatic ligands.<sup>53,72</sup> In other cases, relatively stable MOFs can also be prepared by using divalent metal ions such as  $\text{Zn}^{2+}$ ,  $\text{Co}^{2+}$  or  $\text{Cu}^{2+}$  coordinated to imidazole-derivatives such as 2-methylimidazole (Fig. 10).<sup>53,72,73</sup> Fig. 10 shows some common organic ligands employed for the development of active and robust MOFs as solid catalysts.

## Dicarboxylic organic ligands

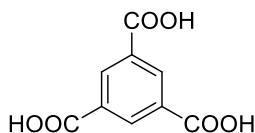


R: H, NH<sub>2</sub>, NO<sub>2</sub>, OH  
 R': H, NH<sub>2</sub>, NO<sub>2</sub>

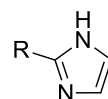


X<sub>1</sub> = H or N  
 X<sub>2</sub> = H or N

## Tricarboxylic organic ligands



## Imidazoles



R: H, CH<sub>3</sub>

**Fig. 10** Common organic ligands used for the preparation of MOFs as catalysts.

One of the MOF families that has attracted most interest for the development of several applications that include catalysis is denoted as MIL-101 (MIL stands for *Matériaux de l'institut Lavoisier*).<sup>48</sup> In MIL-101(Cr) the metal nodes are constituted by three trivalent transition metal cations (such as Cr<sup>3+</sup> or Fe<sup>3+</sup>) connected to a central oxygen atom. The resulting nodes from Cr<sup>3+</sup> and Fe<sup>3+</sup> ions are (Cr<sub>3</sub>-μ<sub>3</sub>O)<sup>7+</sup> and (Fe<sub>3</sub>-μ<sub>3</sub>O)<sup>7+</sup>, respectively. Each metal ion present in the trimeric units is connected with two terephthalate organic ligands. There is an additional coordination position that defines an octahedron around each of the Cr<sup>3+</sup> or Fe<sup>3+</sup> ions. One-third of these positions are occupied by a halogen, frequently F<sup>-</sup> for Cr<sup>3+</sup> and Cl<sup>-</sup> for Fe<sup>3+</sup> (although it could also be a hydroxide ion, Fig. 11). The other two-thirds of positions are occupied by solvent molecules such as DMF or H<sub>2</sub>O. It is important to note that the solvent molecules such as H<sub>2</sub>O can be removed by thermal treatment under vacuum conditions that result in the formation of coordinative unsaturated sites (CUS). The formation of CUS is important from the catalytic point of view as they have frequently been reported as the active sites of the catalyst.

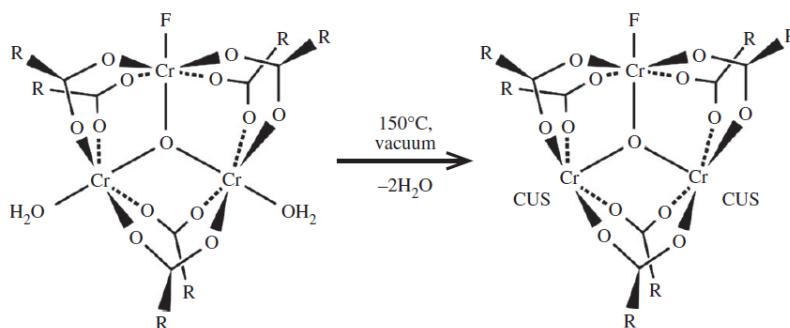


**Fig. 11** Formation of coordinatively unsaturated chromium (CUS) sites in the Cr<sub>3</sub>O-carboxylate cluster of the MIL-101 structure. Reprinted with permission from ref. <sup>74</sup>

The arrangement of four trimeric M<sub>3</sub><sup>3+</sup>-μO metal nodes with the terephthalate organic linkers produces super tetrahedra (ST) building units. These ST building units result in the formation of a rigid zeotype crystal structure consisting of two quasi-spherical mesoporous cages in MIL-101. The larger cage has a diameter of 3.4 nm that is accessible through hexagonal windows of 1.6 nm. The smaller cage with 2.9 nm of diameter is accessible through pentagonal windows of 1.2 nm (Fig. 12). The resulting MIL-101 structure is highly porous with reported surface areas of about 3,000 m<sup>2</sup> g<sup>-1</sup>.



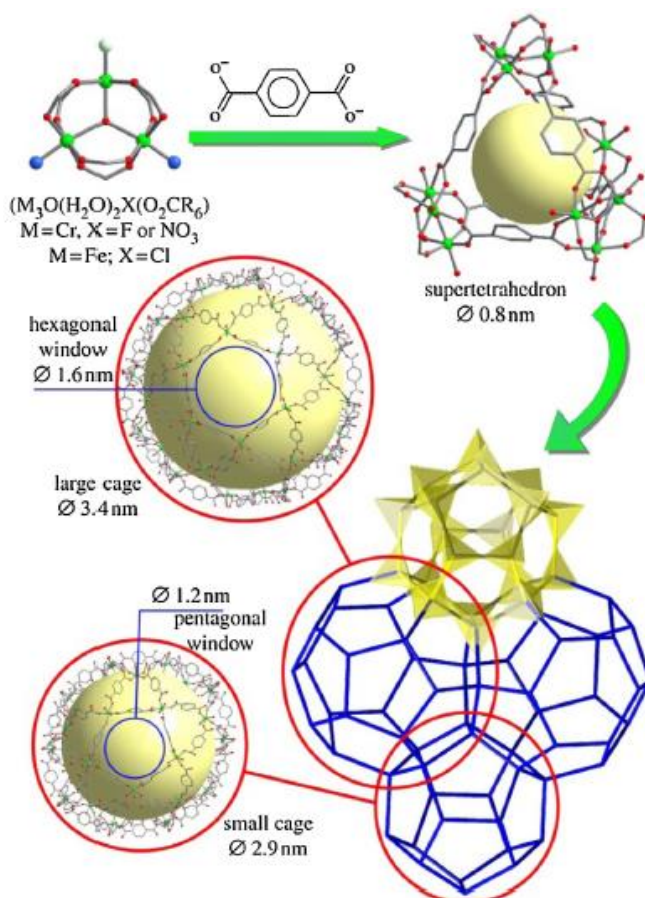


Fig. 12 Schematic of MIL-101 structure. Reprinted with permission from ref.<sup>74</sup>

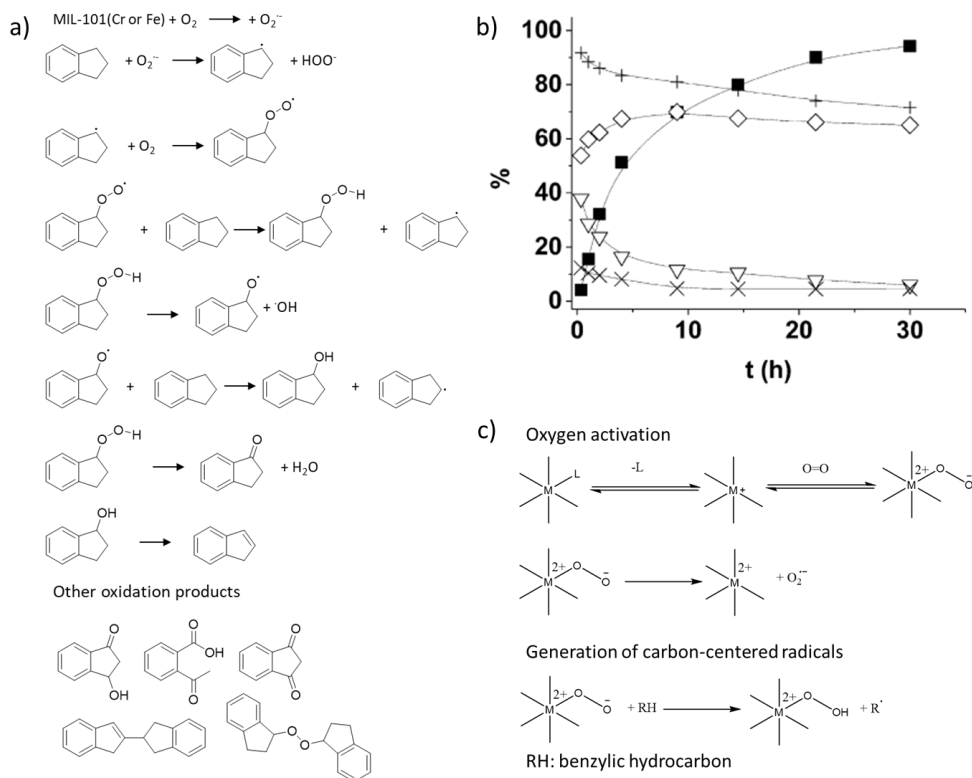
## 1.7 MOFs for oxidation reactions

MOFs have been used in some extent as heterogeneous catalysts for oxidation reactions.<sup>75–79</sup> In a series of studies several MOF families have shown outstanding thermal and chemical stability when used as heterogeneous catalysts for the activation of oxidants such as  $H_2O_2$  or tert-butyl hydroperoxide (as well as other oxidants). As representative examples, the list includes terephthalate-based MOFs

such as: MIL-101(Cr or Fe), MIL-125(Ti), and UiO-66(Zr); trimesate-based MOFs such as MIL-100(Fe or Cr); as well as some imidazolate-based MOFs such as ZIF-8(Zn). In addition, many other MOFs have also been reported as suitable for this purpose.<sup>39,59</sup> Several isostructural-based MOFs in addition to those mentioned have functionalised organic ligands or mixed-metal nodes and have also been reported as solid catalysts for oxidations. Some of common reactions using MOFs for oxidations include the oxidation of alkanes and aromatic hydrocarbons, oxidation of allylic positions, epoxidation of C=C bonds, oxidation of alkylphenols, oxidation of alcohols, and oxidation of S- or N-containing organic compounds.<sup>80</sup>

A step forward in the field of MOFs as heterogeneous catalysts for oxidation reaction has been the use of molecular O<sub>2</sub> as a sole oxidant.<sup>75,76</sup> As one representative example, our group has shown the possibility of using MIL-101(Cr) or MIL-101(Fe) as stable and reusable heterogeneous catalysts for the oxidation of benzylic positions with O<sub>2</sub> under solvent-free conditions.<sup>81</sup> Regardless of the somewhat lower level of activity of MIL-101(Cr) as a catalyst during the aerobic oxidation in date in comparison with MIL-101(Fe), it showed greater stability in terms of metal leaching from the solid to the solution (0.2 vs 1.6 wt% of Cr or Fe leaching with respect to the MOF metal content). After a series of catalytic experiments, it was concluded that the reaction occurs through a radical-chain mechanism with a long propagation chain. Interestingly, the greater selectivity towards desired 1-indanol/1-indanone -ol/ona reaction products when using MIL-101(Cr) as a solid catalyst (when compared to common radical initiators) was interpreted assuming that the reaction takes place within the pore cavities of the MOF. EPR and selective quenching experiments evidenced the formation O<sub>2</sub><sup>•-</sup>/HOO<sup>•</sup> as the primary radical species responsible for the benzylic oxidation accompanied by small amounts of HO<sup>•</sup> radicals. Scheme 2 shows the proposed reaction mechanism for the aerobic oxidation of indane (Scheme 2 a, b) as accelerated by molecular O<sub>2</sub> activation in the CUS of the MIL-101(Cr) catalyst. The

scope of the benzylic oxidation using MIL-101(Cr) as a solid catalyst was expanded to other substrates such as ethylbenzene, n-butylbenzene, iso-butylbenzene, 1-bromo-4-butylbenzene, sec-butylbenzene, and cumene.



**Scheme 2** (a) Proposed reaction pathway for the oxidation of indane using MIL-101(Cr or Fe) as a catalyst and (b) time conversion and product selectivity plot for the oxidation of indane using MIL-101(Cr) for legend: indane conversion (■) and selectivity to 1-indanyl hydroperoxide (x), indanone (◇), indanol (▽) and indanol + indanone (+). Reaction conditions: 75 mg of MIL-101(Cr), catalyst, 20 mmol of substrate, 120 °C, O<sub>2</sub> atmosphere. (c) A possible mechanism for oxygen activation by coordination with a transition metal ion resulting in the generation of radicals. Reprinted with permission from refs.<sup>63,81</sup>

In a series of studies MIL-101(Cr or Fe) and related materials have been employed as stable and reusable solid catalysts for the aerobic oxidation of DBT using n-dodecane or commercial diesel as solvents (Fig. 12a).<sup>14</sup> The aim of these studies was to study the feasibility of the aerobic oxidative desulfuration using

MOFs as an alternative to current hydrodesulfuration. These studies have been considered the related precedents to Chapter 5 in this thesis in which organic ligand functionalised MIL-101(Cr)-based materials have also been used for this purpose. In the case of using MIL-101(Cr or Fe) the reaction exhibits an induction period attributed to the solvent or O<sub>2</sub> diffusion within the MOF cavities. The use of PBN as a spin trap enabled detecting the presence of HOO· radicals during the reaction. Furthermore, a hot filtration test showed that if the catalyst is removed once the reaction is initiated (38 % conversion) the reaction proceeds with the same temporal profile as with the catalyst. The use of commercial diesel as a solvent resulted in longer reaction times (~40 h) with respect to n-dodecane (~24 h) to achieve full DBT conversion. This fact was explained considering the presence of hydrocarbons with longer chain lengths than n-dodecane and the possible presence of additives that can decrease the adsorption and reaction of DBT. Overall, it was proposed that MIL-101(Cr) is acting as a radical initiator and the reaction proceeds via an auto-oxidation mechanism (Fig. 13b).

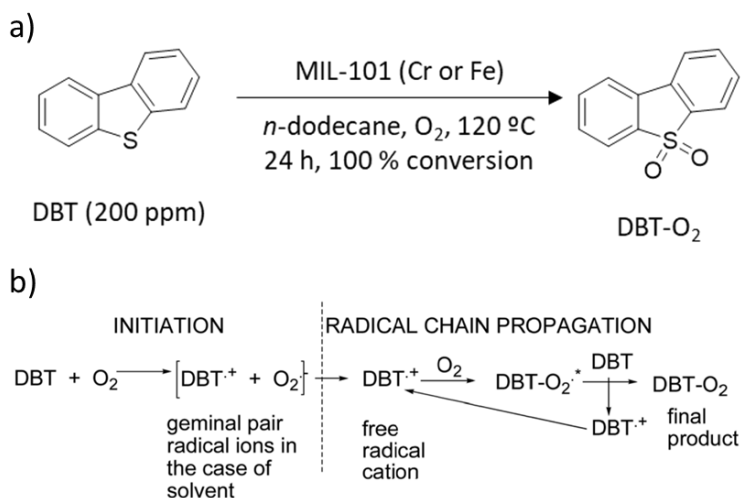


**Fig. 13** a) Aerobic oxidation of DBT to DBT-sulfone using MIL-101(Cr or Fe) as the catalyst. b) Proposed reaction mechanism for the aerobic oxidation of DBT with molecular O<sub>2</sub> in the presence of MIL-101(Cr) as the catalyst. Reprinted with permission from ref. <sup>14</sup>

In a related study, a novel iron-based MOF with larger pores was developed with the aim of reducing the induction period observed when using MIL-101(Cr or Fe) solids for the aerobic oxidation of DBT.<sup>37</sup> The material is prepared from tetrathiafulvalene tetrabenzoic acid ( $H_4TFTB$ ) and a preformed  $[Fe_3O(CH_3COO)_6](ClO_4)$  cluster. Interestingly, the resulting MUV-2 material exhibited the same  $Fe_3-\mu_3O$  active center as MIL-101(Fe) or MIL-100(Fe) while having greater porosity (Fig. 14b). The greater porosity of MUV-2 than MIL-101(Fe) or MIL-100(Fe) is beneficial for enhancing the catalytic activity for the aerobic oxidation of DBT to DBT- $O_2$  and even when using commercial diesel as a solvent.

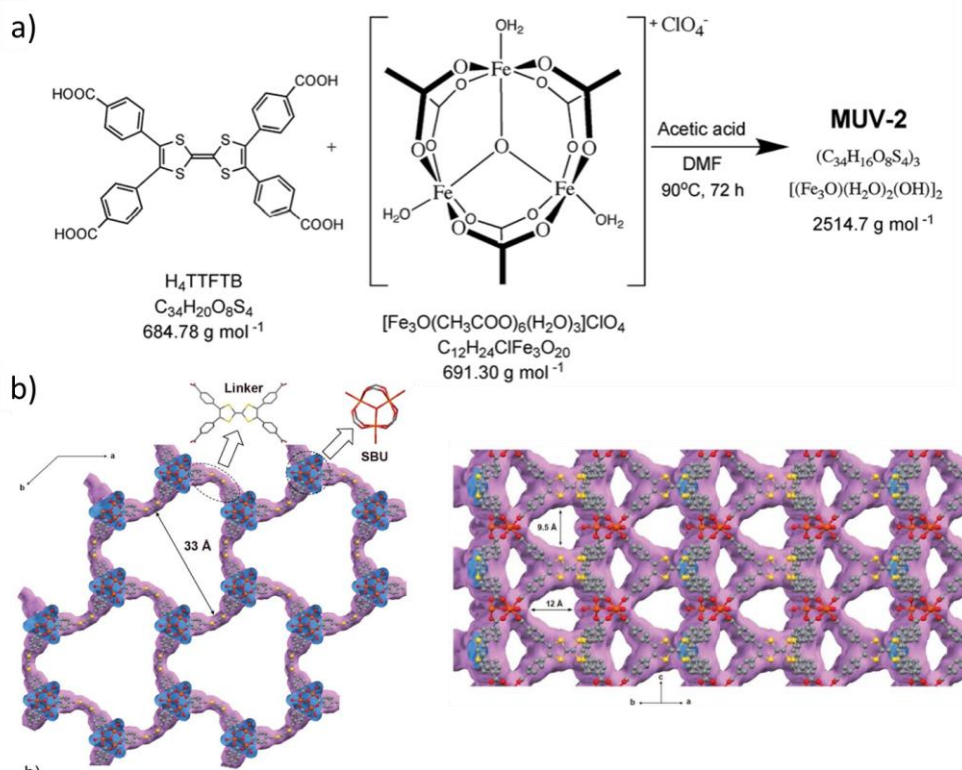


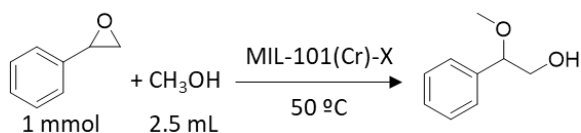
**Fig. 14** a) Synthesis of MUV-2. (a) Representation of the crystal structure of MUV-2 showing mesoporous channels along the  $c$ -axis; and (b) microporous channels orthogonal to the  $c$ -axis. The van der Waals surface is shown in purple. Adapted with permission from ref<sup>37</sup>

## 1.8. MOFs as catalysts for condensation reactions

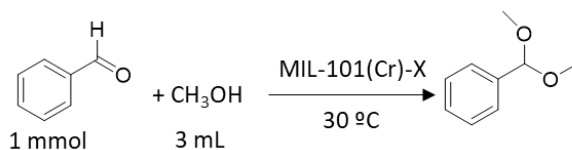
As commented in the introduction, a large variety of organic compounds are prepared in the industry through condensation reactions.<sup>42,43</sup> These types of reactions have also been studied using MOFs as heterogeneous catalysts.<sup>82–84</sup> Particular success has been achieved using MIL-101(Cr) based catalysts in terms of catalytic activity and stability. Importantly, as will be commented later, some of these studies reported the possibility of engineering the catalytic sites in MIL-101(Cr) through metal node or organic ligand modifications.<sup>82</sup> It should be noted that the present thesis in Chapter 3 will study the development of a mixed-metal MIL-101(Cr, Fe) solid acid catalyst for the Prins reaction of  $\beta$ -pinene with formaldehyde for the synthesis of Nopol. Chapter 4 of this thesis studies the development of an active MIL-101(Cr) based multifunctional solid catalyst through organic ligand functionalisation for the synthesis of benzimidazoles from 1,2-benzenediamines and benzaldehyde derivatives. Thus, the following paragraphs will focus on some representative examples of the use of MOFs for these reactions and which will be considered as the precedents for these two chapters.

In one of these studies, our group examined the influence of terephthalic acid substituents on the catalytic activity of MIL-101(Cr) in three Lewis acid catalysed condensation reactions (Fig. 15).<sup>7</sup> The series of isostructural materials included MIL-101(Cr) with electron-withdrawing ( $\text{NO}_2$ ,  $\text{SO}_3\text{H}$ , Cl) or donating functional groups ( $\text{NH}_2$ ,  $\text{CH}_3$ ). Interestingly, a positive linear relationship was found between the electron-withdrawing ability and the observed catalytic activity.

## Ring opening of epoxides



## Acetalization of aldehydes



## Prins reaction

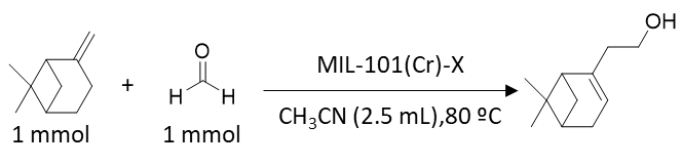


**Fig. 15** Three acid-catalysed reactions that were studied using MIL-101(Cr)-X as heterogeneous catalysts. Reprinted with permission from ref. <sup>7</sup>

In the case of the Prins reaction and the ring opening of styrene oxide using methanol catalysed by MIL-101(Cr)-X, a positive linear relationship with the  $\sigma_{\text{meta}}$  Hammett constant of each substituent of the terephthalate ligand was found (Fig. 16b).<sup>7</sup> In the case of benzaldehyde acetalization with methanol, the NH<sub>2</sub> and CH<sub>3</sub> substituted MOFs showed higher than expected catalytic activity based on the  $\sigma_{\text{meta}}$  Hammett constant of the substituent. In these cases, it was proposed that the presence of the NH<sub>2</sub> and CH<sub>3</sub> functional groups may play a role in the reaction mechanism or favour the absorption processes, respectively, and thus favour the catalytic process. Importantly, the use of CO as probe molecules for Lewis acid sites coupled with in situ FT-IR spectroscopy showed that the presence of NO<sub>2</sub> on the terephthalate ligand of the MOF results in an increase of the Lewis acidity of the metal cluster. In contrast, the presence of NH<sub>2</sub> as an electron-donating

substituent in the ligand of the MOF decreases the Lewis acidity of the MOF metal cluster. Furthermore, the catalyst was found to be stable on reuse. Additionally, the hot filtration test revealed that the MOF is acting as a truly heterogeneous catalyst. Overall, this work exemplifies the possibility of tuning the Lewis acidity of the metal nodes of MIL-101(Cr) with the presence of electron-withdrawing or donating functional groups in the terephthalate organic ligand.

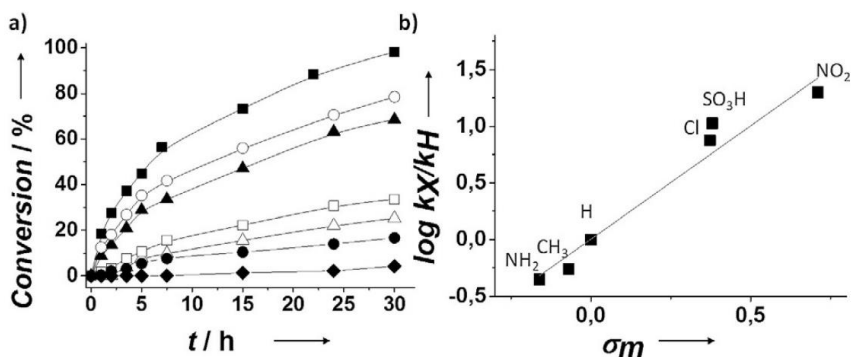


**Fig. 16** a) Time-conversion plot for the Prins coupling of  $\beta$ -pinene catalysed by MIL-101(Cr)-X. Legend: MIL-101(Cr)-H ( $\square$ ), MIL-101(Cr)-NO<sub>2</sub> ( $\blacksquare$ ), MIL-101(Cr)-SO<sub>3</sub>H ( $\circ$ ), MIL-101(Cr)-Cl ( $\blacktriangle$ ), MIL-101(Cr)-CH<sub>3</sub> ( $\triangle$ ), MIL-101(Cr)-NH<sub>2</sub> ( $\bullet$ ) and blank control in the absence of a catalyst ( $\blacklozenge$ ). Reaction conditions: catalyst (0.08 mmol of Cr);  $\beta$ -pinene (1 mmol); formaldehyde (1 mmol); acetonitrile (2.5 mL); 80 °C. b) Plot of the logarithm of the relative initial reaction rate versus the Hammett constant for each substituent on the terephthalate linker. Reprinted with permission from ref. <sup>7</sup>

Another possible strategy to tune the activity of MOFs as solid acid catalysts is the preparation of mixed-metal MOFs.<sup>85</sup> As one representative example, a series of mixed-metal MIL-100(Fe/Ni) materials were found to exhibit enhanced catalytic activity for the Prins reaction when using the MIL-100(Fe) pattern (Fig. 17).<sup>8</sup> The increase in catalytic activity agrees with the increase in Lewis acidity determined by CO titration due to the incorporation of Ni<sup>2+</sup> in the metal node. In addition, the presence of Ni<sup>2+</sup> in the metal node results in a distortion of the frameworks as revealed by EXAFS measurements. It was proposed that the presence of Ni<sup>2+</sup> in



the metal node favours the accessibility to Fe(III) Lewis acid sites and this results in an increase in catalytic activity. Additional catalytic experiments showed that the mixed-metal MIL-101(Fe, Ni) solid can be used as a reusable and truly heterogeneous catalyst. This work clearly exemplifies the possibility of preparing stable mixed-metal MOFs with enhanced catalytic activity.

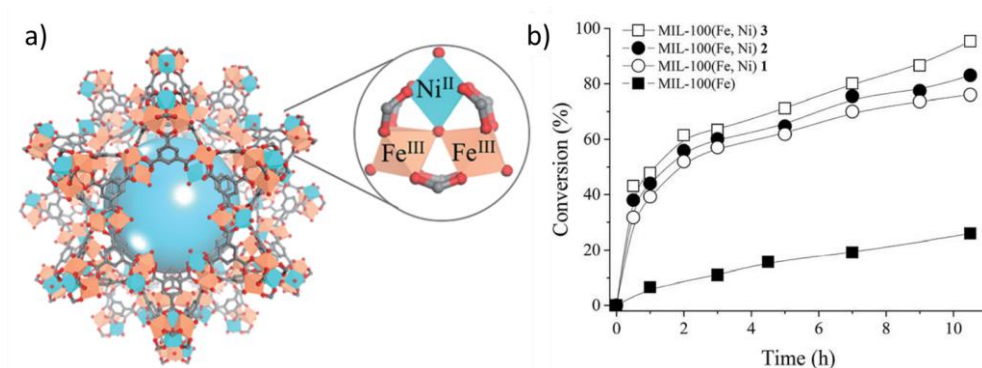


**Fig. 17** (a) Structure of the heterometallic MIL-100 (Fe, Ni) and trimeric heterometallic unit. Iron and nickel octahedra, and carbon and oxygen atoms are shown in orange, blue, grey, and red, respectively. b) Time conversion plot of  $\beta$ -pinene using as a catalyst either the mixed-metal MIL-100(Fe, Ni) 1–3 or homometallic MIL-100(Fe). Reaction conditions: catalyst (15 mg, 0.5 mol% total metal based);  $\beta$ -pinene (1 mmol); and paraformaldehyde (1 mmol) in MeCN at 80 °C. Legend (a): MIL-100(Fe) (■), MIL-100(Fe, Ni) 1 (○), 2 (●) and 3 (□). Reprinted with permission from ref.<sup>8</sup>

In a series of studies, MOFs have been used as heterogeneous catalysts for the synthesis of benzimidazoles. In one of these studies, MIL-101(Cr) was found to be active for the preparation of benzimidazole from *o*-phenylenediamine and benzaldehyde derivatives. The catalyst was reused five times without observing a decrease in catalytic activity.

## 1.9. Metal-free heterogeneous catalysts

As previously commented, most catalysts used worldwide are based on transition metals. For the sake of sustainability, it would be worthwhile

developing metal-free catalysts.<sup>24–27,86–88</sup> In this context, at the beginning of the 20th century several studies reported the possibility of using carbon-based materials as heterogeneous catalysts. One study in 1925 reported the mineralisation of oxalic and malonic acids in the presence of charcoal as a metal-free catalyst and molecular O<sub>2</sub> as an oxidant.<sup>89</sup> It was proposed that molecular oxygen added as an oxidant reacts with charcoal and leads to the formation of surface reactive oxygen species able to degrade the organic compounds. Several subsequent studies observed that the coke deposited on acidic oxides<sup>90,91</sup> or metal phosphates<sup>92</sup> employed during the oxidative dehydrogenation of ethylbenzene was the real catalyst of the process.

In the middle of the 20<sup>th</sup> century several studies reported the possibility of using carbonaceous materials as metal-free catalysts for dehydrogenation reactions.<sup>93</sup> One of the most studied examples included the catalytic dehydrogenation of ethylbenzene to styrene (Fig. 18). Styrene is an important commodity for producing polystyrene. In one of these examples, it was reported that oxidative dehydrogenation of ethylbenzene using Zr(HPO<sub>4</sub>)<sub>2</sub> resulted in the formation of coke in the catalyst.<sup>92</sup> Further investigation concluded that the active sites of the catalyst that promote the styrene dehydrogenation were hydroquinone/quinone- and/or aroxyl/phenol groups.

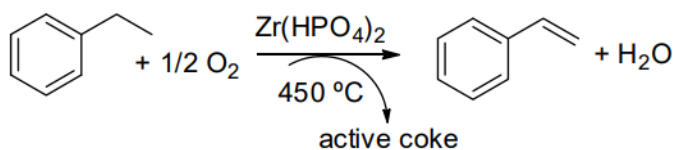


**Fig. 18** Catalytic oxidative dehydrogenation of ethylbenzene to styrene and formation of active coke. Reprinted with permission of ref.<sup>93</sup>

Activated carbons obtained from biomass have proven to be a clear example of sustainability when used as metal-free catalysts.<sup>94</sup> A series of studies have reported the use of activated carbon, for example, for the activation of H<sub>2</sub>O<sub>2</sub> and even molecular O<sub>2</sub> to promote oxidation reactions.<sup>94</sup> The discovery of new carbon allotropes and the development of novel carbon-based materials means that the field of carbocatalysis has further widened. The discovery of graphene in 2004<sup>95</sup> has greatly expanded the field of carbocatalysis.<sup>7,8,24–27,85</sup>

## 1.10. Graphene-based materials as metal-free catalysts

Graphene is a two-dimensional material made of one atom thick sp<sup>2</sup> carbons arranged in a hexagonal lattice.<sup>95,96</sup> However, there are only a few examples of ideal graphene used as a carbocatalyst. In contrast, there are many examples describing the possibility of using defective graphenes as metal-free catalysts.<sup>26,27</sup> Among the various methods to produce defective graphenes the technique based on the Hummer's oxidation followed by exfoliation (with or without reduction) has been the most widely used for the preparation of metal-free catalysts (Fig. 19).<sup>27</sup> This method involves the chemical oxidation of graphite by a mixture of strong mineral acids with KMnO<sub>4</sub> followed by the addition of H<sub>2</sub>O<sub>2</sub>. The resulting graphite oxide material can be later exfoliated by sonication leading to the formation of graphene oxide. As a function of the degree of oxidation, the oxygen content of graphene oxide can range from 40 to 60 wt%. The resulting GO can be further modified by thermal or chemical reduction resulting in the formation of reduced GO (rGO) with an oxygen content that frequently ranges between 5 to 20 wt% and a reconstituted sp<sup>2</sup> layer. Fig. 19 also illustrates the large variety of oxygen functional groups that can be present in varying proportions in GO and rGO as a function of the preparation conditions. It is important to note that the use of transition metal oxidants such as KMnO<sub>4</sub> during the preparation of GO and

rGO can result in the presence of  $Mn^{2+}$  impurities in the materials.<sup>88</sup> Therefore, when using these graphene-based materials as metal-free catalysis the possibility that the presence of metal impurities are the active sites of the process should be discounted.

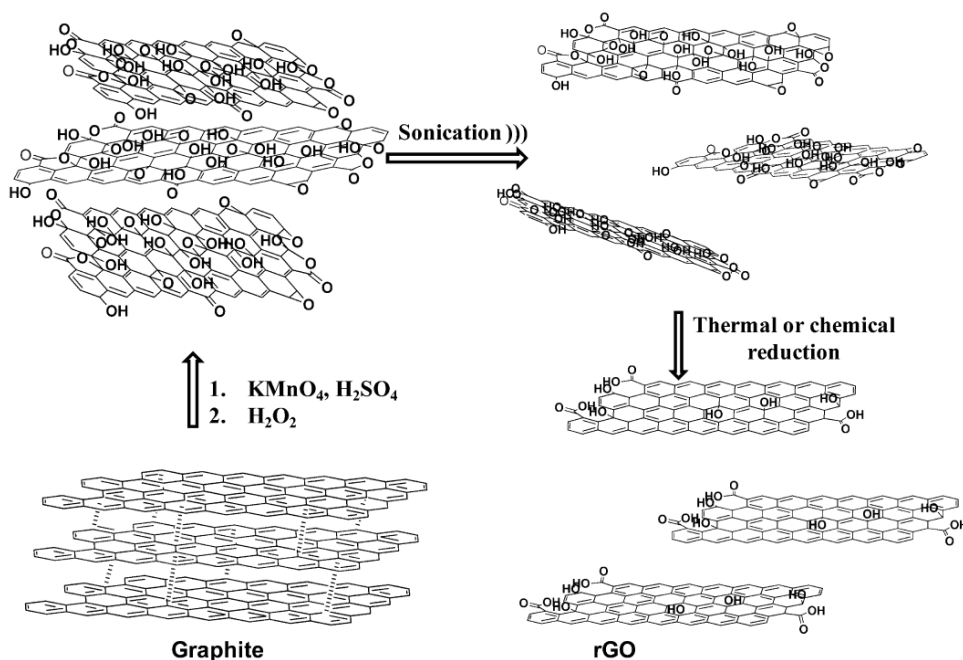


**Fig. 19** Illustration of the preparation of GO and rGO based on the Hummer's oxidation method followed by sonication and reduction processes. Reprinted with permission from ref.<sup>27</sup> (Navalon, S; Dhakshinamoorthy, A.; Alvaro, M.; Garcia, H. Carbocatalysis by Graphene-Based Materials. *Chemical Reviews* 2014, *114*, 6179-6212). Copyright (2021) American Chemical Society.

In one seminal study, Bielawski and co-workers showed for the first time the possibility of using GO as metal-free catalyst for the oxidation of neat benzyl alcohol to benzaldehyde using molecular  $O_2$  as an oxidant (Fig. 20).<sup>97</sup> It is important to note that this reaction has been frequently reported using transition metal and noble metal-based catalysts. Based on experimental evidence and theoretical

calculations, the presence of epoxide functional groups in the GO were proposed as the active sites of the material.



**Fig. 20** Aerobic oxidation of benzyl alcohol to benzaldehyde using GO as metal-free catalyst.

Several examples using GO or rGO as metal-free catalysts have been reported since then.<sup>26,27,98,99</sup> Many studies focussed on determining the active sites present on GO or rGO to promote different reactions. In one of these examples, our group proposed that the presence of hydroquinone/p-benzoquinone-like moieties in rGO were the active centres responsible of the  $\text{H}_2\text{O}_2$  activation to hydroxyl radicals.<sup>31</sup> The classic metal-catalysed  $\text{H}_2\text{O}_2$  decomposition of hydroxyl radicals is called the Fenton reaction. This reaction consists in the one-electron  $\text{H}_2\text{O}_2$  reduction to  $\text{HO}^\cdot$  and  $\text{HO}^\cdot$  together with Fe(II) oxidation to Fe(III). The catalytic cycle is reconstituted by the Fe(III) reduction to Fe(II) by  $\text{H}_2\text{O}_2$  and the formation of  $\text{HOO}^\cdot$ . Fig. 21 shows the proposed reaction mechanism for the  $\text{H}_2\text{O}_2$  activation by the redox pair hydroquinone/p-benzoquinone.

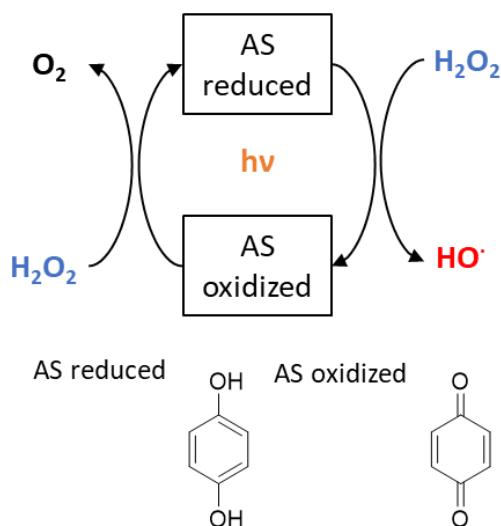


**Fig. 21** Mechanistic proposal for H<sub>2</sub>O<sub>2</sub> activation to hydroxyl radicals using hydroquinone/p-benzoquinone model molecules for the active sites (AS) in rGO. Adapted with permission from ref.<sup>31</sup> (Espinosa, J.C.; Navalón, S.; Álvaro, M.; García, H. Reduced Graphene Oxide as Metal-Free Catalyst for the Light-Assisted Fenton-Like Reaction. *ChemCatChem* 2016, *8*, 2642-2648).

More recently, our group has reported the influence of the chemical GO reduction method on the activity of the resulting rGO for the aerobic oxidation of benzylamine.<sup>100</sup> Previous studies showed that the transformation of GO to rGO using ascorbic acid, hydrazine (N<sub>2</sub>H<sub>4</sub>) or alanina (among other possible reducing agents) occurs through a series of complex reactions leading to the reconstitution of the sp<sup>2</sup> domain in rGO (Fig. 22).<sup>88</sup> Importantly, some specific functionalisation on the graphene sheet is introduced as a function of the reducing agent employed for the preparation of rGO. Furthermore, as previously commented, previous studies have identified the quinone/hydroquinone moieties present in rGO as active sites to promote oxidation reactions using H<sub>2</sub>O<sub>2</sub> as well as molecular O<sub>2</sub>. Therefore, hydroquinone was selected as a reducing agent to promote the transformation of GO to rGO while introducing quinone/hydroquinone-like moieties in the graphene sheet. For comparison, other rGO materials were

prepared using the widely employed ascorbic acid and hydrazine reducing agents. A thermal reduced rGO sample was also prepared.

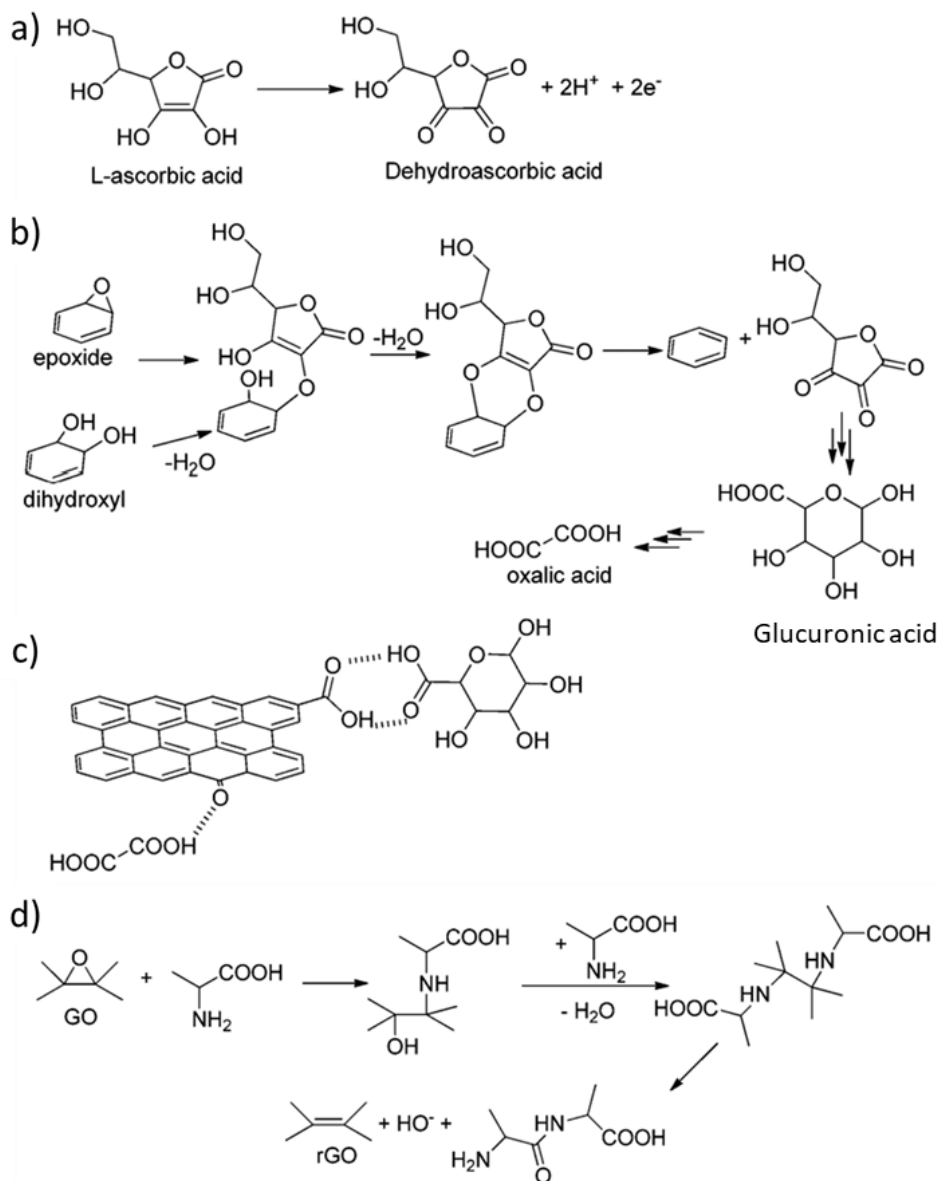


**Fig. 22** a) L-ascorbic oxidation to dehydroascorbic acid; b) proposed mechanisms for the reduction of epoxide and dihydroxyl groups with L-ascorbic acid; c) illustration of rGO association with oxalic and glucuronic acid that improves rGO dispersibility in aqueous suspensions; and d) possible mechanism of reduction of GO to rGO with alanine. Note that

some nitrogenated intermediates could still be present in the final complex structure of rGO. Reprinted with permission from ref.<sup>88</sup>

Interestingly, the most active sample of the series was the rGO prepared using hydroquinone as a reducing agent.<sup>100</sup> The characterisation data of the catalyst together with catalytic experiments and mechanistic studies enabled suggesting the pair of hydroquinone/quinone-like moieties as being responsible for the high level of catalytic activity observed (Fig. 23).

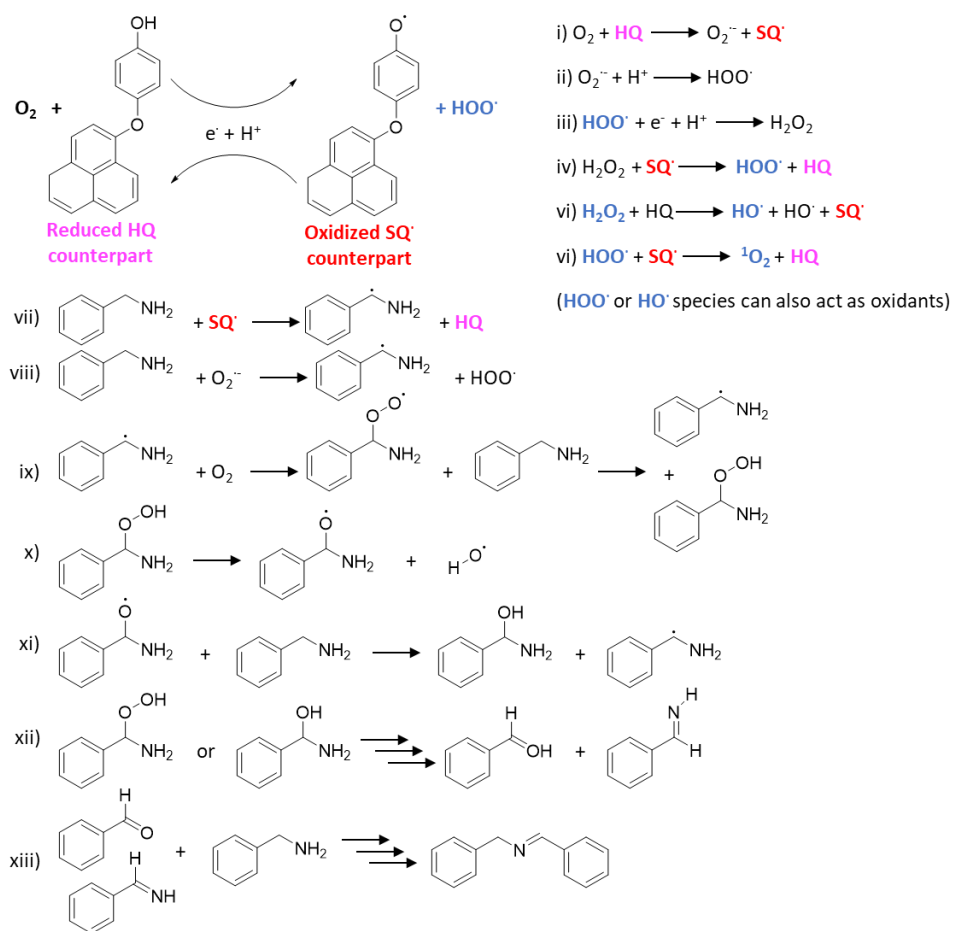


**Fig. 23** Plausible reaction mechanism involving activation of molecular O<sub>2</sub> by hydroquinone-like moieties present in the rGO-HQ1 sample with formation of ROS that generates benzylic radicals resulting in the final N-benzylidene benzylamine. Reprinted with permission from ref.<sup>100</sup>



## 1.11. References

- 1 E. Gallei and E. Schwab, *Catal. Today*, 1999, **51**, 535-546.
- 2 J. Lee, C. Choi and S. Kim, *Catal Today*, 2021, **359**, 1-2.
- 3 B. Liu and Z. Zhang, *ACS Catal.*, 2016, **6**, 326-338.
- 4 S. L. James, *Chem. Soc. Rev.*, 2003, **32**, 276-288.
- 5 C. Locke and H. Rase, *Ind. & Eng. Chem.*, 1960, **52**, 515-516.
- 6 X. Li, J. Yu, J. Low, Y. Fang, J. Xiao and X. Chen, *J. Mat. Chem. A*, 2015, **3**, 2485-2534.
- 7 A. Santiago-Portillo, S. Navalón, P. Concepción, M. Álvaro and H. García, *ChemCatChem.*, 2017, **9**, 2506-2511.
- 8 M. Giménez-Marqués, A. Santiago-Portillo, S. Navalón, M. Álvaro, V. Briois, F. Nouar, H. Garcia and C. Serre, *J. Mat. Chem. A*, 2019, **7**, 20285-20292.
- 9 C. K. Prier, D. A. Rankin and D. W. C. MacMillan, *Chem. Rev.*, 2013, **113**, 5322-5363.
- 10 W. Zhou, L. Xie, J. Gao, R. Nazari, H. Zhao, X. Meng, F. Sun, G. Zhao and J. Ma, *Chem. Eng. J.*, 2021, **410**, 128368.
- 11 S. Li, Y. Gao, N. Li, L. Ge, X. Bu and P. Feng, *Energy Environ. Sci.*, 2021, **14**, 1897-1927.
- 12 A. Dhakshinamoorthy, A. Santiago-Portillo, A. M. Asiri and H. Garcia, *ChemCatChem.*, 2019, **11**, 899-923.
- 13 M. J. Climent, A. Corma and S. Iborra, *RSC Adv.*, 2012, **2**, 16-58.
- 14 A. Gómez-Paricio, A. Santiago-Portillo, S. Navalón, P. Concepción, M. Alvaro and H. Garcia, *Green Chem.*, 2016, **18**, 508-515.
- 15 R. Klaewkla, M. Arend and W. F., in *Mass Transfer - Advanced Aspects*, 2011, 667-684
- 16 A. Dhakshinamoorthy, M. Opanasenko, J. Čejka and H. Garcia, *Catal. Sci. Technol.*, 2013, **3**, 2509-2540.
- 17 A. Corma and J. M. Serra, in *Catal. Today*, 2005, **107-108**, 699-706.
- 18 A. Corma, J. Navas and M. J. Sabater, *Chem. Rev.*, 2018, **118**, 1410-1459.
- 19 A. Gałuszka, Z. M. Migaszewski, P. Konieczka and J. Namieśnik, *TrAC – Trend. Anal. Chem.*, 2012, **37**, 61-72.
- 20 R. A. Sheldon, *ACS Sustainable Chem. Eng.*, 2018, **6**, 32-48.
- 21 B. Mallesham, D. Raikwar and D. Shee, *Advanced Functional Solid Catalysts for Biomass Valorization*, 2020, 1-37.
- 22 H. Li, Z. Fang, R. L. Smith and S. Yang, *Prog. Energ. Combust.*, 2016, **55**, 98-194.
- 23 F. Jérôme, Y. Pouilloux and J. Barrault, *ChemSusChem.*, 2008, **1**, 586-613.
- 24 D. R. Dreyer and C. W. Bielawski, *Chem. Sci.*, 2011, **2**, 1233-1240.
- 25 X. Duan, H. Sun and S. Wang, *Acc.Chem. Res.*, 2018, **51**, 678-687
- 26 S. Navalon, A. Dhakshinamoorthy, M. Alvaro, M. Antonietti and H. García, *Chem. Soc. Rev.*, 2017, **46**, 4501-4529.
- 27 S. Navalon, A. Dhakshinamoorthy, M. Alvaro and H. Garcia, *Chem. Rev.*, 2014, **114**, 6179-6212.

- 28 S. Navalón, J. R. Herance, M. Álvaro and H. García, *Chem.-Eur. J.*, 2017, **23**, 15244-15275.
- 29 J. C. Espinosa, S. Navalon, M. Alvaro, A. Dhakshinamoorthy and H. Garcia, *ACS Sustain. Chem. Eng*, 2018, **6**, 5607-5614
- 30 J. C. Espinosa, S. Navalón, A. Primo, M. Moral, J. F. Sanz, M. Álvaro and H. García, *Chem.-Eur. J.*, 2015, **21**, 11966-11971.
- 31 J. C. Espinosa, S. Navalón, M. Álvaro and H. García, *ChemCatChem*, 2016, **8**, 2642-2648
- 32 Z. Guo, B. Liu, Q. Zhang, W. Deng, Y. Wang and Y. Yang, *Chem. Soc. Rev.*, 2014, **43**, 3480-3524.
- 33 S. Caron, R. W. Dugger, S. G. Ruggeri, J. A. Ragan and D. H. Brown Ripin, *Chem. Rev.*, 2006, **106**, 2943-2989.
- 34 M. E. Ali, M. M. Rahman, S. M. Sarkar and S. B. A. Hamid, *J. Nanomater.*, 2014, **2014**, 1-23.
- 35 A. Franco, S. De, A. M. Balu, A. A. Romero and R. Luque, *ChemistrySelect*, 2017, **2**, 9546-9551.
- 36 R. Xie, G. Fan, L. Yang and F. Li, *Chem. Eng. J.*, 2016, **288**, 169-178.
- 37 M. Souto, A. Santiago-Portillo, M. Palomino, I. J. Vitórica-Yrezábal, B. J. C. Vieira, J. C. Waerenborgh, S. Valencia, S. Navalón, F. Rey, H. García and G. Mínguez Espallargas, *Chem. Sci.*, 2018, **9**, 2413-2418.
- 38 R. Goyal, O. Singh, A. Agrawal, C. Samanta and B. Sarkar, *Catal. Rev.*, 2020.
- 39 A. Dhakshinamoorthy, A. M. Asiri, J. R. Herance and H. Garcia, *Catal. Today*, 2018, **306**, 1-310
- 40 A. Corma and H. García, *Chem. Rev.*, 2003, **103**, 4307-4366.
- 41 A. Dhakshinamoorthy, A. M. Asiri and H. Garcia, *Chem.-Eur. J.*, 2016, **22**, 8012-8024.
- 42 E. Arundale and L. A. Mikeska, *Chem. Rev.s*, 1952, **51**, 505-555.
- 43 G. J. Kelly, F. King and M. Kett, *Green Chem.*, 2002, **4**, 392-399.
- 44 F. Doro, N. Akeroyd, F. Schiet and A. Narula, *Angew. Chem. Int. Edit.*, 2019, **58**, 7174-7179.
- 45 S. I. Alaqeel, *Journal of Saudi Chemical Society*, 2017, **21**, 229-237.
- 46 H. Li, M. Eddaoudi, M. O'Keeffe and O. M. Yaghi, *Nature*, 1999, **402**, 276-279.
- 47 G. Férey, *Chem. Soc. Rev.*, 2008, **37**, 191-214.
- 48 C. Férey, C. Mellot-Draznieks, C. Serre, F. Millange, J. Dutour, S. Surblé and I. Margiolaki, *Science*, 2005, **309**, 2040-2042.
- 49 S. Kitagawa, R. Kitaura and S. I. Noro, *Angew. Chem. Int. Edit.*, 2004, **43**, 2334-2375.
- 50 H. Furukawa, K. E. Cordova, M. O'Keeffe and O. M. Yaghi, *Science*, 2013, **341**, 1230444.
- 51 C. Gropp, S. Canossa, S. Wuttke, F. Gándara, Q. Li, L. Gagliardi and O. M. Yaghi, *ACS Cent. Sci.*, 2020, **6**, 1255-1273.
- 52 T. Devic and C. Serre, *Chem. Soc. Rev.*, 2014, **43**, 6097-6115.
- 53 S. Yuan, L. Feng, K. Wang, J. Pang, M. Bosch, C. Lollar, Y. Sun, J. Qin, X. Yang, P. Zhang, Q. Wang, L. Zou, Y. Zhang, L. Zhang, Y. Fang, J. Li and H. C. Zhou, *Adv. Mater.*, 2018, **30**, 1704303.

- 54 K. S. Park, Z. Ni, A. P. Côté, J. Y. Choi, R. Huang, F. J. Uribe-Romo, H. K. Chae, M. O’Keeffe and O. M. Yaghi, *P. Natl. Acad. Sci. USA*, 2006, **103**, 10186-10197.
- 55 D. Y. Heo, H. H. Do, S. H. Ahn and S. Y. Kim, *Polymers-basel*, 2020, **12**, 2061.
- 56 H. Li, L. Li, R.-B. Lin, W. Zhou, Z. Zhang, S. Xiang and B. Chen, *EnergyChem*, 2016, **1**, 100006.
- 57 H. Deng, S. Grunder, K. E. Cordova, C. Valente, H. Furukawa, M. Hmadeh, F. Gándara, A. C. Whalley, Z. Liu, S. Asahina, H. Kazumori, M. O’Keeffe, O. Terasaki, J. F. Stoddart and O. M. Yaghi, *Science*, 2012, **336**, 1018-1023
- 58 García H and Navalón S, *Focus on Catalysts*, 2017, **2018**, 1-8
- 59 L. M. Aguirre-Díaz, D. Reinares-Fisac, M. Iglesias, E. Gutiérrez-Puebla, F. Gándara, N. Snejko and M. Á. Monge, *Coordin. Chem. Rev.*, 2017, **335**, 1-27.
- 60 J. Gascon, A. Corma, F. Kapteijn and F. X. Llabrés I Xamena, *ACS Cata.*, 2014, **4**, 361-378.
- 61 A. Bavykina, N. Kolobov, I. S. Khan, J. A. Bau, A. Ramirez and J. Gascon, *Chem. Rev*, 2020, **120**, 8468-8535.
- 62 S. M. J. Rogge, A. Bavykina, J. Hajek, H. Garcia, A. I. Olivos-Suarez, A. Sepúlveda-Escribano, A. Vimont, G. Clet, P. Bazin, F. Kapteijn, M. Daturi, E. v. Ramos-Fernandez, F. X. I. Llabrés Xamena, V. van Speybroeck and J. Gascon, *Chem. Soc. Rev.*, 2017, **46**, 3134-3184.
- 63 A. Dhakshinamoorthy, A. M. Asiri and H. García, *Angew. Chem. Int. Edit.*, 2016, **55**, 5414-5445.
- 64 L. E. Kreno, K. Leong, O. K. Farha, M. Allendorf, R. P. van Duyne and J. T. Hupp, *Chem. Rev.*, 2012, **112**, 1105-1125.
- 65 M. Mon, R. Bruno, J. Ferrando-Soria, D. Armentano and E. Pardo, *J. Mater. Chem. A*, 2018, **6**, 4912-4947.
- 66 S. Rojas and P. Horcajada, *Chem. Rev.*, 2020, **120**, 8378-8415.
- 67 L. Ma, X. Feng, S. Wang and B. Wang, *Mater. Chem. Front.*, 2017, **1**, 2474-2486.
- 68 A. M. Rice, C. R. Martin, V. A. Galitskiy, A. A. Berseneva, G. A. Leith and N. B. Shustova, *Chem. Rev.*, 2020, **120**, 8790-8813.
- 69 E. Coronado, *Nat. Rev. Mater.*, 2020, **5**, 87-104.
- 70 W. Zhang and R. G. Xiong, *Chem. Rev.*, 2012, **112**, 1163-1195.
- 71 P. Horcajada, R. Gref, T. Baati, P. K. Allan, G. Maurin, P. Couvreur, G. Férey, R. E. Morris and C. Serre, *Chem. Rev.*, 2012, **112**, 1232-1268.
- 72 S. Wang and C. Serre, *ACS Sustainable Chem. Eng.*, 2019, **7**, 11911-11927.
- 73 N. Li, J. Xu, R. Feng, T. L. Hu and X. H. Bu, *Chem. Commun.*, 2016, **52**, 8501-8513.
- 74 N. v. Maksimchuk, O. v. Zalomaeva, I. Y. Skobelev, K. A. Kovalenko, V. P. Fedin and O. A. Kholdeeva, in *Proc. R. Soc. A*, 2012, 468, 2017-2034.
- 75 A. A. Babaryk, O. R. Contreras Almengor, M. Cabrero-Antonino, S. Navalón, H. García and P. Horcajada, *Inorg. Chem.*, 2020, **59**, 3406-3416
- 76 A. Dhakshinamoorthy, M. Alvaro and H. Garcia, *Catal. Sci. Technol.*, 2011, **1**, 856-867
- 77 A. Dhakshinamoorthy, E. M. Lanzuela, S. Navalon and H. Garcia, *Catalysts*, 2021, **11**, 1-25.
- 78 A. Corma, H. García and F. X. Llabrés I Xamena, *Chem. Rev.*, 2010, **110**, 4606-4655.
- 79 A. Dhakshinamoorthy, Z. Li and H. Garcia, *Chemical Society Reviews*, 2018, **47**, 8134-8172.

- 80 O. Kholdeeva and N. Maksimchuk, *Catalysts*, 2021, **11**, 1-23.
- 81 A. Santiago-Portillo, S. Navalón, F. G. Cirujano, F. X. L. I. Xamena, M. Alvaro and H. Garcia, *ACS Catal.*, 2015, **5**, 3216-3224
- 82 A. Dhakshinamoorthy, M. Opanasenko, J. Čejka and H. Garcia, *Adv. Synth. Catal.*, 2013, **355**, 247-268.
- 83 P. Hu and M. Long, *Appl. Catal. B-Environmental*, 2016, **181**, 103-117-.
- 84 M. Opanasenko, A. Dhakshinamoorthy, Y. K. Hwang, J. S. Chang, H. Garcia and J. Čejka, *ChemSusChem*, 2013, **6**, 865-871
- 85 M. Y. Masoomi, A. Morsali, A. Dhakshinamoorthy and H. Garcia, *Angew. Chem. Int. Edit.*, 2019, **58**, 15188-15205.
- 86 J. Duan, S. Chen, M. Jaroniec and S. Z. Qiao, *ACS Catal.*, 2015, **5**, 5207-5234
- 87 S. Navalón, A. Dhakshinamoorthy, M. Álvaro and H. García, *Chem. Mater.*, 2020, **32**, 4116-4143.
- 88 S. Navalón, J. R. Herance, M. Álvaro and H. García, *Mater. Horiz.*, 2018, **5**, 363-378.
- 89 E. K. Rideal and W. M. Wright, *J. Chem. Soc., Trans.*, 1925, **127**, 1347-1357.
- 90 F. Cavani and F. Trifirò, *Appl. Catal. A- Gen.*, 1995, **133**, 219-239.
- 91 A. E. Lisovskii and C. Aharoni, *Catal. Rev.*, 1994, **36**, 25-74.
- 92 A. Schraut, G. Emig and H. G. Sockel, *Appl. Catal.*, 1987, **29**, 311-326.
- 93 S. Navalón, W. J. Ong and X. Duan, *Processes*, 2020, **8**, 1-18.
- 94 S. Navalon, A. Dhakshinamoorthy, M. Alvaro and H. Garcia, *ChemSusChem*, 2011, **4**, 1712-1730.
- 95 K. S. Novoselov, A. K. Geim, S. v. Morozov, D. Jiang, Y. Zhang, S. v. Dubonos, I. v. Grigorieva and A. A. Firsov, *Science*, 2004, **306**, 666-669.
- 96 A. K. Geim and K. S. Novoselov, *Nat. Mater.*, 2007, **6**, 183-191.
- 97 D. R. Dreyer, S. Park, C. W. Bielawski and R. S. Ruoff, *Chem. Soc. Rev.*, 2010, **39**.
- 98 D. R. Dreyer, H. P. Jia and C. W. Bielawski, *Angew. Chem. Int Edit.*, 2010, **49**, 6813-6816.
- 99 D. R. Dreyer, S. Murali, Y. Zhu, R. S. Ruoff and C. W. Bielawski, *J. Mater. Chem.*, 2011, **21**, 3443-3447.
- 100 J. C. Espinosa, M. Álvaro, A. Dhakshinamoorthy, S. Navalón and H. García, *ACS Sustainable Chem. Eng.*, 2019, **7**, 19.

## **Chapter 2. *Objectives***



The aim of this thesis is the engineering of catalytic sites for oxidation and condensation reactions using metal-organic frameworks or graphene-based materials.

The specific objectives of each of the chapters are the following:

To design stable mixed-metal MIL-101(Cr/Fe) materials with enhanced catalytic activity for the Prins reaction. For this purpose, a series of MIL-101(Cr/Fe) solids with different proportions of metals will be prepared. The solids will be characterised by a series of techniques including PXRD and spectroscopic techniques (such as FT-IR, XPS,  $^{57}\text{Fe}$ -Mössbauer spectroscopy), thermogravimetric analyses, isothermal  $\text{N}_2$  adsorption, and electron microscopy techniques (SEM). The Lewis acidity of the samples will be evaluated using in situ FT-IR using CO and  $\text{CD}_3\text{CN}$  as probe molecules. The catalytic activity of the materials will be tested for the Prins reaction, and the reusability and stability of the most active catalyst will be studied.

The influence of the nature of the substituent of the terephthalate organic ligand used for the preparation of MIL-101(Cr) materials on the catalytic activity for the synthesis of benzimidazoles will be studied. The samples will be characterized using PXRD, spectroscopic, analytical, and electron microscopy techniques. It is expected that the most active catalyst acts as an efficient bifunctional catalyst for the synthesis of benzimidazoles promoting catalysed condensation on the acid sites and subsequent oxidative dehydrogenation. The Lewis acidity of the most active sample will be evaluated by in situ FT-IR spectroscopy using  $\text{CD}_3\text{CN}$  as probe molecules. The most active catalyst will be reused several times and the occurrence of possible metal leaching and/or possible loss of catalyst crystallinity or morphological changes will be evaluated.

The aerobic oxidation of thiophenol and DBT derivatives using MIL-101(Cr) based materials bearing electron-donor or electron-acceptor substituents in the terephthalate organic ligand is studied. It is expected that a relationship will be found between the observed catalytic activities due to the metal centres and the nature of the MOF substituent. The nature of the reactive oxygen species involved in the catalytic processes will be studied by performing selective radical quenching experiments and EPR measurements using radical spin traps in the reactions. The catalytic activity and stability of the most active catalyst will be studied by performing consecutive reuse experiments and characterisation of the used catalyst by PXRD and an analysis of possible metal leaching from the solid to the solution.

Engineering the active sites in reduced graphene oxide for the development of metal-free catalysts with enhanced activity for the aerobic oxidations of thiophenol and indane. A series of rGO will be prepared with hydroquinone, hydrazine, and ascorbic acid to promote the reduction of graphene oxide. The samples will be characterised by a series of spectroscopic techniques (i.e., XPS, FT-IR, and diffuse reflectance UV-Vis). It is expected that the reducing agents will promote the reduction of GO to rGO together with rGO functionalisation with some groups of the reducing agent in its lattice during the functionalisation. The reusability of the most active sample will be studied by performing several consecutive reuses. To gain insight about the reaction mechanism, several selective radical quenching experiments will be performed for both aerobic oxidations.



**Chapter 3. *Desing of stable mixted-metal  
MIL-101(Cr/Fe) materials with enhanced  
catalytic activity for the Prins reaction***



# Desing of stable mixed-metal MIL-101(Cr/Fe) materials with enhanced catalytic activity for the Prins reaction

Cristina Vallés-García,<sup>‡,a</sup> Effrosyni Gkaniatsou,<sup>‡,b</sup> Andrea Santiago-Portillo,<sup>a</sup> Mónica Giménez-Marqués,<sup>c</sup> Mercedes Álvaro,<sup>a</sup> Jean-Marc Greneche,<sup>d</sup> Nathalie Steunou,<sup>b</sup> Clémence Sicard,<sup>b,\*</sup> Sergio Navalón,<sup>a,\*</sup> Christian Serre,<sup>6,\*</sup> Hermenegildo García<sup>f,g,\*</sup>

<sup>a</sup> Departamento de Química, Universitat Politècnica de València, C/Camino de Vera, s/n, 46022 Valencia, Spain.

<sup>b</sup> Institut Lavoisier de Versailles, UMR CNRS 8180, Université de Versailles Saint- Quentin-en-Yvelines, Université Paris Saclay, France.

<sup>c</sup> Instituto de Ciencia Molecular (ICMol), Universidad de Valencia, C/Catedrático José Beltrán 2, Paterna 46980, Spain.

<sup>d</sup> Institut des Molécules et Matériaux du Mans, UMR CNRS 6283, Université du Maine, Le Mans, France.

<sup>e</sup> Institut des Matériaux Poreux de Paris, UMR 8004 CNRS Ecole Normale Supérieure, Ecole Supérieure de Physique et de Chimie Industrielles de Paris, PSL university, Paris, France.

<sup>f</sup> Instituto de Tecnología Química CSIC-UPV, Universitat Politècnica de València, Consejo Superior de Investigaciones Científicas, Av. de los Naranjos s/n, 46022 Valencia, Spain.

<sup>g</sup> Center of Excellence for Advanced Materials Research, King Abdulaziz University, Jeddah, Saudi Arabia.

\*Both are considered as first authors.

Published online: July 23, 2020

(Reprinted with permission from *J. Mater. Chem. A*, 2020, **8**, 17002-17011.

Copyright © 2020, The Royal Society of Chemistry. All rights reserved.)



### 3.1 Abstract

This work highlights the benefit of designing mixed-metal (Cr/Fe) MOFs for enhanced the chemical stability and catalytic activity. A robust and stable mixed-metal MIL-101(Cr/Fe) was prepared through a HF-free direct hydrothermal route with Fe<sup>3+</sup> content up to 21 wt%. The incorporation of Fe<sup>3+</sup> cations in the crystal structure was confirmed by <sup>57</sup>Fe-Mössbauer spectrometry. The catalytic performance of the mixed metal MIL-101(Cr/Fe) was evaluated in the Prins reaction. MIL-101(Cr/Fe) exhibited a higher catalytic activity compared to MIL-101(Cr), improved chemical stability compared to MIL-101(Fe) and a higher catalytic activity for bulky substrates compared to MIL-100(Fe). *In situ* infra-red spectroscopy study suggests that the incorporation of Fe<sup>3+</sup> ions in MIL-101 structure leads to an increase in Lewis acid sites. It was thus concluded that the predominant role of Cr<sup>3+</sup> ions was to maintain the crystal structure, while Fe<sup>3+</sup> ions enhanced the catalytic activity.

### 3.2 Introduction

Metal-organic frameworks (MOFs) have been successfully applied as catalysts for a large variety of liquid-phase reactions.<sup>1-5</sup> Of particular importance are the Lewis acid-catalyzed processes due to the wide reaction range and their general applicability for the production of fine chemicals, pharmaceuticals and agrochemicals.<sup>6</sup> Some examples have shown the superiority as catalysts of MOFs *versus* zeolites to promote Lewis acid-catalyzed reactions in the liquid phase.<sup>7, 8</sup>

Among the most commonly used MOFs as heterogeneous catalysts, MIL-101(Cr) combines a series of desirable properties, including: (i) an exceptional chemical and a suitable thermal stability, (ii) a very high

porosity with wide pentagonal (1.2 nm) and hexagonal (1.4 nm) windows to access to the mesoporous cavities (2.9 and 3.4 nm in diameter), (iii) a large surface area (3000-4200 m<sup>2</sup> g<sup>-1</sup>), and (iv) a tunable composition through organic ligand substitution and metal node modification.<sup>9</sup> Importantly, after the removal of water molecules coordinated to the metal sites, the metal node cluster (Cr<sup>3+</sup>-trimer) presents inherent Lewis acidity.<sup>7</sup> Thus, MIL101-(Cr) has been widely reported as heterogeneous catalyst for those reactions that require Lewis acid sites<sup>7, 10</sup> or redox<sup>11-13</sup> centers.

Heterogeneous catalysis is continuously searching for more active and selective catalysts. In the particular case of MOFs as solid Lewis acids, this target can be achieved, by at least, two alternative ways, either by introducing electron-withdrawing substituents on the organic linker or by selecting metal ions with higher acid strength. In this context, it has been reported that the catalytic activity as Lewis acid of MIL-101(Cr) can be increased up to three orders of magnitude by introducing electron-withdrawing groups such as nitro groups in the organic ligand.<sup>10</sup> However, a complementary strategy would be to partially replace Cr<sup>3+</sup> by other appropriate transition metal. Regarding the possibility to enhance Lewis acidity by proper selection of the transition metal, an obvious choice is the replacement of Cr<sup>3+</sup> by Fe<sup>3+</sup> in MIL-101. It has been previously established that for some reactions MIL-101(Fe) is more efficient as catalyst than MIL-101(Cr),<sup>14</sup> although the direct comparison between the catalytic activity of Cr<sup>3+</sup> and Fe<sup>3+</sup> is in most cases not possible due to the different nature of the accompanying counter anion, particles sizes and other parameters. In addition, MOFs bearing Lewis acid sites such as MIL-100 or MIL-101 suffer from a partial poisoning of the most active metal sites by impurities (ligand, anion...)<sup>15</sup> Thus depending on the activation conditions, the same material

can exhibit a significantly different density of Lewis sites of different strength,<sup>16</sup> making thus comparison between various samples cumbersome.

In this context, the lower chemical stability of MIL-101(Fe), easily converted upon exposure to water or polar organic solvents to the less porous MIL-88B(Fe),<sup>17</sup> has hampered the determination of the real catalytic activity of Fe<sup>3+</sup> ions in the MIL-101 structure in comparison with the Cr<sup>3+</sup> analogue.

Previously, some of us have reported the direct preparation of mixed Cr/Fe MIL-53 materials. It was shown that the introduction of Cr<sup>3+</sup> ions into the Fe-MOF was accompanied by a strong enhancement of the chemical stability.<sup>18</sup> Later on this strategy was further extended to prepare highly porous Cr-MOFs through an easy solvothermal post-synthetic treatment starting from pre-formed Fe-MOFs.<sup>19</sup> However, the synthesis of bimetallic kinetic phase, such as MIL-101, remains challenging as it requires a careful tuning of the kinetic reactivity of the cations.

Preparation of heterometallic MOFs is a well-established strategy to optimize the catalytic activity of these materials.<sup>20-23</sup> For instance, doping MIL-100(Fe) with Ni species was found a convenient way to both increase the activity of the MOF catalyst, while preserving the good chemical stability of the bare Fe-MOF.

Herein, the preparation of a robust and stable mixed-metal MIL-101(Cr/Fe) structure in various Fe<sup>3+</sup> proportions up to 21 wt% is achieved through a direct hydrothermal synthesis reported avoiding the use of toxic HF. <sup>57</sup>Fe-Mössbauer spectrometry supports the successful

incorporation of  $\text{Fe}^{3+}$  cations within the crystal structure of the mixed-metal MIL-101(Cr/Fe) solids. Catalytic data for the Prins reaction indicate that the mixed-metal MIL-101(Cr/Fe) materials exhibit both an increased activity in comparison with the pure MIL-101(Cr) material, as well as a strongly enhanced chemical stability compared with the single-metal MIL-101(Fe) solid. A recent precedent has shown the superior activity of MIL-101(Fe) to catalyzed Nopol synthesis and the present study shows that it can be even further enhanced.<sup>23</sup> The mesoporosity of the mixed-metal MIL-101(Cr/Fe) was found to make this material more adequate as catalyst to promote the Prins addition of bulky substrate compared to MIL-100(Fe), most likely due to a favored substrate diffusion. In addition, a good relationship between the  $\text{Fe}^{3+}$  proportion in the MIL-101(Cr/Fe) catalysts and the observed catalytic activity has been found. Stability data indicate that MIL-101(Cr/Fe) solid acts as a true heterogeneous catalyst that can be reused maintaining its initial crystallinity without undergoing metal leaching. This work illustrates the successful design of heterometallic MOFs exhibiting a superior catalytic activity by having one metal with a predominant role in maintaining the crystal structure ( $\text{Cr}^{3+}$  in the present case) and a second one enhancing the catalytic activity ( $\text{Fe}^{3+}$  in MIL-101).

### **3.3 Results and discussion**

#### **3.3.1 Catalyst preparation**

The synthesis of MIL-101(Cr/Fe) by direct hydrothermal synthesis has been already reported.<sup>24</sup> However, the previously reported synthetic procedure used hydrofluoric acid (HF) as acidic modulator/mineralizing agent. HF is a highly hazardous liquid (highly toxic and corrosive, as well as contact poison) and, therefore, not suitable for green and sustainable



syntheses that are targeted nowadays, particularly for large scale preparation. A hydrothermal synthesis without HF was recently reported, but pure MIL-101(Cr/Fe) phase was only obtained for low Fe content (10 wt% ).<sup>25</sup> In the present case, the target was to introduce much larger Fe proportions and about 20 wt% of the total  $\text{Cr}(\text{NO}_3)_3 \cdot 9\text{H}_2\text{O}$  was replaced by  $\text{Fe}(\text{NO}_3)_3 \cdot 9\text{H}_2\text{O}$ . Consequently, the reported synthesis was optimized to avoid the use of HF, while achieving higher Fe content.

For the synthesis of pure and well crystallized MIL-101(Cr/Fe) solids, one of the most difficult challenges to overcome is the competition between the crystallization of two other polymorphs (*i.e.* same chemical composition, but different structure) typically obtained when dealing with  $\text{M}^{3+}$  cations and terephthalic acid: namely MIL-101,<sup>9</sup> MIL-88<sup>26</sup> and the thermodynamically preferred phase MIL-53.<sup>27, 28</sup> The use of mixed-metals with different reactivity is also known to modify the crystallization process and influence polymorph formation, not mentioning the risk to form metal oxides.<sup>29</sup> Therefore, attempts to obtain mixed-metal MIL-101(Cr/Fe) using iron nitrate as  $\text{Fe}^{3+}$  source and similar synthetic conditions (220 °C, 8 h) as those used for the pure MIL-101(Cr),<sup>30</sup> resulted only in mixtures of MIL-101/MIL-88B (Fig. SI-1†), possibly due to the higher reactivity of iron cations that drives the phase formation towards MIL-88B. The addition of non-toxic acidic modulators, such as acetic acid (HOAc) was also explored, but it resulted as well in MIL-101/MIL-88B mixtures (Fig. SI-1†). A possible way to address this difference in reactivity between  $\text{Fe}^{3+}$  and  $\text{Cr}^{3+}$  is the use of a less reactive iron source such as metal iron.  $\text{Fe}^0$  has already successfully been used for the preparation of the mixed metal MIL-53(Cr/Fe).<sup>23</sup> As seen in Fig. SI-2†, the use of  $\text{Fe}^0$  drastically limited the formation of MIL-88B phase, compared to the use of iron nitrate, but did not fully prevented its

formation. The use of HOAc did not improve the phase purity and resulted in mixture of MIL-101/MIL-88B phases (Fig. SI-2). It was, thus, concluded that this acid modulator was not adequate for the formation of a pure MIL-101(Cr/Fe) phase.

Basic additives, such as NaOH, KOH and tetramethylammonium hydroxide (TMAOH), have also been studied for the synthesis of MIL-101 materials. Their use has been reported to enhance the solubility of the terephthalic acid and to favor the nucleation process, as the pH conditions are shifted around pH 6, thus promoting the synthesis of MIL-101. MIL-101(Cr) synthesized in the presence of low concentrations of TMAOH showed a good crystallinity, high specific surface area and the formation of pure phases.<sup>31, 32</sup> It was hence of interest to investigate the use of this basic additive for the formation of the mixed metal MIL-101(Cr/Fe). To minimize the formation of the thermodynamic phase MIL-53(Cr), the reaction temperature was decreased, while the reaction time increased and various TMAOH concentrations were tested (0.0125-0.09 M). It was found that the purity of MIL-101 (Cr/Fe) varied linearly with TMAOH concentrations (Fig. SI-3<sup>†</sup>). Concentrations above 0.06 M promoted mostly the synthesis of MIL-101 phase, whereas lower concentrations resulted in traces of the MIL-53 phase. When TMAOH concentration was increased above 0.07 M, the crystallinity of the product significantly decreased until an amorphous solid was obtained at 0.09 M of TMAOH. These results are in agreement with previous studies that showed the effect of the TMAOH concentration on the crystallinity of MIL-101.<sup>32</sup>

Further optimization was achieved by further decrease of the reaction temperature minimizing oxide formation. Two pure MIL-101(Cr/Fe) materials with 4:1 and 5.9:1 Cr:Fe ratios were finally successfully obtained by using TMAOH as basic additive at 0.06 M at 150 °C. Both MIL-101(Cr/Fe) materials showed

characteristic Bragg peaks of MIL-101, without any additional peaks, which confirmed the formation of a pure phase (Fig. 1).

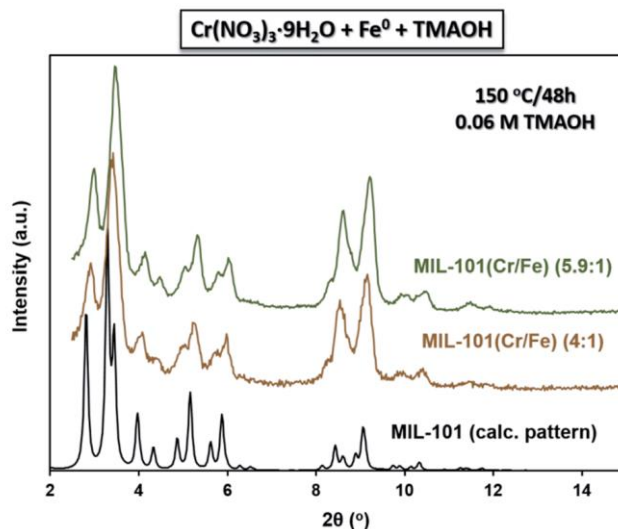


**Fig. 1** Normalized PXRD patterns ( $\lambda = 1.54 \text{ \AA}$ ) of MIL-101(Cr/Fe) (4:1) and MIL-101(Cr/Fe) (5.9:1), compared with the calculated pattern of MIL-101(Cr).

The Cr and Fe atomic content was analyzed by EDX (average of 12 random points) and confirmed by ICP-OES. The composition was found to be  $81 \pm 2\%$  Cr and  $19 \pm 2\%$  Fe for MIL-101(Cr/Fe) (4:1, 21 wt%) and  $85 \pm 1\%$  Cr and  $15 \pm 1\%$  Fe for MIL-101(Cr/Fe) (5.9:1, 14 wt%). The low standard deviation as well as the identical values obtained by EDX and ICP-OES, suggest a homogeneous dispersion of iron in the sample. The chemical formulae of the MOFs deduced from the EDX are  $\text{Cr}_{2.4}\text{Fe}_{0.6}\text{OH}(\text{H}_2\text{O})_2\text{O}[(\text{O}_2\text{C})\text{-C}_6\text{H}_4\text{-(CO}_2\text{)}]_3$ ,  $\text{Cr}_{2.57}\text{Fe}_{0.43}\text{OH}(\text{H}_2\text{O})_2\text{O}[(\text{O}_2\text{C})\text{-C}_6\text{H}_4\text{-(CO}_2\text{)}]_3$  for MIL-101(Cr/Fe) (4:1) and MIL-101(Cr/Fe) (5.9:1), respectively.

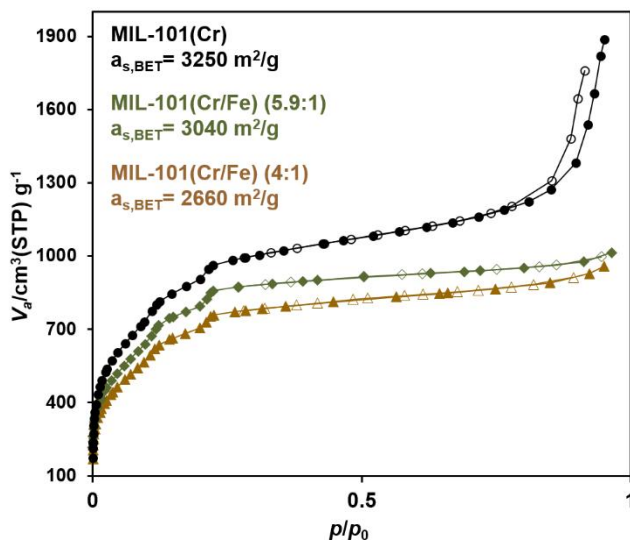


**Fig. 2** N<sub>2</sub> sorption isotherms of MIL-101 (Cr) (black cycles), MIL-101(Cr/Fe) (4:1) (brown triangles) and MIL-101(Cr/Fe) (5.9:1) (green diamonds) at 77 K ( $P_0=1$  atm).

SEM analysis on the two mixed-metal MIL-101(Cr/Fe) solids revealed the formation of particles, without a well-defined morphology. Nonetheless, both MOFs showed uniform particles of around 100 nm (Fig. SI-4<sup>†</sup>). The TGA curves of the two mixed metal MOFs were compared with that of MIL-101(Cr) (Fig. SI-5<sup>†</sup>). The thermal degradation of the structures was observed around 300 °C under oxygen, which is similar to the pure MIL-101(Cr),<sup>9</sup> indicating that the incorporation of Fe<sup>3+</sup> cations, does not affect the thermal stability of the framework. The percentage of Cr<sub>2</sub>O<sub>3</sub> residue obtained in the case of MIL-101(Cr) (31 %) was found to be slightly lower than then global percentage of the oxide residues (Cr<sub>2</sub>O<sub>3</sub> + Fe<sub>2</sub>O<sub>3</sub>) formed in the case of the mixed metal MOFs: 35% for MIL-101(Cr/Fe) (4:1) and 32% for MIL-101(Cr/Fe) (5.9:1). This may indicate that a small part of the metal precursors used for the synthesis of the MOFs could have formed oxides that could not be removed during the activation of the samples.

$N_2$  sorption measurements of the mixed-metal MOFs exhibit type I isotherms, with secondary uptakes at  $p/p_0 \sim 0.1$  and  $p/p_0 \sim 0.2$ , which are characteristic of the two microporous windows (pentagonal and hexagonal) of the two mesoporous cages (Fig. 2). The apparent BET surface areas were calculated to be  $2700 \pm 100$  and  $3040 \pm 60 \text{ m}^2 \text{ g}^{-1}$  for MIL-101(Cr/Fe) (4:1) and MIL-101(Cr/Fe) (5.9:1), respectively. The pore size distributions of the pure MIL-101(Cr) and the mixed-metal MIL-101(Cr/Fe) are very close to each other (Fig. SI-6<sup>+</sup>), suggesting identical pores structure and that both metals are incorporated in the framework. The obtained mixed-metal MOFs exhibited slightly lower surface area than that for the pure MIL-101(Cr) ( $3250 \text{ m}^2 \text{ g}^{-1}$ ), which could be related to the presence of small percentages of metal oxides, in agreement with the TGA measurements.

$^{57}\text{Fe}$ -Mössbauer spectrometry was used to gain information about the oxidation and the spin state of the Fe atoms, along with its electronic environment, in order to confirm that the Fe of the mixed MOFs was indeed incorporated in the lattice and to exclude the possibility of Fe being mainly under the form of Fe oxides or hydroxides. The transmission Mössbauer spectra of MIL-101(Cr/Fe) (4:1) recorded at 300 K and 77 K, consist of quadrupolar doublets with broadened and overlapped lines, indicative of different environments of Fe atoms (Fig. 3, SI-7 and SI-8<sup>+</sup>). They were first recorded at  $4 \text{ mm s}^{-1}$  to check that the samples did not contain any High Spin (HS) Fe(II) species and then at  $2 \text{ mm s}^{-1}$ . Fig. 3 illustrates only the spectra recorded at  $2 \text{ mm s}^{-1}$ . Different fitting models could be applied with two components or three components, resulting in the same mean values of isomer shift ( $0.33$  and  $0.48 \text{ mm s}^{-1}$  at 300 K and 77 K, respectively) and quadrupolar splitting ( $0.68$  and  $0.74 \text{ mm s}^{-1}$  at 300 K and 77 K, respectively). These values are consistent with the presence of HS  $\text{Fe}^{3+}$  in an octahedral

environmental, suggesting that they may be located in the octahedral units of the inorganic building blocks.<sup>33-35</sup> This is further supported by the similarity between the Mössbauer spectra of the mixed MIL-101(Cr/Fe) (4:1) and the reported spectrum of MIL-100(Fe) (Fig. 3 and SI-8†).<sup>35</sup> The isomer shift values of MIL-100(Fe) are significantly higher (0.42 and 0.54 mm s<sup>-1</sup> at 300 K and 77 K, respectively). This difference could result from the amount of fluorine ions contained in the structure, as the presence of F ions in the Fe environment results in higher isomer shifts than Fe surrounded by O.<sup>23</sup> It should be noted that in the reported Mössbauer spectrum of MIL-100(Fe), the synthesis was performed in presence of KF and it has been previously demonstrated that the resulting structure has one fluorine atom per Fe trimer.<sup>35</sup> However, in the case of MIL-101(Cr/Fe), the synthesis was performed without fluorine, and the corresponding coordination position in the structure is occupied by hydroxyl ions.<sup>18</sup> In the present mixed metal MIL-101(Cr/Fe), the mean values of isomer shift are rather typical of Fe<sup>3+</sup> surrounded by oxygen or hydroxyl groups, in fair agreement with the absence of KF during the synthesis of MIL-101(Cr/Fe). When the content of Fe incorporated in the synthesis was decreased (ratio Cr/Fe 5.9:1), no significant differences were observed in the Mössbauer spectrum (Fig. 3), except for a slight increase of the quadrupolar doublet asymmetry. The presence of water molecules in the framework actually influences the Mössbauer spectra and may be responsible for this difference. It is important to emphasize that the lack of resolution of the hyperfine structure does not allow excluding the presence of traces of iron<sup>3+</sup> oxides in MIL-101(Cr/Fe) samples, similarly to the case of MIL-100(Fe).

Our strategy therefore allows the preparation of MIL-101(Cr/Fe) solid with a Fe<sup>3+</sup> loading up to 21 wt% using a HF-free route. It should be

commented that the mesoporous rigid MIL-101 phase exhibits higher BET surface areas and porosity ( $3250 \text{ m}^2 \text{ g}^{-1}$  and  $1.2 \text{ cm}^3 \text{ g}^{-1}$ ) compared to that of the flexible microporous MIL-88B ( $<500 \text{ mg}^2 \text{ g}^{-1}$ ;  $0.6 \text{ cm}^3 \text{ g}^{-1}$ ), whose pores undergo a strong contraction upon drying. Therefore, MIL-101 is better suited as heterogeneous catalyst in comparison to MIL-88B, which shows important diffusion limitations.

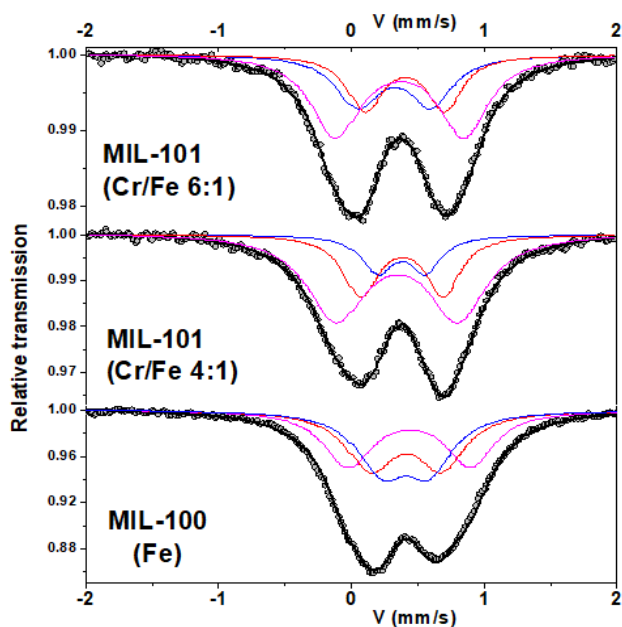


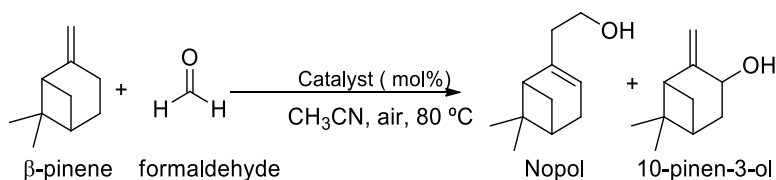
**Fig. 3** Mössbauer transmission spectra of MIL-101(Cr/Fe) (6:1), MIL-101(Cr/Fe) (4:1) and MIL-100(Fe), recorded at 77 K.

### 3.3.2 Catalytic activity

The main purpose of this study was to show that it is possible to overcome the intrinsic structural instability of the single metal MIL-101(Fe) solid by exploiting the structural stability of MIL-101(Cr), while introducing

in nodal positions some Fe<sup>3+</sup> sites in adequate proportion to preserve structural stability due to the prevalence of Cr<sup>3+</sup>, but still sufficiently high to achieve optimal catalytic activity.

To prove the concept of one metal maintaining the MOF structure and other acting as catalytic center, the MIL-101(Cr/Fe) (4:1) sample having about 21 wt% Fe<sup>3+</sup> was initially selected and its catalytic activity studied for the benchmark Lewis acid catalyzed addition of  $\beta$ -pinene to formaldehyde to afford [2-(7,7-dimethyl-4-bicyclo[3.1.1]hept-3-enyl)-ethanol], commonly known as Nopol (Scheme 1). Nopol is an important commodity with woody camphoraceous scent used in perfumery for the large scale production of fragrances.<sup>8, 36</sup> It is also used in the preparation of pesticides in the agrochemical industry.<sup>8, 36</sup> This Prins reaction has been widely studied in the presence of a large range of homogenous (*i.e.* HCl, SnCl<sub>2</sub>, ZnCl<sub>2</sub> etc.) and heterogeneous catalysts including MOFs, observing that Nopol formation is accompanied by the presence of some byproducts, 10-pinen-3-ol being the most common one.<sup>7</sup>



**Scheme 1** Prins reaction of  $\beta$ -pinene with formaldehyde and the chemical structure of the two products observed in the present reaction.

Particularly, formation of Nopol has been reported already using MIL-100(Fe) or MIL-100(Cr) as heterogeneous catalysts, observing that these materials efficiently promote the addition reaction, without



undergoing metal leaching and exhibiting reusability in consecutive batch reactions.<sup>8</sup>

In the present study a preliminary blank control experiment in the absence of catalyst shows that  $\beta$ -pinene conversion does not take place under the present reaction conditions. In contrast, when MIL-101(Cr) was present in the reaction, the addition reaction occurs resulting in the formation of Nopol as main product together with 10-pinen-3-ol (Scheme 1), reaching a conversion of 26 % at 30 h (Fig. 4). The use of MIL-101(Fe) or MIL-88B(Fe) as iron-based catalysts resulted in a slight increase of the catalytic activity ( $\sim 36\%$   $\beta$ -pinene conversion at 30 h) respect to the use of MIL-101(Cr).

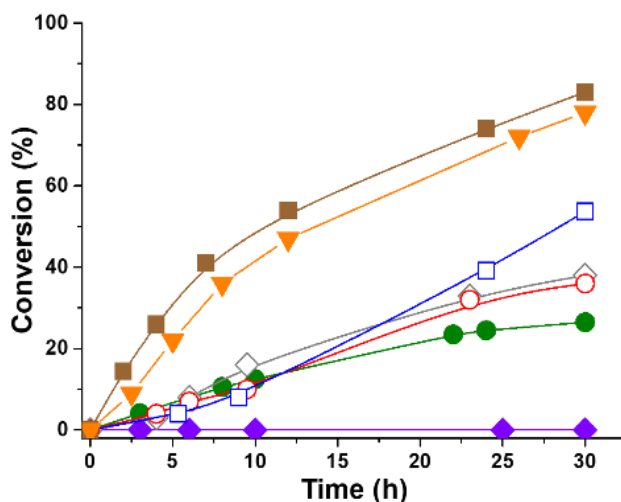


**Fig. 4** Catalytic activity for  $\beta$ -pinene using MIL-101(Cr/Fe) (4:1) (■), MIL-88(Fe) (◇), MIL-101(Fe) (○), MIL-101(Cr) (●), MIL-100(Fe) (▼), Fe<sup>3+</sup> acetate (□) and in the absence of catalyst (◆). Reaction conditions: Catalyst (0.02 mmol of metal),  $\beta$ -pinene (800  $\mu$ L, 5 mmol), formaldehyde (750  $\mu$ L, 5 mmol), acetonitrile (1.26 mL), 80 °C.

PXRD patterns of the used MOFs revealed that MIL-101(Fe) is, however, unstable under the present reaction conditions and is largely transformed into the MIL-88B(Fe) structure (Fig SI-9<sup>†</sup>). Importantly, the use of the novel MIL-101(Cr/Fe) (4:1) solid resulted in a much more robust material, exhibiting a significantly higher catalytic activity (85% at 30 h) than MIL-101(Cr), MIL-101(Fe) or MIL-88(Fe) and even than the homogeneous Fe<sup>3+</sup> acetate catalyst (Fig. 4). It should be noted that the higher catalytic activity of these Fe-based MOFs results, however, in the formation of higher amounts of 10-pinen-3-ol respect to the less active, but more selective MIL-101(Cr) catalyst (Table S1<sup>†</sup>).

To put the catalytic activity of MIL-101(Cr/Fe) (4:1) into context, MIL-100(Fe) with all the metal nodes constituted by iron was used as reference. MIL-100(Fe) exhibited only slightly lower activity than MIL-101(Cr/Fe) (4:1) (Fig. 4 and Table S1<sup>†</sup>), whose Fe<sup>3+</sup> content is about 5 times lower. Thus, it seems that the Fe<sup>3+</sup> sites of MIL-101(Cr/Fe) (4:1) are intrinsically more active than the ones of MIL-100(Fe). The lower intrinsic activity of Fe<sup>3+</sup> in MIL-100(Fe) can be understood considering the smaller dimensions of windows (0.55 and 0.86 nm) and cavities (2.4 and 2.9 nm) in MIL-100 respect to the MIL-101 structure imposing diffusion limitations to the reaction. The higher activity of MIL-101(Cr/Fe) (4:1) respect to MIL-101(Cr) can also be understood considering the benefits of combining the highly porous and stable MIL-101(Cr) structure, with a large percentage of Fe<sup>3+</sup> ions with higher intrinsic catalytic activity than Cr<sup>3+</sup>. In this way, even though the amount Fe<sup>3+</sup> in the catalyst is only 21 wt %, the activity of Fe<sup>3+</sup> ions in this MIL-101 structure is similar or higher than when homometallic MIL-100(Fe) or MIL-88(Fe) are used as catalyst, due to a more impeded accessibility to the Fe<sup>3+</sup> sites.

In agreement with the above proposal to rationalize the activity of mixed Cr/Fe MOF, the benefits of MIL-101(Cr/Fe) (4:1) respect to the MIL-100(Fe) as solid catalyst to promote the Prins reaction of  $\beta$ -pinene are even more clearly evidenced when a bulkier aldehyde such as benzaldehyde is used as substrate. In this case, the use of argon atmosphere during the reaction allowed to achieve a selective addition of  $\beta$ -pinene and benzaldehyde without formation of oxid. Fig. 5 shows a comparison of the time-conversion plot under the same conditions for the Prins reaction with benzaldehyde as reagent using MIL-101(Cr/Fe) (4:1) or MIL-100(Fe) as catalyst. As it can be seen the activity of MIL-101(Cr/Fe) (4:1) is higher than that of MIL-100(Fe) in spite of the 5-fold higher Fe<sup>3+</sup> content of the latter.

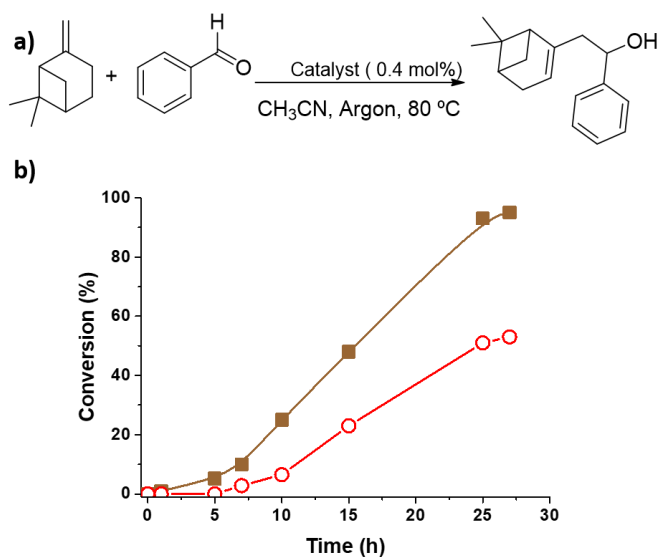


**Fig. 5** a) Prins addition of  $\beta$ -pinene and benzaldehyde. b) Temporal conversion plot of  $\beta$ -pinene using MIL-101(Cr/Fe) (4:1) (■) or MIL-100(Fe) (○) as catalyst. Reaction conditions: Catalyst (0.02 mmol of Cr+Fe),  $\beta$ -pinene (800  $\mu$ L, 5 mmol), benzaldehyde (5 mmol), acetonitrile (1.26 mL), 80  $^{\circ}$ C.

To determine the influence of the  $\text{Fe}^{3+}$  content present in the mixed-metal MIL-101(Cr/Fe) solid on the catalytic activity for the Prins reaction, three MIL-101(Cr/Fe) containing different  $\text{Fe}^{3+}$  contents with values 2.5, 14 and 21 wt% (ratio Cr/Fe 36:1, 5.9:1, 4:1, respectively) were tested. Fig. 6 presents the time-conversion plots for the Prins reaction promoted by these three mixed-metals MIL-101(Cr/Fe) solids. By plotting the initial reaction rate vs. the Fe content it was observed that, although  $\text{Cr}^{3+}$  also catalyzes the reaction as it can be deduced from the initial reaction rate value at 0  $\text{Fe}^{3+}$  content, the initial reaction rate increases with the  $\text{Fe}^{3+}$  content. This increase in the initial reaction rate means that  $\text{Fe}^{3+}$  is more active than  $\text{Cr}^{3+}$  to promote the reaction. Furthermore, an increase of TOF value at higher  $\text{Fe}^{3+}$  loadings was observed. In principle, the TOF value should be constant if all the  $\text{Fe}^{3+}$  sites were equally active. Therefore, the TOF increase along the  $\text{Fe}^{3+}$  percentage suggests some degree of cooperation among the  $\text{Fe}^{3+}$  sites. Furthermore, the higher the iron content in the mixed-metal MIL-101(Cr/Fe) solid the higher the activity accompanied also by increased formation of the by-products 10-pinen-3-ol (Fig. 7b and Table S1†).

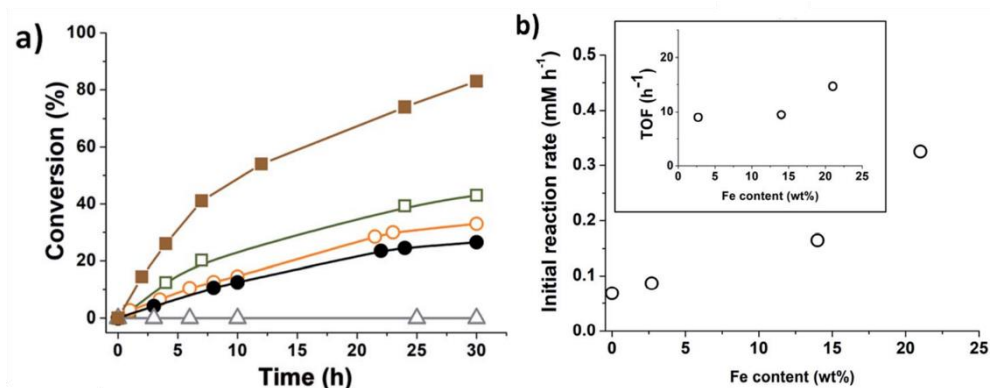


**Fig 6** (a) Time-conversion plot for the Prins reaction between  $\beta$ -pinene and formaldehyde in the presence of MIL-101(Cr/Fe) (4:1) (■), MIL-101(Cr/Fe) (5.9:1) (□), MIL-101(Cr/Fe) (36:1)

(○), MIL-101(Cr) (●) and in the absence of catalyst (Δ). (b) Influence of the iron MIL-101 iron content on the initial reaction. The inset shows the influence of the iron content on the TOF; note that the activity of the MIL-101(Cr) has been subtracted to calculate the TON of mixed-metal MIL-101(Cr/Fe) solids. Reaction conditions: Catalyst (0.02 mmol of Fe+Cr),  $\beta$ -pinene (800  $\mu$ L, 5 mmol), formaldehyde (750  $\mu$ L, 5 mmol), acetonitrile (1.26 mL), 80 °C.

The catalytic activity of mixed-metal MIL-101(Cr/Fe) (4:1) was finally compared with that of homogeneous  $\text{Cr}^{3+}$  acetate and heterogeneous  $\text{Cr}_2\text{O}_3$  or  $\text{Fe}_2\text{O}_3$  solids (Fig. 7). MIL-101(Cr/Fe) (4:1) exhibits the highest initial reaction rate in the series followed by the soluble  $\text{Cr}^{3+}$  salt. This observation is in agreement with previous results showing the benefits of metal ion isolation by immobilization in highly accessible metal clusters of porous MOFs acting as single-site catalysts.<sup>37</sup> On one hand, they exhibit similar or higher intrinsic activity to that of the homogeneous sites catalysts, and on the other, they undergo much slower deactivation by aggregation due to site immobilization.

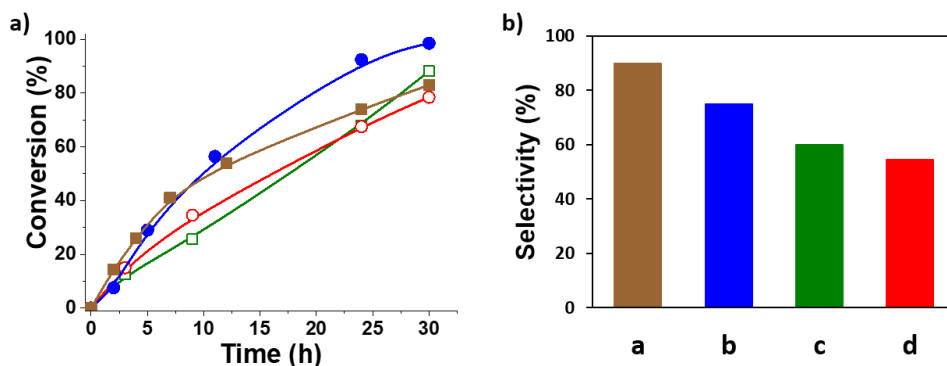


**Fig. 7** (a): Time-conversion plots of  $\beta$ -pinene using MIL-101(Fe/Cr) (4:1) (■),  $\text{Cr}^{3+}$  acetate hydroxyde (●),  $\text{Fe}_2\text{O}_3$  (□) or  $\text{Cr}_2\text{O}_3$  (○) as catalysts and (b): Nopol selectivity for  $\text{Cr}^{3+}$  acetate hydroxyde (a), MIL-101(Fe/Cr) (4:1) (b),  $\text{Fe}_2\text{O}_3$  (c) or  $\text{Cr}_2\text{O}_3$  (d) as catalysts. Reaction conditions: Catalyst (0.02 mmol metal),  $\beta$ -pinene (800  $\mu$ L, 5 mmol), formaldehyde (750  $\mu$ L, 5 mmol),  $\text{CH}_3\text{CN}$  (1.15 mL), 80 °C.

As mentioned above and shown in Scheme 1, besides Nopol the formation of 10-pinen-3-ol was also observed in the presence of MIL-101. Selectivity values are presented in Fig. 7b. As described in previous reports, 10-pinen-3-ol arises from the allylic oxidation of  $\beta$ -pinene by molecular oxygen.<sup>38, 39</sup> There are in the literature several studies showing that, besides as solid Lewis acid, MIL-101 can act also as oxidation catalyst.<sup>14,40</sup> Under the present reaction conditions, the highest conversion and highest Nopol selectivity at final reaction time (30 h) was achieved using the homogeneous  $\text{Cr}^{3+}$  salt. Importantly, the use of the heterogeneous MIL-101(Cr/Fe) (4:1) catalyst results in a higher catalytic activity and higher Nopol selectivity respect to the metal oxides  $\gamma\text{-Fe}_2\text{O}_3$  or  $\alpha\text{-Cr}_2\text{O}_3$  (Fig. 7 and Table S1†).

In the case of the mixed-metal MIL101(Cr/Fe) (4:1), the heterogeneity of the reaction was supported by performing a hot filtration test, observing that the reaction almost completely stopped after filtration of the solid (Fig. 8a). The minor conversion from 26 to 30 % from 4 to 30 h in the absence of solid after filtration of the catalyst was due to the occurrence of  $\beta$ -pinene oxidation to 10-pinen-3-ol, but not to the  $\beta$ -pinene addition to formaldehyde.

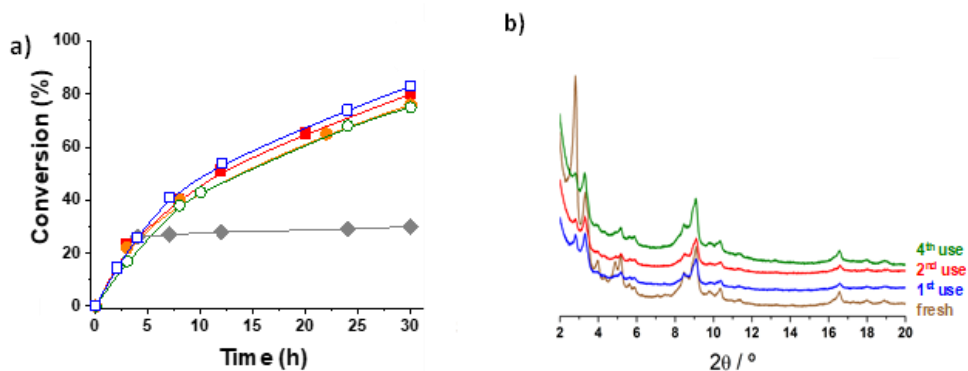


**Fig. 8** a) Hot filtration and reusability tests 1<sup>st</sup> use (□), 2<sup>nd</sup> use (■), 3<sup>th</sup> use (●), 4<sup>th</sup> use (○) and upon filtration of the catalyst at 2.5 h (◆). b) PXRD patterns for the fresh and used MIL-101(Cr/Fe) (4:1). Reaction conditions: Catalyst (0.02 mmol metal), β-pinene (800 μL, 5 mmol), formaldehyde (750 μL, 5 mmol), CH<sub>3</sub>CN (1.15 mL), 80 °C.

Catalyst stability was finally studied by performing four consecutive runs using the same MIL-101(Cr/Fe) (4:1) sample. Comparison of the temporal profiles of first and consecutive reactions showed only a slight decrease of the catalytic activity, while maintaining the same product selectivity of about 75% (Fig. 8a). This partial deactivation is not due to degradation of the MIL-101(Cr/Fe) (4:1) catalyst, since little changes were observed in PXRD patterns recorded after each run compared to the fresh material (Fig. 8b). A loss of intensity of the first Bragg reflections was observed, likely due to remaining reactants in the pores. Analysis by ICP-OES of the chromium and iron content in the liquid reaction phase after filtration of the solid catalyst showed that the concentration of these metals in the liquid phase corresponds to about 0.002 and 0.02 wt% of the initial chromium and iron content of the fresh catalyst, respectively, in agreement with the absence of degradation of the MIL-101(Cr/Fe). A minor catalyst deactivation was observed upon consecutive reuse which might be attributed to adsorption of reaction products or by-products within the

pores. It is important to note that all molecules involved in the catalytic process have molecular dimensions smaller than 1 nm and are suitable for entering the pores of the catalysts through the windows (Fig. SI-10<sup>†</sup>). However, despite the favoured molecule diffusion, a partial blocking of the pores and/or active sites may not be excluded, which may cause an apparent decrease on the performance of the material. To corroborate the possibility of products or by-products adsorption in consecutive cycles, N<sub>2</sub> physisorption measurements were conducted for the used and washed MIL-101(Cr/Fe) material. It was observed that used and washed catalysts exhibit a slightly lower surface area as compared to the fresh catalyst, whereas a drastic loss of sorption capacity was observed when the catalyst was not washed, pointing to the presence of physisorbed molecules filling the pores (Fig. SI-11 in ESI<sup>†</sup>).

### 3.3.3 Characterization of acid sites

In order to get some insight on the higher catalytic activity of the mixed-metal MIL-101(Cr/Fe) respect to MIL-101(Cr), an *in situ* infrared spectroscopy study was undertaken to investigate the Lewis acid sites on those solids.<sup>41</sup> Following previous works using MIL-100(Fe)<sup>42,43</sup> or MIL-100(Cr)<sup>44</sup> materials, the MIL-101 samples under study were activated at 150 °C under vacuum for 3 h to remove the water molecules coordinated to the metal centers. Then, the acid strength of the resulting coordinatively unsaturated sites (CUS) of the MIL-101 solids was studied using CD<sub>3</sub>CN and CO as probe molecules.

In the case of CD<sub>3</sub>CN adsorption on activated MIL-101(Cr/Fe) (4:1), the characteristic  $\nu(\text{CN})$  and  $\nu(\text{CD}_3)$  bands due to the presence of CD<sub>3</sub>CN on both



the CUS or physisorbed in the solid were recorded (Fig. 9). The broad  $\nu(\text{CN})$  band with the maximum appearing at  $2320\text{ cm}^{-1}$  can be assigned to the coordinated deuterated acetonitrile on the  $\text{Cr}^{3+}$  and/or  $\text{Fe}^{3+}$  Lewis sites present in the MIL-101(Cr/Fe) (4:1) solid. This  $\nu(\text{CN})$  wavenumber is slightly lower than that found for MIL-100(Al) ( $2321\text{ cm}^{-1}$ ), a fact that agrees with the polarizing power of  $\text{Al}^{3+} > \text{Fe}^{3+} > \text{Cr}^{3+}$ .<sup>45</sup> In the case of MIL-101(Cr/Fe) (4:1) solid an additional  $\nu(\text{CN})$  band at higher wavenumber ( $2350\text{ cm}^{-1}$ ) appeared and could be assigned to adsorption of  $\text{CD}_3\text{CN}$  on metal defects with a higher Lewis acidity as it has been proposed in the case of the MIL-100(Al) ( $\nu(\text{CN})\ 2341\text{ cm}^{-1}$ ).<sup>45</sup> Physisorbed acetonitrile is characterized by the  $\nu(\text{CN})$  band appearing at lower wavenumbers ( $2274\text{--}2261\text{ cm}^{-1}$ ). The band corresponding to the  $\nu(\text{CD}_3)$  can be observed at  $2112\text{ cm}^{-1}$ . For comparison,  $\text{CD}_3\text{CN}$  adsorption on activated MIL-101(Cr) was also studied. The higher  $\nu(\text{CN})$  wavenumbers of MIL-101(Cr/Fe) (4:1) ( $2320$  and  $2350\text{ cm}^{-1}$ ) vs. MIL-101(Cr) ( $2318$  and  $2344\text{ cm}^{-1}$ ) is an indication of the stronger Lewis acidity of the former. Again, this observation agrees with the charge to radius ratio of the  $\text{Cr}^{3+}$  vs.  $\text{Fe}^{3+}$  and, then, with the expected higher polarizing power of  $\text{Fe}^{3+}$  vs.  $\text{Cr}^{3+}$  as Lewis center.<sup>45</sup> Once the  $\text{CD}_3\text{CN}$  equilibrium was reached for MIL-101(Cr/Fe), outgassing the samples led to a decrease of the area under the peak at  $2350\text{ cm}^{-1}$  in lesser extent than that of  $2320\text{ cm}^{-1}$ . This suggests that the higher the Lewis acid strength of the metal nodes, the higher the observed  $\nu(\text{CN})$  wavenumber and, therefore, the stronger the adsorption of the probe.

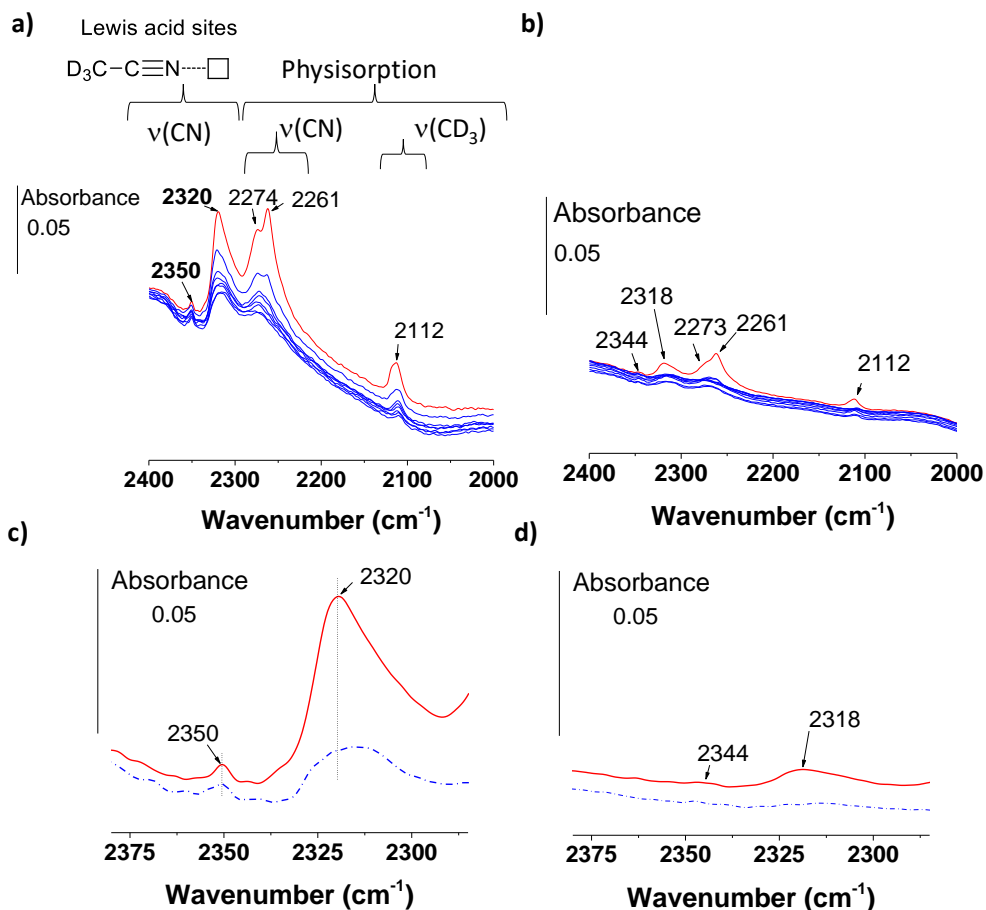


**Fig. 9** FT-IR spectra of  $CD_3CN$  adsorbed in MIL-101(Cr/Fe) (a, c) or MIL-101(Cr) (b, d). Red line spectra show the equilibrated  $CD_3CN$  adsorbed in MOFs; Blue line spectra show the retained  $CD_3CN$  after outgassing the corresponding MOF for 1 h period.

Importantly, for the same weight of MIL-101(Cr/Fe) and MIL-101(Cr) solids the  $CD_3CN$  adsorption measurements indicated a ten-fold increase of the area corresponding to the peaks at 2350 and 2320  $cm^{-1}$  in MIL-101(Cr/Fe) (4:1) compared to that of MIL-101(Cr). The higher  $\nu(CN)$  wavenumber value and the higher peak area in the case of MIL-101(Cr/Fe) respect to MIL-101(Cr), indicates the presence of higher density and stronger Lewis acidity of the metal nodes in MIL-101(Cr/Fe) respect to

MIL-101(Cr). These results are in sharp contrast with those previously reported for MIL-100(Cr) vs. MIL-100(Fe) that indicate a higher Lewis acid density for MIL-100(Cr).<sup>45</sup> This might be a consequence of the partial poisoning of the strongest Lewis sites in MIL-100(Fe) and/or the presence of structural defects in MIL-100(Cr). In any case, it seems that for the mixed metal Cr/Fe solid, the presence of the two metals is associated with a higher density of structural defects characterized by the  $2350\text{ cm}^{-1}$   $\nu(\text{CN})$  band and stronger CUS Lewis sites corresponding to the  $2320\text{ cm}^{-1}$   $\nu(\text{CN})$  band.

The acidity of the MIL-101(Cr/Fe) (4:1) material was further characterized by IR spectroscopy by using CO as probe molecule. Fig. SI-12† shows three main  $\nu(\text{CO})$  bands corresponding to CO coordinated with Lewis acid sites [ $\nu(\text{CO})$  at  $2195\text{ cm}^{-1}$ ], CO interacting with Brönsted acid sites [ $\nu(\text{CO})$  at  $2161\text{ cm}^{-1}$ ] and physisorbed species [ $\nu(\text{CO})$  at  $2136\text{ cm}^{-1}$ ]. In the case of MIL-101(Cr), similar CO bands were also observed although slightly shifted to lower wavenumber values for the Lewis and Brönsted acid sites respect to the mixed-metal MIL-101(Cr/Fe) (4:1). These observations are in agreement with the higher acidity of the MIL-101(Cr/Fe) (4:1) solid in respect to MIL-101(Cr) observed using  $\text{CD}_3\text{CN}$  as probe. Once the CO equilibrium was achieved in each MIL-101 sample, a vacuum treatment slightly decreased the peak intensity of the Lewis centers, while the signals of the weaker Brönsted acid sites as well as those of physisorbed CO species were almost completely vanished.

This IR spectroscopy study allowed us concluding that the higher catalytic activity observed for MIL-101(Cr/Fe) arises mainly from the increase of Lewis acidity due to the incorporation of Fe ions at the metal nodes. In agreement with this conclusion, when the Prins reaction was carried out

using the MIL-101(Cr/Fe) (4:1) solid adding pyridine as a base,<sup>46</sup> the resulting catalytic activity was drastically reduced (Fig. SI-13<sup>†</sup> in ESI<sup>†</sup>).

### **3.4 Conclusions**

The present study illustrates the advantages of combining the structural robustness and porosity, characteristic of MIL-101(Cr) material with the presence of Fe<sup>3+</sup> as active Lewis sites. Overall, the present study exemplifies the potential that mixed-metal MOF offer in catalysis, particularly when preparation methods make possible to prepare crystalline materials with a wide range of metal proportions as it is the case of the present MIL-101(Cr/Fe) materials.

### **3.5 Experimental section**

#### **3.5.1 Materials**

All the reagents and solvents employed in this work were of analytical or HPLC grade and supplied by Sigma-Aldrich.

#### **3.5.2 Catalyst preparation**

MIL-101(Cr),<sup>10,12</sup> MIL-101(Fe)<sup>14</sup> and MIL-88B(Fe)<sup>47</sup> have been prepared as previously reported. MIL-101(Cr/Fe) materials were prepared by mixing 1.5 mmol terephthalic acid, 1 mmol metal source (Cr and Fe) and 10 mL tetramethylammonium hydroxide (TMAOH) solution (0.06 M) in a Teflon reactor. More precisely, 0.75 mmol Cr(NO<sub>3</sub>)<sub>3</sub>·9H<sub>2</sub>O and 0.25 mmol of Fe<sup>0</sup> were used for MIL-101(Cr/Fe) (4:1) and 0.85 mmol Cr(NO<sub>3</sub>)<sub>3</sub>·9H<sub>2</sub>O and 0.15 mmol of Fe<sup>0</sup> for MIL-101(Cr/Fe) (5.9:1). The reaction mixtures were heated at 150 °C for 48 h under autogenous pressure. The obtained solids were

isolated by centrifugation (20 min, 14500 rpm) and washed three times with water and three times with abs. EtOH. Density separation was performed to remove any iron oxide impurities from the MOFs. In order to remove the residual ligand molecules from the pores, the solids were treated with a solution of KF (0.1 M) for 1 h. The purified products were dried at 100 °C overnight, prior to their characterization.

### 3.5.3 Characterization

Powder X-ray diffraction patterns were obtained on a Siemens D5000 diffractometer using Cu K $\alpha$  1,2 radiation ( $\lambda=1.5406\text{\AA}$ ).

N<sub>2</sub> sorption measurements were performed at 77 K on a BELL Japan Belsorp Max apparatus, after an overnight activation of the samples at 150 °C, under primary vacuum.

<sup>57</sup>Fe-Mössbauer spectra were recorded at 300 and 77 K using a <sup>57</sup>Co/Rh  $\gamma$ -ray source moving with a triangular velocity form and mounted on a conventional electromagnetic drive. The hyperfine structure was modeled by a least-square fitting procedure involving quadrupolar doublets composed of Lorentzian lines. The isomer shift values (IS) are referred to  $\alpha$ -Fe at 300 K, while the samples consist of a thin layer of powder containing about 15 mg of Fe.

The metal content (Cr or Fe) of the MOF samples was determined by using inductively coupled plasma optical emission spectroscopy (ICP-OES, Perkin-Elmer). Previously to ICP-OES analysis, the solid samples (10 mg) were digested using concentrated HNO<sub>3</sub> (65 wt%; 20 mL) at 80 °C for 24 h.

The resulting solution was diluted with Milli-Q water and, then, analyzed by ICP-OES.

FTIR spectroscopy was performed by compression the solid samples at 2 ton  $\text{cm}^{-2}$  in air prior to recording the spectra. In some cases the sample was mixed with  $\text{SiO}_2$  as binder. Then, the samples were placed in a quartz cell equipped with KR5-5 (thallium bromoiodide) windows. The cell was connected to a vacuum line for activation ( $P_{\text{residual}} = 10^{-5}$  mbar for 2 h) prior to CO or  $\text{CD}_3\text{CN}$  adsorption. For the CO adsorption experiments, the temperature of the pellet was decreased to about  $-170$  °C by cooling the sample holder with liquid  $\text{N}_2$ .  $\text{CD}_3\text{CN}$  adsorption experiments have been carried out at room temperature. The addition of CO in the cell was from 0 to 2.56 mbar, approximately.  $\text{CD}_3\text{CN}$  adsorption was performed at 0.26 or 0.82/0.35 mbar for MIL-101(Cr/Fe) or MIL-101(Cr), respectively. Transmission IR spectra were recorded in the  $4000\text{-}400$   $\text{cm}^{-1}$  range, at  $4$   $\text{cm}^{-1}$  resolution, on a VERTEX 70 spectrophotometer equipped with DTGS (Deuterated triglycine sulfate detector).

### 3.5.4 Catalytic reaction

**Prins reaction.** Prior to its use as catalyst, the corresponding amount of the solid (typically 0.02 mmol of Cr + Fe metal) was dried in a two-necked round bottom flask (25 mL) at  $100$  °C for 12 h. Then, the system was heated at  $150$  °C under vacuum for 16 h. Subsequently, the system was cool down to  $80$  °C and the reagents added to the system under continuous magnetic stirring in the following order: acetonitrile (1.26 mL), formaldehyde (750  $\mu\text{L}$ , 5 mmol) and  $\beta$ -pinene (800  $\mu\text{L}$ , 5 mmol).

Selective quenching experiments were carried out as described above, but adding pyridine at 20 mol % respect to the substrate.

Reuse experiments were carried out under the general reaction conditions. At the end of each run, the catalyst was recovered by filtration through a Nylon membrane (0.2  $\mu\text{m}$ ). The retained solid was washed by flushing hot acetonitrile (50  $^{\circ}\text{C}$ , 400 mL) and, then, ethanol (20  $^{\circ}\text{C}$ , 600 mL). The resulting solid was dried in an oven at 100  $^{\circ}\text{C}$  for at least 12 h before being employed in a subsequent catalytic cycle.

The progress of the reaction was followed by gas chromatography (GC) using a flame ionization detector (FID). During the reaction several aliquots (100  $\mu\text{L}$ ) were sampled, then diluted with acetonitrile (0.5 mL) and filtered using syringe filters (0.2  $\mu\text{m}$  Nylon). Nitrobenzene was finally added as external standard (10  $\mu\text{L}$ ) to each reaction aliquot. Quantification was carried out using a calibration plot for each commercially available compound. The samples were analyzed immediately after being taken from the reaction mixture.

### **3.6 Acknowledgments**

Financial support by the Spanish Ministry of Economy and Competitiveness (Severo Ochoa, CTQ2018-890237-CO2-R1 and Maria de Maeztu, CEX2019-000919-M), is gratefully acknowledged. Generalidad Valenciana is also thanked for funding (Prometeo 2017/083). S.N. thanks financial support by the Ministerio de Ciencia, Innovación y Universidades (RTI 2018-099482-A-100 project), Fundación Ramón Areces (XVIII Concurso Nacional para la Adjudicación de Ayudas a la Investigación en Ciencias de la

Vida y de la Materia, 2016), and Generalitat Valenciana grupos de investigación consolidables 2019 (ref: AICO/2019/214) Project. E. G. thanks the ANR-11-LABEX-0039 (LabEx CHARM3AT) for financial support. M.G.-M thanks support from “la Caixa” Foundation (LCF/BQ/PI19/11690022) and Generalitat Valenciana (SEJI/2020/036).



### 3.7 References

1. H. Chughtai, N. Ahmad, H. A. Younus, A. Laypkov and F. Verpoort, *Chem. Soc. Rev.*, 2015, **44**, 6804-6849.
2. Corma, H. Garcia and F. X. Llabrés i Xamena, *Chem. Rev.*, 2010, **110**, 4606-4655.
3. H. Furukawa, Cordova, K.E., O'Keeffe, M., Yaghi, O.M., *Science*, 2013, **341**, 1230444.
4. J. Gascon, A. Corma, F. Kapteijn and F. X. Llabrés i Xamena, *ACS Catal.*, 2014, **4**, 361-378.
5. M. Yoon, R. Srirambalaji and K. Kim, *Chem. Rev.*, 2012, **112**, 1196-1231.
6. A. Dhakshinamoorthy, Opanasenko, M., Čejka, J., Garcia, H., *Catal. Sci. Technol.*, 2013, **3**, 2509-2540.
7. Z. Hu and D. Zhao, *CrystEngComm*, 2017, **19**, 4066-4081.
8. M. Opanasenko, A. Dhakshinamoorthy, Y. K. Hwang, J.-S. Chang, H. Garcia and J. Cejka, *ChemSusChem* 2013, **6**, 865 - 871.
9. G. Férey, C. Mellot-Draznieks, C. Serre, F. Millange, J. Dutour, S. Surble and I. Margiolaki, *Science*, 2005, **309**, 2040-2042.
10. A. Santiago-Portillo, S. Navalón, P. Concepción, M. Álvaro and H. García, *ChemCatChem*, 2017, **9**, 2506-2511
11. A. Dhakshinamoorthy, M. Alvaro and H. Garcia, *Catal. Sci. Technol.*, 2011, **1**, 856-867.
12. A. Santiago-Portillo, J. F. Blandez, S. Navalón, M. Álvaro and H. García, *Catal. Sci. Technol.*, 2017, **7**, 1351-1362.
13. A. Dhakshinamoorthy, A. M. Asiri and H. Garcia, *Chem. Eur. J.*, 2016, **22**, 8012-8024.
14. A. Santiago-Portillo, S. Navalon, F. Cirujano, F. Llabrés i Xamena, M. Alvaro and H. Garcia, *ACS Catal.*, 2015, **5**, 3216–3224.
15. P. L. Llewellyn, S. Bourrelly, C. Serre, A. Vimont, M. Daturi, L. Hamon, G. D. Weireld, J.-S. Chang, D.-Y. Hong, Y. K. Hwang, S. H. Jung and G. Férey, *Langmuir*, 2008, **24**, 7245-7250.
16. D.-Y. Y. K. H. Hong, Serre, C. Férey, G. Chang, J.-S., *Adv. Funct. Mater.*, 2009, **19**, 1537-1552.
17. P. C. Horcajada, H. Heurtaux, D. Benyettou, F. Salles, F. Devic, T. Garcia-Marquez, A. Yu, C. Lavrard, H. Dutson, C.L. Magnier, E. Maurin, G. Elkaïm, E. Serre, C., *Chem. Commun.*, 2014, **50**, 6872-6874.
18. A. Vimont, J.-M. Goupil, J.-C. Lavalley, M. Daturi, S. Surblé, C. Serre, F. Millange, G. Férey and N. Audebrand, *J. Am. Chem. Soc.*, 2006, **128**, 3218-3227.
19. J. H. Wang, Y. Zhang, M. Li, S. Yan, D. Li and X. M. Zhang, *Angew. Chem. Int. Ed.*, 2016, **56**, 6478-6482.
20. S. Abednatanzi, P. G. Derakhshandeh, H. Depau, F.-X. Coudert, P. Van Der Voort and K. Leus, *Chem. Soc. Rev.*, 2019, **48**, 2535-2565.
21. M. Giménez-Marqués, A. Santiago-Portillo, S. Navalón, M. Álvaro, V. Briois, F. Nouar, H. Garcia and C. Serre, *J. Mater. Chem. A.*, 2019, **7**, 20285-20292.

22. M. Y. Masoomi, A. Morsali, A. Dhakshinamoorthy and H. Garcia, *Angew. Chem. Int. Ed.*, 2019, **58**, 15188-15205.
23. F. Nouar, T. Devic, H. Chevreau, N. Guillou, E. Gibson, G. Clet, M. Daturi, A. Vimont, J. M. Grenèche, M. I. Breeze, R. I. Walton, P. L. Llewellyne and C. Serre, *Chem. Commun.*, 2012, **48**, 10237-10239
24. T. A. Vu, G. H. Le, C. D. Dao, L. Q. Dang, K. T. Nguyen, P. T. Dang, H. T. K. Tran, Q. T. Duong, T. V. Nguyen and G. D. Lee, *RSC Adv*, 2014, **4**, 41185-41194.
25. T. Tanasaro, K. Adpakpang, S. Ittisanronnachai, K. Faungnawakij, T. Butburee, S. Wannapaiboon, M. Ogawa and S. Bureekaew, *Cryst. Growth Des.*, 2018, **18**, 16–21.
26. S. Surlblé, C. Serre, C. Mellot-Draznieks, F. Millange and G. Férey, *Chem. Commun.*, 2006, 284-286.
27. C. Serre, F. Millange, C. Thouvenot, M. Noguès, G. Marsolier, D. Louër and G. Férey, *J. Am. Chem. Soc.*, 2002, **124**, 13519-13526.
28. E. Stavitski, M. Goesten, J. Juan-Alcaçiz, A. Martinez-Joaristi, P. Serra-Crespo, A. V. Petukhov, J. Gascon and F. Kapteijn, *Angew. Chem. Int. Ed.*, 2011, **50**, 9624 -9628.
29. C. Castillo-Blas, N. Snejko, V. A. de la Peña-O'Shea, J. Gallardo, E. Gutiérrez-Puebla, M. A. Monge and F. Gándara, *Dalton Trans.*, 2016, **45**, 4327-4337.
30. P. B. S. Rallapalli, M. C. Raj, S. Senthilkumar, R. S. Somani and H. C. Bajaja, *Environ. Prog. Sustain. Energy.*, 2016, **35**, 461-468.
31. M. H. Wickenheisser, A.; Tannert, R.; Milow, B.; Janiak, C., *Micropor. Mesopor. Mat.*, 2015, **215**, 143-153.
32. J. Z. Yang, Q.; Li, J.; Dong, J., *Micropor. Mesopor. Mat.*, 2010, **130**, 174-179.
33. B. G. Abeykoon, J.-M.; Jeanneau, E.; Chernyshov, D.; Goutaudier, C.; Demessence, A.; Devic, T.; and A. Fateeva, *Dalton Trans. T*, 2017, **46**, 517-523.
34. G. M. Férey, F.; Morcrette, M.; Serre, C.; Doublet, M.-L.; Grenèche, J.-M.; Tarascon, J.-M, *Angew. Chem. Int. Ed.*, 2007, **46**, 3259-3263.
35. P. S. Horcajada, S.; Serre, C.; Hong, D.-Y.; Seo, Y.-K.; Chang, J.-S.; Grenèche, J.-M.; Margiolaki, I.; and G. Férey, *Chem Commun* 2007, **27**, 2820-2822.
36. F. G. Delolo, K. C. B. Oliveira, E. N. dos Santos and G. E.V., *Mol. Catal.*, 2019, **462**, 1-9.
37. S. J. Rogge, A. Bavykina, J. Hajek, H. Garcia, A. I. Olivos-Suarez, A. Sepúlveda-Escribano, A. Vimont, G. Clet, P. Bazin, F. Kapteijn, M. Daturi, E. V. Ramos-Fernandez, F. X. Llabrés i Xamena, V. Van Speybroeck and J. Gascon, *Chem. Soc. Rev.*, 2017, **46**, 3134-3184.
38. I. Y. Skobelev, K. A. Kovalenko, V. P. Fedin, A. B. Sorokin and O. A. Kholdeeva, *Kinet. Catal.*, 2013, **54**, 607-614.
39. I. Y. Skobelev, A. B. Sorokin, K. A. Kovalenko, V. P. Fedin and O. A. Kholdeeva, *J. Catal.*, 2013, **298**, 61-69.
40. A. Gómez-Paricio, A. Santiago-Portillo, S. Navalón, P. Concepción, M. Alvaro and H. Garcia, *Green Chem.*, 2016, 508-515.
41. A. Vimont, F. Thibault-Starzyk and M. Datur, *Chem. Soc. Rev.*, 2010, **39**, 4928-4950.
42. A. Dhakshinamoorthy, M. Alvaro, P. Horcajada, E. Gibson, M. Vishnuvarthan, A. Vimont, J.-M. Grenèche, C. Serre, M. Daturi and H. Garcia, *ACS Catal.*, 2012, **2**, 2060-2065.

43. H. Leclerc, A. Vimont, J.-C. Lavalley, M. Daturi, A. D. Wiersum, P. L. Llwellyn, P. Horcajada, G. Férey and C. Serre, *Phys. Chem. Chem. Phys.*, 2011, **13**, 11748-11756.
44. J. W. Yoon, H. Chang, S.-J. Lee, Y. K. Hwang, D.-Y. Hong, S.-K. Lee, J. S. Lee, S. Jang, T.-U. Yoon, K. Kwac, Y. Jung, R. S. Pillai, F. Faucher, A. Vimont, M. Daturi, G. Férey, C. Serre, G. Maurin, Y.-S. Bae and J.-S. Chang, *Nat. Mater.*, 2017, **16**, 526-531.
45. C. Volkringer, H. Leclerc, J.-C. Lavalley, T. Loiseau, G. Férey, M. Daturi and A. Vimont, *J. Phys. Chem. C*, 2012, **116**, 5710–5719.
46. T. Barzetti, E. Selli, D. Moscotti and L. Forni, *J. Chem. Soc. Faraday Trans.*, 1996, **92**, 1401-1407
47. P. Horcajada, F. Salles, S. Wuttke, T. Devic, D. Heurtaux, G. Maurin, A. Vimont, M. Daturi, O. David, E. Magnier, N. Stock, Y. Filinchuk, D. Popov, C. Riekkel, G. Férey and C. Serre, *J. Am. Chem. Soc.*, 2011, **44**, 17839-17847.

### 3.8 Supplementary Material

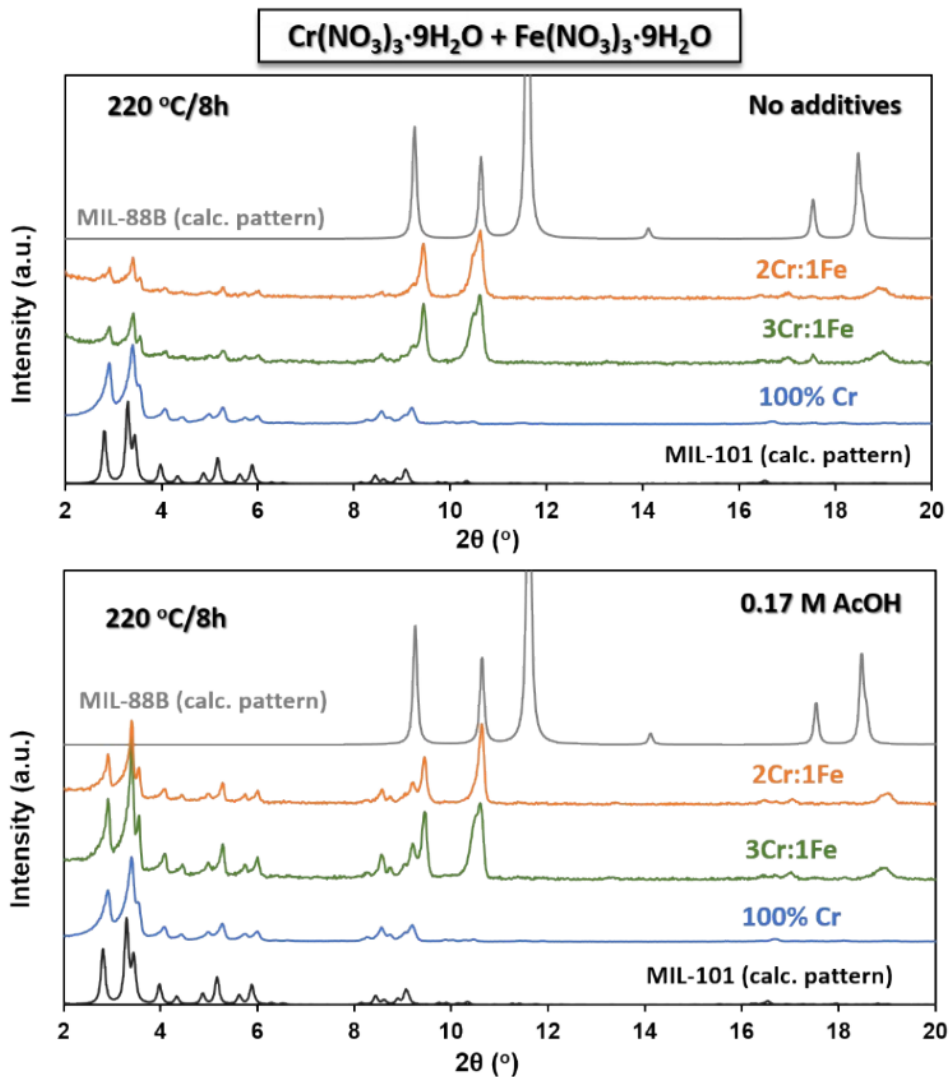


**Fig. SI-1** Normalized PXRD patterns ( $\lambda = 1.54 \text{ \AA}$ ) of the obtained products using different ratios of the metal sources  $\text{Cr}(\text{NO}_3)_3 \cdot 9\text{H}_2\text{O}$  and  $\text{Fe}(\text{NO}_3)_3 \cdot 9\text{H}_2\text{O}$ . Hydrothermal conditions: 220 °C for 8 h; without additives (top) and with 0.17 M AcOH (down).

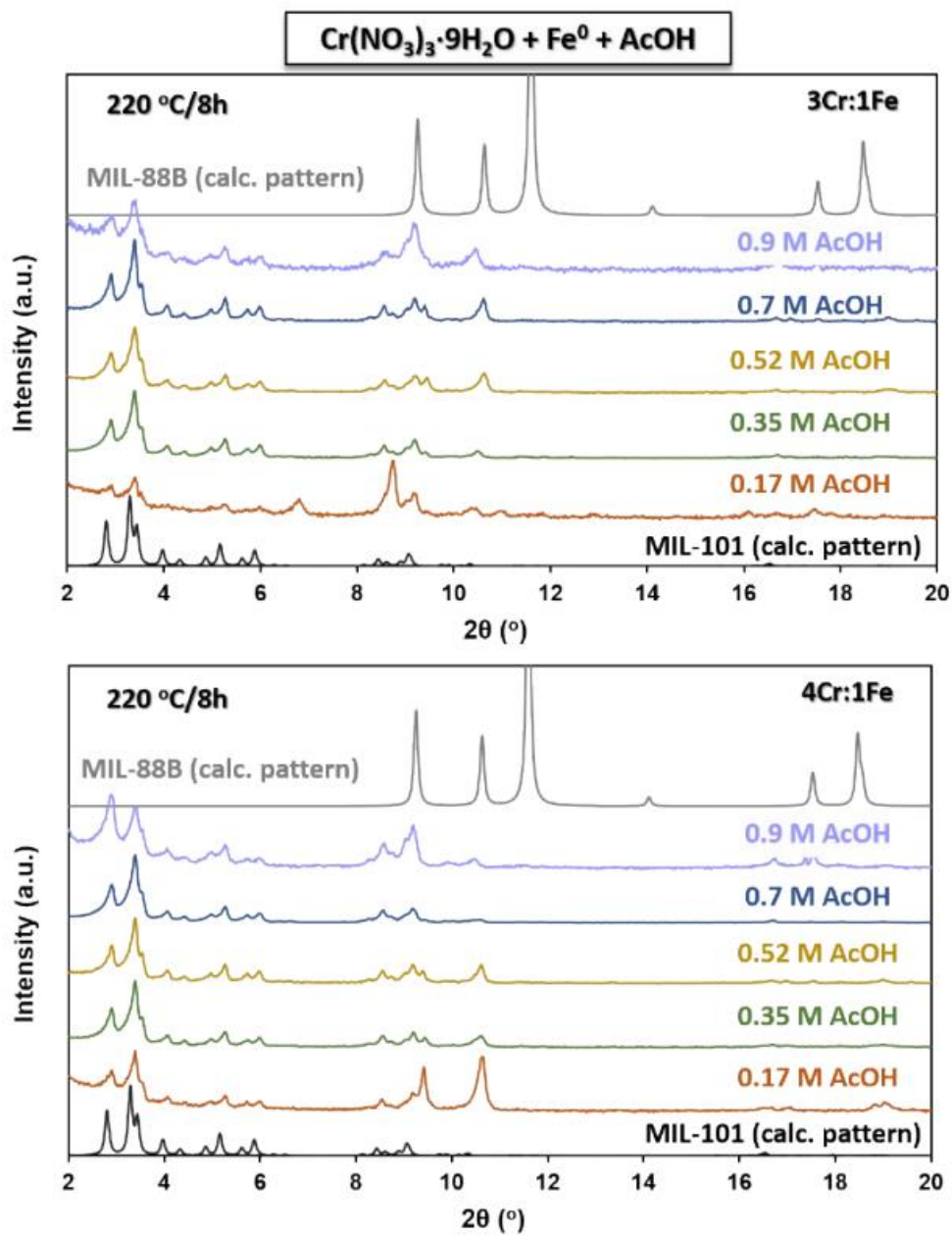


**Fig. SI-2** Normalized PXRD patterns ( $\lambda = 1.54 \text{ \AA}$ ) of the obtained products using as metal sources Cr(NO<sub>3</sub>)<sub>3</sub>·9H<sub>2</sub>O and Fe<sup>0</sup> with different concentrations of AcOH (0.17-0.9 M). Hydrothermal conditions: 220 °C for 8 h; metal ratio 3Cr:1Fe (top) and 4:Cr:Fe (down).

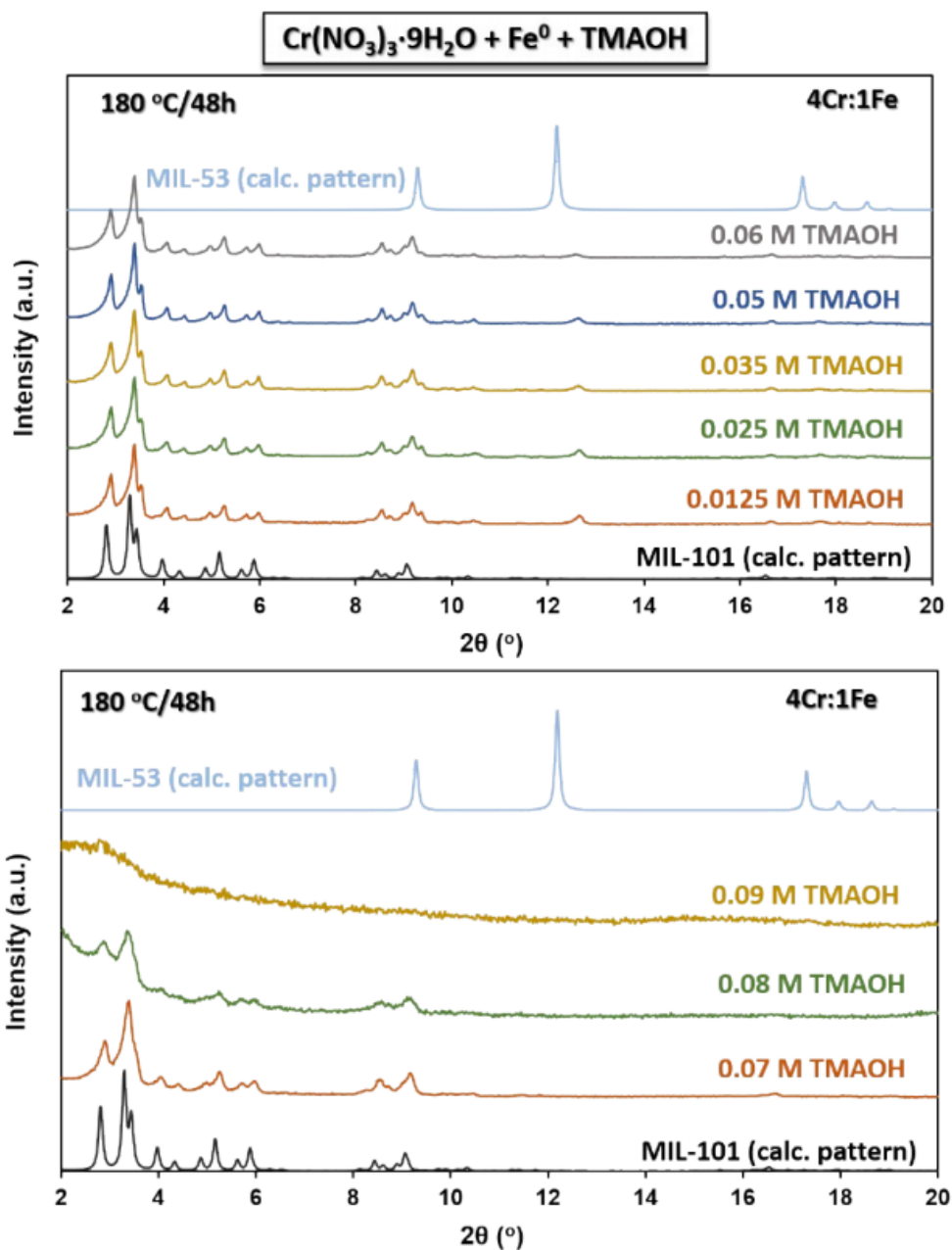


**Fig. SI-3** Normalized PXRD patterns ( $\lambda = 1.54 \text{ \AA}$ ) of the obtained products using as metal sources  $\text{Cr}(\text{NO}_3)_3 \cdot 9\text{H}_2\text{O}$  and  $\text{Fe}^0$ , with different concentrations of TMAOH and metal ratio 4Cr:Fe. Hydrothermal conditions: 180 °C for 48 h;  $[\text{TMAOH}] = 0.0125\text{-}0.06 \text{ M}$  (top) and  $0.07\text{-}0.09 \text{ M}$  (down).

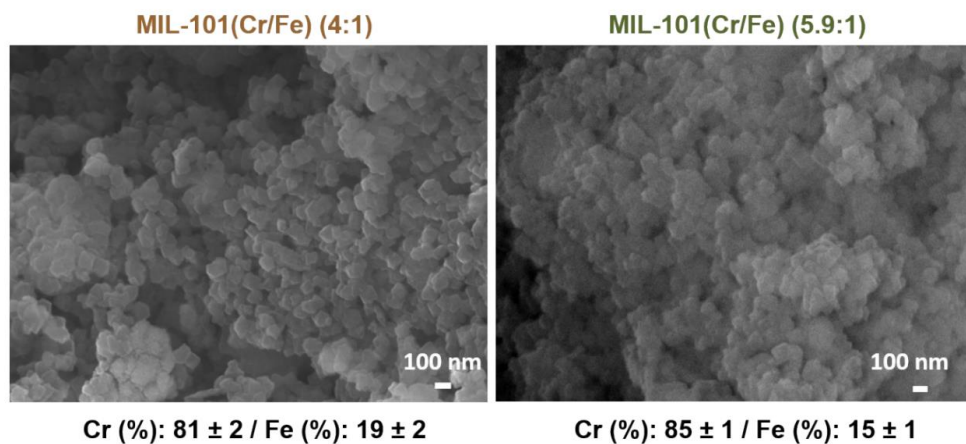
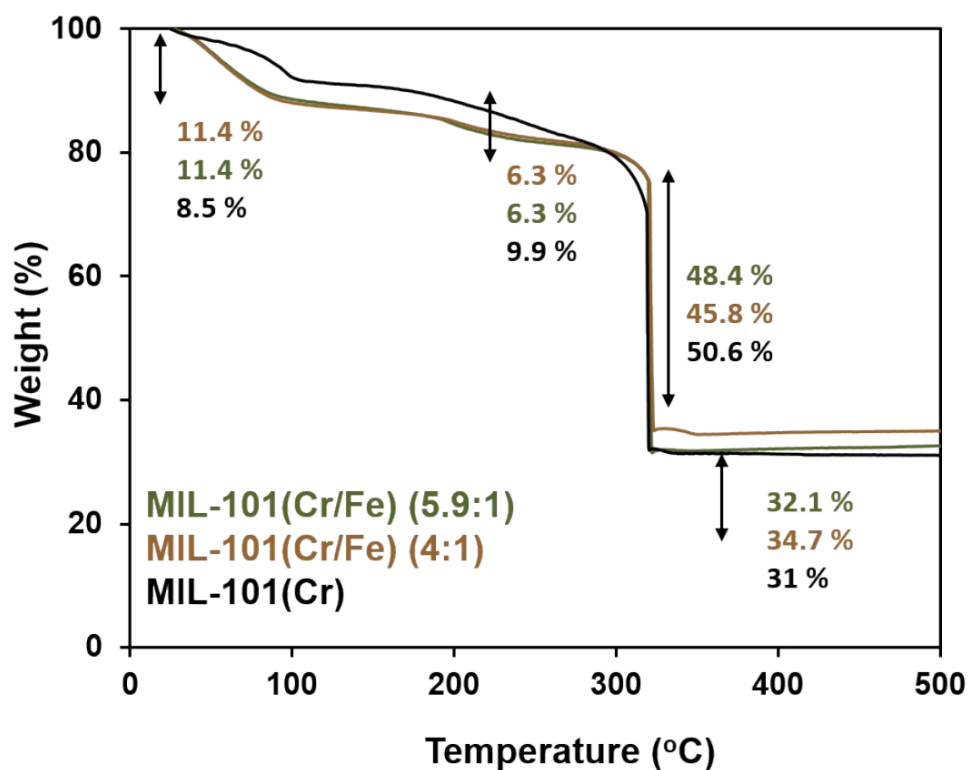


Fig. SI-4 SEM-EDX analysis of MIL-101(Cr/Fe) (4:1) and MIL-101(Cr/Fe) (5.9:1).

Fig. SI-5 TGA curves of MIL-101(Cr/Fe) (4:1), MIL-101(Cr/Fe) (5.9:1) and MIL-101(Cr), under O<sub>2</sub> flow.

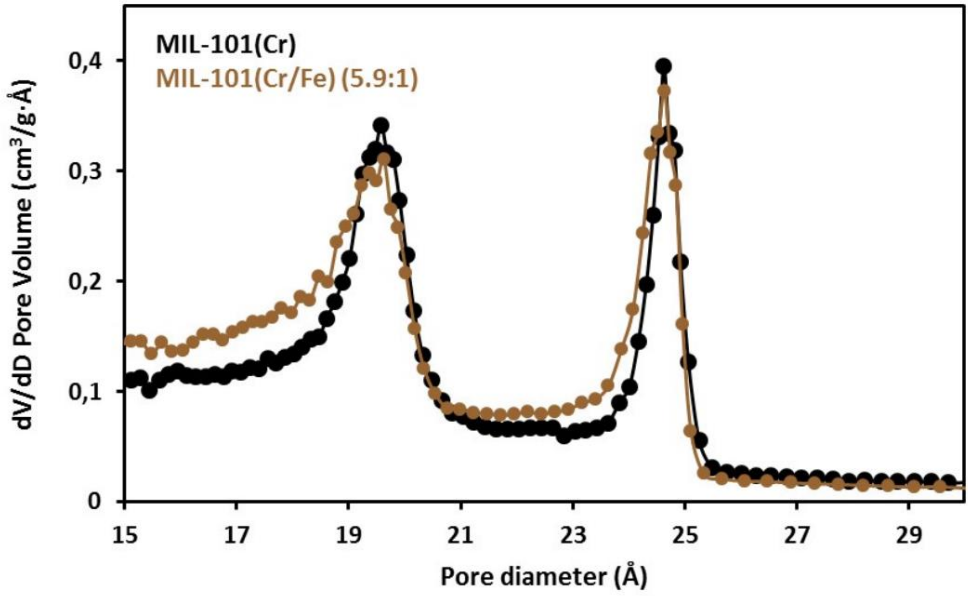
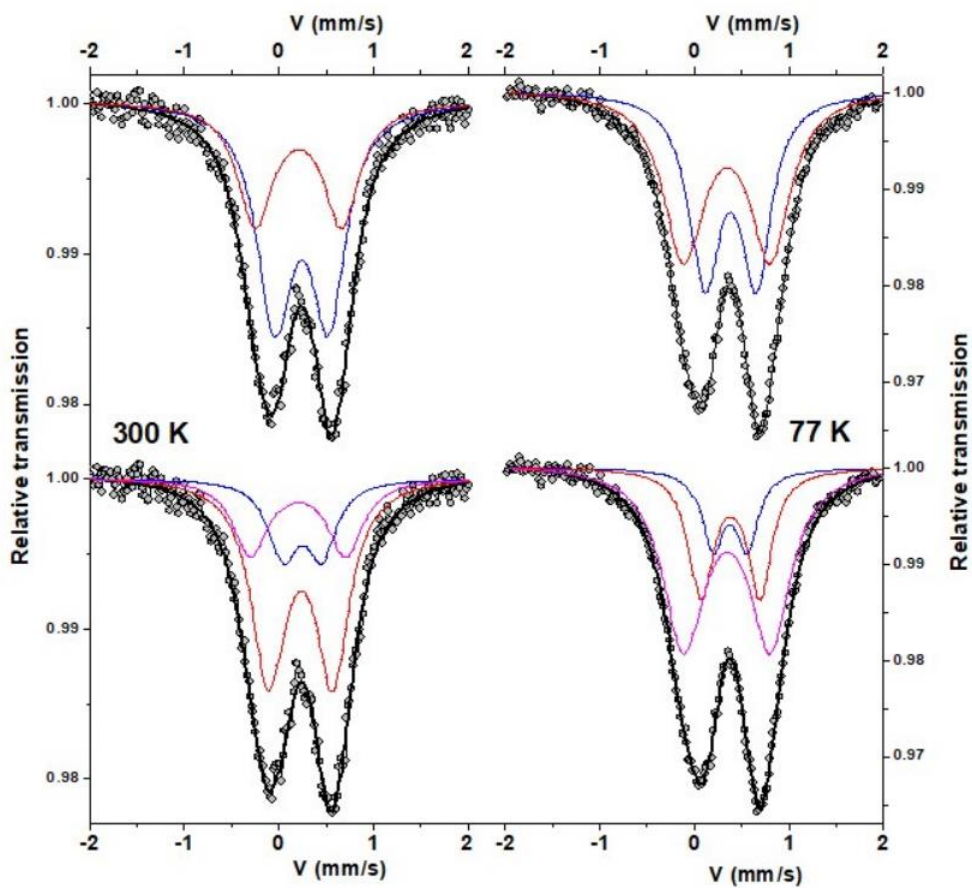
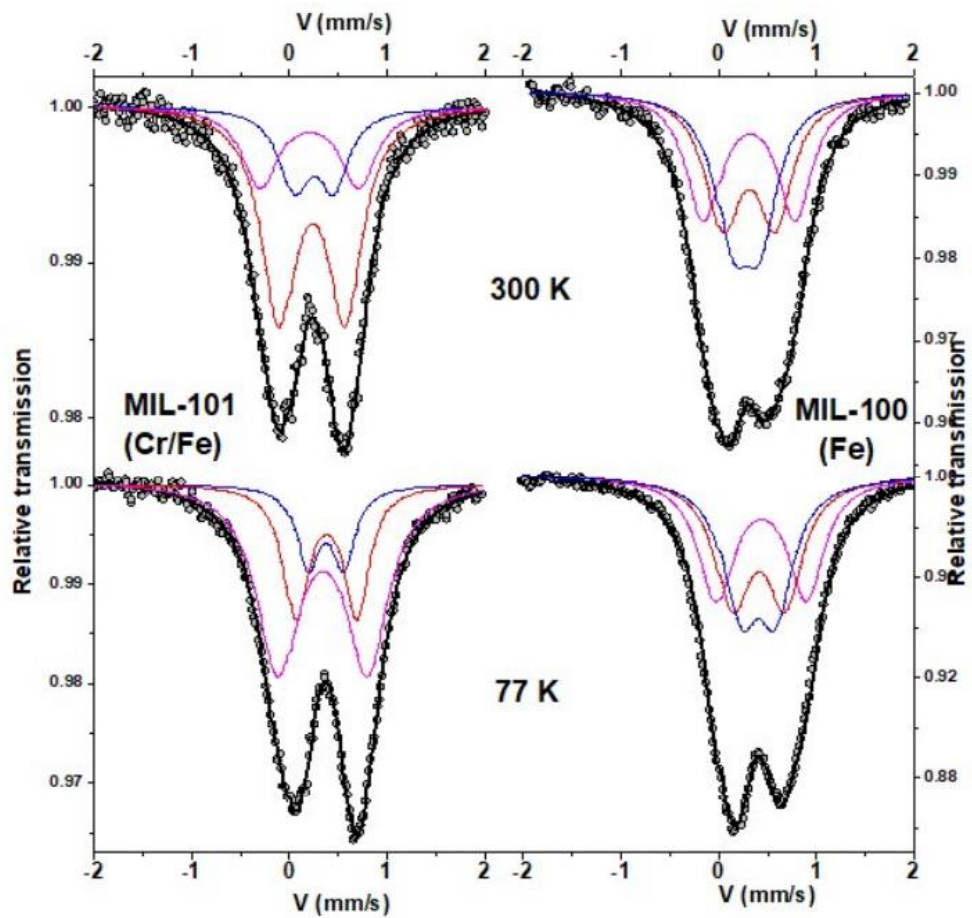


Fig. SI-6 BJH pore size distribution of MIL-101(Cr) and MIL-101(Cr/Fe) (5.9:1). Sample activation: 150 °C/16 h, under vacuum.





**Fig. SI-7** Mössbauer transmission spectra of MIL-101(Cr/Fe) (4:1), recorded at 300 K and 77 K with 2 fitting models.



**Fig. S1-8** Mössbauer transmission spectra of MIL-101(Cr/Fe) (4:1) and MIL-100(Fe), recorded at 300 K and 77 K.

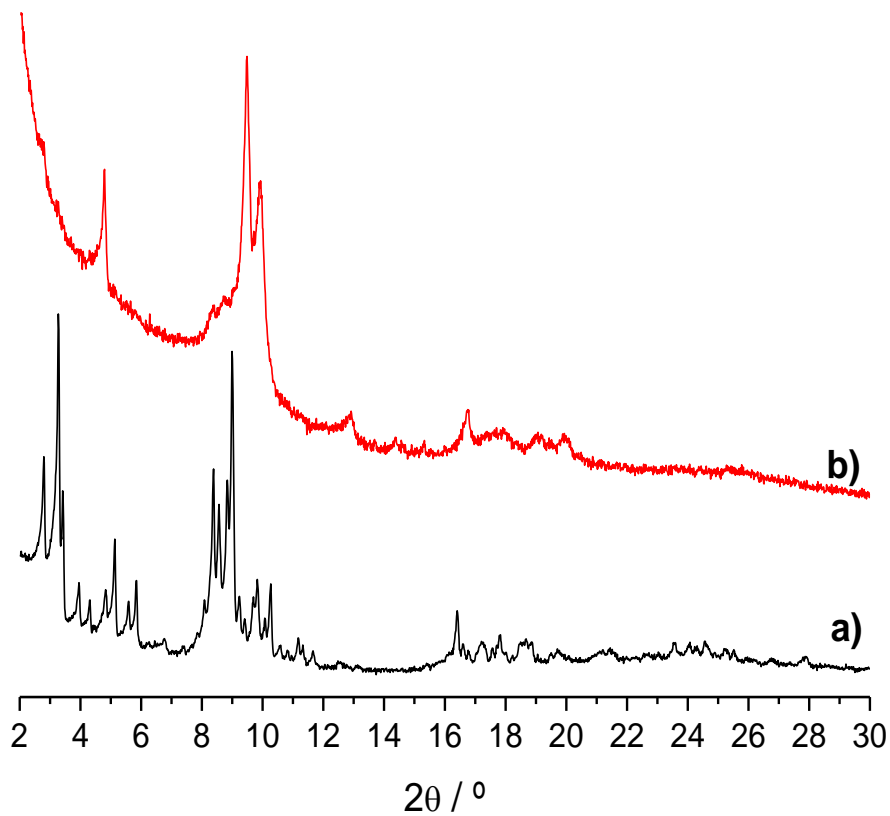


**Fig. SI-9** PXRD of fresh (a) and used in the Prins reaction (b) MIL-101(Fe). Reaction conditions: Catalyst (0.02 mmol metal),  $\beta$ -pinene (800  $\mu$ L, 5 mmol), formaldehyde (750  $\mu$ L, 5 mmol),  $\text{CH}_3\text{CN}$  (1.15 mL), reaction temperature (80  $^\circ\text{C}$ ).

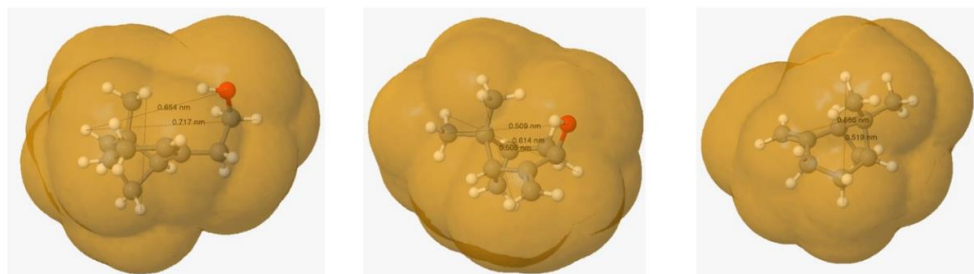


**Fig. SI-10** Representation of Nopol (lefts), 10-pinen-3-ol (middle) and  $\beta$ -pinene (right) molecules with selected largest atomic distances. The measured solvent accessible surface is represented in place orange and calculated as de Van der Waals distances + 1.4 Angstrom. Calculations performed using the molecular calculator software MolCalc.

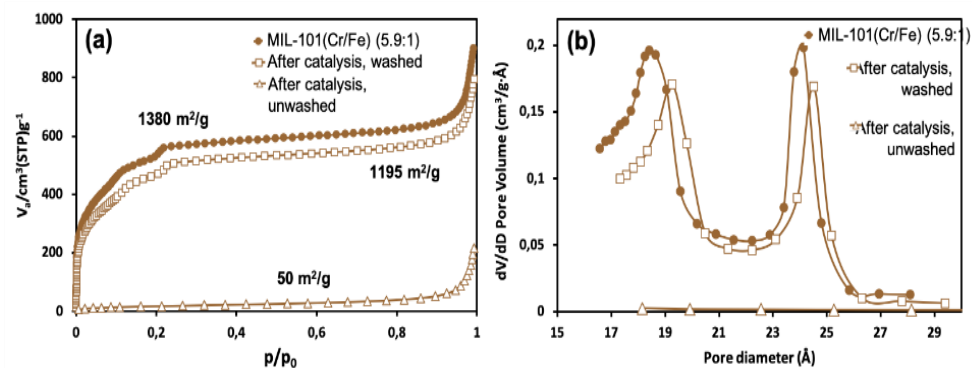


**Fig. SI-11** (a) Adsorption isotherms and (b) BJH pore size distribution of fresh MIL-101(Cr/Fe) (5.9:1) and after catalysis with ( $\square$ ) or without ( $\Delta$ ) washing. Sample activation: 80 °C/1 h, under vacuum.

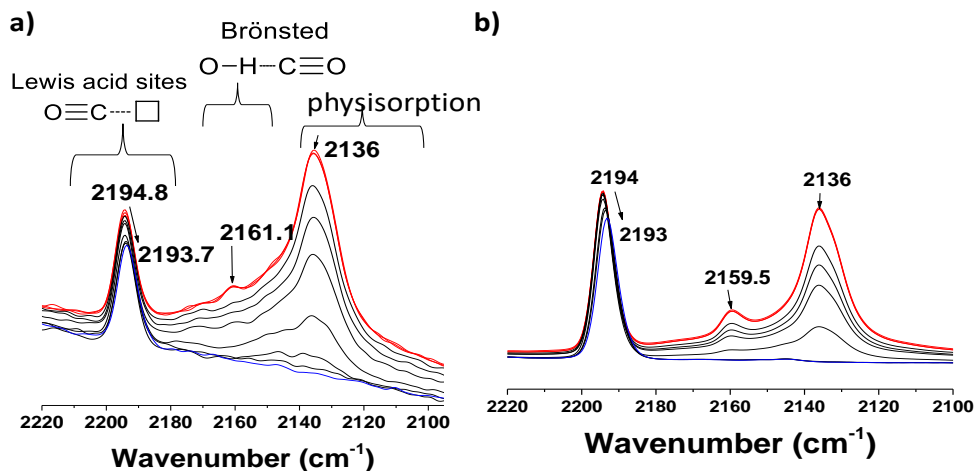


**Fig. SI-12** FT-IR spectra of CO adsorbed in MIL-101(Cr/Fe) (a) or MIL-101(Cr) (b). Red line spectra show the equilibrated CO adsorbed in the two MOFs; other color line spectra show the retained CO after outgassing the corresponding MOF for 1 h periods.

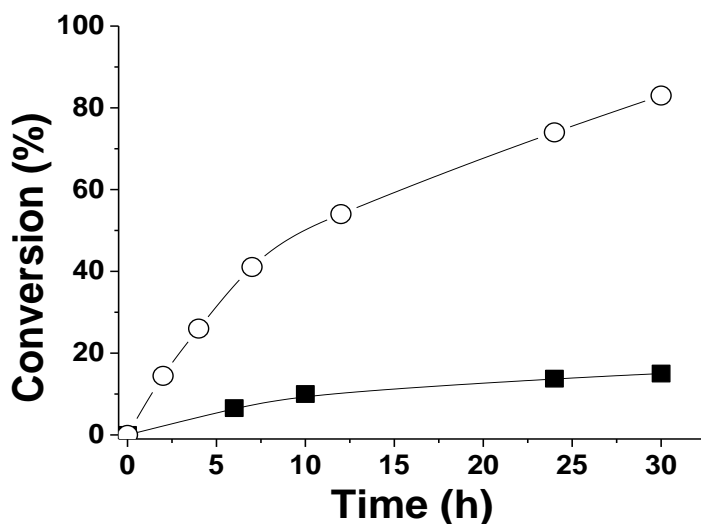


**Fig. SI-13** Influence of the presence (■) or absence (○) of pyridine as Lewis acid sites quencher in the resulting catalytic activity for the Prins reaction using MIL-101(Cr/Fe) (4:1) as catalyst. Reaction conditions: Catalyst (0.02 mmol of Fe+Cr), β-pinene (800 μL, 5 mmol), formaldehyde (750 μL, 5 mmol), pyridine (1 mmol) acetonitrile (1.26 mL), 80 °C.

**Table S1.** Summary of the Nopol and 10-pinen-3-ol yields achieved using several catalysts under study.<sup>a</sup>

Entry	Catalyst	Yield (%)	
		Nopol	10-pinen-3-ol
1	MIL-101(Cr)	25.18	0.31
2	MIL-101(Fe)	25.41	7.59
3	MIL-88(Fe)	32.95	2.05
4	MIL-101(Cr/Fe) (4:1)	63.75	21.25
5	Fe(III) acetate	41.60	10.40
6	MIL-100(Fe)	62.32	13.68
7	MIL-101(Cr/Fe) (5.9:1)	38.92	4.07
8	MIL-101(Cr/Fe) (36:1)	29.08	2.33
9	Cr <sup>+3</sup> acetate hydroxide	88.50	10.05
10	Cr <sub>2</sub> O <sub>3</sub>	52.91	35.27
11	Fe <sub>2</sub> O <sub>3</sub>	42.84	35.62

<sup>a</sup>Reaction conditions: Catalyst (0.02 mmol of metal), β-pinene (800 μL, 5 mmol), formaldehyde (750 μL, 5 mmol), acetonitrile (1.26 mL), 80 °C, reaction time 30 h.

**Chapter 4. *Nitro functionalized chromium terephthalate metal-organic framework as multifunctional solid acid for the synthesis of benzimidazoles***





# Nitro functionalized chromium terephthalate metal-organic framework as multifunctional solid acid for the synthesis of benzimidazoles.

Cristina Vallés-García,<sup>a</sup> María Cabrero-Antonino,<sup>a</sup> Sergio Navalón,<sup>\*,a</sup>  
Mercedes Álvaro,<sup>a</sup> Amarajothi Dhakshinamoorthy,<sup>\*,b</sup> Hermenegildo  
García<sup>\*,c,d</sup>

<sup>a</sup>Departamento de Química, Universitat Politècnica de València, C/Camino de Vera, s/n, 46022 Valencia, Spain

<sup>b</sup>School of Chemistry, Madurai Kamaraj University, Madurai-625 021, Tamil Nadu, India.

<sup>c</sup>Departamento de Química and Instituto Universitario de Tecnología Química (CSIC-UPV), Av. De los Naranjos s/n, 46022 Valencia, Spain.

<sup>d</sup>Center of Excellence for Advanced Materials Research, King Abdulaziz University, Jeddah, Saudi Arabia

Published online: October 25, 2019

(Reprinted with permission from *J. Colloid Interf. Sci.*, 2020, **560**, 885-893.

Copyright © 2020, Elsevier. All rights reserved.)



## 4.1 Abstract

In the present work, nitro functionalized chromium terephthalate [MIL-101(Cr)-NO<sub>2</sub>] metal-organic framework is prepared and characterized by powder X-ray diffraction (XRD), elemental analysis, infrared spectroscopy (IR), X-ray photoelectron spectroscopy (XPS), scanning electron microscopy (SEM) and Brunauer–Emmett–Teller (BET) surface area. The inherent Lewis acidity of MIL-101(Cr)-NO<sub>2</sub> is confirmed by FT-IR spectroscopy using CD<sub>3</sub>CN as a probe molecule. The performance of MIL-101(Cr)-NO<sub>2</sub> as bifunctional catalyst (acid and redox) promoting the synthesis of wide range of benzimidazoles has been examined by catalyzed condensation on acid sites and subsequent oxidation dehydrogenation. The catalytic activity of MIL-101(Cr)-NO<sub>2</sub> is found to be superior than analogues catalysts like MIL-101(Cr)-SO<sub>3</sub>H, MIL-101(Cr)-NH<sub>2</sub>, UiO-66(Zr), UiO-66(Zr)-NO<sub>2</sub>, MIL-100(Fe) and Cu<sub>3</sub>(BTC)<sub>2</sub> (BTC: 1,3,5-Benzenetricarboxylate) under identical reaction conditions. The structural stability of MIL-101(Cr)-NO<sub>2</sub> is supported by leaching analysis and reusability tests. MIL-101(Cr)-NO<sub>2</sub> solid is used five times without decay in its activity. Comparison of the fresh and five times used MIL-101(Cr)-NO<sub>2</sub> solids by powder XRD, SEM and elemental analysis indicate identical crystallinity, morphology and the absence of chromium leaching, respectively.

## 4.2 Introduction

Metal organic frameworks (MOFs) are crystalline porous materials whose crystal structure is assembled by the coordination of metal ions or clusters with rigid organic linkers defining one, two and three-dimensional structures. Since the discovery of MIL-101 (MIL: *Materiaux de l'Institute Lavoisier*) by Ferey and co-workers,<sup>1</sup> this solid has been extensively used as Lewis acid for wide range of

organic reactions<sup>2-6</sup> including acetalization, condensation, oxidation, CO<sub>2</sub> fixation and coupling reactions due to its robust stability.<sup>7, 8</sup> The catalytic activity derives from the presence of coordinatively unsaturated metal centres around Cr<sup>3+</sup> ions upon removal of solvent molecules by thermal activation and its robust structure. Furthermore, isostructural MIL-101 MOFs were also prepared by replacing terephthalic acid present in the parent MIL-101 by 2-aminotheterephthalic acid or 2-hydroxysulfonylterephthalic acid, among others, to obtain MIL-101(Cr)-NH<sub>2</sub> or MIL-101(Cr)-SO<sub>3</sub>H, respectively. The activity of MIL-101(Cr)-NH<sub>2</sub> and MIL-101(Cr)-SO<sub>3</sub>H has been studied in base catalyzed reactions including Knoevenagel condensation<sup>9-14</sup> and Brønsted acid catalyzed reactions<sup>15-17</sup>, respectively. Besides introducing active sites on the ligand, the Lewis acidity around Cr<sup>3+</sup> can also be enhanced by electron withdrawing substituents on the linker, thus, increasing the catalytic performance of MIL-101(Cr)-H<sup>18</sup>. Hence, compared to MIL-101(Cr)-H, MIL-101(Cr)-NO<sub>2</sub> has shown improved activity in the oxidative coupling of benzyl amine<sup>18</sup> and acetalization of benzaldehyde.<sup>19</sup> However, the number of examples determining the promotional effect in the catalytic activity of MIL-101(Cr)-H due to the presence of NO<sub>2</sub> is still limited.

Many biologically relevant compounds, natural products and drug molecules contain benzimidazole<sup>20, 21</sup> as a common core unit and hence considerable efforts have been made to develop new and efficient methods for the synthesis of benzimidazole and its derivatives. Benzimidazoles have been synthesised through the reaction between benzaldehydes and *o*-phenylenediamine, either with homogeneous or heterogeneous catalysts which include sulfamic acid,<sup>22</sup> FeCl<sub>3</sub>·6H<sub>2</sub>O,<sup>23</sup> In(OTf)<sub>3</sub>,<sup>24</sup> Sc(OTf)<sub>3</sub>,<sup>25</sup> ionic liquids,<sup>26</sup> iodine,<sup>27</sup> activated carbon,<sup>28</sup> claytic,<sup>29</sup> and FeCl<sub>3</sub>/Al<sub>2</sub>O<sub>3</sub>.<sup>30</sup> On other hand, benzimidazole has also been synthesised by a series of MOFs as heterogeneous catalysts with different active centres. For example, a zinc-based MOF was reported to promote the

condensation of aldehyde with diamines to obtain benzimidazoles.<sup>31</sup>  $I_2@Cd$ -MOF was used as heterogeneous catalyst to perform the condensation of aldehydes and amines to give benzimidazoles.<sup>32</sup> On other hand, UiO-66(Zr)-NHSO<sub>3</sub>H (UiO: University of Oslo) was reported as a heterogeneous Brønsted acid catalyst for the synthesis of benzimidazole derivatives.<sup>33</sup> In another report, UiO-66(Zr)-NH<sub>2</sub>-TC-Cu (TC: thiophene-2-carbaldehyde) was employed as solid catalyst for the synthesis of various benzimidazoles.<sup>34</sup> These catalysts require post-synthetic modification of the as-synthesised material to install the active sites while such post-synthetic treatment is not required in the present work.

MOFs comprising Lewis acid metal nodes as part of a highly porous lattice are currently under investigation as solid catalysts.<sup>35-37</sup> One of the current interests in heterogeneous catalysis by MOFs is to show the ability of these materials to act as multifunctional catalysts promoting reactions in where the reaction mechanism requires more than one type of active site.<sup>38-44</sup> Multifunctionality in MOFs can arise from the activity of transition metal centers as Lewis acid as well as their ability to act as oxidation centers to promote oxidation reactions.<sup>41</sup> In a previous study, we have shown that MOFs can promote aerobic oxidations by activation of molecular oxygen and generation of hydroperoxyl and other reactive oxygen species.<sup>45-49</sup> Moreover it has been shown that the catalytic activity to promote aerobic oxidations is also strongly influenced by the presence of substituents on the linker. Inductive effects can increase the electronegativity of the linker and, as consequence, the oxidation potential of the nodal metal cation.<sup>18, 50</sup>

In the present study two robust MOF solids are used to demonstrate the bifunctional catalytic activity. These MOFs were selected based on their catalytic and structural stability. Specifically herein we have used MIL-101 both of the Cr and Fe forms and UiO-66(Zr) as solid catalysts due to their high stability. Both

MOFs have in common terephthalic acid as organic linker and for both types of structures preparation of isostructural materials with organic substituents in the terephthalic acid has been reported in the literature.<sup>18</sup> Other common points between these two MOFs are their large specific BET surface area and their high porosity that allow easy diffusion of the reagents and products within the internal pores. Therefore, the catalytic performance of a series of MOFs like MIL-101(Cr)-H, MIL-101(Cr)-NO<sub>2</sub>, MIL-101(Cr)-SO<sub>3</sub>H, MIL-101(Cr)-NH<sub>2</sub>, UiO-66(Zr), UiO-66(Zr)-NO<sub>2</sub>, MIL-100(Fe) and Cu<sub>3</sub>(BTC)<sub>2</sub> is studied in the cyclocondensation between benzaldehyde and o-phenylenediamine to achieve 2-phenylbenzimidazole involving Lewis and redox active sites.

## **4.3 Experimental**

### **4.3.1 Materials**

All the reagents, solvents were purchased from Sigma-Aldrich with analytical or HPLC grade and used as received.

### **4.3.2 Catalyst preparation**

MIL-101(Cr)-X (X: H, NO<sub>2</sub>, NH<sub>2</sub>, SO<sub>3</sub>H) solids have been prepared according to previous reports.<sup>1, 51</sup> Briefly, the corresponding amount (1.5 mmol) of terephthalic acid or 2-nitroterephthalic acid and Cr(NO<sub>3</sub>)<sub>3</sub>·9H<sub>2</sub>O (for the synthesis of MIL-101(Cr)-H) or CrCl<sub>3</sub> (for the synthesis of MIL-101(Cr)-NO<sub>2</sub>) (1 mmol) were introduced into a Teflon autoclave containing demineralized water (8 mL). Then, HF (10 μL) was added for the synthesis of MIL-101(Cr)-H. The autoclave was closed and heated at 200 °C for 8 h or 180 °C for 120 h for the preparation of MIL-101(Cr)-H and MIL-101(Cr)-NO<sub>2</sub>, respectively. Then, the autoclave was cooled down to room temperature and the obtained solid was washed two consecutive

times using dimethylformamide (DMF, 120 °C for 1 h) and then, three consecutive times with ethanol (80 °C) both under continuous magnetic stirring. MIL-101(Cr)-NH<sub>2</sub> was prepared by the post-synthetic reduction of the nitro groups present in preformed MIL-101(Cr)-NO<sub>2</sub> solid with SnCl<sub>2</sub>·H<sub>2</sub>O according to previous reports.<sup>18, 52</sup> Further, MIL-101(Cr)-SO<sub>3</sub>H was obtained by post-synthetic sulfonation of the parent MIL-101(Cr)-H with chlorosulfonic acid as previously reported.<sup>18, 53</sup> These resulting solids were dried in an oven at 100 °C for 24 h.

UiO-66(Zr)-X (X: H or NO<sub>2</sub>) solids have been prepared by adopting previously reported procedures.<sup>48, 54</sup> Briefly, terephthalic acid or 2-nitroterephthalic acid (1 mmol) and ZrCl<sub>4</sub> (1 mmol) were added to a Teflon autoclave containing DMF (3 mL). The autoclave was closed and heated at 220 °C for 12 or 24 h for the preparation of UiO-66(Zr) and UiO-66(Zr)-NO<sub>2</sub>, respectively. Once the autoclave was cooled to room temperature by standing at the ambient, the resulting solids were collected and washed with DMF at 60 °C for 1 h. Then, the solids were submitted to Soxhlet extraction using methanol as solvent for 12 h. The resulting solids were dried in an oven at 100 °C for 24 h.

### 4.3.3 Catalyst characterization

Powder XRD of MIL-101(Cr)-X (X: H, NO<sub>2</sub>, NH<sub>2</sub>, SO<sub>3</sub>H) and UiO-66(Zr)-X (X: H or NO<sub>2</sub>) were recorded using a Philips XPert diffractometer equipped with a graphite monochromator (40 kV and 45 mA) employing Ni-filtered CuK<sub>α</sub> radiation. ATR-FTIR spectra of the MIL-101(Cr)-X and UiO-66(Zr)-X series were measured with a Bruker Tensor 27 instrument. Prior to ATR-FTIR measurements the solid samples were dried in an oven at 100 °C for 16 h to remove physisorbed water. X-ray photoelectron spectra (XPS) of the solids prepared were collected on a SPECS spectrometer with a MCD-9 detector using a monochromatic Al (K<sub>α</sub>= 1486.6 eV)

X-ray source. Spectra deconvolution was performed with CASA software using the C 1s peak at 284.4 eV as binding energy reference. Isothermal nitrogen adsorption measurements were collected at 77 K using a Micromeritics ASAP 2010 apparatus. The metal content of the MOFs was determined by inductively coupled plasma-atomic emission spectroscopy (ICP-AES). The solid MOF samples were digested in concentrated HNO<sub>3</sub> (15 mL, 80 °C, 24 h) prior to ICP-AES analyses. Thermogravimetric analyses (TGA) were measured on a TGA/SDTA851e Mettler Toledo station. SEM images were captured using a Zeiss instrument.

#### **4.3.4 Reaction procedure**

In a typical reaction procedure, 1,2-benzenediamine (**1**, 0.5 mmol) and benzaldehyde (**2**, 0.55 mmol) were dissolved in 2 mL of solvent. To this solution 30 mg (0.1 mmol of Cr) MIL-101(Cr)-NO<sub>2</sub> catalyst was added. The catalyst loading of other tested catalysts was 0.1 mmol of metal. This suspension was placed in hot plate preheated at 70 °C. The progress of the reaction was monitored by gas chromatography by sampling periodically aliquots of the reaction mixture using known amounts of nitrobenzene as internal standard. The conversion of **2** and the selectivity of the final product were determined by gas chromatography using calibration plots. Product identity was confirmed by GC-MS and <sup>1</sup>H-NMR spectroscopy.

Hot-filtration experiment was performed following the typical reaction procedure as described above. However, the catalyst was filtered after 10 min reaction time and the reaction mixture without solid was allowed to react further for the remaining time. Also, the course of the reaction was followed as indicated above determining the reaction mixture at identical time intervals as in the case



when the MOF was not filtered. Kinetic plots with and without solid catalyst were compared.

Reusability experiments were performed following the typical reaction procedure as described above. After the reaction time, the catalyst was recovered by filtration and repeatedly washed with acetonitrile and dried at 100 °C in an oven for 24 h. Then, this used catalyst was employed for subsequent runs with fresh reactants and solvents.

## 4.4 Results and discussion

### 4.4.1 Structural description of catalysts

MIL-101(Cr)-H and its isostructural materials were prepared following earlier reported procedures.<sup>1, 18, 51</sup> Powder XRD confirms that the MIL-101(Cr)-X (X: H, NO<sub>2</sub>, NH<sub>2</sub> and SO<sub>3</sub>H) are isostructural with the parent MIL-101(Cr)-H (Fig. 1). FT-IR spectroscopy shows the presence of the corresponding functional groups on the terephthalate ligand by providing their characteristic vibrations peaks (Fig. S1-S4). The chromium metal content was determined by ICP-AES of previously digested MIL-101(Cr)-X samples and the values are in good agreement with the theoretical formula of these MOFs (Table 1). Isothermal nitrogen adsorption measurements confirm the high surface area and pore volume of the parent MIL-101(Cr)-H solid. The presence of functional groups on the terephthalate linker decreases these values reflecting the space occupied by the substituents. Thermogravimetric analysis of MIL-101(Cr)-H and MIL-101(Cr)-NO<sub>2</sub> are provided in Fig. S5. No significant differences in thermal stability were observed for both materials. XPS of the MIL-101(Cr)-X (X: H, NO<sub>2</sub>, SO<sub>3</sub>H and NH<sub>2</sub>) solids confirms the presence and types of the individual atoms expected for the corresponding MOF (C, O, Cr, N or S) in agreement with previous reports (Fig. S6-S9).<sup>48</sup> Specifically, it shows the

presence of two individual components attributed to the aromatic carbons at 284.6 eV and carboxylate groups at 288.06 eV. The experimental O 1s peak contains in some cases a single component attributed to the carboxylate groups. All the samples also present a single component for Cr based on the Cr 2p peak with only very minor shift in the binding energy. In contrast, the position of the N 1s peak in MIL-101(Cr)-NH<sub>2</sub> compared to that of MIL-101(Cr)-NO<sub>2</sub> undergoes a remarkable change in binding energy from 395.0 to 405.5 eV, respectively.

Similar to powder XRD (Fig. 1), metal content determination by ICP-AES (Table 1), isothermal nitrogen adsorption (Table 1) and XPS also support the successful preparation of UiO-66(Zr) and UiO-66(Zr)-NO<sub>2</sub> samples (Fig. S10-S11).<sup>48</sup>

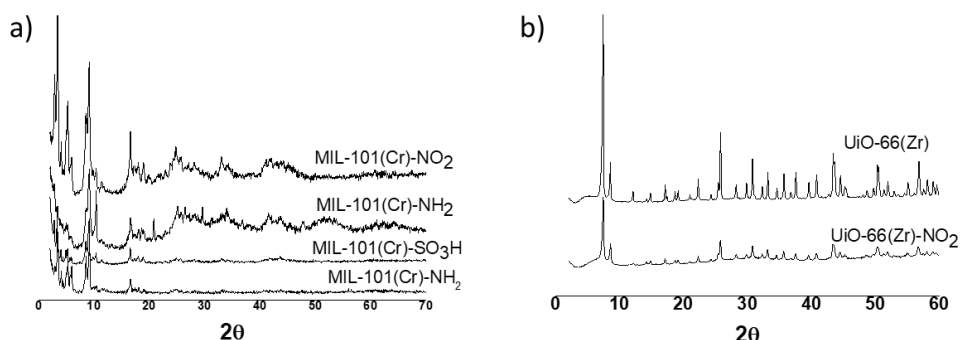


**Fig. 1** Powder XRD of (a) MIL-101(Cr)-X and (b) UiO-66(Zr)-X solids.

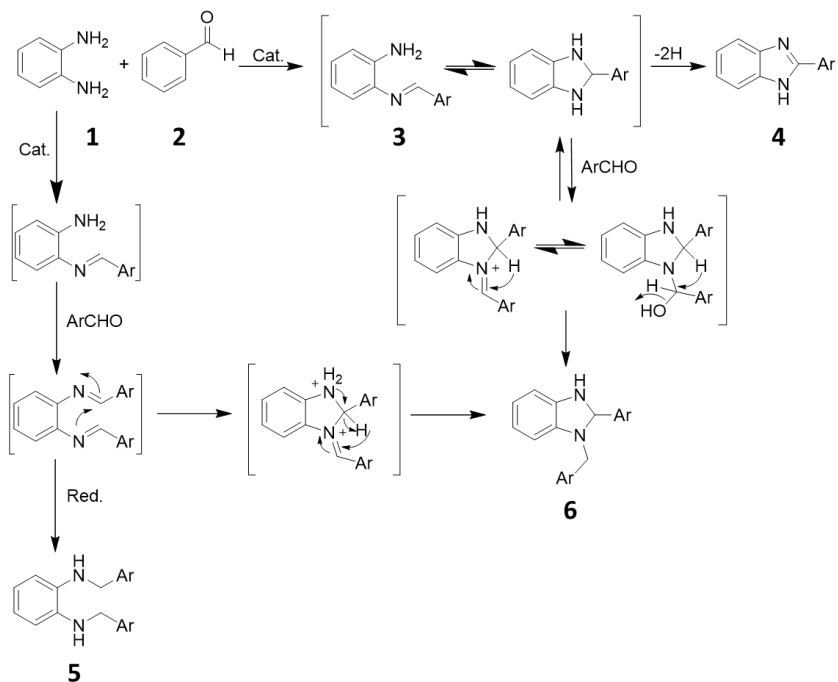
**Table 1** List of MOFs employed as catalysts in this work together with some relevant textural and analytical data.

Entry	Catalyst	BET Surface area (m <sup>2</sup> g <sup>-1</sup> )	Pore volume (cm <sup>3</sup> g <sup>-1</sup> )	Theoretical metal content (%) / Calculated by ICP (%)
1	MIL-101(Cr)-H {Cr <sub>3</sub> F(H <sub>2</sub> O) <sub>2</sub> O(BDC) <sub>3</sub> }	2740	2.20	21.77 / 22.84
2	MIL-101(Cr)-NO <sub>2</sub> {Cr <sub>3</sub> Cl(H <sub>2</sub> O) <sub>2</sub> O(BDC-NO <sub>2</sub> ) <sub>3</sub> }	1848	1.47	17.73 / 16.40
3	MIL-101(Cr)-SO <sub>3</sub> H {Cr <sub>3</sub> Cl(H <sub>2</sub> O) <sub>2</sub> O(BDC-SO <sub>3</sub> H) <sub>3</sub> }	1550	1.30	16.96 / 17.01
4	MIL-101(Cr)-NH <sub>2</sub> {Cr <sub>3</sub> Cl(H <sub>2</sub> O) <sub>2</sub> O(BDC-NH <sub>2</sub> ) <sub>3</sub> }	1555	1.15	20.97 / 21.50
5	UiO-66(Zr)	1258	0.73	32.80 / 34.70
6	UiO-66(Zr)-NO <sub>2</sub>	700	0.23	28.20 / 32.60
7	MIL-100(Fe) {Fe <sub>3</sub> F <sub>3</sub> O(BTC) <sub>3</sub> }	1205	0.55	23.00 / 22.20
8	Cu <sub>3</sub> (BTC) <sub>2</sub>	1250	0.57	31.20 / 32.40

#### 4.4.2 Catalytic activity

Aimed at demonstrating the influence of substituents on the activity of MOFs as bifunctional catalysts, the present study has focused on a model reaction of general interest in heterocyclic chemistry such as the cyclocondensation of *o*-phenyldiamine (**1**) with benzaldehyde (**2**) to form 2-phenylbenzimidazole (**4**). Benzimidazoles are nitrogenated heterocycles that find application as therapeutic agents and pharmaceutical compounds.<sup>55</sup> The reaction mechanism leading to the formation of the benzimidazole from **2** and **1** is well understood and comprises one step leading to the dihydrobenzimidazole that is catalyzed by acids and a subsequent step involving the oxidative dehydrogenation of the dihydrobenzimidazole intermediate resulting in the final heterocycle.<sup>56</sup> In those cases in where the oxidation step does not occur at a sufficient rate, formation of

byproducts such as *N,N'*-dibenzylidenediimine (**5**) and 1-benzyl-2-phenyl-1*H*-benzimidazole (**6**) can be observed. Scheme 1 illustrates the elementary steps of the accepted reaction mechanism involved in the formation of the various products.



**Scheme 1** Elementary steps with indication of the nature of the catalytic site in the reaction pathway leading to **4** from **2** and **1** and by-products **5** and **6**.

According to the reaction mechanism shown in Scheme 1, a suitable catalyst for the cyclocondensation of **1** and **2** leading to **4** should be able to promote two elementary steps, the acid-catalyzed formation of 2-(benzylideneamino)aniline **3** and its oxidative aromatization towards **4**.<sup>56</sup> In principle imine formation does not require strong acid sites and can be promoted by acids of weak or medium acid strength. Regarding the oxidative step, although aromaticity of the ring is driving towards the final benzimidazole product, oxidation sites are required, particularly

to avoid by-product formation. Considering that earlier results have shown the positive influence of electron withdrawing groups on the linker on the catalytic activity, it can be expected that the same trend should be found here in the benzimidazole formation. The results presented below confirm the bifunctional activity of MOF in this cyclocondensation/oxidation showing the beneficial influence of nitro groups on the terephthalate linker to promote the oxidative steps in the mechanism.

The reaction of **1** with **2** to obtain **4** is typically catalyzed either by Lewis<sup>29, 57</sup> or Brönsted acids and redox centers.<sup>56, 58</sup> Initial attempts were made to synthesize these compounds using Cu<sub>3</sub>(BTC)<sub>2</sub> MOFs, due to its intrinsic Lewis acid sites and redox activity of dimeric Cu metal centres. However, the chemical stability of Cu<sub>3</sub>(BTC)<sub>2</sub> MOFs used for the condensation of **1** and **2** for benzimidazole synthesis is limited and the solid decomposes.<sup>59</sup> Hence, the present work aims to employ some of the structurally most robust MOFs as heterogeneous solid catalysts for the synthesis of benzimidazole. The results achieved are summarized in Table 2. The reaction of **1** and **2** in the presence of MIL-101(Cr)-H at room temperature afforded 32 % selectivity of **4** at room temperature after 5 h (entry 1, Table 2). Under identical conditions, the use of MIL-101(Cr)-NO<sub>2</sub> afforded 42 % selectivity (entry 2, Table 2). These results show the increase of activity for the synthesis of product **4** when using MIL-101(Cr)-NO<sub>2</sub> (TOF 0.38 h<sup>-1</sup>) respect to MIL-101(Cr)-H (TOF 0.21 h<sup>-1</sup>) working at room temperature. In a related work, Hamadi and co-workers also showed the benefits of using the heterogeneous UiO-66(Zr)-NHSO<sub>3</sub>H solid as Brönsted acid catalyst respect to the parent UiO-66(Zr)-NH<sub>2</sub> for the preparation of benzimidazole.<sup>33</sup> The reaction of **1** with **2** in the presence of MIL-101(Cr)-H and MIL-101(Cr)-NO<sub>2</sub> was carried out at 70 °C and the selectivity were 54 and 79 %, respectively after 5 h (entries 3 and 5, Table 2). Then, the activity of MIL-101(Cr)-NO<sub>2</sub> was screened for the reaction between **1** and **2** under identical

conditions in various solvents including acetonitrile/ethanol and toluene, observing 55 and 37 % selectivity of **4**, respectively (entries 4 and 6 Table 2). The highest selectivity (82 %) was achieved after 4 h in acetonitrile (entry 8, Table 2). It is likely that protic solvents such as ethanol interact strongly with the acid and basic sites, therefore decreasing the catalytic activity, while aromatic solvents may interact with the organic ligand and are typically strongly adsorbed in some MOF. A control experiment for the reaction of **1** and **2** under argon atmosphere resulted in a conversion of about 94 % with around 10 % selectivity of **4**. This result reinforces the need of oxygen to promote the oxidative dehydrogenation to form the imidazole ring. This oxidative dehydrogenation could involve either metal-oxygen adducts such as metaloxirane or metalo hydroperoxide and together with Lewis acidity required in the amino-carbonyl condensation, determines that MIL-101(Cr)-NO<sub>2</sub> acts as bifunctional (acid and redox) catalyst. In agreement with the role of oxygen as reagent to promote dehydrogenation, an additional control reaction was performed with similar conditions in the presence of pure oxygen atmosphere (Table 2, entry 20). A selectivity of 90 % to **4** with 100 % conversion of **1** (Fig. S12) was observed under pure oxygen atmosphere, thus reinforcing the role of the oxygen to promote imidazole formation as indicated in the Scheme 1. Table S1 summarizes the obtained turnover number (TON) and turnover frequency (TOF) values for the series of catalysts tested in this work at 70 °C. SEM images comparing the morphology of MIL-101(Cr)-NO<sub>2</sub> before and after catalytic uses showed no significant differences suggesting catalyst stability (Fig. S13). Further, SEM images of the recovered after one use of MIL-101(Cr)-H, MIL-101(Cr)-NH<sub>2</sub>, MIL-101(Cr)-SO<sub>3</sub>H, MIL-100(Fe), UiO-66(Zr), UiO-66(Zr)-NO<sub>2</sub> and solids showed almost similar morphology compared to their respective fresh catalysts (Figs. S14-19) while Cu<sub>3</sub>(BTC)<sub>2</sub> indicated some change in its morphology (Fig. S20).

**Table 2** Summary of the catalytic results for the cyclocondensation of **1** and **2** to form **4** using MIL-101(Cr)-H and UiO-66(Zr)-based solid catalysts.<sup>a</sup>

Entry	Catalyst	Solvent	Time (h)	T (°C)	Conversion (%) <sup>b</sup>	Selectivity (%) <sup>b</sup>			
						<b>3</b>	<b>4</b>	<b>5</b>	<b>6</b>
1	MIL-101(Cr)-H	CH <sub>3</sub> CN	5	rt	72	4	32	36	28
2	MIL-101(Cr)-NO <sub>2</sub>	CH <sub>3</sub> CN	5	rt	79	7	42	24	27
3	MIL-101(Cr)-H	CH <sub>3</sub> CN	5	70	78	5	54	23	18
4	MIL-101(Cr)-NO <sub>2</sub>	CH <sub>3</sub> CN /EtOH	5	70	67	3	55	8	34
5	MIL-101(Cr)-NO <sub>2</sub>	CH <sub>3</sub> CN	2	70	93	1	79	11	9
6	MIL-101(Cr)-NO <sub>2</sub>	Toluene	3	70	88	2	37	25	36
7	MIL-101(Cr)-NO <sub>2</sub>	CH <sub>3</sub> CN	3	70	82	6	56	22	16
8	MIL-101(Cr)-NO <sub>2</sub>	CH <sub>3</sub> CN	4	70	100	2	82	6	10
9	MIL-101(Cr)-SO <sub>3</sub> H	CH <sub>3</sub> CN	4	70	93	18	67	9	6
10	MIL-101(Cr)-NH <sub>2</sub>	CH <sub>3</sub> CN	4	70	99	30	40	8	22
11	MIL-100(Fe)	CH <sub>3</sub> CN	4	70	99	15	54	14	17
12	UiO-66(Zr)	CH <sub>3</sub> CN	4	70	90	26	19	47	8
13	UiO-66(Zr)-NO <sub>2</sub>	CH <sub>3</sub> CN	4	70	99	17	59	22	2
14	Cu <sub>3</sub> (BTC) <sub>2</sub>	CH <sub>3</sub> CN	4	70	98	31	51	15	3
15	Cr <sub>2</sub> O <sub>3</sub>	CH <sub>3</sub> CN	4	70	95	22	51	23	4
16	Cr(OAc) <sub>3</sub>	CH <sub>3</sub> CN	4	70	96	15	47	30	8
17	-	CH <sub>3</sub> CN	4	70	98	27	44	25	4
18	2-nitroterephthalic acid	CH <sub>3</sub> CN	4	70	100	1	6	1	92
19	MIL-101(Cr)-NO <sub>2</sub> <sup>c</sup>	CH <sub>3</sub> CN	4	70	100	4	69	0	27
20	MIL-101(Cr)-NO <sub>2</sub> <sup>e</sup>	CH <sub>3</sub> CN	4	70	100	0	90	0	10

<sup>a</sup> Reaction condition: **1** (0.5 mmol), **2** (0.55 mmol), catalyst (0.1 mmol of metal), solvent (2 mL).

<sup>b</sup> Determined by GC.

<sup>c</sup> Reaction was performed in the presence of pyridine (0.1 mmol).

<sup>e</sup> Reaction was performed in the pure oxygen atmosphere.

As commented earlier, a wide range of Lewis and Brønsted acids have been reported as catalysts for the synthesis of benzimidazole derivatives. Therefore, it was of special interest to study the activity of MIL-101(Cr)-SO<sub>3</sub>H that combines the Lewis acidity of Cr metal nodes with the Brønsted acid sites of sulfonic groups. In this context, MIL-101(Cr)-SO<sub>3</sub>H has already been reported as an efficient Brønsted acid catalyst for a series of reactions particularly in biomass valorisation.<sup>60, 61</sup> It was observed that MIL-101(Cr)-SO<sub>3</sub>H exhibits 67 % of selectivity for the reaction of **1** and **2** in acetonitrile at 70 °C after 4 h (entry 9, Table 2). Further, the use of MIL-101(Cr)-NH<sub>2</sub> afforded 40 % selectivity of **4** under similar reaction conditions (entry 10, Table 2). On other hand, the reaction of **1** with **2** using MIL-100(Fe) as

catalyst reached 54 % selectivity of **4** under identical reaction conditions (entry 11, Table 2).

To further expand the study on the influence of substituents on the catalytic activity of robust MOFs, UiO-66(Zr) was also tested as catalyst for the condensations between **1** and **2**. The selectivity of **4** was 19 % with UiO-66(Zr) under the optimized reaction conditions (entry 12, Table 2) which is comparatively lower than using MIL-101(Cr)-H and MIL-100(Fe) as catalysts. Interestingly, the selectivity of product **4** under identical conditions increased to 59 % using UiO-66(Zr)-NO<sub>2</sub> as solid catalyst under identical conditions (entry 13, Table 2). These control experiments have clearly demonstrated that under identical reaction conditions the activity of MIL-101(Cr)-H or UiO-66(Zr) is lower compared to MIL-101(Cr)-NO<sub>2</sub> or UiO-66(Zr)-NO<sub>2</sub> solid catalysts. This higher activity of nitro-functionalized MIL-101(Cr)-NO<sub>2</sub> or UiO-66(Zr)-NO<sub>2</sub> is attributed due to the higher strength of the Lewis acid centres in these catalysts due to the electron-withdrawing effect of NO<sub>2</sub> group on the aromatic ring. Furthermore, Cu<sub>3</sub>(BTC)<sub>2</sub> was also employed as solid catalyst for this reaction, observing 51 % selectivity of **4** (entry 14, Table 2) under identical conditions.

In order to understand the role of MIL-101(Cr)-NO<sub>2</sub> in this reaction, a series of control experiments were performed and the results are given in Table 2. The use of homogeneous metal salts such as Cr<sub>2</sub>O<sub>3</sub> and Cr(OAc)<sub>3</sub> as catalysts resulted in 51 and 47 % selectivity of **4** under identical conditions (entries 15-16, Table 2). On other hand, the reaction of **1** with **2** under similar conditions in the presence of 2-nitroterephthalic acid afforded 6 % selectivity of the product (entry 18, Table 2). These experiments clearly reveal that the catalytic activity of MIL-101(Cr)-NO<sub>2</sub> originates from the Lewis acidity around the nodal Cr<sup>3+</sup> atoms in MIL-101(Cr)-NO<sub>2</sub>. These results are in agreement with earlier reports in a wide range of



reactions.<sup>18, 50</sup> Fig. 2 shows the evolution of selectivity of **4** from **1** and **2** using MIL-101(Cr)-H and MIL-101(Cr)-NO<sub>2</sub> as catalysts. Furthermore, the activity of MIL-101(Cr)-NO<sub>2</sub> was significantly reduced for the reaction of **1** with **2** upon addition of pyridine as a catalyst poison. This lower activity of MIL-101(Cr)-NO<sub>2</sub> in the presence of pyridine can be explained considering neutralization of Lewis sites (Cr<sup>3+</sup>) by pyridine (entry 19, Table 2).

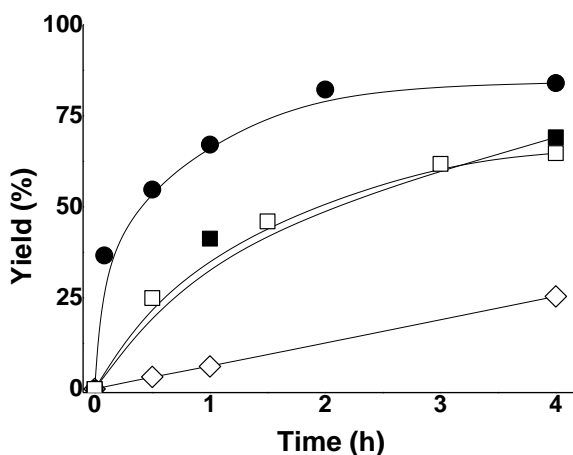


**Fig. 2** Time-yield plot for benzimidazole formation using MIL-101(Cr)-NO<sub>2</sub> (●) or MIL-101(Cr)-H (■) as catalysts. Control experiments using pyridine in the presence (□) or in the absence of MIL-101(Cr)-NO<sub>2</sub> (◇) are also shown. Reaction condition: **1** (0.5 mmol), **2** (0.55 mmol), catalysts (0.1 mmol of metal), CH<sub>3</sub>CN (2mL), 70 °C.

Reusability tests using the most active MIL-101(Cr)-NO<sub>2</sub> catalyst show that the activity decreases from the first to the third catalytic cycle, while, then, the activity is maintained up to the fifth cycle. Importantly, it was observed that the catalyst retains its initial crystallinity upon extensive use as catalyst and SEM analysis of the samples show no changes in the particle morphology (Fig. S13). Furthermore, elemental analysis by ICP-AES of the liquid phase after removal of the solid indicated negligible amount of Cr 0.02 wt%, thus supporting the heterogeneity of the process in the case of MIL-101(Cr)-NO<sub>2</sub>. Combustion elemental analysis of the used MIL-101(Cr)-NO<sub>2</sub> catalyst showed slight increase of

the nitrogen content, even though it has been thoroughly washed with  $\text{CH}_3\text{CN}$  (see experimental section), respect to the fresh sample. This increase of nitrogen content has been attributed to the occurrence of strong adsorption of the basic nitrogen reagents and intermediates on to the acid sites of the  $\text{MIL-101}(\text{Cr})\text{-NO}_2$  and, therefore, partially blocking the active sites (Table S2).

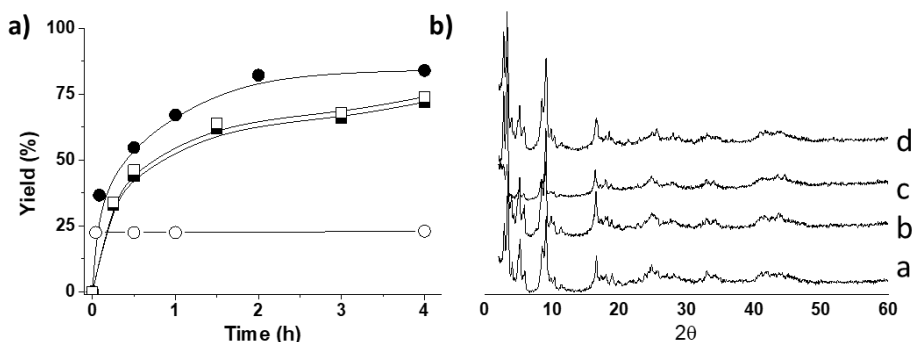


**Fig. 3** a) Reusability of the  $\text{MIL-101}(\text{Cr})\text{-NO}_2$  for the condensation of **1** with **2** to form the corresponding benzimidazole **4**; b) PXRD of the fresh (a), 1<sup>st</sup> use (b), 3<sup>rd</sup> use (c) and 5<sup>th</sup> use (d)  $\text{MIL-101}(\text{Cr})\text{-NO}_2$  catalyst. Reaction condition: **1** (0.5 mmol), **2** (0.55 mmol), catalysts (0.1 mmol of metal),  $\text{CH}_3\text{CN}$  (2mL), 70 °C.

An important issue in heterogeneous catalysis is to confirm that the process is promoted by the active sites on the solid or not by any possible leached metal species present in the solution. To address this point, hot-filtration experiment was performed starting the reaction under the conventional conditions and removing the solid catalyst by filtration at about 50 % conversion. Then, the reaction mixture was stirred in the absence of catalyst for the remaining time. The results are presented in Fig. 3. It was observed that the reaction did not progress without the solid catalyst and the product yield remains constant. These data are compatible with the conclusion that the reaction is being promoted exclusively by the active sites of  $\text{MIL-101}(\text{Cr})\text{-NO}_2$  solid rather than by any leached species.

Table 3 provides a comparison of the catalytic performance of  $\text{MIL-101}(\text{Cr})\text{-NO}_2$  with some of the catalysts reported in the literature for the synthesis of **4** in terms

of solvent, reaction temperature, time and the number of reuses. As it can be seen there, the activity of MIL-101(Cr)-NO<sub>2</sub> is slightly lower or comparable to other reported catalysts. However, MIL-101(Cr)-NO<sub>2</sub> appears as a stable catalyst at least for five uses. Further, MIL-101(Cr)-NO<sub>2</sub> is one of the few examples in where the solid is used without the requirement of post-synthetic modification.

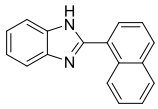
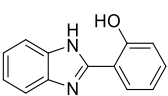
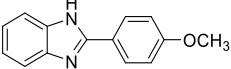
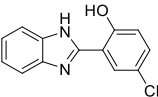
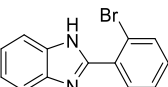
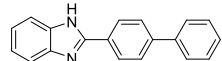
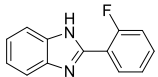
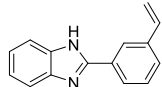
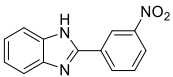
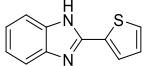
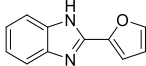
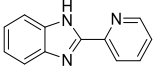
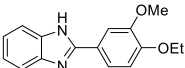
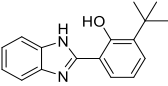
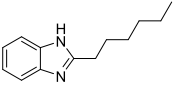
**Table 3** Comparison of the catalytic activity of MIL-101(Cr)-NO<sub>2</sub> with other catalysts for the synthesis of **4**.

Catalyst	Conditions	Yield (%)	Reuses	Ref.
CuO/SiO <sub>2</sub>	MeOH, RT, 4 h	93	5	[62]
Ag <sub>2</sub> CO <sub>3</sub> /celite	EtOH, 70 °C, 3 h	94	-	[63]
Fe(III)-Schiff base/SBA-15	H <sub>2</sub> O, reflux, 3 h	92	6	[64]
N,N-DMA/graphite (DMA: N,N-dimethylaniline)	EtOH, 75 °C, 3 h	67	3	[65]
CoO	EtOH, RT, 6 h	93	4	[66]
Nano ZnO	EtOH, reflux, 2 h	88	3	[67]
Nano sulphated zirconia	EtOH, 78 °C, 5 h	92	3	[67]
Nano-γ-alumina	EtOH, 75 °C, 5 h	85	3	[67]
Nano ZSM-5	EtOH, 75 °C, 5 h	75	3	[67]
SiO <sub>2</sub> -OSO <sub>3</sub> H	EtOH, 80 °C, 0.5 h	92	3	[68]
UiO-66(Zr)-NH-SO <sub>3</sub> H	EtOH, RT, 1 h	97	5	[33]
TiCl <sub>3</sub> OTf	EtOH, RT, 1.25 h	84	-	[69]
VOSO <sub>4</sub>	EtOH, RT, 1 h	92	4	[70]
MIL-101(Cr)-NO <sub>2</sub>	ACN, 70 °C, 4 h	82	5	This work

After screening different catalysts and various reaction conditions for the synthesis of **4**, the scope of MIL-101(Cr)-NO<sub>2</sub> was explored as heterogeneous solid catalyst for the synthesis of a wide range of benzimidazole derivatives (Table 4). The reaction of 1-naphthylbenzaldehyde with **1** using MIL-101(Cr)-NO<sub>2</sub> as catalyst afforded the corresponding naphthyl benzimidazole derivative in 84 % yield. 2-Hydroxy- and 4-methoxybenzaldehydes were reacted successfully with **1** in the presence of MIL-101(Cr)-NO<sub>2</sub> to afford 71 and 78 % yields of their corresponding products. On other hand, the reaction between 2-hydroxy-5-chlorobenzaldehyde and **1** afforded the expected benzimidazole in 60 % yield. Furthermore, 4-phenylbenzaldehyde also reacted with **1** to give 54 % yield of the corresponding product. These lower yields may be due to the bulkier nature of these aldehydes

which may experience some diffusion limitations to reach the active sites. Interestingly, aldehydes bearing electron withdrawing substrates like 2-fluoro-, 2-bromo- and 3-nitrobenzaldehydes reacted with **1** to provide respective benzimidazoles in 80, 71 and 92 % yields under the optimized conditions. The enhanced activity of these aldehydes respect to aldehydes with electron donating groups may be due to the rapid formation of the corresponding imine due to the higher reactivity of carbonyl groups with higher positive charge density. Analogously, 3-styrylbenzaldehyde reacted with **1** in the presence of MIL-101(Cr)-NO<sub>2</sub> to give the respective product in 91 % yield. This enhanced yield is highly promising since the final heterocyclic product bears vinyl groups which can be readily used as monomers in the synthesis of polymers. Heterocyclic aldehydes like 2-thiophenecarbaldehyde, 2-furfural and 2-pyridinecarbaldehyde also reacted with **1** using MIL-101(Cr)-NO<sub>2</sub> as catalyst to afford the corresponding benzimidazoles in 72, 64 and 51 % yields under identical conditions. These lower yields may be due to the competitive binding of heteroatoms with the Lewis acid sites, but further studies are necessary to prove this hypothesis. 4-Ethoxy-3-methoxybenzaldehyde and 3-t-butyl-2-hydroxybenzaldehydes also gave the respective benzimidazoles in 84 and 70 % yields using MIL-101(Cr)-NO<sub>2</sub> as solid catalyst without much diffusion limitations. Finally, the reaction between 1-heptanal and **1** exhibited 53 % yield of the hexylbenzimidazole under identical conditions. This moderate activity may be due to the lower reactivity of aliphatic aldehyde than aromatic aldehydes. These results indicate that MIL-101(Cr)-NO<sub>2</sub> is a general and convenient solid catalyst for the synthesis of wide ranges of benzimidazoles in moderate to high yields.

**Table 4** Structures and the corresponding yields of benzimidazole derivatives prepared using MIL-101(Cr)-NO<sub>2</sub> as a multifunctional solid catalyst.<sup>a</sup>

		
84	71	78
		
60	71	54
		
80	91	92
		
72	64	51
		
84	70	53

<sup>a</sup> Reaction conditions: aldehyde (0.5 mmol), **2** (0.55 mmol), MIL-101(Cr)-NO<sub>2</sub> (0.1 mmol Cr), ACN (2 mL), 70 °C, 4 h.

<sup>b</sup> Determined by GC.

#### 4.4.3 Characterization of the Lewis acid centers

In order to get some understanding of the higher catalytic activity achieved with MIL-101(Cr)-NO<sub>2</sub> as solid Lewis acid catalyst respect to the parent MIL-101(Cr)-H, infrared spectroscopy was employed as a spectroscopic tool for CD<sub>3</sub>CN as a probe molecule to determine the relative Lewis acid sites.<sup>71</sup> Prior to the FT-IR measurements, the solid samples were activated at 150 °C under vacuum for 3 h to remove the water molecules coordinated to the Cr<sup>3+</sup> metal centers.<sup>72, 73</sup> Subsequently, CD<sub>3</sub>CN was supplied to the thermally activated solids. Fig. 4 shows the equilibrated curve corresponding to the adsorption of CD<sub>3</sub>CN on

the activated solids. In agreement with previous reports, the characteristic  $\nu(\text{CN})$  and  $\nu(\text{CD}_3)$  vibration bands corresponding to  $\text{CD}_3\text{CN}$  physisorbed or coordinated to the  $\text{Cr}^{3+}$  Lewis centers can be clearly distinguished.<sup>73</sup> It should be noted that for the FT-IR experiments the same amount of solid was employed, thus, the higher intensity of the band at about  $2323\text{ cm}^{-1}$  for the MIL-101(Cr)- $\text{NO}_2$  respect to the MIL-101(Cr)-H indicates the higher population of  $\text{Cr}^{3+}$  Lewis centers present in this sample. In addition, the higher  $\nu(\text{CN})$  wavenumber measured for MIL-101(Cr)- $\text{NO}_2$  solid respect to that observed for MIL-101(Cr)-H ( $2320\text{ cm}^{-1}$ ) is an indication of the stronger Lewis character of the former sample. Interestingly, the Lewis acidity of the MIL-101(Cr)- $\text{NO}_2$  characterized by the  $\nu(\text{CN})$  at  $2323\text{ cm}^{-1}$  is higher than that observed for related MIL-100(Fe) or MIL-100(Al) material with analogous metal nodes.<sup>74</sup> It is well-known that the Lewis acidity of  $\text{Al}^{3+}$  ions is higher than that of  $\text{Cr}^{3+}$  ones, while in this case the presence of the nitro group in the terephthalate organic ligand of the MIL-101(Cr)- $\text{NO}_2$  has a positive effect inducing a stronger acidity on the  $\text{Cr}^{3+}$  metal centers respect to  $\text{Al}^{3+}$  ones. All these observations support that the higher catalytic activity observed for the MIL-101(Cr)- $\text{NO}_2$  solid derives from the increased Lewis acidity around  $\text{Cr}^{3+}$  nodes that enhances both the acid and redox steps in benzimidazole formation.

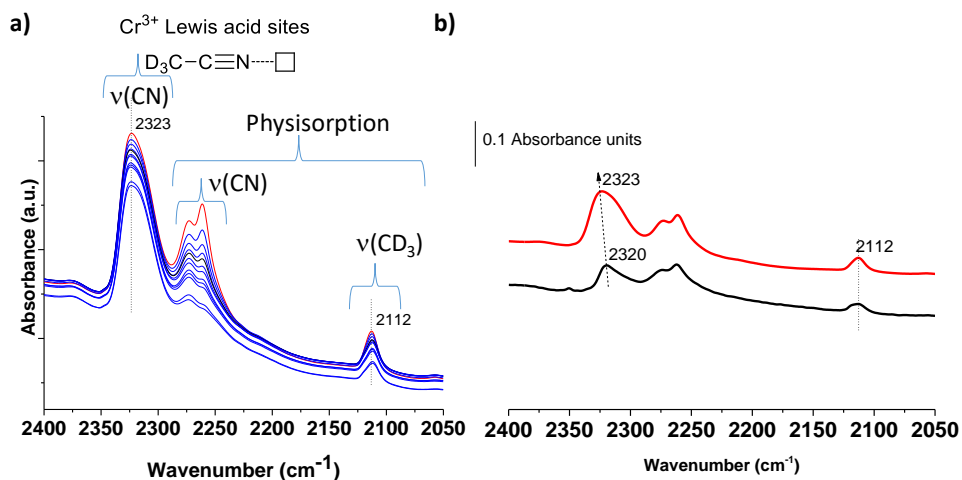


**Fig. 4** a) FT-IR spectra of CD<sub>3</sub>CN adsorbed in MIL-101(Cr)-NO<sub>2</sub> at 6 mbar and -170 °C; Blue line spectra show the CD<sub>3</sub>CN desorption from MIL-101(Cr)-NO<sub>2</sub>. b) Comparison of the FT-IR spectra of CD<sub>3</sub>CN adsorbed on MIL-101(Cr)-NO<sub>2</sub> (red line) or MIL-101(Cr)-H (black line) at 6 mbar and -170 °C.

## 4.5. Conclusions

The results provided here show that the activity and selectivity of MIL-101(Cr)-H for the cyclocondensation of **1** and **2** to give **4** can be improved by nitro substitution on the terephthalate linker resulting in MIL-101(Cr)-NO<sub>2</sub>. The process requires a bifunctional (Lewis acid and oxidation sites) catalyst.<sup>18</sup> Further, MIL-101(Cr)-NO<sub>2</sub> is stable up to five uses without activity decay as shown by leaching tests to prove the heterogeneity of the reaction. The catalyst exhibited a wide scope respect to the benzaldehyde derivatives to obtain different benzimidazole derivatives. MIL-101(Cr)-NO<sub>2</sub> does not need any post-synthetic treatment, while some of previously reported catalysts require post-synthetic modifications.<sup>33, 34, 59</sup> Overall, the present catalytic data provide additional insights to the existing literature in using MIL-101(Cr)-NO<sub>2</sub> as heterogeneous bifunctional catalyst for the synthesis of nitrogen heterocycles.

## **4.6 Acknowledgements**

AD thanks the University Grants Commission, New Delhi, for the award of an Assistant Professorship under its Faculty Recharge Programme. AD also thanks the Department of Science and Technology, India, for the financial support through Extra Mural Research Funding (EMR/2016/006500). Financial support by the Spanish Ministry of Science and Innovation (Severo Ochoa and RTI2018-098237-CO21) and Generalitat Valenciana (Prometeo 2017/083) is gratefully acknowledged. S.N. thanks financial support by the Fundación Ramón Areces (XVIII Concurso Nacional para la Adjudicación de Ayudas a la Investigación en Ciencias de la Vida y de la Materia, 2016), Ministerio de Ciencia, Innovación y Universidades RTI2018-099482-A-I00 project and Generalitat Valenciana grupos de investigación consolidables 2019 (AICO/2019/214) project.



## 4.7 References

1. G. Ferey, C. Mellot-Draznieks, C. Serre, F. Millange, J. Dutour, S. Surble and I. Margiolaki, *Science*, 2005, **309**, 2040-2042.
2. L. Bromberg and T.A. Hatton, *ACS Appl. Mater. Interfaces*, 2011, **3**, 4756-4764.
3. F.G. Cirujano, A. Leyva-Pérez, A. Corma and F.X. Llabrés i Xamena, *ChemCatChem*, 2013, **5**, 538-549.
4. J. Kim, S.-N. Kim, H.-G. Jang, G. Seo and W.-S. Ahn, *Appl. Catal. A: Gen.*, 2013, **453**, 175.
5. B. Li, K. Leng, Y. Zhang, J.J. Dynes, J. Wang, Y. Hu, D. Ma, Z. Shi, L. Zhu, D. Zhang, Y. Sun, M. Chrzanowski and S. Ma, *J. Am. Chem. Soc.*, 2015, **137**, 4243-4248.
6. L. Mitchell, B. Gonzalez-Santiago, J.P.S. Mowat, M.E. Gunn, P. Williamson, N. Acerbi, M.L. Clarke and P.A. Wright, *Catal. Sci. Technol.*, 2013, **3**, 606-617.
7. S. Bhattacharjee, C. Chen and W.-S. Ahn, *RSC Adv.*, 2014, **4**, 52500.
8. E. Niknam, F. Panahi, F. Daneshgar, F. Bahrami and A. Khalafi-Nezhad, *ACS Omega*, 2018, **3**, 17135-17144.
9. L.A. Darunte, A.D. Oetomo, K.S. Walton, D.S. Sholl and C.W. Jones, *ACS Sustainable Chem. Eng.*, 2016, **4**, 5761-5768.
10. L. Gao, C.-Y.V. Li, H. Yung and K.-Y. Chan, *Chem. Commun.*, 2013, **49**, 10629.
11. M. Hartmann and M. Fischer, *Micropor. Mesopor. Mater.*, 2012, **164**, 38-43.
12. W. Ma, L. Xu, Z. Li, Y. Sun, Y. Bai and H. Liu, *Nanoscale*, 2016, **8**, 10908.
13. T. Toyao, M. Fujiwaki, Y. Horiuchi and M. Matsuoka, *RSC Adv.*, 2013, **3**, 21582-21587.
14. H. Yu, J. Xie, Y. Zhong, F. Zhang and W. Zhu, *Catal. Commun.*, 2021, **29**, 101.
15. L. Ma, L. Xu, H. Jiang and X. Yuan, *RSC Adv.*, 2019, **9**, 5692.
16. M. Saikia and L. Saikia, *RSC Adv.*, 2016, **6**, 15846-15853.
17. Y.-X. Zhou, Y.-Z. Chen, Y. Hu, G. Huang, S.-H. Yu and H.-L. Jiang, *Chem. Eur. J.*, 2014, **20**, 14976.
18. A. Santiago-Portillo, J.F. Blandez, S. Navalón, M. Álvaro and H. García, *Catal. Sci. Technol.*, 2017, **7**, 1351-1362.
19. A. Herbst, A. Khutia and C. Janiak, *Inorg. Chem.*, 2014, **53**, 7319-7333.
20. A. Kumar, R.A. Maurya and D. Saxena, *Mol. Diversity*, 2010, **14**, 331-341.
21. L.A. Reddy, G.C. Malakondaiah, A.S. Reddy, B.V. Bhaskar, V. Himabindu, A. Bhattacharya and R. Bandichhor, *Org. Process Res. Dev.*, 2009, **13**, 1122-1124.
22. Z.-H. Zhang, T.-S. Li and J.-J. Li, *Monat. Chem.*, 2007, **138**, 89.
23. M.P. Singh, S. Sasmal, W. Lu and M.N. Chatterjee, *Synthesis*, 2000, **10**, 1380.
24. R. Trivedi, S.K. De and R.A. Gibbs, *J. Mol. Catal. A: Chem.*, 2006, **245**, 8-11.
25. K. Nagata, T. Itoh, H. Ishikawa and A. Ohsawa, *Heterocycles*, 2003, **61**, 93.
26. H.Q. Ma, Y.L. Wang, J.P. Li and J.Y. Wang, *Heterocycles*, 2007, **71**, 135.
27. P. Gogoi and D. Konwar, *Tetrahedron Lett.*, 2006, **47**, 79-82.

28. Y. Kawashita, N. Nakamichi, H. Kawabata and M. Hayashi, *Org. Lett.*, 2003, **5**, 3713-3715.
29. A. Dhakshinamoorthy, K. Kanagaraj and K. Pitchumani, *Tetrahedron Lett.*, 2011, **52**, 69.
30. G.-F. Chen and X.-Y. Dong, *J. Chem.*, 2012, **9**, 289.
31. K. Madasamy, S. Kumaraguru, V. Sankar, S. Mannathan and M. Kathiresan, *New J. Chem.*, 2019, **43**, 3793-3800.
32. H. Kaur, M. Venkateswarlu, S. Kumar, V. Krishnan and R.R. Koner, *Dalton Trans.*, 2018, **47**, 1488-1497.
33. M. Homaee, H. Hamadi, V. Nobakht, M. Javaherian and B. Salahshournia, *Polyhedron*, 2019, **165**, 152-161.
34. R. Kardanpour, S. Tangestaninejad, V. Mirkhani, M. Moghadam, I. Mohammadpoor-Baltork and F. Zadehahmadi, *J. Solid State Chem.*, 2016, **235**, 145-153.
35. J. Canivet, M. Vandichel and D. Farrusseng, *Dalton Trans.*, 2016, **4**, 4090-4099.
36. A. Dhakshinamoorthy, A.M. Asiri and H. Garcia, *Chem. Soc. Rev.*, 2015, **44**, 1922-1947.
37. S. Yuan, L. Feng, K. Wang, L. Zou, Y. Zhang, J. Li and H.-C. Zhou, *Adv. Mater.*, 2018, **30**, 1704303.
38. A. Dhakshinamoorthy and H. Garcia, *ChemSusChem*, 2014, **7**, 2392-2410.
39. M.-L. Hu, V. Safarifard, E. Doustkhah, S. Sadegh Rostamnia, A. Morsali, N. Nouruzi, S. Beheshti and K. Akhbari, *Micropor. Mesopor. Mater.*, 2018, **256**, 111-127.
40. Y.-B. Huang, J. Liang, X.-S. Wang and R. Cao, *Coord. Chem. Rev.*, 2017, **46**, 126-157.
41. C. Xu, R. Fang, R. Luque, L. Chen and Y. Li, *Coord. Chem. Rev.*, 2019, **388**, 268-292.
42. D. Azarifar, R. Ghorbani-Vaghei, S. Daliran and A.R. Oveisi, *ChemCatChem*, 2017, **9**, 1992-2000.
43. M.R. Ghaleno, M. Ghaffari-Moghaddam, M. Khajeh, A.R. Oveisi and M. Bohlooli, *J. Colloid Interf. Sci.*, 2019, **535** 214-226.
44. A. Kirchon, L. Feng, H.F. Drake, E.A. Joseph and H.-C. Zhou, *Chem. Soc. Rev.*, 2018, **47**, 8611-8638.
45. A. Dhakshinamoorthy, M. Alvaro and H. Garcia, *ChemCatChem*, 2010, **2**, 1438-1443.
46. A. Dhakshinamoorthy, M. Alvaro and H. Garcia, *ACS Catal.*, 2011, **1**, 836-840.
47. A. Dhakshinamoorthy, A.M. Asiri and H. Garcia, *Chem. Eur. J.*, 2016, **22**, 8012-8024.
48. A. Santiago-Portillo, S. Navalón, M. Álvaro and H. García, *J. Catal.*, 2018, **365**, 450-463.
49. A. Santiago-Portillo, S. Navalon, F. Cirujano, F. Llabrés i Xamena, M. Alvaro and H. Garcia, *ACS Catal.*, 2015, **5**, 3216-3224.
50. A. Santiago-Portillo, S. Navalón, P. Concepción, M. Álvaro and H. García, *ChemCatChem*, 2017, **9**, 2506-2511.
51. M. Lammert, S. Bernt, F. Vermoortele, D.E. De Vos and N. Stock, *Inorg. Chem.*, 2013, **52**, 8521-8528.
52. S. Bernt, V. Guillerme, C. Serre and N. Stock, *Chem. Commun.*, 2011, **47**, 2838-2840.
53. B. Li, Y. Zhang, D. Ma, L. Li, G. Li, G. Li, Z. Shi and S. Feng, *Chem. Commun.*, 2012, **48**, 6151.

54. M. Kandiah, M.H. Nilsen, S. Usseglio, S. Jakobsen, U. Olsbye, M. Tilset, C. Larabi, E.A. Quadrelli, F. Bonino and K.P. Lillerud, *Chem. Mater.*, 2010, **22**, 6632-6640
55. Y. Bansal and O. Silakari, *Bioorg. Med. Chem.*, 2012, **20**, 6208.
56. D. Kumar, D.N. N. Kommi, R. Chebolu, S.K. Garg, R. Kumar and A.K. Chakraborti, *RSC Adv.*, 2013, **3**, 91.
57. M. Curini, F. Epifano, F. Montanari, O. Rosati and S. Taccone, *Synlett*, 2011, 1832.
58. R. Wang, X. Lu, X. Yu, L. Shi and Y. Sun, *J. Mol. Catal. A: Chem.*, 2007, **266**, 198.
59. A. Dhakshinamoorthy, M. Alvaro and H. Garcia, *Catal. Lett.*, 2015, **145**, 1600-1605.
60. J. Chen, K. Li, L. Chen, R. Liu, X. Huang and D. Ye, *Green Chem.*, 2014 **16**, 2490-2499.
61. A. Herbst and C. Janiak, *CrystEngComm*, 2017, **19**, 4092-4117.
62. S.M. Inamdar, V.K. More and S.K. Mandal, *Tetrahedron Lett.*, 2013, **54**, 579-583.
63. E. Soleimani, M.M. Khodaei, H. Yazdani, P. Saei and J. Zavar Reza, *J. Iran. Chem. Soc.*, 2015, **12**, 1281-1285.
64. G.R. Bardajee, M. Mohammadi, H. Yari and A. Ghaedi, *Chin. Chem. Lett.*, 2016, **27**, 265-270.
65. H. Sharghi, O. Asemani and S.M.H. Tabaei, *J. Heterocycl. Chem.*, 2008, **45**, 1293-1298.
66. M.A. Chari, D. Shobha and T. Sasaki, *Tetrahedron Lett.*, 2011, **52**, 5575-5580.
67. A. Teimouri, A.N. Chermahini, H. Salavati and L. Ghorbanian, *J. Mol. Catal. A: Chem.*, 2013, **373**, 38-45.
68. B. Sadeghi and M. Ghasemi Nejad, *J. Chem.*, 2013, 1-5.
69. J. Azizian, P. Torabi and J. Noei, *Tetrahedron Lett.*, 2016, **57**, 185-188.
70. C.S. Digwal, U. Yadav, A.P. Sakla, P.S. Ramya, S. Aaghaz and A. Kamal, *Tetrahedron Lett.*, 2016, **57**, 4012-4016.
71. A. Vimont, F. Thibault-Starzyk and M. Datur, *Chem. Soc. Rev.*, 2010, **39**, 4928-4950.
72. H. Leclerc, A. Vimont, J.-C. Lavalley, M. Daturi, A.D. Wiersum, P.L. Llwellyn, P. Horcajada, G. Férey and C. Serre, *Phys. Chem. Chem. Phys.*, 2011, **13**, 11748-11756.
73. A. Vimont, J.M. Goupil, J.C. Lavalley, M. Daturi, S. Surblé, C. Serre, F. Millange, G. Férey and N. Audebrand, *J. Am. Chem. Soc.*, 2006, **128**, 3218.
74. C. Volkringer, H. Leclerc, J.-C. Lavalley, T. Loiseau, G. Férey, M. Daturi and A. Vimont, *J. Phys. Chem. C.*, 2012, **116**, 5710-5719.

## 4.8 Supporting information

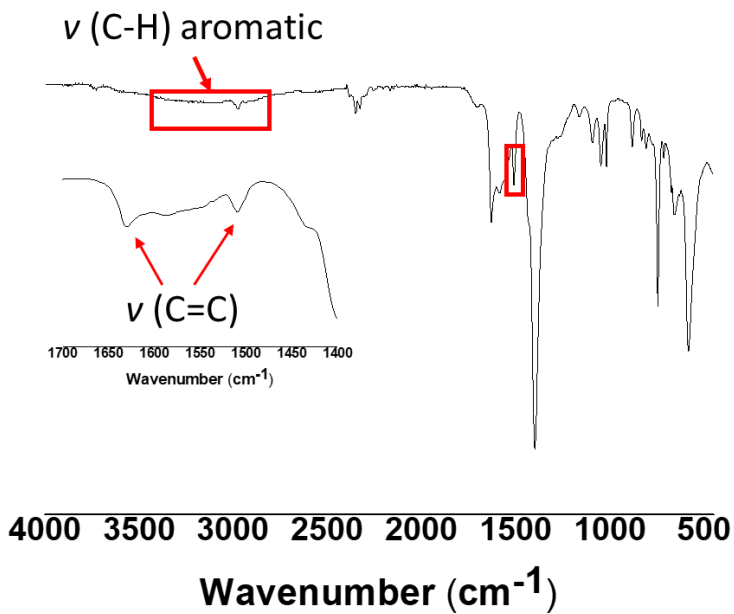


**Fig. S1** FT-IR spectrum recorded for MIL101(Cr)-H. The inset shows an expansion of the 1700-1400  $\text{cm}^{-1}$  region. The arrows show some of the characteristic vibration bands.

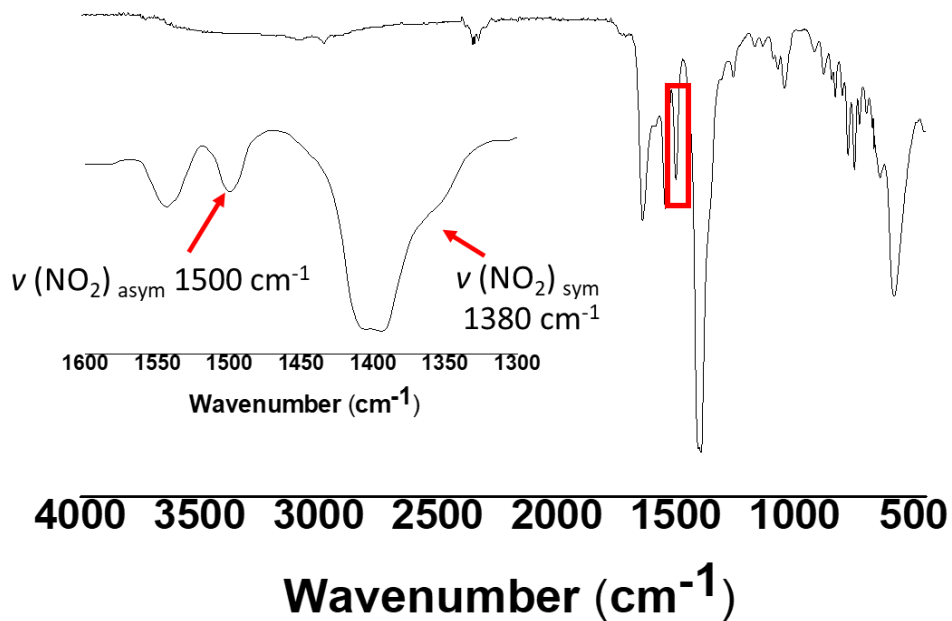


**Fig. S2** FT-IR spectrum recorded for MIL101(Cr)-NO<sub>2</sub>. The inset shows an expansion of the 1600-1300 cm<sup>-1</sup> region. The arrows show some of the characteristic asymmetric and symmetric vibration bands.

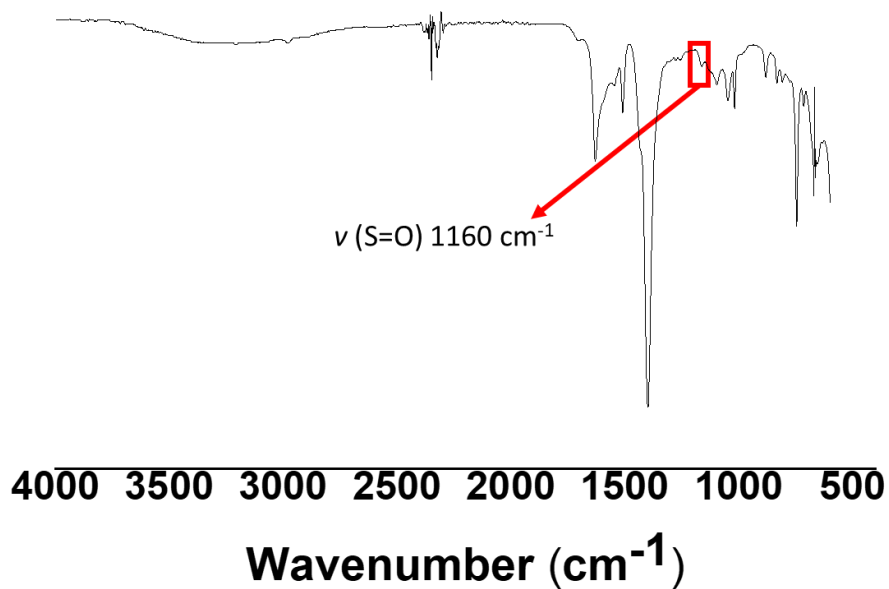


**Fig. S3** FT-IR spectrum recorded for MIL101(Cr)-SO<sub>3</sub>H. The inset shows an expansion of the 1300-1100 cm<sup>-1</sup> region. The arrows show some of the characteristic vibration bands.

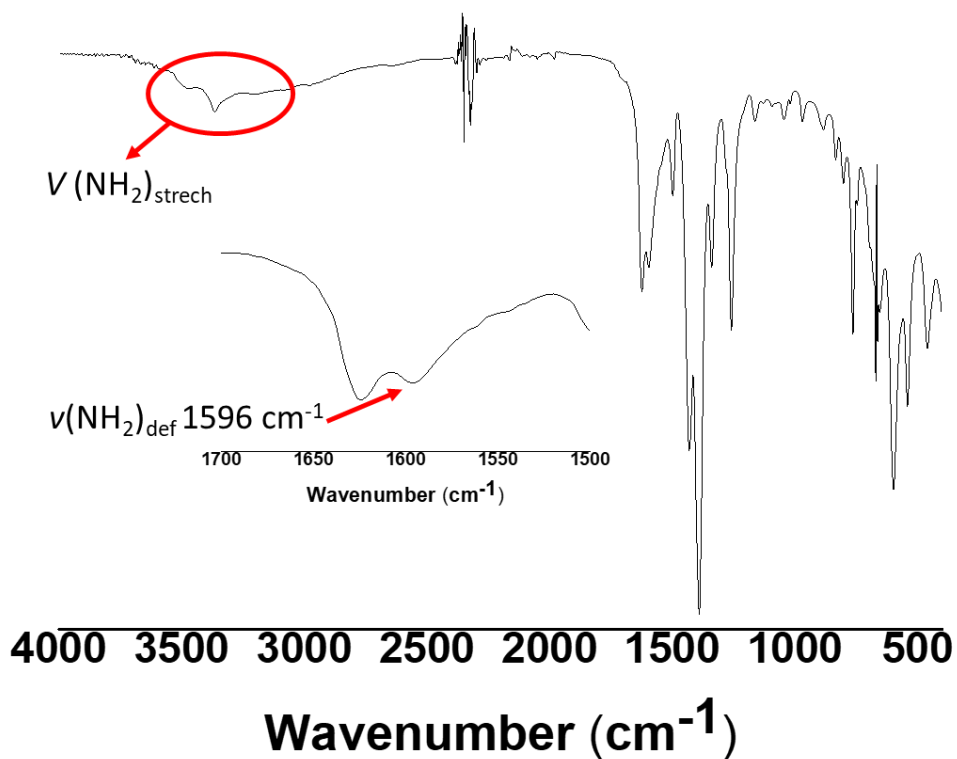


**Fig. S4** FT-IR spectrum recorded for MIL101(Cr)-NH<sub>2</sub>. The inset shows an expansion of the 1700-1500 cm<sup>-1</sup> region. The arrows show some of the characteristic vibration bands.

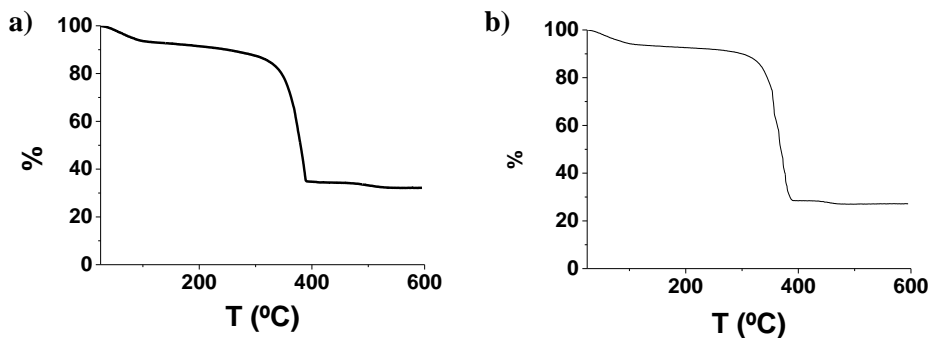


**Fig. S5** Thermogravimetric profiles of the MIL-101(Cr)-H (a), % Cr (experimental) = 21.77 %; % Cr (theoretical) = 22.84 %, and MIL-101(Cr)-NO<sub>2</sub> (b), % Cr (experimental) = 18.28 %; % Cr (theoretical) = 17.89 %, fresh materials.

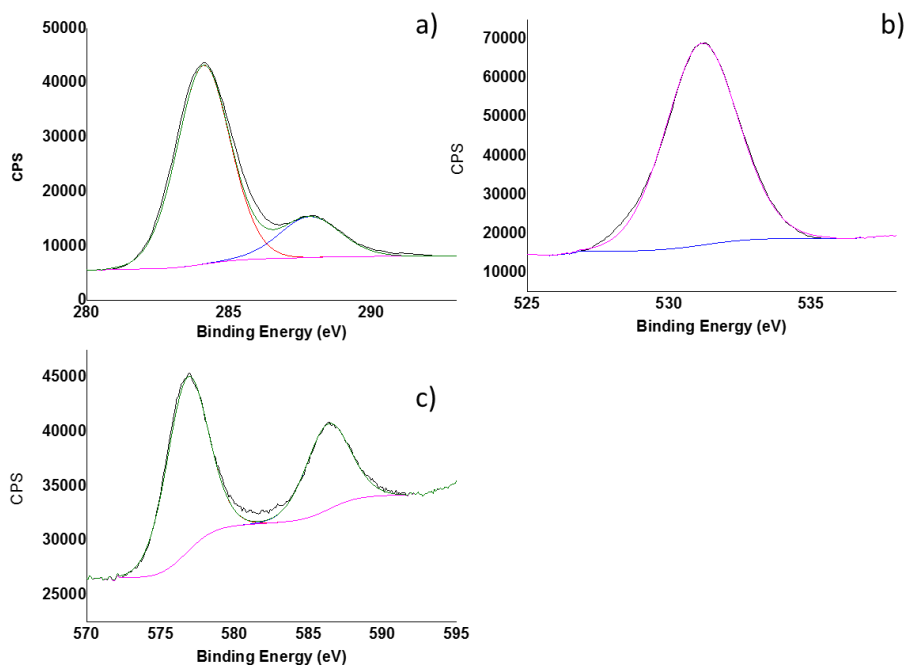


**Fig. S6** XPS spectra of MIL-101(Cr)-H. (a) C1s, (b) O1s and (c) N1s peaks with the corresponding best fit to individual components.



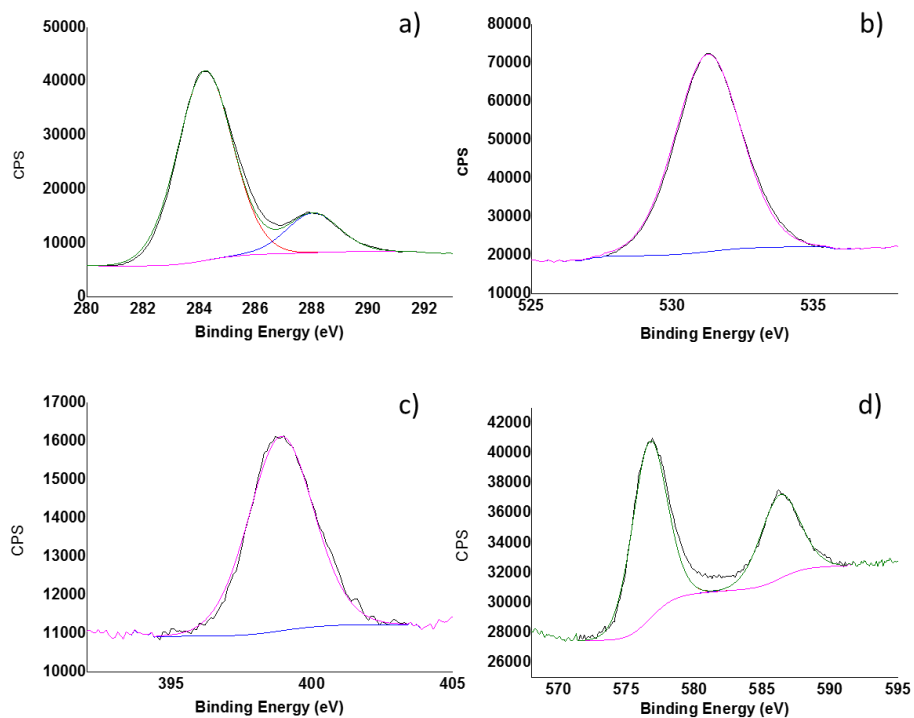


**Fig. S7** XPS spectra of MIL-101(Cr)-NH<sub>2</sub>. (a) C1s, (b) O1s, (c) N1s and (d) Cr2p peaks with the corresponding best fit to individual components.

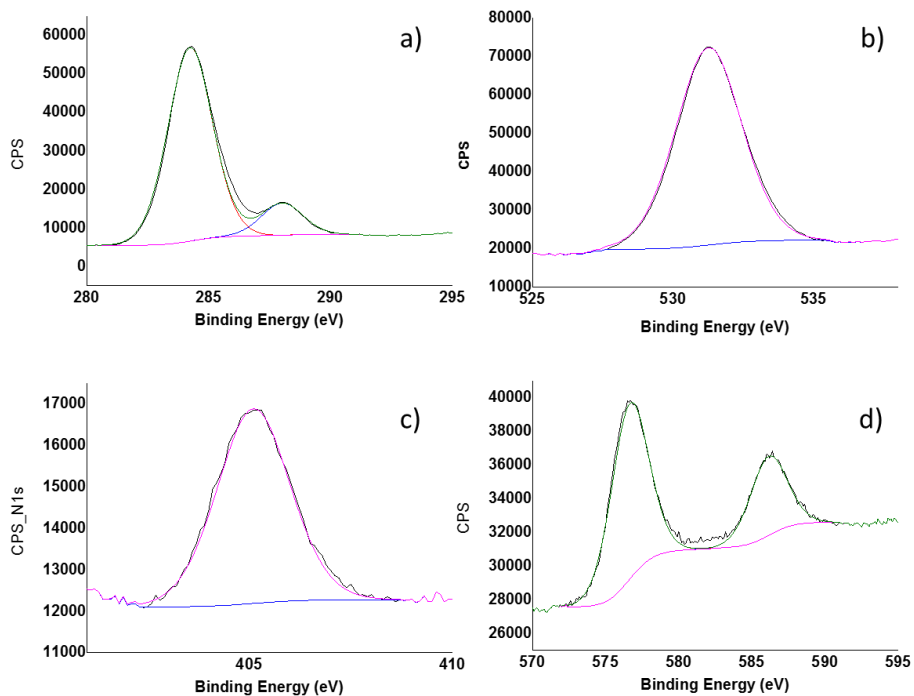


**Fig. S8** XPS spectra of MIL-101(Cr)-NO<sub>2</sub>. (a) C1s, (b) O1s, (c) N1s and (d) Cr2p peaks with the corresponding best fit to individual components.

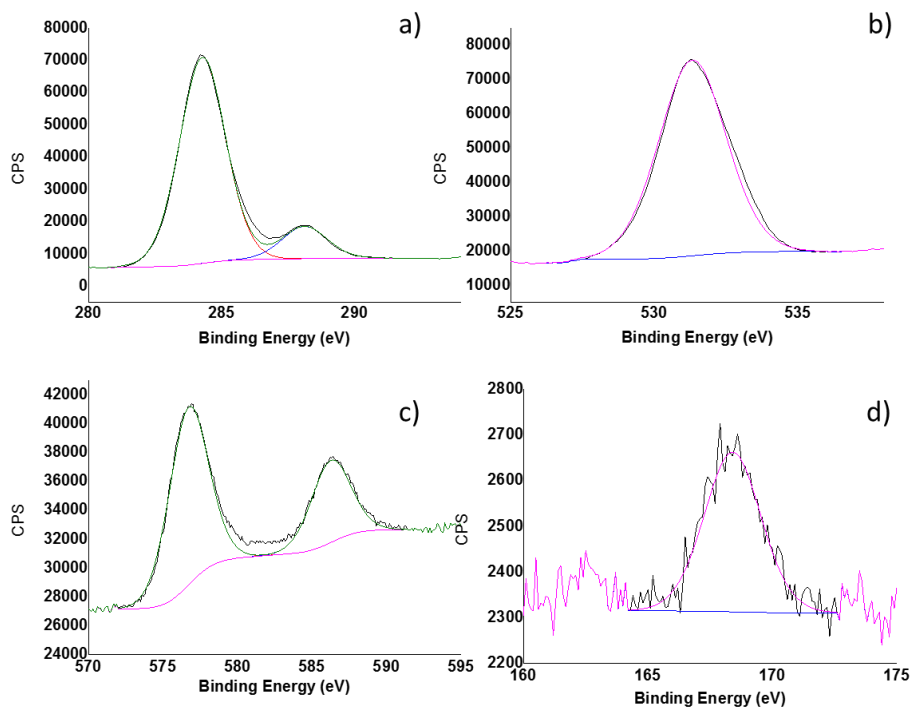


**Fig. S9** XPS spectra of MIL-101(Cr)-SO<sub>3</sub>H. (a) C1s, (b) O1s, (c) Cr2p and (d) S2p peaks with the corresponding best fit to individual components.

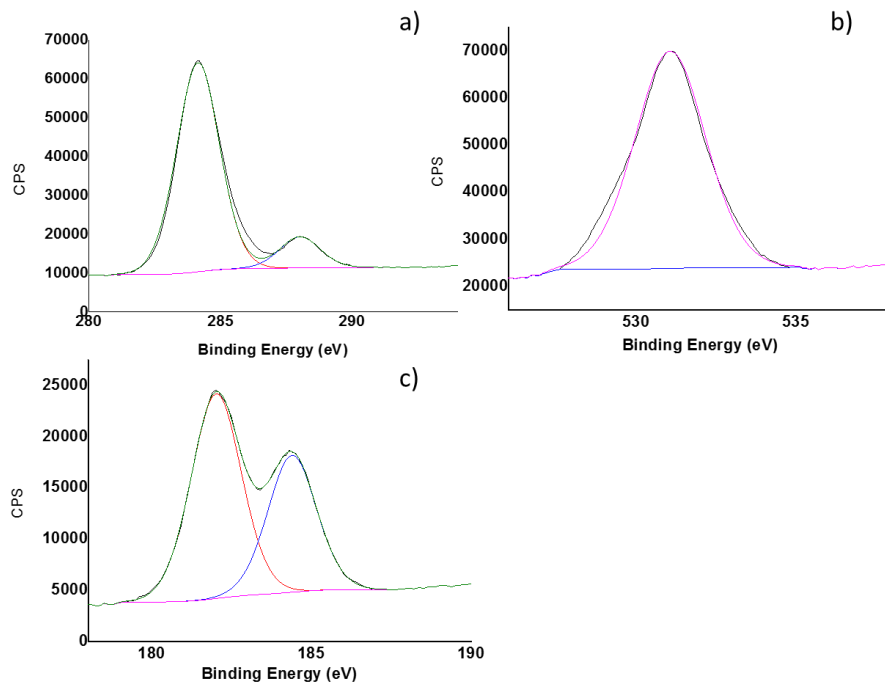


**Fig. S10** XP spectra of UiO-66(Zr)-H. (a) C1s, (b) O1s and (c) Zr2p peaks with the corresponding best fit to individual components.

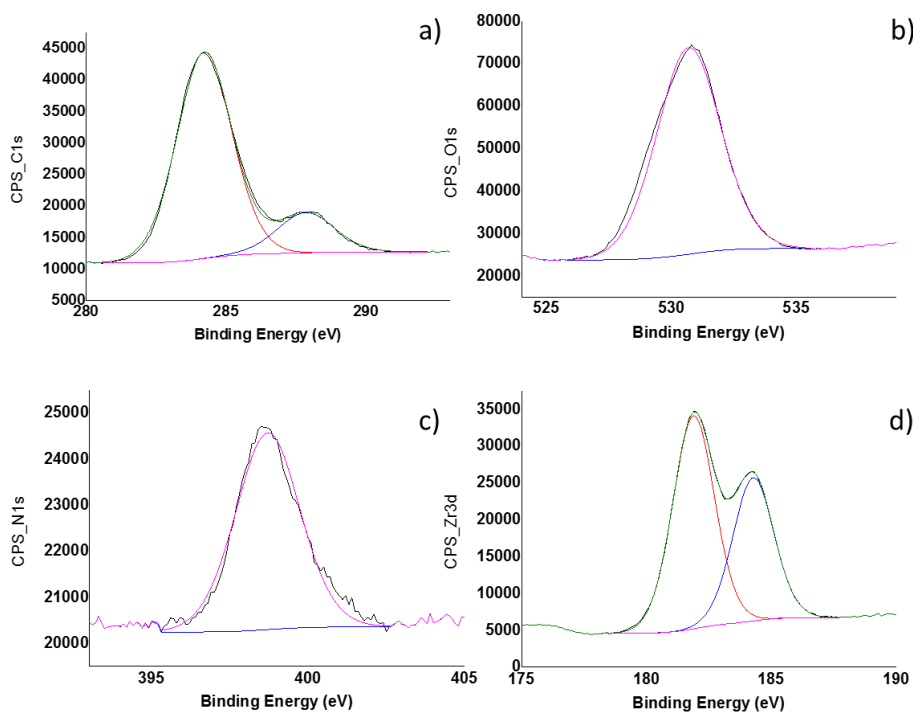


**Fig S11** XPS spectra of UiO-66(Zr)-NO<sub>2</sub>. (a) C1s, (b) O1s, (c) N1s and (d) Zr2p peaks with the corresponding best fit to individual components.

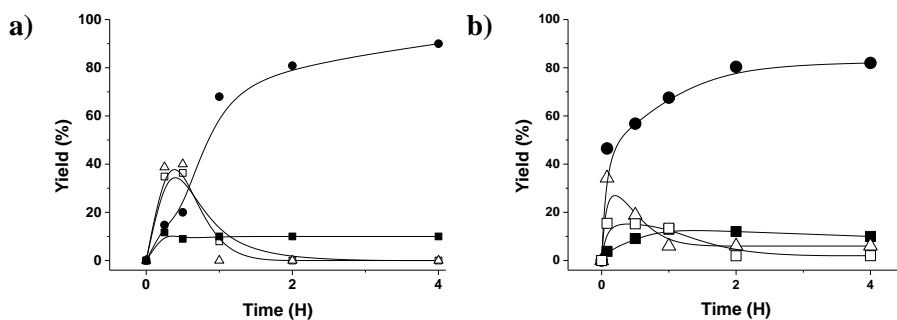


**Fig. S12** Time-yield plot for the formation of benzimidazole (4) and other byproducts with pure oxygen atmosphere (a) and air atmosphere (b); yield 3 (□); yield 4 (●); yield 5 (Δ); yield 6 (■). Reaction conditions: 1 (0.5 mmol), 2 (0.55 mmol), catalyst (30 mg, 0.1 mmol of metal, 20 wt%), ACN (2 mL).

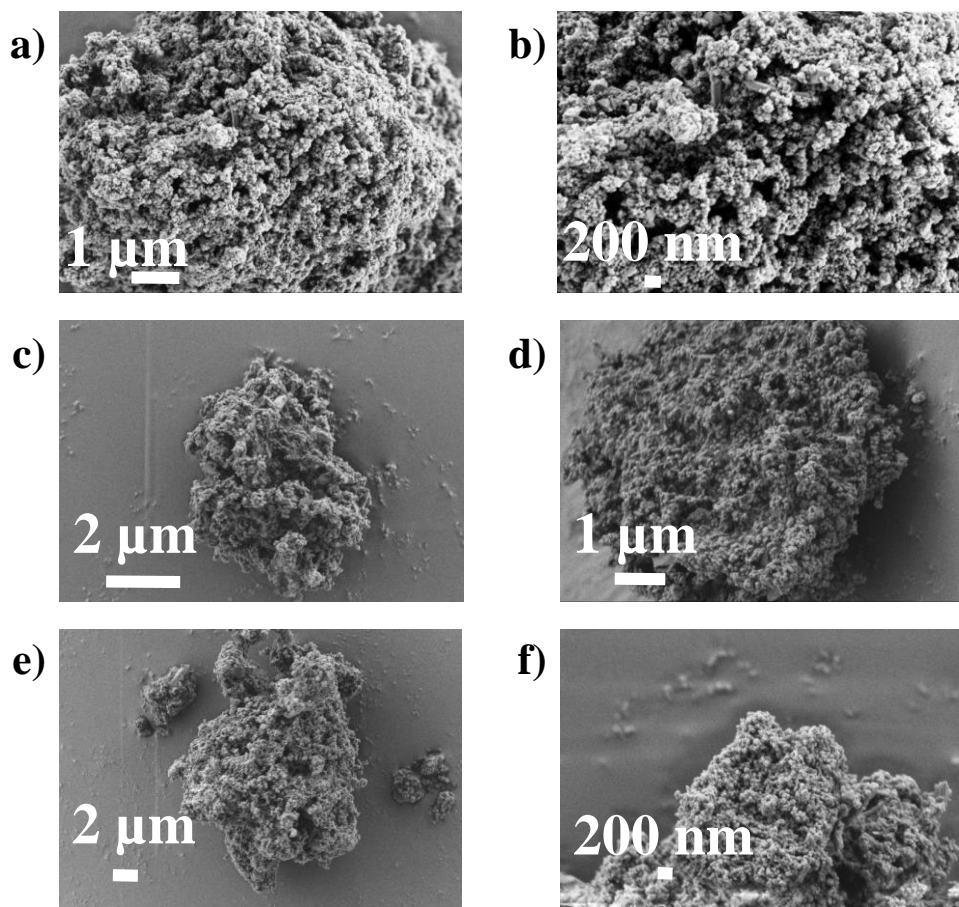


**Fig. S13** SEM images of the fresh MIL-101(Cr)-NO<sub>2</sub> catalyst (a, b), after one use (c, d) and after five uses (e, f) in the synthesis of **4**. Reaction conditions: **1** (0.5 mmol), **2** (0.55 mmol), catalyst (0.1 mmol of metal), ACN (2 mL).

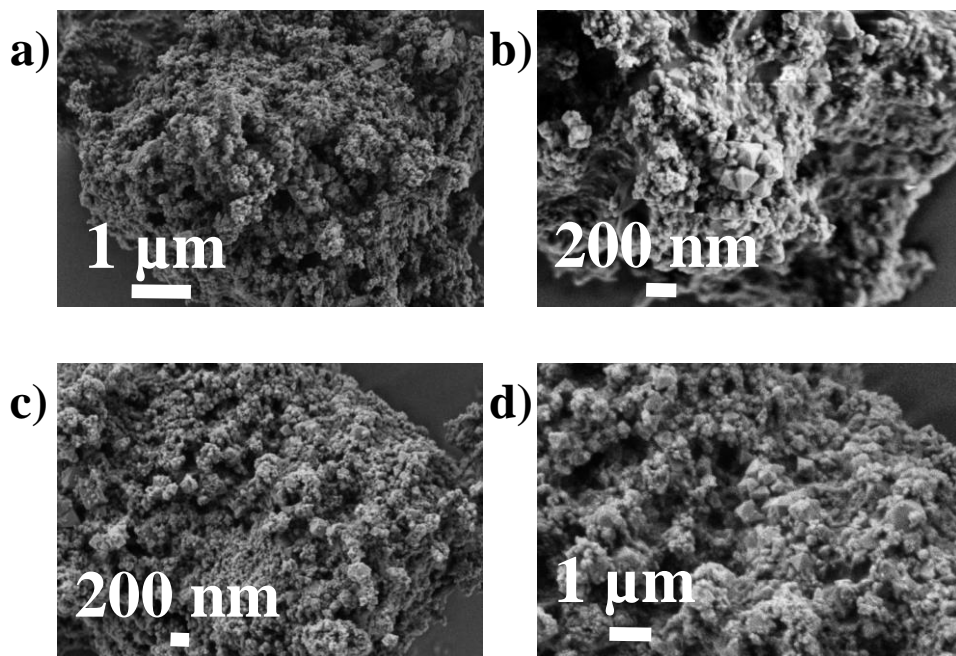


**Fig. S14** SEM images of the fresh MIL-101(Cr)-H catalyst (a, b) or after one use (c, d) as catalyst for the synthesis of **4**. Reaction conditions: **1** (0.5 mmol), **2** (0.55 mmol), catalyst (0.1 mmol of metal), ACN (2 mL).

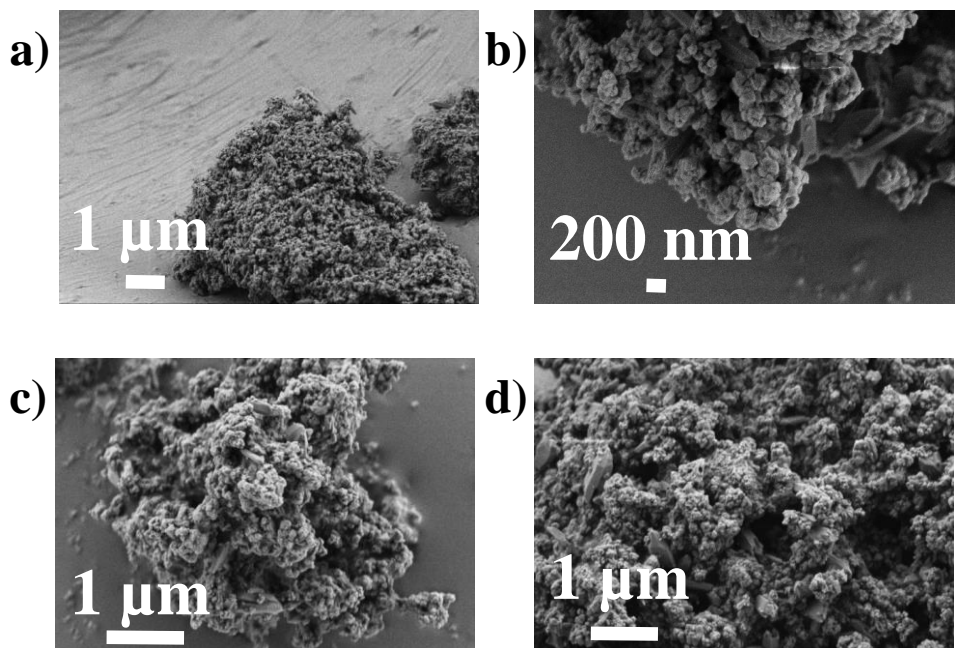


**Fig. S15** SEM images of the fresh MIL-101(Cr)-NH<sub>2</sub> catalyst (a, b) or after one use (c, d) as catalyst for the synthesis of **4**. Reaction conditions: **1** (0.5 mmol), **2** (0.55 mmol), catalyst (0.1 mmol of metal), ACN (2 mL).



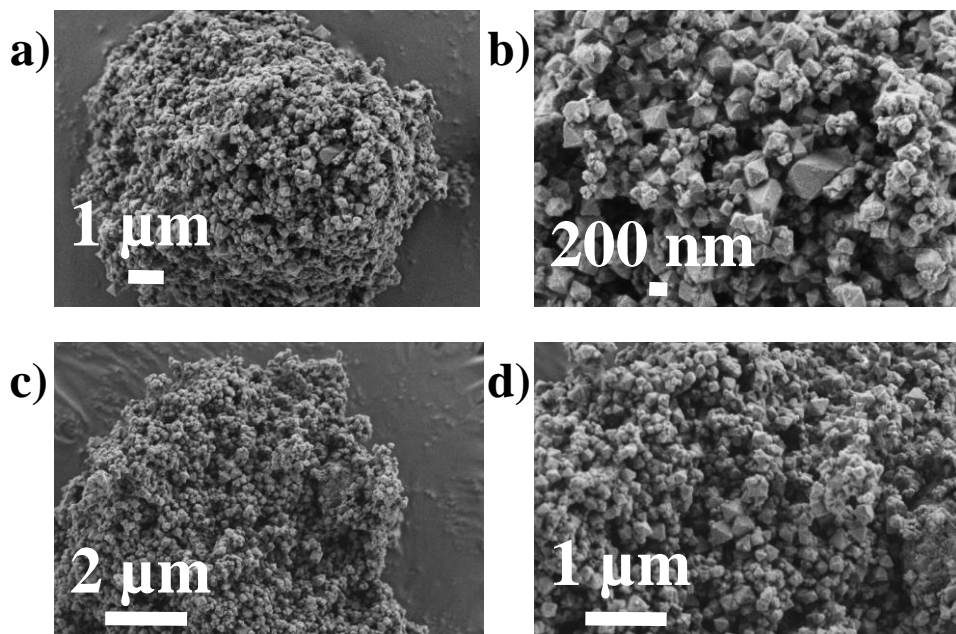


**Fig. S16** SEM images of the fresh MIL-101(Cr)-SO<sub>3</sub>H catalyst (a, b) or (c, d) after one use (c, d) as catalyst for the synthesis of **4**. Reaction conditions: **1** (0.5 mmol), **2** (0.55 mmol), catalyst (0.1 mmol of metal), ACN (2 mL).

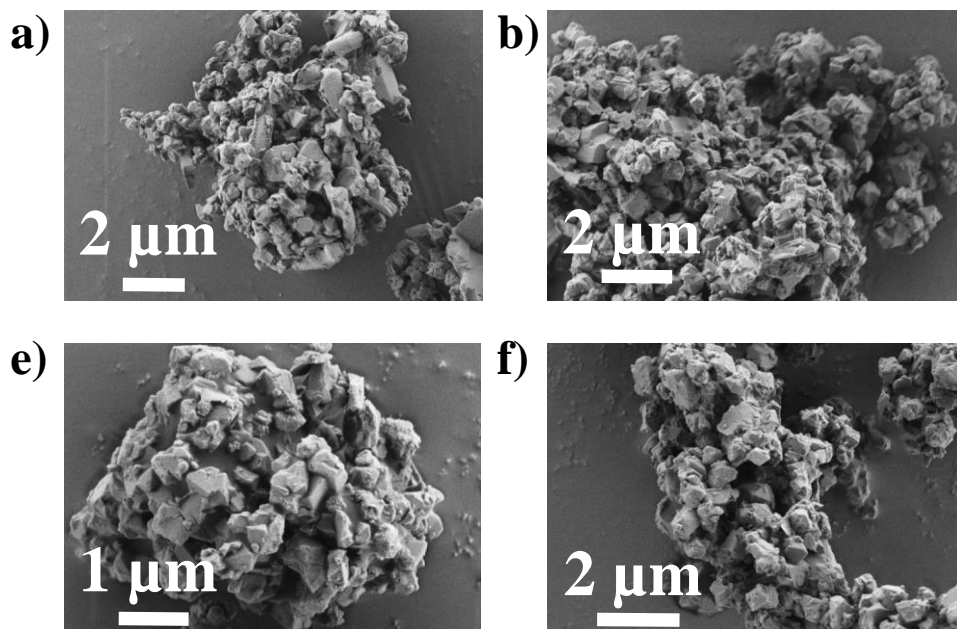


**Fig. S17** SEM images of the fresh MIL-100(Fe) catalyst (a, b) or after one use (c, d) as catalyst for the synthesis of **4**. Reaction conditions: **1** (0.5 mmol), **2** (0.55 mmol), catalyst (0.1 mmol of metal), ACN (2 mL).

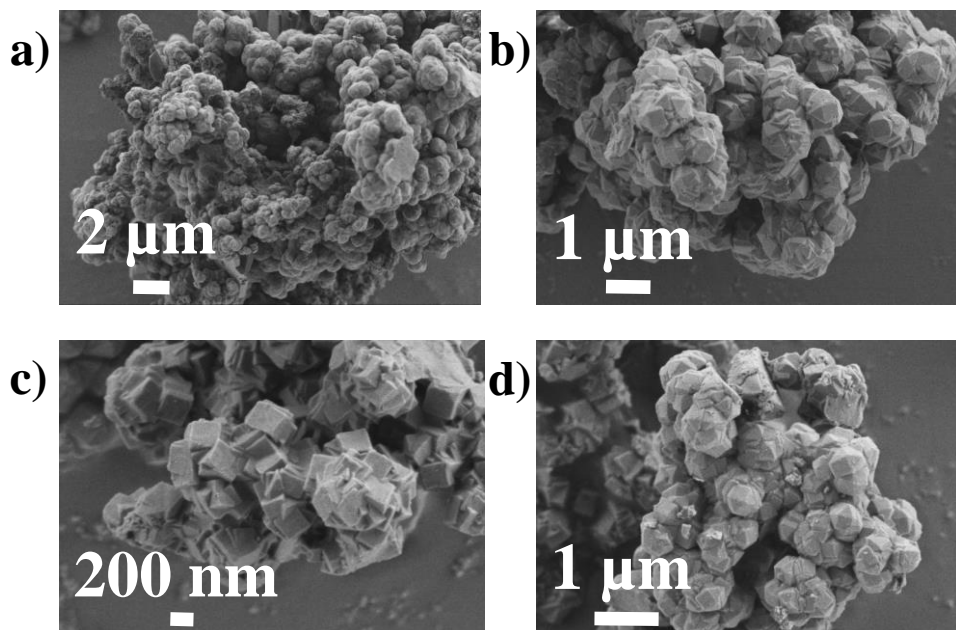


**Fig. S18** SEM images of the fresh UiO66(Zr)-H catalyst (a, b) or after one use (c, d) as catalyst for the synthesis of **4**. Reaction conditions: **1** (0.5 mmol), **2** (0.55 mmol), catalyst (0.1 mmol of metal), ACN (2 mL).

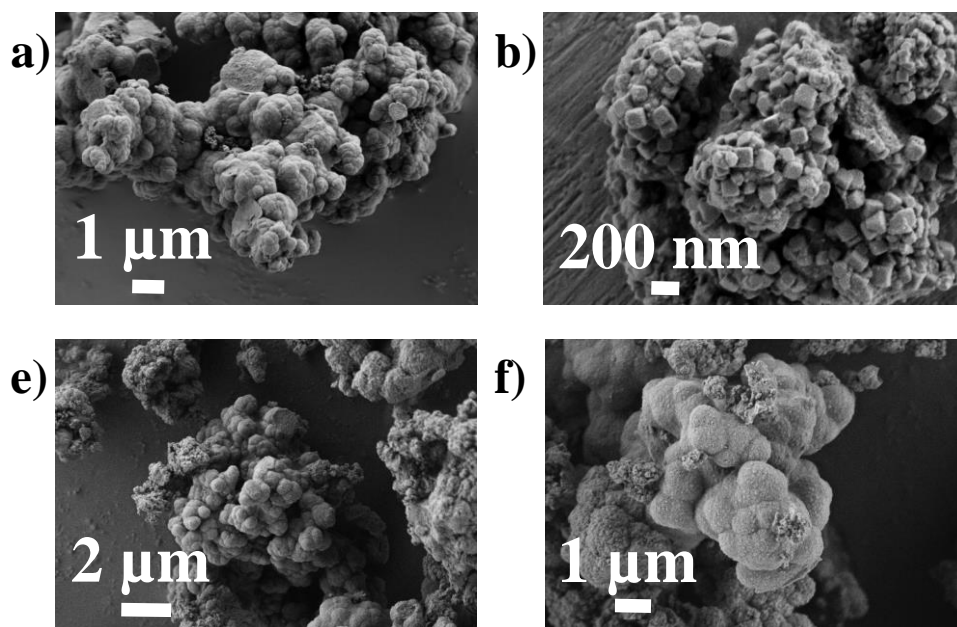


**Fig. S19** SEM images of the fresh UiO66(Zr)-NO<sub>2</sub> catalyst (a, b) or after one use (c, d) as catalyst for the synthesis of **4**. Reaction conditions: **1** (0.5 mmol), **2** (0.55 mmol), catalyst (0.1 mmol of metal), ACN (2 mL).

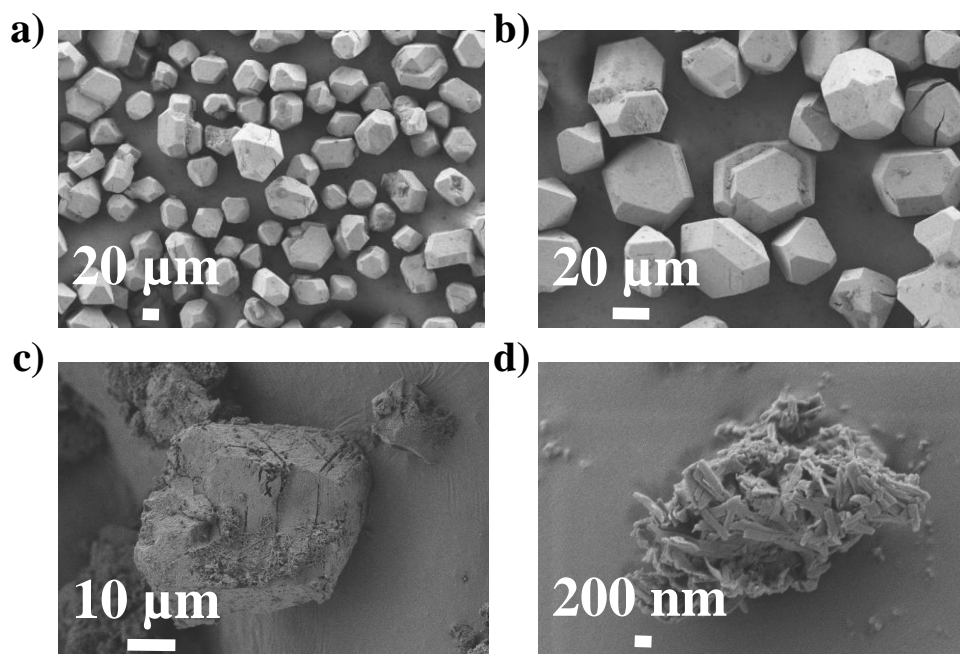


**Fig. S20** SEM images of the fresh  $\text{Cu}_3(\text{BTC})_2$  catalyst (a)-(b) or (c, d) after one use as catalyst for the synthesis of **4**. Reaction conditions: **1** (0.5 mmol), **2** (0.55 mmol), catalyst (0.1 mmol of metal), ACN (2 mL).

**Table S1.** TON and TOF values for the different catalysts under study.<sup>a</sup>

Entry	Catalyst	TON	TOF ( $\text{h}^{-1}$ )
1	MIL-101(Cr)-NO <sub>2</sub>	4.1	13.2 <sup>c</sup>
2	MIL-101(Cr)-SO <sub>3</sub> H	3.3	2.0 <sup>d</sup>
3	MIL-101(Cr)-NH <sub>2</sub>	2.0	3.0 <sup>c</sup>
4	MIL-100(Fe)	2.7	1.7 <sup>d</sup>
5	UiO-66(Zr)	0.9	0.8 <sup>d</sup>
6	UiO-66(Zr)-NO <sub>2</sub>	2.9	0.9 <sup>d</sup>
7	$\text{Cu}_3(\text{BTC})_2$	2.5	0.6 <sup>d</sup>
8	$\text{Cr}_2\text{O}_3$	2.5	2.0 <sup>d</sup>
9	$\text{Cr}(\text{OAc})_3$	2.3	2.6 <sup>d</sup>
10	MIL-101(Cr)-NO <sub>2</sub> <sup>b</sup>	4.5	14.4 <sup>c</sup>

<sup>a</sup>Reaction condition: **1** (0.5 mmol), **2** (0.55 mmol), catalyst (30 mg, 0.1 mmol of metal, 20 wt%), solvent (2 mL), reaction temperature (70 °C).

<sup>b</sup>Reaction was performed in the pure oxygen atmosphere.

<sup>c</sup>Values at 0.25 h.

<sup>d</sup>Values at 1h.

**Table S2** Elemental analysis of fresh MIL-101(Cr)-NO<sub>2</sub> catalyst and after being used before and after washings. The data show that after the washing there is still NH<sub>2</sub> adsorbed in the catalyst. Reaction conditions: **1** (0.5 mmol), **2** (0.55 mmol), catalyst (30 mg), ACN (2 mL).

	N %	C %	H %	O %
Fresh catalyst	4.5	34	2.7	58.8
Catalyst before washed	10.5	57.4	3.6	28.5
Catalyst After washed	6.3	36.5	2.4	54.8

**Chapter 5. MIL-101(Cr)-NO<sub>2</sub> as efficient  
catalysts for the aerobic oxidation of thiophenols  
and the oxidative desulfurization of  
dibenzothiophenes**





# MIL-101(Cr)-NO<sub>2</sub> as efficient catalyts fot the aerobic oxidation of thiophenols and the oxidative desulfurization of dibenzothiophenes.

Cristina Vallés-García,<sup>a</sup> Andrea Santiago-Portillo,<sup>a</sup> Mercedes Álvaro,<sup>a</sup> Sergio Navalón,<sup>a,\*</sup> Hermenegildo García<sup>a,b,c,\*</sup>

<sup>a</sup> Departamento de Química, Universitat Politècnica de València, C/Camino de Vera s/n, 46022, Valencia, Spain.

<sup>b</sup> Instituto de Tecnología Química CSIC-UPV, Universitat Politècnica de València, Consejo Superior de Investigaciones Científicas, Av. de los Naranjos s/n, 46022 Valencia, Spain.

<sup>c</sup> Center of Excellence for Advanced Materials Research, King Abdulaziz University, Jeddah, Saudi Arabia.

Published online: July 30, 2019

(Reprinted with permission from *Appl. Catal. A-Gen*, 2020, **590**, 117340.

Copyright © 2020, Elsevier. All rights reserved.)



## 5.1 Abstract

A series of MIL-101(Cr)-X functionalized with electron withdrawing ( $\text{NO}_2$ ,  $\text{SO}_3\text{H}$  or  $\text{Cl}$ ) or electron donor ( $\text{NH}_2$  or  $\text{CH}_3$ ) groups has been tested for the solvent-free oxidative coupling of thiophenol to disulfides. No byproducts were observed. A relationship between the catalytic activity of these MOFs with the substituent meta Hammett constant on the terephthalate ligand and with their redox potential was found, MIL-101(Cr)- $\text{NO}_2$  being the most active catalyst.  $\text{NO}_2$ -substituted MIL-101 is also more efficient than the parent MIL-101(Cr) to promote the aerobic desulfurization of dibenzothiophenes in n-dodecane or commercial diesel as solvent. No byproduct formation was observed. Mechanistic studies reveal that MIL-101(Cr)- $\text{NO}_2$  is acting as heterogeneous catalyst in thiophenol oxidation and as radical initiator for the aerobic desulfurization. For both reactions, the catalyst can be reused without deactivation, maintaining its crystallinity and with negligible metal leaching.

## 5.2 Introduction

Metal-organic frameworks (MOFs) are a class of crystalline porous materials constituted by metal ions or metal clusters coordinated to multipodal organic ligands<sup>1-5</sup>. Since the first reports about the preparation and characterization of MOFs at the end of 90s, a vast number of these materials combining many types of organic linkers and inorganic units have been reported.<sup>6,7</sup> MOFs have found applications in different areas<sup>8</sup> including adsorption and separation<sup>9,10</sup>, catalysis<sup>11,12</sup>, photocatalysis<sup>13</sup>, sensing<sup>14,15</sup> or biological applications<sup>16</sup>, among others. The superior catalytic activity of MOFs respect to other alternative solids has been frequently reported.<sup>17-20</sup>

In particular, the interest of MOFs as heterogeneous catalysts is continuously increasing due to their fascinating possibilities to tune their composition and structure to each specific reaction.<sup>21-30</sup> Among them, MIL-101(Cr) (MIL: Matériaux de l'institut Lavoisier) prepared by Férey and co-workers has attracted a large interest due to its remarkable porosity, surface area and structural stability.<sup>1</sup> MIL-101(Cr) is constituted by terephthalate ligands and Cr<sub>3</sub>-μ<sub>3</sub>O-carboxylate nodes where octahedrally coordinated metal ions are bond to carboxylate groups and to water molecule or one fluoride ion.<sup>1,31,32</sup>

Assembly of the nodes and linkers results in supertetrahedral units forming two mesoporous cavities of 1.6 and 1.2 nm diameter accessible through hexagonal (8.6 Å) and pentagonal (5.5 Å) windows, respectively (Fig. 1a). The wide MIL-101(Cr) windows allow the diffusion of substrates through the large surface area (2700 m<sup>2</sup> g<sup>-1</sup>) and pore volume (2.1 cm<sup>3</sup> g<sup>-1</sup>) of the solid. Of special interest in catalysis is the possibility to remove adsorbed molecules present in the MOF by thermal treatment (150 °C) under vacuum resulting in the formation of coordinatively unsaturated sites (CUS) that can act as Lewis acid or redox centers (Fig. 1b).<sup>33,34</sup> More recently it has been reported that the presence of electron donor and electron acceptor functional groups at the terephthalate linker can tune the Lewis acidity<sup>35</sup> and the redox properties<sup>36</sup> of MIL-101(Cr) metallic nodes. In particular, the NO<sub>2</sub> substitution on the terephthalate linker enhances the catalytic activity with respect to the parent terephthalate for three common Lewis-catalyzed reactions as well as for the oxidative coupling of benzylamine using molecular oxygen as oxidant (Fig. 1).<sup>35,36</sup>

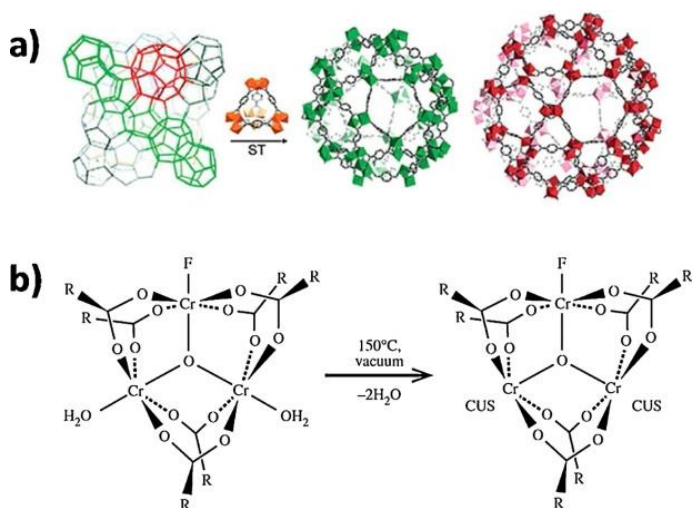


**Fig. 1** a) Schematic 3D representation of the MIL-101 structure made of smaller (green) and larger (red) cages connected through supertetrahedra (ST). Left: the ensemble of the two types of cages. Right: isolated cages of each type of cavity. b) Formation of CUS in the MIL-101(Cr) metal node by thermal treatment under vacuum. (For interpretation of the references to colour in this figure legend, the reader is referred to the web version of this article). Reprinted with permission from ref. 1

In previous studies, some of us have reported the aerobic oxidation of organosulfur compounds using MIL-101(Cr or Fe) and MIL-100(Fe).<sup>37</sup> MIL-100(Fe) (BET 1800 m<sup>2</sup> g<sup>-1</sup> and 0.9 cm<sup>3</sup> g<sup>-1</sup> pore volume) is a MOF constituted by benzene-1,3,5-tricarboxylate as ligand and Fe<sub>3</sub>-μ<sub>3</sub>O as metal nodes. In particular, MIL-101(Cr) solid has been reported as a stable catalyst to promote the aerobic oxidative desulfurization of di-benzothiophenes in n-dodecane or diesel.<sup>38</sup> The applicability of the system is, however, somehow limited due to the need of long reaction times, especially in diesel solution (~ 48 h). In other study, the aerobic oxidation of thiols to disulfides was promoted by MIL-100(Fe) as catalyst in acetonitrile as solvent and molecular oxygen as oxidant.<sup>39</sup> Regardless the good results obtained in that study, it is always of interest to develop alternative system to perform the reaction under solvent-free conditions, while still presenting a high catalytic activity.

With these precedents, in the present work it is reported that MIL-101(Cr)-NO<sub>2</sub> solid while still stable is more efficient catalyst than the parent MIL-101(Cr) to promote both the solvent-free oxidative coupling of thiophenols to disulfides and the aerobic oxidative desulfurization of fuels using dibenzothiophenes as model substrates in n-dodecane or commercial diesel as solvent. Importantly, the catalytic activity of MIL-101(Cr)-NO<sub>2</sub> is higher than that of isorecticular MIL-101(Cr)-X (X: SO<sub>3</sub>H, Cl, CH<sub>3</sub>, H), MIL-100(Fe) solid, or the corresponding Cr<sub>2</sub>O<sub>3</sub> oxide. Importantly, the activity of MIL-101(Cr)-NO<sub>2</sub> is higher or comparable to that obtained using the homogeneous chromium acetate salt. In addition, MIL-101(Cr)-NO<sub>2</sub> can be reused several times for both reactions without observing decrease of the resulting catalytic activity or metal leaching from the solid to the solution and maintaining the initial crystallinity of the solid.

## **5.3 Materials and methods**

### **5.3.1 Materials**

The reagents such as Cr<sub>2</sub>O<sub>3</sub> powder (ref. 393,703) and solvents employed in the present study were of analytical or HPLC grade and supplied by Sigma-Aldrich. Commercial diesel was provided by Repsol. The MIL-101(Cr)-X (X: NO<sub>2</sub>, SO<sub>3</sub>H, Cl, CH<sub>3</sub>, NH<sub>2</sub>) materials employed in this work are the same batch as those previously prepared and characterized by us (see Fig. S1 in supporting information for XRD patterns of the samples used).<sup>35,36</sup>

### **5.3.2 Catalyst characterization**

Powder XRD measurements were recorded with a Philips XPert diffractometer equipped with a graphite monochromator (40 kV and 45 mA) employing Ni-filtered CuK<sub>α</sub> radiation.

### 5.3.3 Catalytic experiments

The corresponding amount of catalyst (i.e. 20 mg) was previously dried in an oven at 100 °C for 24 h and, then, immediately introduced in a dried two neck round-bottom flask (25 mL). The catalyst was further activated by heating at 150 °C under vacuum for 12 h. Subsequently, the flask was heated at the reaction temperature (120, 130, 140 or 150 °C). The required reaction atmosphere was obtained by purging the system with a balloon containing molecular O<sub>2</sub> or Ar. In the case of the aerobic oxidation of thiophenol the reaction started by the addition of the substrate (20 mmol). In the case of the aerobic oxidation of dibenzothiophenes (DBTs) the reaction started by the addition of a solution of DBT (200 mg L<sup>-1</sup>; 20 mL) prepared in n-dodecane or commercial diesel. During the catalytic experiments the reactions were magnetically stirred at 500 rpm with a magnetic bar.

To study the catalyst reusability, the catalyst was recovered at the end of the reaction by filtration, washed with acetonitrile (thiophenol oxidation) or with thioanisole and acetonitrile (DBT oxidation) and, then, dried before use in a new catalytic cycle.

The reactions have been carried out at least in duplicate. The catalytic data presented in this article corresponds to the average values of independent runs. Standard deviations have been included in the plots. In all cases, mass balances were higher than 95 %.

### 5.3.4 Product analysis

Aliquots of the reaction mixture (100 µL) at different times were diluted in 2 ml of a solution of acetonitrile (for thiophenol oxidation) or anisole (for the oxidative desulfurization of DBT) containing a known amount of nitrobenzene as external

standard. Subsequently, the samples were filtered to remove the catalyst (Nylon filter 0.2  $\mu\text{m}$  adapted to a syringe) and analyzed by gas chromatography (GC) using a flame ionization detector and a methyl-phenyl silicone column (TRB-5MS; 30 m x 0.32 mm x 0.25  $\mu\text{m}$ ). Quantification was carried out by using calibration curves of commercial samples and nitrobenzene as the standard. Identity of the products was confirmed by injecting the mixture in a GC–MS (Agilent 5973) with quadrupole and comparing the retention time with authentic samples.

Analyses of the posible metal leaching were carried out at the end of the reaction by quantitative ICP-OES determination. Briefly, at the end of the reaction the catalyst was removed by filtration using a 0.2  $\mu\text{m}$  Nylon filter. Then, a nitric acid aqueous solution (30 mL, 3 M) was added to the organic phase and the System heated under magnetic stirring at 80  $^{\circ}\text{C}$  for 24 h. Finally, the aqueous phase was analyzed by ICP-OES.

## **5.4 Results and discussion**

### **5.4.1 Catalyst properties**

As commented before, the catalysts employed for this study are from the same batch that those previously reported by some of us.<sup>35,36</sup> Table 1 summarizes the composition and porosity of these solids employed in the present study. Commercially available  $\text{Cr}_2\text{O}_3$  powder was also employed as catalyst for comparison.



**Table 1** List of catalysts employed in the present study<sup>a</sup>

Catalyst / Formula <sup>b</sup>	BET surface area (m <sup>2</sup> g <sup>-1</sup> )	Pore volume (cm <sup>3</sup> g <sup>-1</sup> )
MIL-101(Cr)-H {Cr <sub>3</sub> F(H <sub>2</sub> O) <sub>2</sub> O(bdc) <sub>3</sub> }	2750	2.2
MIL-101(Cr)-NO <sub>2</sub> {Cr <sub>3</sub> Cl(H <sub>2</sub> O) <sub>2</sub> O(bdc-NO <sub>2</sub> ) <sub>3</sub> }	1850	1.3
MIL-101(Cr)-SO <sub>3</sub> H {Cr <sub>3</sub> Cl(H <sub>2</sub> O) <sub>2</sub> O(bdc-SO <sub>3</sub> H) <sub>3</sub> }	1900	1.4
MIL-101(Cr)-Cl {Cr <sub>3</sub> Cl(H <sub>2</sub> O) <sub>2</sub> O(bdc-Cl) <sub>3</sub> }	1300	1.1
MIL-101(Cr)-CH <sub>3</sub> {Cr <sub>3</sub> Cl(H <sub>2</sub> O) <sub>2</sub> O(bdc-CH <sub>3</sub> ) <sub>3</sub> }	1800	1.8
MIL-101(Cr)-NH <sub>2</sub> {Cr <sub>3</sub> Cl(H <sub>2</sub> O) <sub>2</sub> O(bdc-NH <sub>2</sub> ) <sub>3</sub> }	1950	2.0
MIL-100(Fe) {Fe <sub>3</sub> Cl(H <sub>2</sub> O) <sub>2</sub> O(btc) <sub>3</sub> }	1700	0.8

<sup>a</sup> For preparation and additional characterization data see refs.<sup>35,36</sup>

<sup>b</sup> bdc: benzenedicarboxylate; btc: 1,3,5-benzenetricarboxylate.

### 5.4.2 Aerobic oxidation of thiophenols to disulfides

As commented in the introduction, the MIL-101(Cr) and MIL100(Fe) materials are characterized by their excellent chemical and thermal stability and the possibility to be employed for the molecular oxygen activation.<sup>35,37,38</sup> With these precedents, in the first stage of this work, the influence of substituents at the 1,4-benzenedicarboxylate (bdc) linkers on the catalytic activity of MIL-101(Cr)-X (X: NO<sub>2</sub>, SO<sub>3</sub>H, Cl, CH<sub>3</sub>, NH<sub>2</sub>) for the solvent-free aerobic oxidative coupling of thiophenol to diphenyl disulphide was explored. Previous studies have established that the functionalization of the terephthalate organic ligand of the MIL-101(Cr) with electron donor or electron withdrawing groups influences the redox properties of the metal nodes and, therefore, their catalytic activity for oxidation reactions.<sup>36</sup> A blank control in the absence of catalyst reveals that thiophenol conversion is lesser than 12 % under the reaction conditions employed in the study. This observation can be attributed to the occurrence of same degree of spontaneous autoxidation.<sup>37</sup> The presence of several substituents in the organic ligand of the MIL-101(Cr)-X (X: NO<sub>2</sub>, SO<sub>3</sub>H, Cl, H, CH<sub>3</sub>, NH<sub>2</sub>) influences both the initial reaction rate and the substrate conversion at a given reaction time (Fig. 2). In all cases the only observed product was diphenyl

disulphide with complete selectivity and mass balances, without observation of any byproduct formation. MIL-101(Cr)-NO<sub>2</sub> resulted the most active catalyst to promote the solvent-free aerobic oxidation of thiophenol with an initial reaction rate 4 times higher than that of the parent MIL-101(Cr)-H and a final yield at 24 h of 90 %, about 3 times higher than that of the parent MIL-101(Cr)-H.

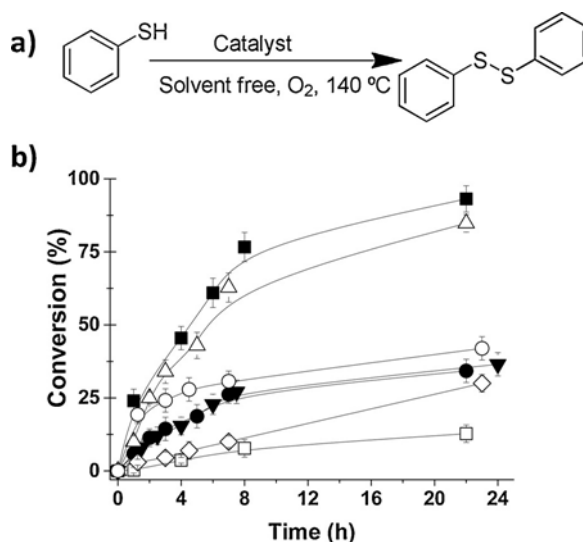


**Fig. 2** a) Oxidative coupling of the aerobic oxidation of thiophenol to diphenyl disulphide by oxygen. b) Time-conversion plot for the aerobic oxidation of thiophenol to diphenyl disulphide using MIL-101(Cr)-H (●), MIL-101(Cr)-SO<sub>3</sub>H (Δ), MIL-101(Cr)-Cl (○), MIL-101(Cr)-NO<sub>2</sub> (■), MIL-101(Cr)-NH<sub>2</sub> (▼), MIL-101(Cr)-CH<sub>3</sub> (◇) and without catalyst (□). Reaction conditions: Catalyst (0.04 mmol Cr), thiophenol (2 mL, 20 mmol), O<sub>2</sub> atmosphere (balloon), reaction temperature (140 °C).

In order to understand the observed catalytic activity using the series of MIL-101(Cr)-X (X: NO<sub>2</sub>, SO<sub>3</sub>H, Cl, H, CH<sub>3</sub>, NH<sub>2</sub>) solids, the logarithm of the relative first order rate constant ( $k_x/k_0$ ) as a function of the different meta Hammett constant for each substituent in MIL-101(Cr)-X catalysts was plotted. A good linear relationship between  $\log k_x/k_H$  vs  $\sigma_m$  was observed for the MIL-101(Cr)-X catalysts having both electron donor or electron withdrawing groups in the

organic ligand. This observation is compatible with previous reports showing that the presence of electron donor or electron withdrawing groups at the organic ligand of the MIL-101(Cr) solids decreases or increases, respectively, the Lewis acidity of the metal center, due to inductive effects of the terephthalate linker on the metal ions of the nodes.<sup>35,36,40</sup> In connection with the previous finding, a good relationship between the initial reaction rate and the reported oxidation potential of the MIL-101(Cr)-X (X: H, NO<sub>2</sub>, SO<sub>3</sub>H, Cl) was also found here, the higher the redox potential the higher the catalytic activity (Fig. 3).

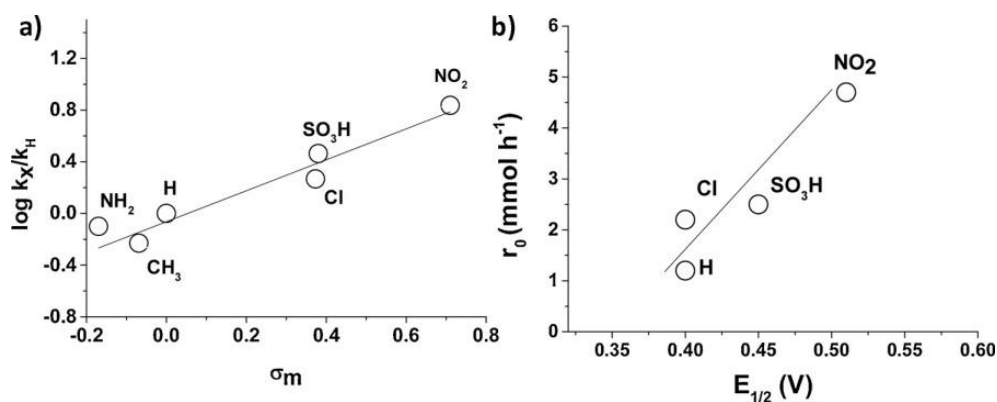


**Fig. 3** a) Plot of the logarithm of the relative first order rate constant measured at initial reaction time for thiophenol oxidation versus the meta Hammett constant of each substituent on the terephthalate linker of MIL-101(Cr)-X solids; Regression coefficient (R<sup>2</sup>) 0.9147; b) Plot of the initial reaction rate versus the halfwave potential ( $E_{1/2}$ ) for the aerobic oxidation of thiophenol promoted by MIL-101(Cr)-X solids with different substituent at the bdc ligand; Regression coefficient (R<sup>2</sup>) 0.8313.

Importantly, the initial reaction rate for thiophenol conversion using MIL-101(Cr)-NO<sub>2</sub> is five times higher than that of the homogeneous chromium acetate and six-times higher than that of the heterogeneous Cr<sub>2</sub>O<sub>3</sub>. This comparison highlights the benefits of using functionalized MIL-101(Cr)-X solid with nitro groups as heterogeneous catalysts respect to the use of analogous

soluble metal salts or heterogeneous metal oxides. Even though MIL-100(Fe) solid possesses higher Lewis acidity and, therefore, catalytic activity ( $r_0$  1.21  $\text{mM h}^{-1}$ ) than MIL-101(Cr)-H ( $r_0$  1.13  $\text{mM h}^{-1}$ ), the presence of the nitro group in the MIL-101(Cr)-NO<sub>2</sub> increases its catalytic activity in a large extent ( $r_0$  4.8  $\text{mM h}^{-1}$ ). The superior catalytic activity observed for MIL-101(Cr)-NO<sub>2</sub> should be a reflection of the higher Lewis acid strength of the Cr<sup>3+</sup> ions with coordinatively unsaturated sites, resulting in a decrease of the apparent activation energy ( $E_a$ ) for the solvent-free aerobic oxidation of thiophenol. From the Arrhenius plot of the influence of the temperature on the reaction rate for MIL-101(Cr)-NO<sub>2</sub> a value of 32  $\text{kJ mol}^{-1}$  was estimated (Fig. 4).

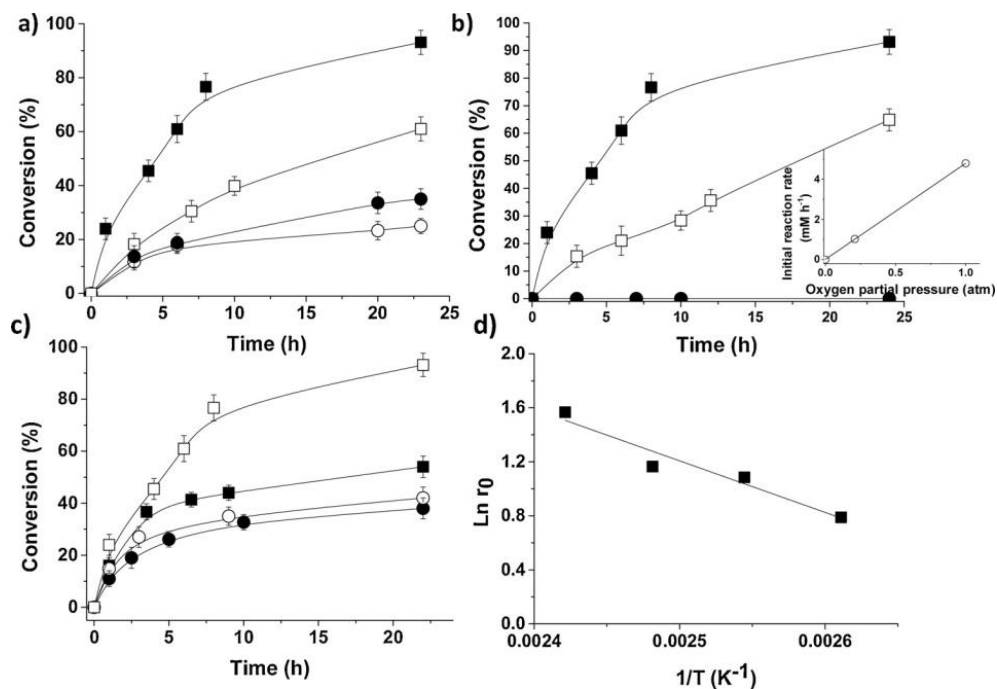


**Fig. 4** a) Comparison of the catalytic activity for the aerobic oxidation of thiophenol to dis- ulphide using MIL-101(Cr)-NO<sub>2</sub> (■), MIL-100(Fe) (□), commercial Cr<sub>2</sub>O<sub>3</sub> (●) or Cr(III) acetate (○). b) Time profile of thiophenol conversion in the presence of O<sub>2</sub> (■), Air (□) or Ar (●). The inset show a plot of the initial reaction rate vs the O<sub>2</sub> pressure showing a first order relationship. c) Time conversion plots for the aerobic oxidation of thiophenol in the presence of MIL-101(Cr)-NO<sub>2</sub> at different

reaction temperatures: 140 °C (□), 130 °C (■), 120 °C (○), 110 °C (●). d) Arrhenius plot of the natural logarithm of the initial reaction rate obtained from panel c versus  $1/T$  ( $K^{-1}$ ). Reaction conditions: catalyst (0.04 mmol Cr), thiophenol (2 mL, 20 mmol),  $O_2$  atmosphere (balloon) and reaction temperature (140 °C for panels a, b); Regression coefficient ( $R^2$ ) 0.9088.

The influence of the reaction atmosphere on the resulting catalytic activity using MIL-101(Cr)- $NO_2$  was evaluated. Fig. 4 shows a good linear relationship between oxygen pressure and the initial reaction rate, indicating that that relation is first order respect to oxygen pressure.

The heterogeneity of the reaction using MIL-101(Cr)- $NO_2$  as catalyst was confirmed by performing the so-called hot filtration test. In this experiment the reaction was started under typical conditions and once conversion has reached about 25 %, a portion of the reaction medium is filtered to remove the solid catalyst and placed in a parallel reaction setup and the reaction allowed to proceed further on the absence of any solid. Fig. 5 shows that once the catalyst is removed the reaction stops, confirming that the reaction is truly heterogeneous. Furthermore, the stability of the MIL-101(Cr)- $NO_2$  catalyst was evidenced by performing ten consecutive catalytic reactions without observing any decrease of the catalytic activity. Powder XRD measurements of the fresh and used catalysts confirm that the solid retains its initial crystallinity upon reuse. The almost absence of chromium leaching from the solid to the solution at the end of the reaction (ICP-OES analytical data in the supporting information, Table S1) reinforces the stability of the heterogeneous MIL-101(Cr)- $NO_2$  catalyst. Also ICP-OES analysis of the MIL-101(Cr)- $NO_2$  sample after the catalysis confirms that the Cr content of the solid does not decrease after the reaction. To put the stability of MIL-101(Cr)- $NO_2$  into context, it should be commented that  $Cu_3(btc)_2$ , also frequently reported as catalyst, undergoes a complete decomposition in a single run under similar conditions.<sup>41</sup> Fig. S3 in supporting information provides a comparison of the SEM images of the fresh

and reused MIL-101(Cr)-NO<sub>2</sub> catalyst showing no significant changes in morphology.

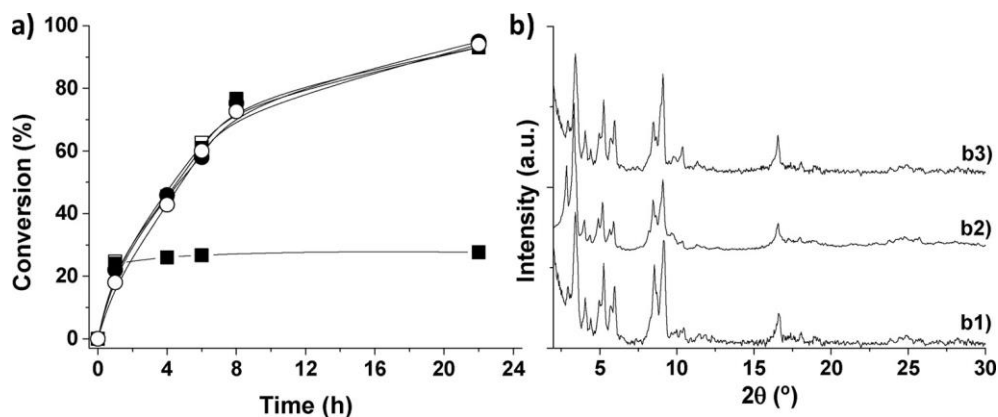


**Fig. 5** a) Hot filtration test (black squares) and reusability experiments (ten times, open circles) for the aerobic oxidation of thiophenol to disulphide using MIL-101(Cr)-NO<sub>2</sub> as catalyst. b) PXRD of the fresh (b1), six-times (b2) and ten-times (b3) used MIL-101(Cr)-NO<sub>2</sub> catalyst.

To further address catalyst stability, a productivity test in where the amount of substrate was increased by a factor of 25 times and the reaction was allowed running for more than three weeks was performed. The results are present in the Fig. S7 in supporting information. No deactivation was observed even under these unfavourable conditions, thus confirming catalyst stability.

Based on the present experimental data and previous results using MIL-101(Cr)-X materials, Fig. 6 summarizes a plausible reaction pathway for the aerobic oxidation of thiophenol to diphenyl disulphide using MIL-101(Cr)-NO<sub>2</sub>. The observation that the higher the electron withdrawing character of the terephthalate substituent in the MIL-101(Cr)-X, the higher the redox potential of the metal center and consequently the higher the catalyst activity is rationalized with the proposed electron transfer process from the electron rich SH functional group to the catalyst.<sup>36</sup> The catalytic cycle is restored by the

presence of  $O_2$  that becomes reduced to  $O_2^{\cdot-}$ . Then, the  $O_2^{\cdot-}$  can lead to the formation of  $HOO^{\cdot}$  radicals that eventually will form  $H_2O_2$  and/or  $H_2O$  by a series of consecutive electron and proton transfer steps through the intermediacy of the corresponding reactive oxygen species.<sup>35,36</sup> It should be noted that any of these reactive oxygen species would react with thiophenol forming the phenylsulfide radical due to the relative strength of O-H bonds respect to SH-bonds.

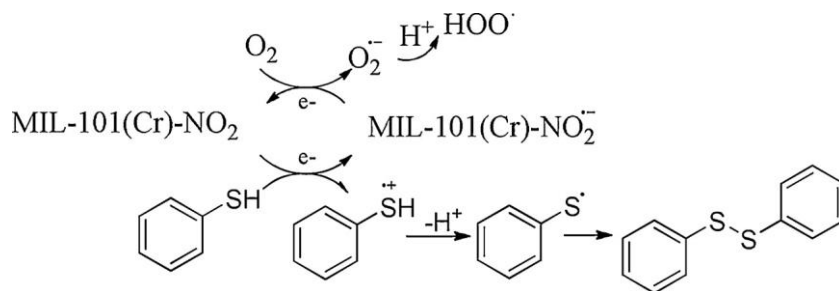


**Fig. 6** Proposed pathway for the aerobic oxidation of thiophenol to benzene disulphide using MIL-101(Cr)-NO<sub>2</sub> as catalyst.

The MIL-101(Cr)-NO<sub>2</sub> can be also employed as catalyst for the solvent-free oxidative coupling of a series substituted thiophenols having electron donor (CH<sub>3</sub>) or electron withdrawing groups (Fig. S2).

### 5.4.3 Aerobic oxidative desulfurization of diesel fractions. Use of DBTs

The second part of the work is focused on the study of the applicability of MIL-101(Cr)-NO<sub>2</sub> solid to promote the aerobic oxidation of DBTs in both n-dodecane or commercial diesel, a process that has been proposed for the deep oxidative desulfurization of gasoil (Fig. 7).<sup>38,42</sup>

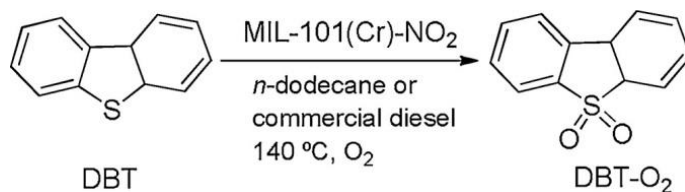


**Fig. 7.** Aerobic oxidation of DBT to DBT-O<sub>2</sub> using MIL-101(Cr)-NO<sub>2</sub> as catalyst.

Initially, a blank control in the absence of catalyst using *n*-dodecane as solvent shows that DBT conversion is less than 10 % under the reaction conditions employed in the present study. Analogously to the results obtained for the aerobic oxidation of thiophenol, it was also observed that the catalytic activity of MIL-101(Cr)-NO<sub>2</sub> is about 3 times higher than that of MIL-101(Cr) to promote the aerobic oxidation of DBT to DBT-O<sub>2</sub> in *n*-dodecane as solvent. Formation of the corresponding DBT sulfoxide or any other byproduct was not observed. In good agreement with this observation, the estimated *E<sub>a</sub>* value for the aerobic oxidation of DBT in *n*-dodecane using MIL-101(Cr)-NO<sub>2</sub> catalyst is lower (117 kJ mol<sup>-1</sup>; Fig. S8) than that previously reported for MIL-101(Cr)-H under the same conditions (137 kJ mol<sup>-1</sup>).<sup>38</sup> SEM analysis of the used MIL-101(Cr)-NO<sub>2</sub> samples at different reaction temperatures does not reveal any significant morphology change respect to the fresh one (Fig. S5-S6). ICP-OES of the acid digested MIL-101(Cr)-NO<sub>2</sub> samples reveal a chromium content of the used samples at different reaction temperatures almost coincident with that of the ideal MOF formula (Cr<sub>3</sub>Cl(H<sub>2</sub>O)<sub>2</sub>O(C<sub>8</sub>H<sub>3</sub>O<sub>4</sub>-NO<sub>2</sub>). Notably, the catalytic activity of MIL-101(Cr)-NO<sub>2</sub> was also higher than that of the MIL-100(Fe) or Cr<sub>2</sub>O<sub>3</sub> solids as heterogeneous catalysts or the soluble Cr(III) acetate salt (Fig. 8).



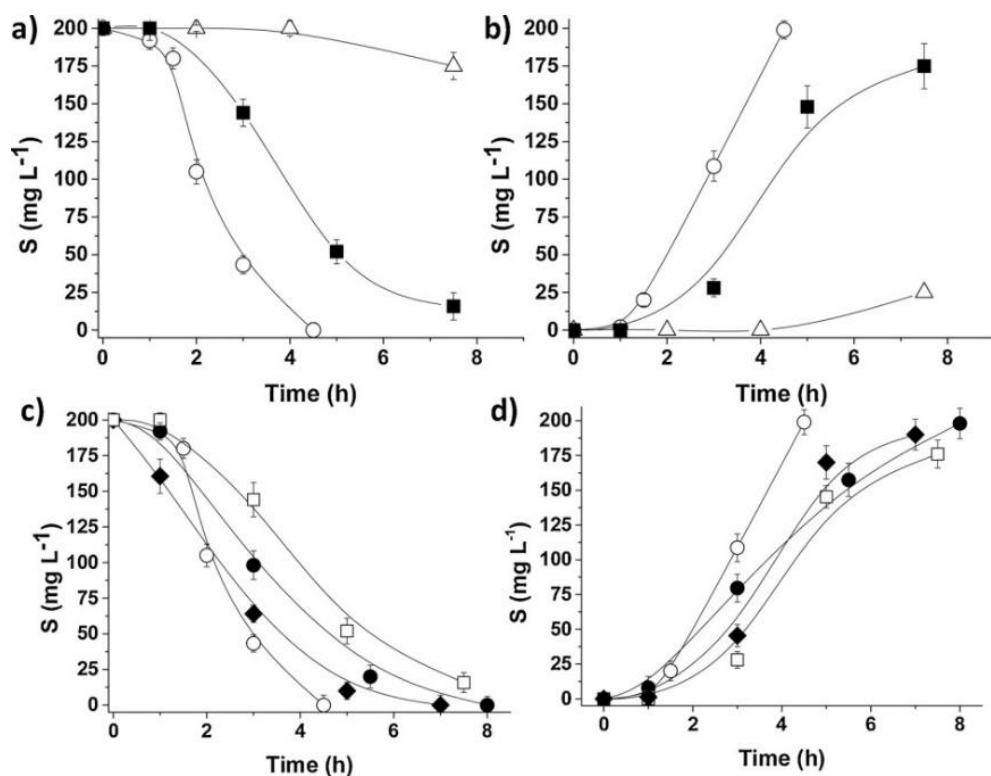


**Fig. 8** DBT oxidation (a, c) to DBT-O<sub>2</sub> (b, d) acetate (◆). A control experiment in the absence of catalyst (Δ) is also shown. Reaction conditions: Catalyst (0.04 mmol Cr), DBT (11.5 mg, 200 ppm S), n-dodecane (10 mL), O<sub>2</sub> atmosphere (balloon), reaction temperature (140 °C).

The stability of the MIL-101(Cr)-NO<sub>2</sub> was assessed by performing five consecutive reaction cycles without observing any decrease of catalytic activity for DBT disappearance or DBT-O<sub>2</sub> formation, while the solid crystallinity is maintained as revealed by powder XRD (Fig. 9).

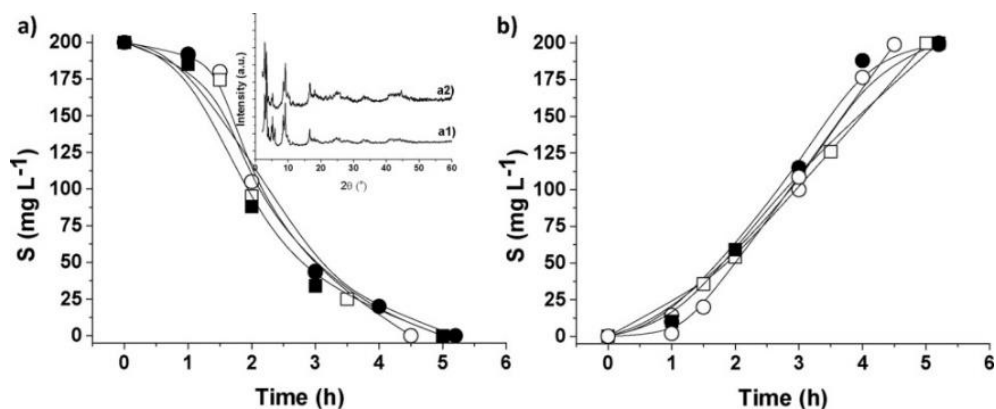


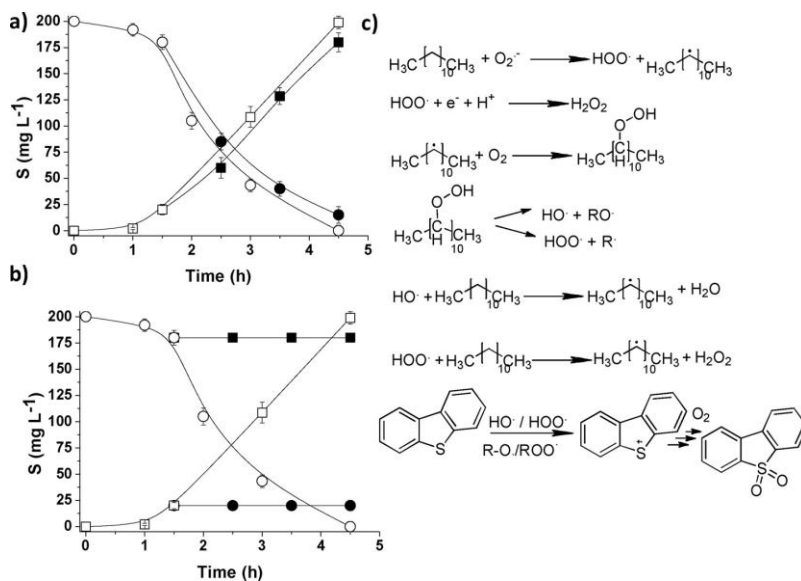
**Fig. 9** Reusability experiments of MIL-101(Cr)-NO<sub>2</sub> for the aerobic oxidation of DBT (a) to DBT-O<sub>2</sub> in n-dodecane as solvent. Legend: 1<sup>st</sup> use (○), 3<sup>th</sup> use (□), 4<sup>th</sup> use (■) and 5<sup>th</sup> use (●). The inset in panel a shows from bottom to top the XRD of the fresh (a1) and three-times used catalyst (a2). Reaction conditions: Catalyst (0.04 mmol Cr), DBT (115 mg), n-dodecane (10 mL), O<sub>2</sub> atmosphere (Ballon), reaction temperature (140 °C).

ICP-OES analysis of the liquid phase at the end of the reaction shows that chromium leaching occurs in negligible amounts (0.7 μg L<sup>-1</sup>; Table S1). Fig. S4 in supporting information provides a comparison of the SEM images of the fresh and used MIL-101(Cr)-NO<sub>2</sub> catalyst.

As in the case of thiophenols, also for DBTs, catalyst stability was confirmed by performing a productivity test, increasing by five times DBT concentration and running the reaction for one week. The temporal profile of this productivity test is presented in Fig. S7. As it can be seen there, even under these unfavourable conditions the MIL-101(Cr)-NO<sub>2</sub> catalyst does not deactivate, and the reaction progresses until complete DBT conversion without any sign of catalyst deactivation. Non-detectable chromium leaching from the solid to the solution was observed under the present reaction conditions. In this case, however, the hot filtration test reveals that the reaction still progresses once the solid catalyst is removed from the reaction. If TEMPO is added to the filtered reaction, however, the reaction stops. In addition, the presence of organic hydroperoxides was

confirmed indirectly by their quenching with  $\text{PPh}_3$  resulting in the formation of  $(\text{Ph}_3)\text{P} = \text{O}$ .<sup>37</sup> Thus, it can be proposed that the MIL-101(Cr)- $\text{NO}_2$  solid is acting in the aerobic oxidation of DBT to DTB- $\text{O}_2$  in n-dodecane as a radical initiator rather than a real catalyst. In addition to DBT oxidation, some solvent oxidation to the positional isomeric ketone derivatives occurs (about 1 %) during the reaction.

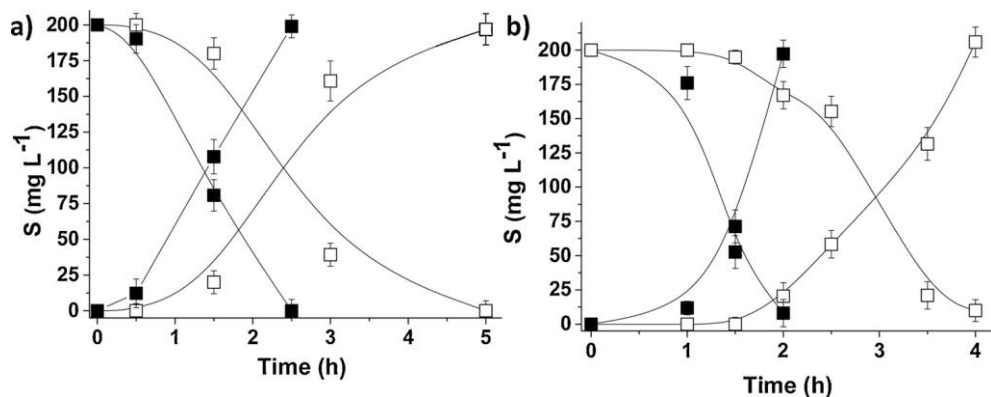
Previous studies have reported that MIL-101(Cr)- $\text{NO}_2$  activates molecular  $\text{O}_2$  leading to the formation of  $\text{O}^{\cdot-}/\text{HOO}^{\cdot}$  species.<sup>35</sup> In this work, a control experiment using an inert  $\text{N}_2$  atmosphere instead  $\text{O}_2$  reveals that the catalytic oxidation does not occur in the absence of  $\text{O}_2$ . With these data Fig. 10c summarizes a plausible reaction mechanism for the aerobic oxidation of DBT to DBT- $\text{O}_2$  by MIL-101(Cr)- $\text{NO}_2$  as radical initiator that is in accordance with previous proposals.<sup>38</sup>



**Fig. 10** a) Hot filtration experiment showing DBT oxidation (○, ●) to DBT- $\text{O}_2$  (□, ■) in the presence of catalyst (open symbols) or once the catalyst is removed by filtration (close symbols). b) Hot filtration experiment showing DBT oxidation (○) to DBT- $\text{O}_2$  (□) in the presence of catalyst (open symbols) or once the catalyst is removed by filtration and TEMPO as radical

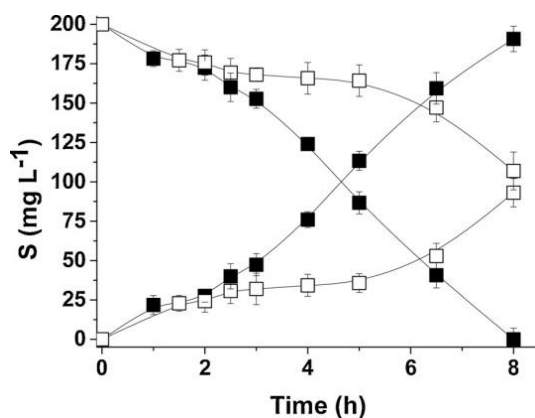
quencher is added (close symbols). Reaction conditions: Catalyst (0.04 mmol Cr), DBT (115 mg), n-dodecane (10 mL), O<sub>2</sub> atmosphere (balloon), reaction temperature (140 °C), when the catalyst is filtered and TEMPO added (20 mol%). c) Proposed pathway for the aerobic oxidative of DBT to DBT-O<sub>2</sub> in the presence of MIL-101(Cr) solid and n-dodecane as solvent.

Fig. 11 shows that MIL-101(Cr)-NO<sub>2</sub> is also catalytically more active than MIL-101(Cr)-H to promote also the 4-MeDBT and 4,6-diMeDBT oxidation to their corresponding sulfones. The observed order of reactivity 4,6-diMeDBT > 4-MeDBT > DBT can be rationalized considering the increase of the electron density on the sulfur atom due to the presence of electron donor methyl groups in positions 4 and/or 6.<sup>38</sup> This relative reactivity order compares favourably respect to the conventional hydrodesulfurization process in which the methyl substituted DBTs are increasingly more difficult to be removed due to steric encumbrance around the S atom, thus requiring high hydrogen pressures (200 atm) combined with high temperatures (> 300 °C) to make 4-MeDBT and 4,6-diMeDBT reactive.<sup>43,44</sup> In addition, the above reactivity in where the electronic density of DBT prevails over kinetic dimensions suggests that the reaction takes place in the same site without diffusion control. Considering the high activity of MIL-101(Cr)-NO<sub>2</sub> as catalyst, the most reasonable sites are those present on the internal pores. Otherwise, either the activity of MIL-101(Cr)-NO<sub>2</sub> would be much lower, or the larger kinetic diameter of methyl substituted DBTs would have made these compounds less reactive due to diffusion limitations less reactive in comparison with the parent DBT.



**Fig. 11** Oxidation of 4-DBT (a) and 4,6-DBT (b) to their corresponding sulfones (a, b) using MIL-101(Cr)-NO<sub>2</sub> (■) or MIL-101(Cr)-H (□). Reaction conditions: Catalyst (0.04 mmol Cr), 4-DBT (200 ppm S) or 4,6-DBT (200 ppm S), n-dodecane (10 mL), O<sub>2</sub> atmosphere (balloon), reaction temperature (140 °C).

Importantly, the oxidative desulfurization of DBT using MIL-101(Cr)-NO<sub>2</sub> as catalyst can be carried out efficiently in commercial diesel exhibiting higher activity respect to MIL-101(Cr)-H (Fig. 12). The increase of reaction time required for the conversion of DBT and formation of DBT-O<sub>2</sub> in commercial diesel respect to the n-dodecane is easily rationalised considering the chain length in diesel that is constituted by a complex mixture of alkanes and/or the presence antioxidant additives. In any case, oxidative desulfurization process is about two times higher using MIL-101(Cr)-NO<sub>2</sub> as catalyst respect to its parent MIL-101(Cr)-H.<sup>38</sup>



**Fig. 12** Aerobic oxidation of DBT to DBT-O<sub>2</sub> using MIL-101(Cr)-NO<sub>2</sub> (■) or MIL-101(Cr) (□) in commercial diesel as solvent. Reaction conditions: Catalyst (0.04 mmol Cr), DBT (200 ppm S), diesel (10 mL), O<sub>2</sub> atmosphere (balloon), reaction temperature (140 °C).

## 5.5 Conclusions

The present work has shown that the catalytic activity of the benchmark MIL-101(Cr)-H MOF can be tuned by the presence of electron donor (CH<sub>3</sub> or NH<sub>2</sub>) or withdrawing (NO<sub>2</sub>, Cl or SO<sub>3</sub>H) substituents on the terephthalate organic ligand. MIL-101(Cr)-NO<sub>2</sub> is the most active catalyst of the series by a factor of 4 and 3 respect to MIL-101(Cr)-H, promoting the solvent-free aerobic oxidation of benzenethiol to diphenylsulfide and the aerobic oxidation of dibenzothiophenes in n-dodecane or commercial diesel, respectively. No new products were observed for any of two reactions. The activity of MIL-101(Cr)-NO<sub>2</sub> is also higher than MIL-101(Fe), Cr<sub>2</sub>O<sub>3</sub> or soluble Cr(III) salts for the aerobic oxidation of thiophenol and the aerobic desulfurization of dibenzothiophenes. Catalytic experiments reveal that MIL-101(Cr)-NO<sub>2</sub> is acting as a truly heterogeneous catalyst in the case of aerobic oxidation of thiophenol, while for the oxidation of dibenzothiophenes it is acting as a radical initiator. For both processes, the catalyst can be reused several times without any decrease in activity, maintaining its initial crystallinity with negligible metal leaching. In summary, this work

exemplifies how the activity of the benchmark MIL-101(Cr) solid to promote oxidations using exclusively molecular oxygen can be enhanced by introducing NO<sub>2</sub> groups on the organic ligand.

## 5.6 Acknowledgements

Financial support by the Spanish Ministry of Science and Innovation (Severo Ochoa and RTI2018-098237-CO21) and Generalitat Valenciana (Prometeo 2017/083) is gratefully acknowledged. S.N. thanks financial support by the Fundación Ramón Areces (XVIII Concurso Nacional para la Adjudicación de Ayudas a la Investigación en Ciencias de la Vida y de la Materia, 2016), Ministerio de Ciencia, Innovación y Universidades CTQ-2018 RTI2018-099482-A-I00 project and Generalitat Valenciana grupos de investigación consolidables 2019 (AICO2019/214 project).

## 5.7 Reference

1. G. Férey, C. Mellot-Draznieks, C. Serre, F. Millange, J. Dutour, S. Surble, and I. Margiolaki, *Science*, 2005, **309**, 2040-2042.
2. H. Furukawa, K.E. Cordova, M. O’Keeffe and O.M. Yaghi, *Science*, 2013 **341**, 1230444.
3. M. Eddaoudi, J. Kim, N. Rosi, D. Vodak, J. Wachter, M. O’Keeffe and O.M. Yaghi, *Science*, 2002, **295**, 469-472.
4. S. Kitagawa, R. Kitaura and S.-I. Noro, *Angew. Chem., Int. Ed.* 2004, **43**, 2237-2334.
5. O.M. Yaghi, M. O’Keeffe, N.W. Ockwig, H.K. Chae, M. Eddaoudi and J. Kim, *Nature*, 2003, **423**, 705-714.
6. T. Devic and C. Serre, *Chem.Soc.Rev.* 2014, **43**, 6097-6115.
7. N. Stock and S. Biswas, *Chem. Rev.* 2012, **112**, 933-969.
8. P. Silva, S.M.F. Vilela, J.P.C. Tomé and F.A. Almeida Paz, *Chem. Soc. Rev.* 2015, **44**, 6774-6803.
9. J.-R. Li, J. Sculley and H.-C. Zhou, *Chem. Rev.* 2012, **112**, 869-932.
10. K. Sumida, D.L. Rogow, J.A. Mason, T.M. McDonald, E.D. Bloch, Z.R. Herm, T.- H. Bae and J.R. Long, *Chem. Rev.* 2012, **112**, 724-781.
11. A. Corma, H. Garcia and F.X. Llabrés i Xamena, *Chem. Rev.* 2010, **110**, 4606-4655.
12. S.M.J. Rogge, A. Bavykina, J. Hajek, H. Garcia, A.I. Olivos-Suarez, A. Sepúlveda-Escribano, A. Vimont, G. Clet, P. Bazin, F. Kapteijn, M. Daturi, E.V. Ramos-Fernandez, F.X.I. Llabrés Xamena, V. Van Speybroeck and J. Gascon, *Chem. Soc. Rev.* 2017, **46**, 3134-3184.
13. A. Dhakshinamoorthy, A.M. Asiri and H. García, *Angew. Chem. Int. Ed.* 2016, **55**, 5414-5445.
14. Y. Cui, Y. Yue, G. Qian and B. Chen, *Chem. Rev.* 2012, **112**, 1126-1162.
15. L.E. Kreno, K. Leong, O.K. Farha, M. Allendorf, R.P. Van Duyne and J.T. Hupp, *Chem. Rev.* 2012, **112**, 1105-1125.
16. P. Horcajada, R. Gref, T. Baati, P.K. Allan, G. Maurin, P. Couvreur, G. Férey, R.E. Morris and C. Serre, *Chem. Rev.* 2012, **112**, 1232-1268.
17. Y. Wu, X. Song, S. Li, J. Zhang, X. Yang, P. Shen, L. Gao, R. Wei, J. Zhang and G. Xiao, *J. Ind. Eng. Chem.* 2018, **58**, 296-303.
18. Y. Wu, X. Song, S. Xu, J. Zhang, Y. Zhu, L. Gao and G. Xiao, *Catal. Lett.* 2019, **149**, 2575-2585.
19. Y. Wu, X. Song, J. Zhang, S. Xu, L. Gao, J. Zhang and G. Xiao, *Chem. Eng. Sci.* 2019, **201**, 288-297.
20. Y. Wu, X. Song, J. Zhang, S. Xu, N. Xu, H. Yang, Y. Miao, L. Gao, J. Zhang and G. Xiao, *Chem. Eng. Res. Des.* 2018, **140**, 273-282.
21. A.H. Chughtai, N. Ahmad, H.A. Younus, A. Laypkov and F. Verpoort, *Chem. Soc. Rev.* 2015, **44**, 6804-6849.
22. A. Dhakshinamoorthy, M. Opanasenko, J. Čejka and H. Garcia, *Catal. Sci. Technol.* 2013, **3**, 2509-2540.



23. A. Dhakshinamoorthy, A.M. Asiri and H. Garcia, *Chem. Eur. J.* 2016, **22**, 8012-8024.
24. D. Farrusseng, S. Aguado and C. Pinel, *Angew. Chem. Int. Ed.* 2009, **48**, 7502-7513.
25. J. Gascon, A. Corma, F. Kapteijn and F.X. Llabrés i Xamena, *ACS Catal.* 2014, **4**, 361-378.
26. J. Lee, O.K. Farha, J. Roberts, K.A. Scheidt, S.T. Nguyen and J.T. Hupp, *Chem. Soc. Rev.* 2009, **38**, 1450-1459.
27. L. Ma, C. Abney and W. Lin, *Chem. Soc. Rev.* 2009, **38**, 1248-1256.
28. P. Valvekens, F. Vermoortele and D. De Vos, *Catal. Sci. Technol.* 2013, **3**, 1435-1445.
29. M. Yoon, R. Srirambalaji and K. Kim, *Chem. Rev.* 2012, **112**, 1196-1231.
30. O.A. Kholdeeva, *Catal. Today* 2016, **278**, 22-29.
31. Y.F. Chen, R. Babarao, S.I. Sandler and J.W. Jiang, *Langmuir* 2010, **26**, 8743-8750.
32. S.H. Jhung, J.-H. Lee, J.W. Yoon, C. Serre, G. Férey and J.-S. Chang, *Adv. Mater.* 2007, **19**, 121-124.
33. Z. Hu and D. Zhao, *CrystEngComm* 2017, **19**, 4066-4081.
34. N.V. Maksimchuk, O.V. Zalomaeva, I.Y. Skobelev, K.A. Kovalenko, V.P. Fedin and O.A. Kholdeeva, *Proc. R. Soc. A* 2012, **68**, 2017-2034.
35. A. Santiago-Portillo, S. Navalón, P. Concepción, M. Álvaro and H. García, *ChemCatChem* 2017, **9**, 2506-2511.
36. A. Santiago-Portillo, J.F. Blandez, S. Navalón, M. Álvaro and H. García, *Catal. Sci. Technol.* 2017, **7**, 1351-1362
37. A. Santiago-Portillo, S. Navalon, F. Cirujano, F. Llabrés i Xamena, M. Alvaro, H. Garcia, *ACS Catal.* 2015, **5**, 3216-3224.
38. A. Gómez-Paricio, A. Santiago-Portillo, S. Navalón, P. Concepción, M. Alvaro and H. Garcia, *Green Chem.* 2016, **18**, 508-515.
39. A. Dhakshinamoorthy, M. Alvaro, P. Horcajada, E. Gibson, M. Vishnuvarthan, A. Vimont, J.-M. Grenèche, C. Serre, M. Daturi and H. Garcia, *ACS Catal.* 2012, **2**, 2060-2065.
40. F. Vermoortele, M. Vandichel, B.V. de Voorde, R. Ameloot, M. Waroquier, V. Van Speybroeck and D.E. De Vos, *Angew. Chem. Int. Ed.* 2012, **51**, 4887-4890.
41. A. Dhakshinamoorthy, M. Alvaro, P. Concepcion and H. Garcia, *Catalan J. Commun. Cult. Stud.* 2011, **12**, 1018-1021.
42. Y. Zhang, R. Wang and Mini-Rev *Org. Chem.* 2018, 15.
43. C. Song, *Catal. Today* 2003, **86**, 211-263.
44. V.C. Srivastava, *RSC Adv.* 2012, **2**, 759-783.

## 5.8 Supplementary Material

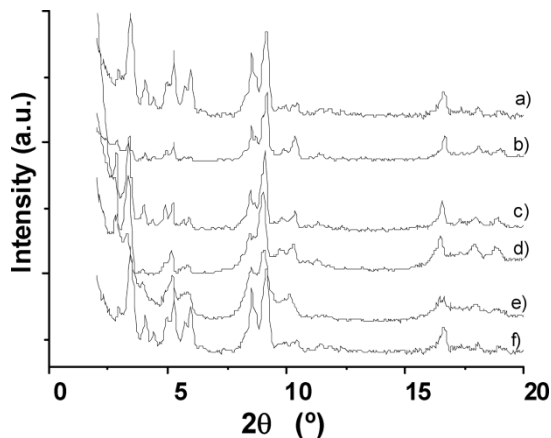


**Fig. S1** XRD patterns of MIL-101(Cr)-X sample study in the present Word; MIL-101(Cr)-H (a); MIL-101(Cr)-NO<sub>2</sub> (b); MIL-101(Cr)-SO<sub>3</sub>H (c); MIL-101(Cr)-Cl (d); MIL-101(Cr)-CH<sub>3</sub> (e); MIL-101(Cr)-NH<sub>2</sub> (f).

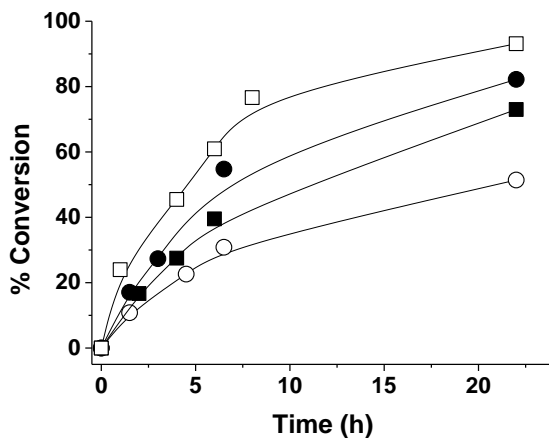


**Fig. S2** Time-conversion plot for the aerobic oxidation of benzenethiol (□), 4-fluorothiophenol (●), 4-chlorothiophenol (■) and 4-methylbenzenethiol (○) to corresponding disulphides, using MIL-101(Cr)-NO<sub>2</sub>. Reaction conditions: Catalyst (0.04 mmol Cr), substrate (20 mmol), O<sub>2</sub> atmosphere (balloon), reaction temperature (140 °C).

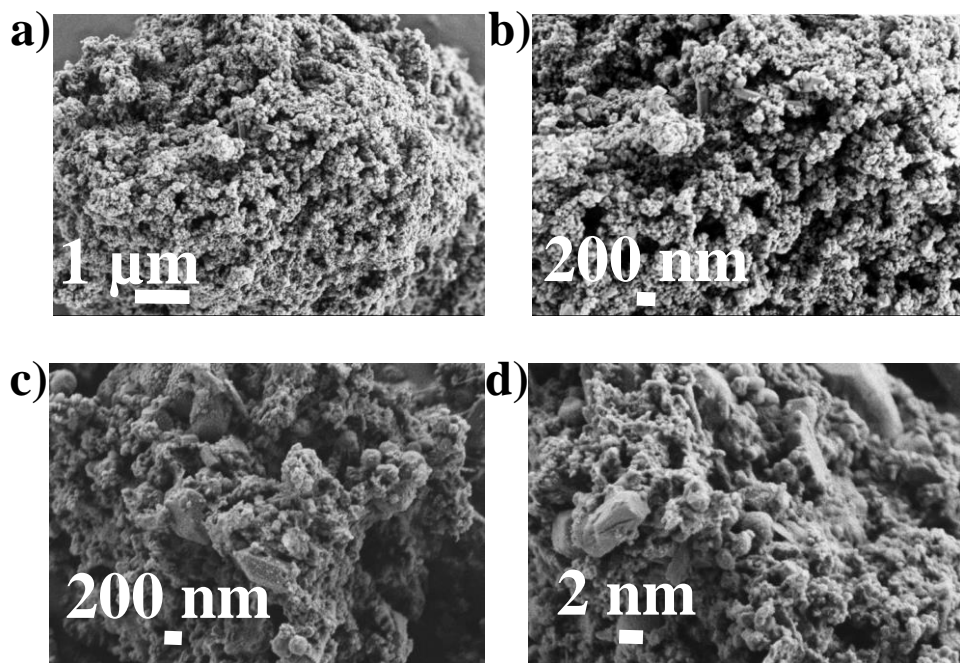


**Fig. S3** SEM images of the fresh and used MIL-101(Cr)-NO<sub>2</sub> catalyst. (a)-(b) Fresh catalyst; (c)-(d) after productivity test of thiophenol by the factor 25 times.

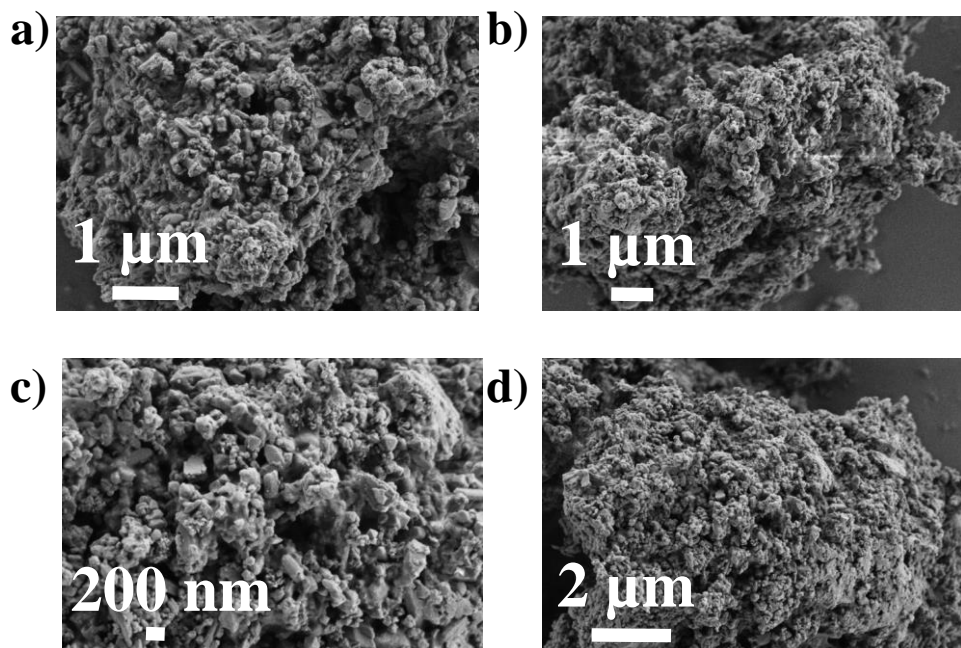


**Fig. S4** SEM images of the MIL-101(Cr)-NO<sub>2</sub> material after (a)-(b) after productivity test of DBT by the factor 5 time; (c)-(d) after 5 use of DBT.

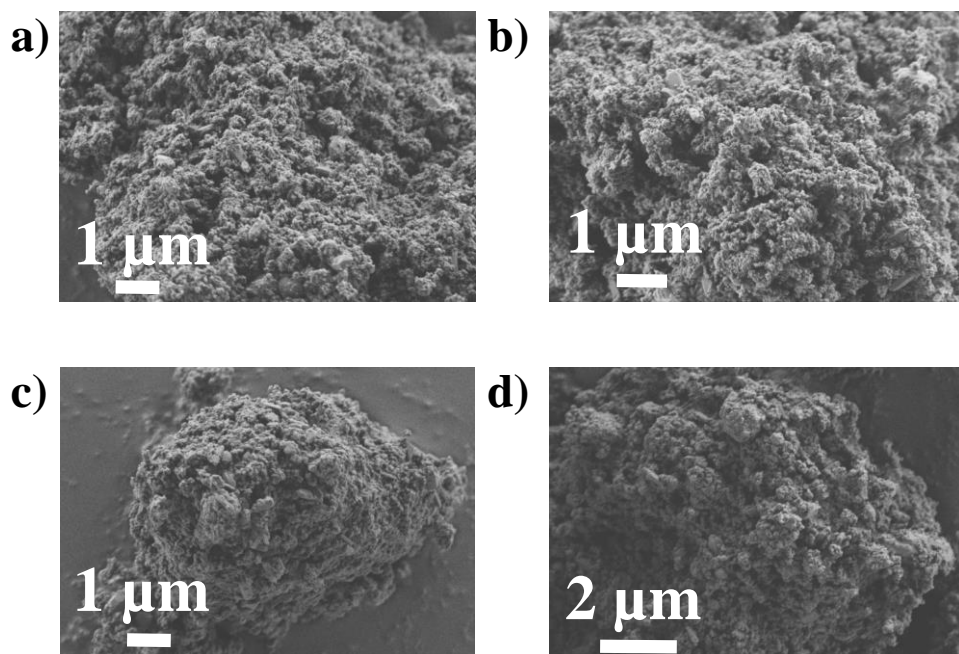


**Fig. S5** SEM images to MIL-101(Cr)-NO<sub>2</sub> after oxidative desulfuration of DBT a different temperature, (a)-(b) 120 °C and (c)-(d) 130 °C.

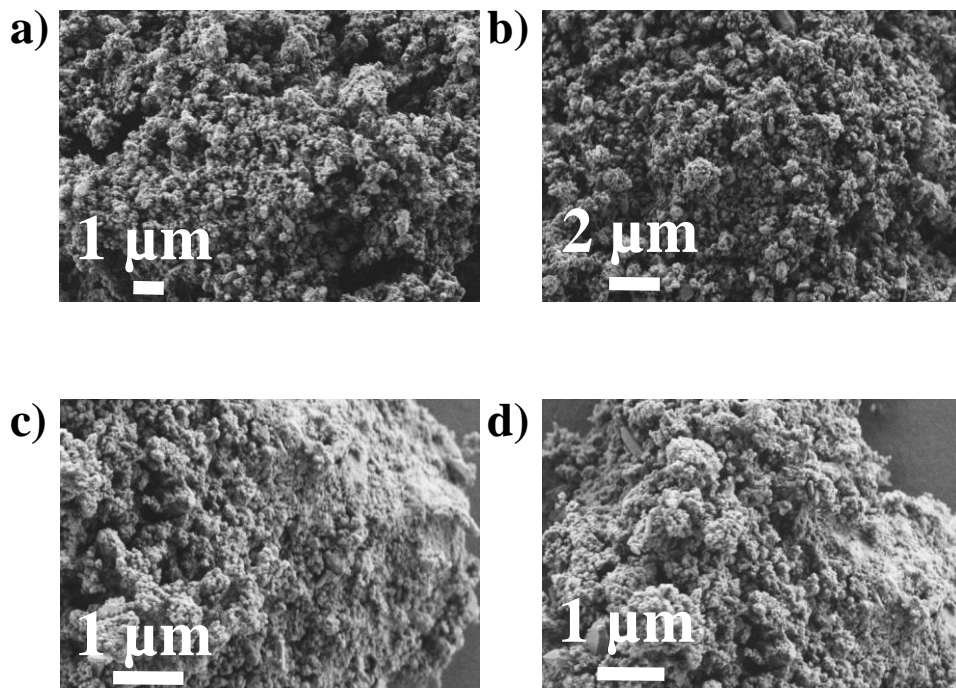


Fig. S6 SEM images to MIL-101(Cr)-NO<sub>2</sub> after oxidative desulfuration DBT a different temperature, (a)-(b) 140 °C or (c)-(d) 150 °C.

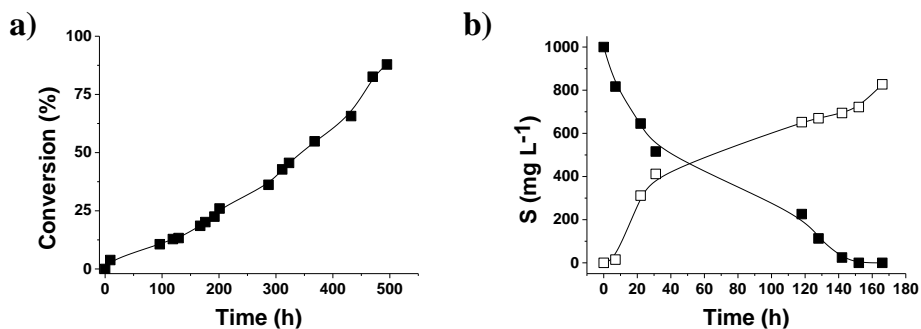
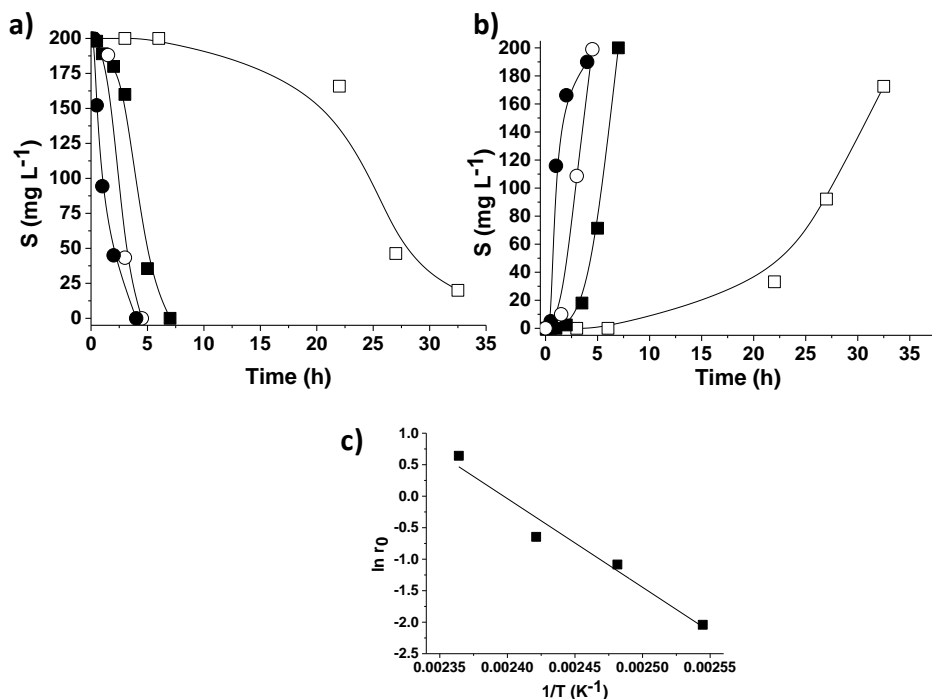


Fig. S7 Time-conversion plot for productivity test to (a) oxidative coupling of the aerobic oxidation of thiophenol and (b) oxidative desulfuration of DBT; DBT (■) or DBT-O<sub>2</sub> (□).



**Fig. S8** Influence of the temperature in the oxidation of DBT (a) to DBT- $\text{O}_2$  (b) in n-dodecane as solvent, 120 °C ( $\square$ ), 130 °C ( $\blacksquare$ ), 140 °C ( $\circ$ ) and 150 °C ( $\bullet$ ). c) Plot of the logarithm of the relative initial reaction rate versus the  $1/T$  ( $\text{K}^{-1}$ ) of each reaction temperature. Reaction conditions: Catalyst (0.04 mmol Cr), DBT (200 ppm S), n-dodecane (10 mL),  $\text{O}_2$  atmosphere (balloon).

**Table S1** ICP-OES analytical data of Cr concentration in the liquid phase after reuses of MIL-101(Cr)- $\text{NO}_2$ .

Reaction	Number of reuses	Cr (mg/L)
Aerobic oxidation of thiophenols	10	$9 \cdot 10^{-4}$
Oxidative desulfurization of DBTs	5	$7 \cdot 10^{-4}$





**Chapter 6. *Tuning the active sites in reduced  
grapheme oxide by hydroquinone  
functionalization for the aerobic oxidations of  
thiophenol and indane***



# Tuning the active sites in reduced graphene oxide by hydroquinone functionalization for the aerobic oxidations of thiophenol and indane.

Cristina Vallés-García<sup>a</sup>, Eva Montero-Lanzuela<sup>a</sup>, Sergio Navalon<sup>a,\*</sup>, Mercedes Álvaro<sup>a</sup>, Amarajothi Dhakshinamoorthy<sup>b,\*</sup>, Hermenegildo Garcia<sup>a,c,d,\*</sup>

<sup>a</sup> Departamento de Química, Universitat Politècnica de València, C/Camino de Vera s/n, 46022, Valencia, Spain.

<sup>b</sup> School of Chemistry, Madurai Kamaraj University, Madurai, 625 021, Tamil Nadu, India.

<sup>c</sup> Instituto Universitario de Tecnología Química, CSIC-UPV, Universitat Politècnica de València, Av. de los Naranjos, Valencia, 46022, Spain.

<sup>d</sup> Center of Excellence in Advanced Materials Research, King Abdulaziz University, Saudi Arabia.

Published online: July 7, 2020

(Reprinted with permission from *Mol. Cat.*, 2020, **493**, 111093.

Copyright © 2020, Elsevier. All rights reserved.)



## 6.1 Abstract

Sustainable reduced graphene oxide (rGO) carbocatalysts for molecular oxygen activation have been developed based on the concept that chemical reduction of graphene oxide to rGO introduces functional groups that can become active sites. Thus, a series of rGOs prepared using hydroquinone (HQ), hydrazine (HZ) and ascorbic acid (ASC) as reducing agents have been tested as catalysts in the aerobic oxidations of thiophenol and indane. In both oxidation reactions, rGO reduced by HQ (rGO-HQ) exhibited the highest catalytic activity and stability. A high selectivity of ol/one (90 %) at around 30 % indane conversion in the absence of transition metals was achieved. Reusability test showed that the activity of rGO-HQ is mostly retained in three consecutive runs. Quenching experiments indicated that the reaction proceeds with the generation of hydroxyl and carbon centered radicals. The higher activity of rGO-HQ was attributed to the covalent anchoring of some HQ molecules on rGO during the chemical reduction. This knowledge has been used to develop a HQ-functionalized Merrifield resin that in spite of its very different textural properties compared to rGO also exhibits catalytic activity for O<sub>2</sub> activation. The present work illustrates the potential to develop rGO carbocatalysts with an increased density of active sites by selecting an appropriate reducing agent during the chemical reduction of graphene oxide.

## 6.2 Introduction

Reduced graphene oxide is among the most widely used carbocatalysts due to its availability and the catalytic activity to promote a large variety of reactions, including oxidations,<sup>1-4</sup> reductions<sup>5-9</sup> and acid catalyzed

reactions,<sup>10,11</sup> among others.<sup>12-17</sup> In recent years, rGO was also used as support for the deposition of metal and metal oxide nanoparticles and their activity was reported in the oxidation as well as oxidative degradation of pollutants.<sup>18-23</sup> Furthermore, rGO can be conveniently obtained in multigram scale by exfoliation of graphite oxide and subsequent chemical reduction of single layer graphene oxide (GO).<sup>24,25</sup>

Due to the mild reaction conditions, hydrazine in aqueous solution has been among the most widely used reducing agents, but other chemicals such as ASC<sup>26,27</sup> and HQ have also been used to convert GO into rGO.<sup>28-31</sup> The mechanism of the reduction of GO into rGO has been studied in detail and it has been shown that the resulting rGO can incorporate some groups from the reducing agent in its lattice during its formation. These functional groups present in rGO would depend on the nature and conditions of the reduction from GO.<sup>8,32-34</sup>

As consequence of the specific functionalization introduced during its formation,<sup>35,36</sup> rGO could exhibit distinctive catalytic activity depending on the conditions employed for the reduction of GO.<sup>37,38</sup> The active sites of rGO are structural defects and adventitious functional groups and, therefore, from the catalytic point of view, the possibility to introduce certain functional groups represents an opportunity to obtain rGO with the optimal catalytic activity for each process. Thus, it has been recently shown that the rGO obtained by HQ reduction (rGO-HQ) of GO is a more efficient catalyst for benzylamine oxidation than other two rGO solids obtained using other reducing agents.<sup>34</sup> This higher activity catalytic activity of rGO-HQ was justified as derived from the presence of HQ-like units covalently anchored on the rGO sheet during the conversion of GO into rGO.

Continuing with this line of research and considering that hydroquinone/quinone moieties have been proposed as active centres for aerobic oxidations, it would be of interest to extend the above methodology to other process showing that rGO-HQ outperforms twin rGO prepared by other reductive treatments. Accordingly, the present study shows that rGO-HQ is the most active among other four related rGOs to promote the aerobic oxidation of thiols to disulfides and the benzylic oxidation of indane to indanol/indanone. The role of HQ as active centres in the process has been supported by preparing a Merrifield resin with covalently anchored HQ units, observing that, in spite of the difference in particle morphology and size, this resin behaves also as a solid catalyst for those processes.

## **6.3 Experimental section**

### **6.3.1 Materials**

The reactants and reagents used in this work were purchased from Sigma-Aldrich and were of analytical or HPLC grade. In particular, the Merrifield resin (100-200 mesh) is a chloromethylpolystyrene-divinylbenzene copolymer. Substrates used in this study like thiophenol, indane, HQ and other reducing agents were also purchased from Sigma Aldrich. These reactants were used without further purification/modification processes.

### **6.3.2 Catalyst preparation**

The various carbocatalysts and their functionalized materials employed in this work were prepared by adopting procedures reported elsewhere.<sup>34</sup> The detailed experimental procedures for the preparation of various

carbocatalysts and their characterization data are provided in the supporting Information. GO was prepared by the Hummers method. In brief, commercial graphite powder was subjected to a chemical oxidation in the presence of  $\text{KMnO}_4$ ,  $\text{KNO}_3$  and  $\text{H}_2\text{SO}_4$  and the resulting solid was subsequently exfoliated to obtain GO by ultrasonication. Later, GO was transformed into rGO either by thermal or chemical methods. The thermally reduced GO (rGO-T) was obtained by heating GO (200 mg) in a tubular furnace under argon atmosphere at 200 °C for 4 h.<sup>34</sup> In addition, the structural analysis of GO and rGO-T by elemental analysis clearly indicated a significant changes introduced upon thermal reduction (Table S1). Further, the as-prepared GO was also reduced with a series of chemical reducing agents like HQ, HZ and ASC and the resulting solids were named as rGO-HQ, rGO-HZ and rGO-ASC, respectively. In addition, the rGO-HQ solid was further submitted to a thermal treatment under inert atmosphere at 300 or 700 °C for 4 h and the samples were labelled as rGO-HQ-300 and rGO-HQ-700, respectively.

HQ-functionalized Merrifield resin has been prepared via synthesis of Williamson. Briefly, the resin as fine powder (500 mg) was suspended in dimethylsulfoxide (DMSO) (20 mL) by sonication (450 W, 20 min) using a round-bottom flask (100 mL). Then, HQ (500 mg, 4.55 mmol) and NaOH (4.55 mmol) were added to the resin suspension. The mixture was heated at 140 °C for 16 h and, then, cooled down to room temperature. The solid was recovered by filtration (Nylon membrane, 0.45  $\mu\text{m}$ ) and washed under stirring with Milli-Q under neutral pH. The resin was further washed in a Soxhlet system using acetonitrile as solvent for 16 h. Finally, the resin was dried in an oven at 100 °C for 16 h. The same washing procedure has been applied to the as received Merrifield resin before use.



### 6.3.3 Instrumentation

X-ray photoelectron (XP) spectra were recorded on a SPECS spectrometer equipped with a MCD-9 detector using a monochromatic Al ( $K\alpha = 1486.6$  eV) X-ray source. Spectra deconvolution has been performed with the CASA software using the C 1s peak at 284.4 eV as binding energy reference. Attenuated total reflectance Fourier transform infrared (ATR-FT-IR) measurements were carried out with a Bruker Tensor 27 spectrophotometer. Diffuse reflectance UV–vis spectra of previously compressed powders were recorded using a Cary 5000 Varian spectrophotometer having an integrating sphere.

### 6.3.4 Aerobic oxidation of thiophenol

In a typical reaction, thiophenol (1 mmol), 20 mg of catalyst and 2 mL of acetonitrile were placed in a 25 mL of round bottom flask. This was connected to oxygen balloon and the reaction was maintained in oxygen atmosphere. This reaction mixture was placed in a preheated oil bath maintained at 70 °C. The reaction was monitored by gas chromatography (GC) and the oxidized product was confirmed by GC coupled with mass spectrometer (GC–MS).

### 6.3.5 Aerobic oxidation of indane

In a 25 mL round bottom flask, 20 mg of catalyst was placed and indane (20 mmol) was added to this flask. This reaction flask was connected to oxygen atmosphere. This heterogeneous reaction mixture was placed in a preheated oil bath maintained at 130 °C. The reaction progress was monitored by sampling at different time intervals using nitrobenzene as internal standard. The oxidized products were confirmed by co-injection with authentic samples and

analyzing by GC-MS.

Quenching experiments with (2,2,6,6-tetramethylpiperidin-1-yl) oxyl (TEMPO) and DMSO were performed under identical conditions in the presence of 20 mol % of these quenchers. Further, reusability tests were conducted under identical conditions described above except by the use of recovered catalyst. After the catalytic reaction, the solid was separated by filtration, washed with acetonitrile and dried at 90 °C. This solid was reused in subsequent cycles with the fresh reactants.

The catalytic data presented in this work correspond to the values of at least two independent experiments.

## **6.4 Results and discussion**

### **6.4.1 Functionalizations of rGO**

One of the main objectives of this work is to study the influence of different active sites present in rGO on the resulting catalytic activity for the aerobic oxidation of thiophenol and for the solvent-free oxidation of indane. Active site engineering on rGO has been performed by reducing GO to rGO using different reducing agents like thermal treatment (rGO-T), HQ (rGO-HQ), HZ (rGO-HZ) and ASC (rGO-ASC). The detailed preparation of these catalysts and their characterization data have been recently reported.<sup>34</sup> Fig. 1 illustrates the procedures employed to obtain different rGO samples employed in this study having different functional groups. Table S1 in the supplementary material summarizes the experimental procedure employed for the preparation of the graphene-based catalysts employed in this study together with some characterization data obtained from elemental analysis and XPS.<sup>34</sup> These results

indicate that both thermal and chemical methods are convenient treatments to promote the reduction of GO as revealed by an increase of the carbon content and concomitant decrease of the oxygen proportion in the rGO samples (Table S1). Further characterization of the rGO-HQ sample by thermogravimetric analysis, FT-IR,  $^{13}\text{C}$ -NMR and temperature programmed desorption (TPD) coupled to a mass-spectrometer (TPD-MS) analysis confirmed the presence of HQ-like moieties (8 wt%) covalently grafted to the rGO sheet.<sup>34</sup> Furthermore, rGO-HQ was subjected to thermal treatment under argon atmosphere at 300 or 700 °C and the resulting solids rGO-HQ-300 and rGO-HQ-700 were found to contain lower oxygen contents (Table S1), thus meaning lower density of active sites. In addition, the removal of oxygen-functional groups including the HQ-like moieties from rGO-HQ was highly dominant at 700 °C (Table S1). In order to demonstrate the differences in the catalytic activity of rGO solid catalysts depending on its reduction conditions, two model aerobic oxidation reactions of thiophenol and indane were selected and the observed results are discussed below.

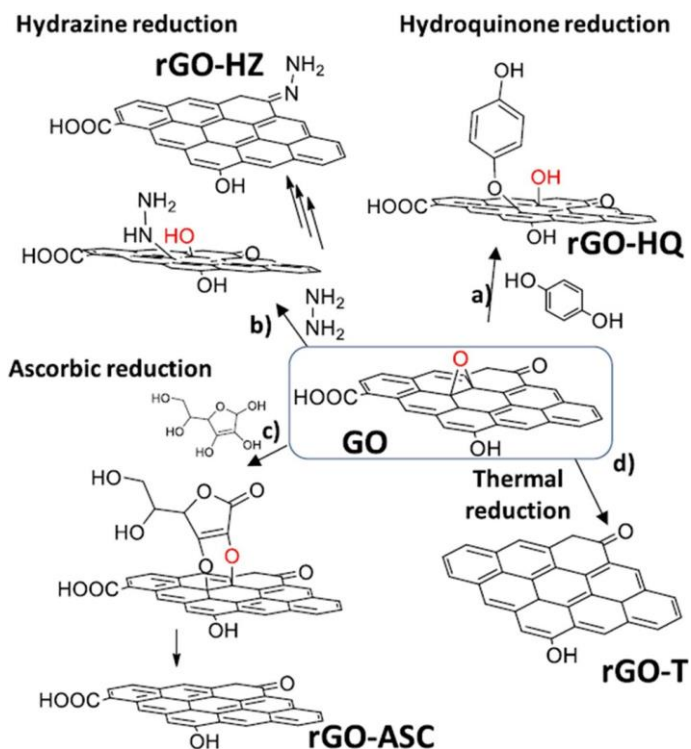


**Fig. 1** Procedures used to obtain the rGO samples under study and plausible functional groups present on their structure: (a) HQ; (b) HZ; (c) ASC as reducing agents, or (d) by thermal treatment. Reprinted with permission from ref.<sup>34</sup>

For comparison, the Merrifield resin has been functionalized with HQ units in basic medium forming an ether bond. Merrifield resin is constituted by particles between 100-200 mesh of cross-linked polystyrene. The presence of HQ covalently anchored through the ether bond to the Merrifield resin was confirmed by ATR-FT-IR spectroscopy by observing two new FT-IR bands appearing at 3330 and 1225  $\text{cm}^{-1}$  attributable to the presence of phenolic and phenyl ether groups, respectively (Fig. S1a). In agreement with the FT-IR data, diffuse reflectance UV–vis spectrum of the HQ-functionalized Merrifield resin exhibits a red shift absorbance respect to the pristine resin due to the presence of HQ molecules anchored through an ether bond (Fig. S1b).

### 6.4.2 Aerobic oxidation of thiophenol

Selective aerobic oxidation of thiophenol to 1,2-diphenyldisulfide is an important reaction in organic chemistry (Fig. 2). This oxidation reaction has often been catalyzed by various transition metals and replacing these transition metals by carbocatalysts would certainly contribute to the green chemistry principles by using renewable catalysts. Further, this reaction is also one of the model reactions to compare various catalysts prepared by different methods.

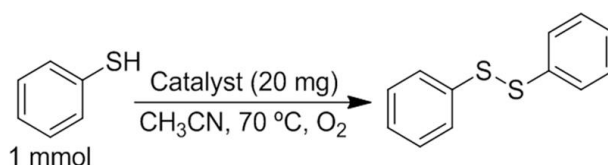


**Fig. 2** Aerobic oxidation of thiophenol to 1,2-phenyldisulfide using different rGO catalysts.

Hence, this reaction is selected to rank the series of catalysts prepared in this work and the observed catalytic data are given in Table 1. The aerobic oxidation of thiophenol was performed with these solid catalysts in acetonitrile at 70 °C. In the absence of catalyst thiophenol conversion was negligible (Table 1, entry 1). In agreement with previous studies, GO is able to catalyze thiophenol oxidation to its corresponding disulfide (Table 1, entry 2).<sup>39</sup> Interestingly, the catalytic activity for thiophenol conversion strongly depends on the solid employed as catalyst. rGO-HQ solid was the most active catalyst of the series with full conversion and selectivity after 24 h (Table 1, entry 3). Considering the loading of HQ-like moieties as active sites in rGO-HQ (8 wt%), this solid showed turnover frequency (TOF) value of 6.6 h<sup>-1</sup> [turnover number (TON): 68] while other metal-based catalysts like Co catalyst (49.2 h<sup>-1</sup>),<sup>40</sup> Au/CeO<sub>2</sub> (14.2 h<sup>-1</sup>),<sup>41</sup> Fe<sub>2</sub>O<sub>3</sub>/silica (1143 h<sup>-1</sup>)<sup>42</sup> provided comparable or significantly higher TOF values. Although these data cannot be directly compared since carbocatalysts and metal-based

catalysts are operated through different reaction mechanisms, the main focus of this work is to forecast the possibility to tune carbocatalysts to promote aerobic oxidation reactions rather than ranking with reported catalysts. On other hand, the aerobic oxidation of thiophenol in the presence of rGO-HQ-300 and rGO-HQ-700 solid catalysts showed 58 and 14 % conversions under identical conditions (Table 1, entries 4-5). These results indicate that the HQ moieties attached to rGO act as active sites for the aerobic oxidation of thiophenol to 1,2-diphenyldisulfide, while thermally treated rGO-HQ-300 and rGO-HQ-700 resulted in decreased activity due to partial decomposition of the HQ moiety, thus lowering the population of active sites. On the other hand, the activity of rGO-HZ or rGO-ASC (Table 1, entries 6-7) as catalysts in the conversion of thiophenol to its respective disulfide was 60 and 10 %, respectively, under similar conditions. In addition, the catalytic performance of rGO-T or HQ (Table 1, entries 8-9) as catalysts in the aerobic oxidation of thiophenol was 47 and 12 %, respectively, which is comparatively much lower than the activity observed with rGO-HQ. These results clearly infer that the synergism between rGO and HQ is dominant by generating high density of active sites which are capable of producing the radicals to promote this aerobic oxidation. Interestingly, the activity of rGO-HQ catalyst in the 1<sup>st</sup> run (Table 1, entry 3) was retained for at least three catalytic cycles (Table 1, entries 10 and 11).

**Table 1** Selective aerobic oxidation of thiophenol to 1,2-diphenyldisulfide by several carbocatalysts.<sup>a</sup>

S. No	Catalysts	Conversion (%) <sup>b</sup>
1	-	< 2
2	GO	70
3	rGO-HQ	100
4	rGO- HQ-300	58
5	rGO- HQ-700	14
6	rGO- Hz	60
7	rGO- ASC	10
8	rGO-T	47
9	HQ	12
10	rGO-HQ <sup>c</sup>	100
11	rGO-HQ <sup>d</sup>	100

<sup>a</sup> Reaction conditions: thiophenol (1 mmol), catalyst (20 mg), CH<sub>3</sub>CN (2 mL), oxygen purged, 70 °C, 24 h.

<sup>b</sup> Determined by CG. The conversions are the average values of two independent experiments. Selectivities were 100 % for all entries.

<sup>c</sup> Second use.

<sup>d</sup> Third use.

In order to rationalize the importance of the presence of HQ-like active sites dispersed in a solid, the HQ molecule was anchored to the so-called Merrifield resin (Fig. 3a) and the resulting solid tested as catalyst for the aerobic oxidation of thiophenol. Notice that the textural properties of the Merrifield resin in terms of particle morphology and size, surface area and porosity are totally different from rGO. However, if the structure of the active sites promoting the aerobic oxidation is related to the quinone/hydroquinone redox pair, both materials rGO-HQ and Merrifield-HQ could promote the aerobic oxidation.

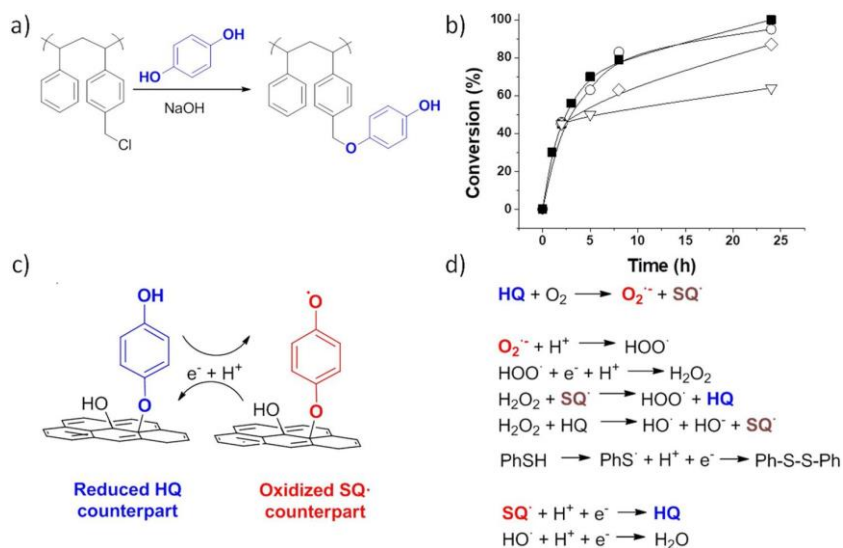


**Fig. 3** a) Merrifield resin functionalization using HQ units; b) Time-conversion plot for the aerobic oxidation of thiophenol under different conditions: rGO-HQ as catalyst in the absence (○) or in the presence of DMSO (▽); hot filtration test using rGO-HQ as catalyst at 43 % conversion (◇); HQ-functionalized Merrifield resin (■) as catalyst. c) Simplified illustration of redox catalytic cycle for HQ/phenoxy-like radical anchored on rGO-HQ catalyst during the aerobic oxidation of thiophenol to 1,2-diphenyldisulfide (d).

Importantly, the HQ-functionalized Merrifield resin is able to efficiently promote the aerobic oxidation of thiophenol to 1,2-diphenyldisulfide (Fig.3b). Control experiments using the as-received Merrifield resin as catalyst results in a negligible thiophenol conversion. These results highlight the role of anchored HQ moieties on support as active sites to promote molecular  $\text{O}_2$  activation.

To obtain some evidence about the reaction pathway for the aerobic oxidation of thiophenol using rGO-HQ as carbocatalyst some additional experiments including the hot filtration test and the selective quenching of hydroxyl radicals have been performed (Fig. 3b). In the hot filtration test, once the reaction was initiated the catalyst is removed by filtration at 43 % conversion of thiophenol and the reaction supernatant allowed to react under the standard reaction. It was



observed that the reaction only partially stopped (Fig. 3b). This observation is in agreement with the general radical reaction mechanism involving the formation of thiyl radicals during the aerobic oxidation of thiophenol to 1,2-diphenyldisulfide. In order to get some evidences of the presence of oxygen radical species a quenching experiment using DMSO as selective hydroxyl radical scavenger has been carried out. Thus, if once the reaction is initiated, the conservation of thiophenol considerably decreases upon addition of DMSO, a fact that indirectly indicates the presence of HO. In the reaction medium. These experimental data together with the known ability of rGO-HQ to activate  $O_2$  to  $O_2^{\cdot-}$ <sup>34</sup> allows to propose a reaction pathway for the oxidation of thiophenol to 1,2-diphenyldisulfide (Fig. 3c-d). The HQ moieties in rGO-HQ with the presence of  $O_2$  leads to the formation of  $O_2^{\cdot-}$  that subsequently promotes the formation of reactive oxygen species (ROS) (Fig. 3d). These ROS are responsible of the thiophenol oxidation to thiyl radicals that couple forming 1,2-diphenyldisulfide. The catalytic cycle is restored by the reduction of the phenoxyl-like radical present in rGO to rGO-HQ.

### 6.4.3 Aerobic oxidation of indane

The preliminary catalytic results on the aerobic oxidation of thiophenol highlight the efficient role of rGO-HQ solid in which HQ units covalently attached to the rGO sheet act as active sites to promote the aerobic oxidation of thiophenol to 1,2-diphenyldisulfide. To further demonstrate the ability of rGO-HQ to activate molecular  $O_2$ , the aerobic oxidation of benzylic hydrocarbon, namely, indane was selected and the aerobic oxidation reactions were performed under solvent-free conditions (Fig. 4).

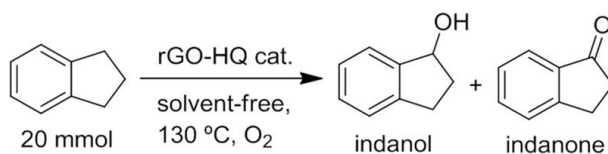


**Fig. 4** Aerobic oxidation of indane to indanol and indanone.

Aerobic oxidation of benzylic hydrocarbons to their corresponding alcohol/ketone (ol/one) products is one of the challenging industrial processes that often requires transition metal catalysts either in the homogeneous or heterogeneous nature.<sup>43,44</sup> However, development of sustainable catalytic systems consisting carbocatalysts is one of the appropriate alternatives to the use of transition metal catalysts,<sup>45</sup> without compromising the ol/one selectivity. With these objectives in mind, the aerobic oxidation of indane was performed with these solid carbocatalysts under solvent-free conditions. The observed results are summarized in Table 2. In agreement with previous reports, an inefficient indane autoxidation reaction takes place working at 130 °C under molecular oxygen (1 bar). Importantly, the presence of rGO-HQ in the reaction medium boosted the conversion of indane (90 %) to 1-indanol and 2-indanone (Fig. 5a). The TON and TOF values for indane oxidation using rGO-HQ catalyst were 1215 and 388 h<sup>-1</sup>, respectively. Interestingly, this TOF value is comparable to Pd@C (452 h<sup>-1</sup>)<sup>46</sup> in the absence of any additive, but however, is lower with Pd@C with 2-acetylpyridine as an additive (863 h<sup>-1</sup>).<sup>46</sup> These data imply that carbocatalysts can also be tuned to achieve activity at par with metal-based catalysts. As in the case of thiophenol oxidation using rGO-HQ, a thermal treatment of rGO-HQ especially at 700 °C decreases the activity (56 %) due to the removal of oxygen-functional groups including HQ-like units. These experiments indirectly show that HQ-like groups present in rGO are active sites for O<sub>2</sub> activation and indane oxidation. The use of rGO

solids prepared using ASC or HZ as reducing agents or by hydrothermal GO reduction (rGO-T) results in a lower catalytic activity. These data highlight the importance of an adequate GO reduction to obtain an rGO solid with the reduction of specific functional groups by lowering the active sites for the O<sub>2</sub> activation.

**Table 2** Aerobic oxidation of indane to indanol and indanone by several carbocatalysts.<sup>a</sup>

S. No	Catalysts	Conversion (%) <sup>b</sup>	Selectivity (%) <sup>b</sup>
1	-	16	-
2	GO	31	88
3	rGO-HQ	90	80
4	rGO-HQ-300	70	83
5	rGO-HQ-700	56	88
6	rGO-Hz	60	88
7	rGO-ASC	52	87
8	rGO-T	68	81
9	rGO-HQ <sup>c</sup>	85	81
10	rGO-HQ <sup>d</sup>	84	82

<sup>a</sup> Reaction conditions: indane (20 mmol), catalyst (20 mg), oxygen purged, 130 °C, 7 h.

<sup>b</sup> Determined by CG. The numbers are the average values of three independent experiments.

<sup>c</sup> Second use.

<sup>d</sup> Third use.

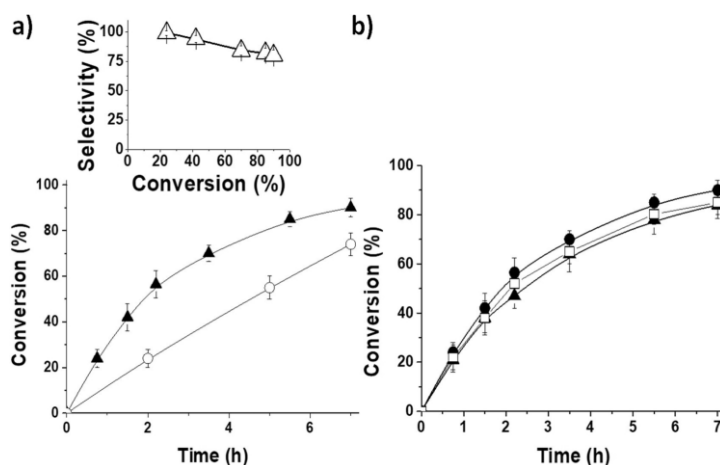


**Fig. 5 a)** Time-conversion profile for the aerobic oxidation of indane using different rGO-HQ (▲)

or HQ-functionalized Merrifield resin (o) as catalysts. The inset shows the selectivity-conversion plot using rGO-HQ catalyst. b) Time profile for the conversion of indane during three consecutive cycles using rGO-HQ as catalyst. Reaction conditions: Catalyst (10 mg), indane (20 mmol), oxygen (1 bar), 130 °C. The bars indicate the standard deviation of two independent experiments.

Importantly, the use of the HQ-functionalized Merrifield resin have resulted an active solid for the aerobic oxidation of indane (Fig. 5a). Control experiments using the non-functionalized Merrifield resin show an inefficient indane conversion attributed to the autooxidation process using O<sub>2</sub>. These experiments reinforce the possibility to anchor HQ molecules in a solid for its use as heterogeneous catalyst for the molecular oxygen activation.

One of the effective strategies to study the catalyst stability in heterogeneous catalysis is to perform reusability tests under the optimized reaction conditions. In this context, the reusability test of rGO-HQ was performed in the oxidation of indane under oxygen atmosphere in solvent free conditions at 130 °C. The time conversion plot for the aerobic oxidation indane in the 1<sup>st</sup>, 2<sup>nd</sup> and 3<sup>rd</sup> runs are shown in Fig. 5b. It can be seen that the conversion of indane slightly decreased during these three runs. Further, the activity loss of rGO-HQ in promoting the aerobic oxidation for indane conversions was 6 and 7 % for 2<sup>nd</sup>, 3<sup>rd</sup> run, respectively compared to 1<sup>st</sup> run. In order to assess this decrease of activity the three times used catalyst was characterized by XPS. Fig. 6, shows the XPS C1s and O1s for the fresh and used rGO-HQ catalysts. The XPS C1s and O1s of the three-times used rGO-HQ catalyst shows a decrease of the C=C component, accompanied by an increase of the bands related with the C-OH, C=O and -COO respect to the fresh catalyst. Considering the presence of the HQ-like moieties in the fresh rGO-HQ of about 20.2 % (Fig. 6b), it is reasonable to propose their partial oxidation to quinone-like moieties (Fig. 6d) and, therefore, decrease of activity.

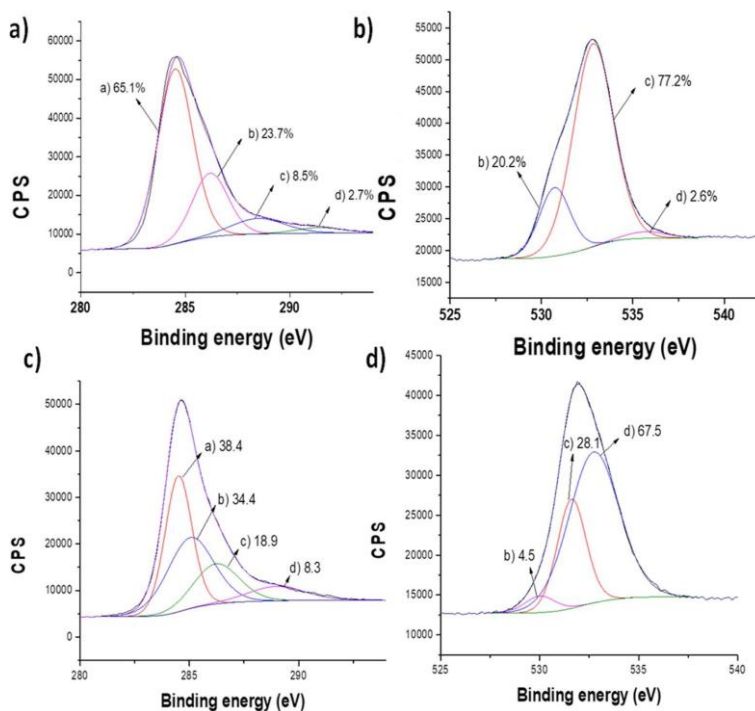


**Fig. 6** XPS C1s (a, c) and O1s (b, d) for the fresh (a, b) and three-times used (c, d) rGO-HQ catalyst. The best deconvolution for fresh and three-times used rGO-HQ sample is shown. Legend: (a) C sp<sup>2</sup>, (b) alcohol/ether, (c) carbonyl, (d) carboxyl. Panels a-b are reprinted with permission from ref.<sup>34</sup>

A series of control experiments were also performed to gain some insights on the reaction pathway for the aerobic oxidation of indane using rGO-HQ as carbocatalyst (Fig. 7). A hot filtration test shows that once the reaction has been initiated reaching 23 % conversion, oxidation does not completely stop if the catalyst is removed and the clear supernatant is allowed to react under the same reaction conditions. In addition, if TEMPO is added to the filtered reaction and the mixture is allowed to react further under the same reaction conditions, the reaction completely stops. These experiments indirectly indicate that the reaction proceeds via carbon centred radicals that can be quenched by TEMPO.

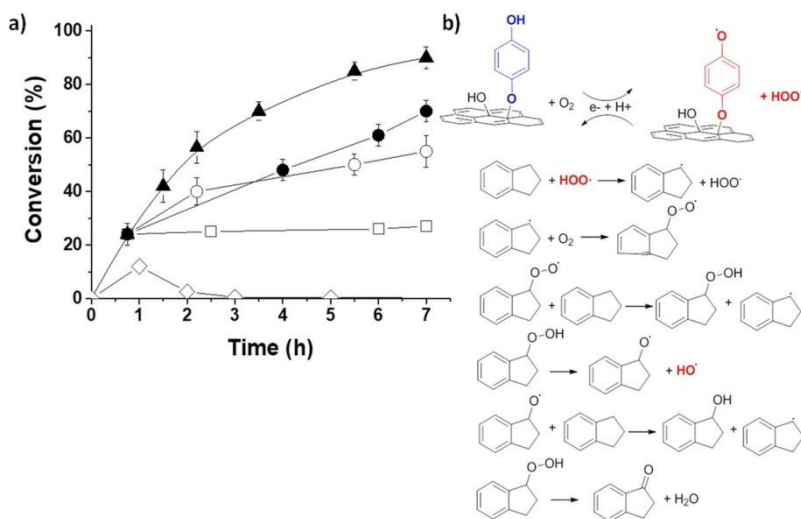


**Fig. 7** a) Time-conversion plot for the aerobic oxidation of indane using rGO-HQ as catalyst ( $\blacktriangle$ ), after catalyst removal at 23 % conversion ( $\bullet$ ), in the presence of catalyst and DMSO ( $\circ$ ), addition of TEMPO at 23 % conversion of indane ( $\square$ ). The indanyl hydroperoxide yield evolution in the reaction in the presence of catalyst is also shown in the graph ( $\diamond$ ). Reaction conditions: indane (20 mmol), catalyst (20 mg), reaction temperature (130 °C); b) Proposed reaction mechanism for the aerobic oxidation of indane using rGO-HQ catalyst.

In order to get further evidence about the reaction mechanism of indane oxidation by rGO-HQ, the possible presence of indanyl hydroperoxide was analyzed. As previously reported, indanyl hydroperoxide can be indirectly determined by monitoring the formation of triphenylphosphine oxide upon addition of triphenylphosphine to the reaction aliquots sampled at different reaction times. It should be noted that indanyl hydroperoxide cannot be directly determined by GC due to its decomposition to indanol and/or indanone. Using the triphenylphosphine reagent, formation of indanyl hydroperoxide with a selectivity of 12 % at about 32 % conversion was estimated in the presence of rGO-HQ as catalyst. Furthermore, the addition of DMSO to the reaction medium at 30 % conversion results in partial decrease of indane conversion. These catalytic data are attributed to the presence of hydroxyl radicals in the reaction system. Similarly, the initiated reaction (23 % conversion) was completely quenched upon

addition of TEMPO to the reaction medium, thus indicating the presence of carbon center radicals in the reaction system.

Based on these observations, Fig. 7 shows a plausible reaction pathway for the oxidation of indane with molecular  $O_2$  using rGO-HQ as catalyst. According to a recent report,<sup>34</sup> the formation of free hydroperoxides and semiquinone-like radicals on the rGO-HQ catalyst is proposed to occur in the initial reaction steps. Then, these radicals can react with the benzylic position of indane leading to the formation of indanyl hydroperoxide, indanol and indanone. In addition, indanyl hydroperoxide can decompose leading to the formation of hydroxyl radicals that can be quenched using DMSO as selective radical scavenger. It should be noted that once the reaction is initiated hydroxyl radicals as well as semiquinone like radicals can promote the benzylic oxidation of indane.

## 6.5 Conclusions

The present study has shown that the catalytic activity of rGO samples prepared by different procedures differs depending on the GO reduction conditions. Considering that among the most active sites for aerobic oxidations on rGO are unsaturated ketones with quinone-like structure, the possibility exists to introduce extra density of these centres by performing the GO reduction to rGO with HQ. Hence, rGO-HQ is the most active catalyst for the two aerobic oxidation reactions like thiophenol and indane. Furthermore, the catalytic activity of thermally treated rGO-HQ is decreased due to the lower density of HQ sites than rGO-HQ catalyst. Rationalization of the nature of the active sites has served not only to engineer the most active rGO, but also to prepare a Merrifield resin with remarkable catalytic activity to promote aerobic oxidations by grafting HQ units in the aryl rings. Overall, this study shows the

ability to design metal-free catalysts based on the understanding of the structure of the active sites.

## **6.6 Acknowledgements**

S.N. thanks financial support by the Fundación Ramón Areces (XVIII Concurso Nacional para la Adjudicación de Ayudas a la Investigación en Ciencias de la Vida y de la Materia, 2016), Ministerio de Ciencia, Innovación y Universidades RTI2018-099482-A-I00 project and Generalitat Valenciana grupos de investigación consolidables 2019 (ref: AICO/2019/214) project. A.D. thanks the University Grants Commission, New Delhi, for the award of an Assistant Professorship under its Faculty Recharge Programme. A.D. also thanks the Department of Science and Technology, India, for the financial support through Extramural Research Funding (EMR/2016/006500). Financial support by the Spanish Ministry of Economy and Competitiveness (Severo Ochoa and RTI2018-089231-CO2-R1) and Generalitat Valenciana (Prometeo 2017-083) is gratefully acknowledged.



## 6.7 References

1. M. Masteri-Farahani and S. Mirshekar, *Colloids Surf. A Physicochem. Eng. Asp.* 2018, **538**, 387-392.
2. S. Sakthinathan, H.F. Lee, S.-M. Chen and P. Tamizhdurai, *J. Colloid Interface Sci.* 2016, **468**, 120-127.
3. X. Gao, Y. Ji, S. He, S. Li and J.M. Lee, *Catal. Sci. Technol.* 2016, **6**, 3143-3148.
4. B. Sang, J. Li, X. Tian, F. Yuan and Y. Zhu, *Mol. Catal.* 2019, **470**, 67-74.
5. A. Kumar, J.M. Gonçalves, A.R. Lima and T.A. Matias, M. Nakamura, J.S. Bernardes, K. Araki and M. Bertotti, *Electrochim. Acta* 2019, **326**, 134984.
6. N. Garino, A. Sacco, M. Castellino, J.A. Muñoz-Tabares, A. Chiodoni, V. Agostino, V. Margaria, M. Gerosa, G. Massaglia and M. Quaglio, *ACS Appl. Mater. Interfaces* 2016, **8**, 4633-4643.
7. N. Garino, A. Sacco, M. Castellino, J.A. Muñoz-Tabares, M. Armandi, A. Chiodoni and C.F. Pirri, *ChemistrySelect.* 2016, **1**, 3640-3646.
8. C.K. Chua and M. Pumera, *ACS Nano* 2015, **9**, 4193-4199.
9. M. Nasrollahzadeh, Z. Nezafat, M.G. Gorab and M. Sajjadi, *Mol. Catal.* 2020, **484**, 110758.
10. J. Porwal, N. Karanwal, S. Kaul and S.L. Jain, *New J. Chem.* 2016, **40**, 1547-1553.
11. M. Karthik and P. Suresh, *New J. Chem.* 2018, **42**, 17931-17938.
12. M. Azloul, M. Durmaz, E. Zor and H. Bingol, *Mater. Chem. Phys.* 2020, 239, 122298.
13. S. Gupta, R. Banu, C. Ameta, R. Ameta and P.B. Punjabi, *Top. Curr. Chem.* 2019, **377**, 13.
14. A. Dandia, A. Sharma, V. Parewa, B. Kumawat and K.S. Rathore, *RSC Adv.* 2015, 5, 91888-91902.
15. A. Dhakshinamoorthy, M. Alvaro, M. Puche, V. Fornes and H. Garcia, *ChemCatChem.* 4 (2012) 2026-2030.
16. G. Shivudu, K. Chandraraj and P. Selvam, *Mol. Catal.* 2020, **484**, 110745.
17. J. Xu, L.-Z. Wen, Y.-L. Gan and B. Xue, *Mol. Catal.* 2020, **485**, 110848.
18. J. Sánchez-García, A.M. Benito, W.K. Maser and E. García-Bordejé, *Mol. Catal.* 2020, **484**, 110737.
19. K.V. Ashok Kumar, L. Chandana, P. Ghosal and C. Subrahmanyam, *Mol. Catal.* 2018, **451**, 87-95.
20. D. Li, W. Li and J. Zhang, *Mol. Catal.* 2019, **470**, 48-55.
21. H. Sharma, S. Sharma, C. Sharma, S. Paul and J.H. Clark, *Mol. Catal.* 2019, **469**, 27-39.
22. L. Fang, Q. Xu, Y. Qi, X. Wu, Y. Fu, Q. Xiao, F. Zhang and W. Zhu, *Mol. Catal.* 2020, **486**, 110863.
23. C. Wu and I.D. Gates, *Mol. Catal.* 2019, **469**, 40-47.
24. Y. Qiu, F. Guo, R. Hurt and I. Kulaots, *Carbon* 2014, **72**, 215-223.

25. A. Yar, J.O. Dennis, M.S.M. Saheed, N.M. Mohamed, M.I. Irshad, A. Mumtaz and R. Jose, *J. Alloys Comp.* 2020, **822**, 153636.
26. A.B. Bourlinos, D. Gournis, D. Petridis, T. Szabó, A. Szeri and I. Dékány, *Langmuir* 2003, **19**, 6050-6055.
27. J. Zhang, H. Yang, G. Shen, P. Cheng, J. Zhang and S. Guo, *Chem. Commun.* 2010, **46**, 1112-1114.
28. L.G. Guex, B. Sacchi, K.F. Peuvot, R.L. Andersson, A.M. Pourrahimi, V. Ström, S. Farris and R.T. Olsson, *Nanoscale* 2017, **9**, 9562-9571.
29. S. Eigler, S. Grimm, M. Enzelberger-Heim, P. Müller and A. Hirsch, *Chem. Commun.* 2013, **49**, 7391-7393.
30. L. Bellucci and V. Tozzini, *Molecules* 2020, **25**, 339.
31. X. Zhang, L. Hou, F. Richard and P. Samorì, *Chem. Eur. J.* 2018, **24**, 18518-18528.
32. S. Navalon, A. Dhakshinamoorthy, M. Alvaro, M. Antonietti and H. García, *Chem. Soc. Rev.* 2017, **46**, 4501-4529.
33. D. Majumdar, *Carbon Nanostructures* 2019, 63-103.
34. J.C. Espinosa, M. Álvaro, A. Dhakshinamoorthy, S. Navalón and H. García, *ACS Sustain. Chem. Eng.* 2019, **7**, 15948-15956.
35. R. Estevez, L. Aguado-Deblas, V. Montes, A. Caballero and F.M. Bautista, *Mol. Catal.* 2020, **488**, 110921.
36. X. Lin, S. Jie and Z. Liu, *Mol. Catal.* 455 2018, 143-149.
37. K. Muthoosamy and S. Manickam, *Ultrason. Sonochem.* 2017, **39**, 478-493.
38. D. Wang, H. Duan, J. Lü and C. Lü, *J. Mater. Chem. A* 2017, **5**, 5088-5097.
39. D.R. Dreyer, H.-P. Jia, A.D. Todd, J. Geng and C.W. Bielawski, *Org. Biomol. Chem.* 2011, **9**, 7292-7295.
40. L. Menini, M.C. Pereira, A.C. Ferreira, J.D. Fabris and E.V. Gusevskaya, *Appl. Catal. A Gen.* 2011, **392**, 151-157.
41. A. Corma and T. Rodenas, M.J. Sabater, *Chem. Sci.* 2012, **3**, 398-404.
42. S. Paul, S. and Manirul Islam, *RSC Adv.* 2016, **6**, 95753-95759.
43. R. Burch, D.J. Crittle and M.J. Hayes, *Catal. Today* 1999, **47**, 229-234.
44. G. Bilisa, K.C. Christoforidis, Y. Deligiannakis and M. Louludi, *Catal. Today* 2010, **157**, 101-106.
45. S. Biswas, M. Maes, A. Dhakshinamoorthy, M. Feyand, D.E. De Vos, H. Garcia and N. Stock, *J. Mater. Chem.* 2012, **22**, 10200-10209.
46. P. Zhang, Y. Gong, H. Li, Z. Chen and Y. Wang, *Nature Commun.* 2013, **4**, 1593-1603.

## 6.8 Supplementary information

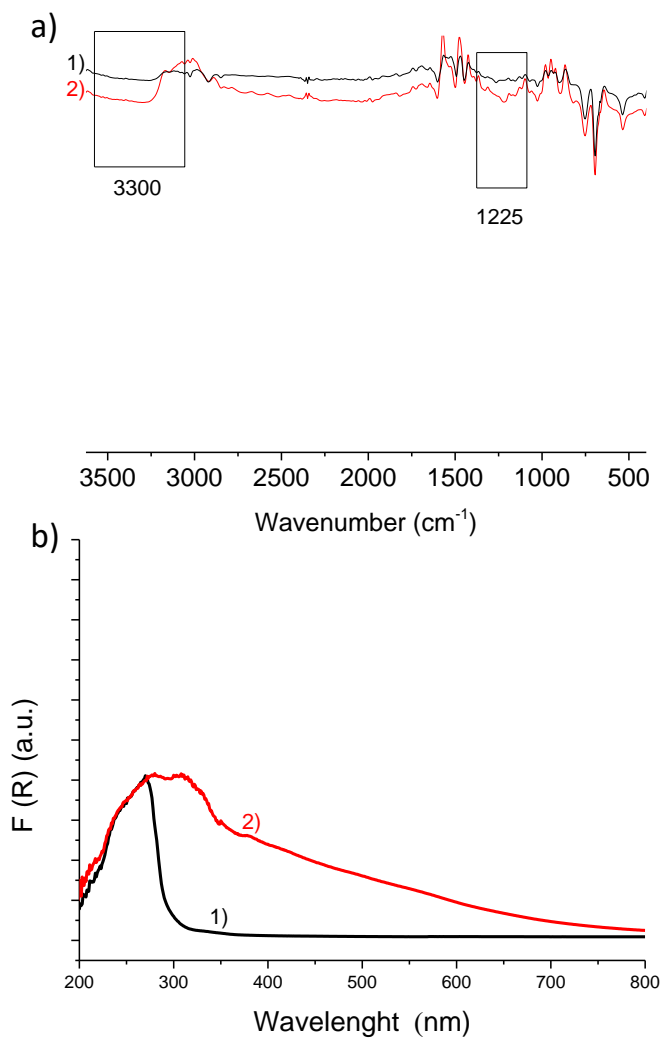


**Fig. S1** ATR-FT-IR (a) and diffuse reflectance UV-Vis (b) spectra of pristine (1, black colour) and hydroquinone-functionalized (2, red colour) Merrifield resin.

**Table S1** Summary of the catalysts employed and their characterization data. Reprinted with permission from ref.<sup>1</sup>

	Preparation method	Elemental analysis		
		C (wt %)	H (wt %)	O (wt %)
GO	Graphite oxidation by Hummers method	50.0 (46) <sup>b</sup>	2.3	47.7 (54) <sup>b</sup>
rCO-HQ	GO chemical reduction using HQ (32 mmol) at 100 °C in water for 24 h	80.9 (79.5) <sup>b</sup>	1.0	18.1 (20.5) <sup>b</sup>
rCO-HQ-300	rGO-HQ1pyrolysis at 300 °C for 2 h	83.0 (75.6) <sup>b</sup>	1.1	15.9 (24.4) <sup>b</sup>
rCO-HQ-700	rGO-HQ pyrolysis at 700 °C for 2 h	92.9 (86.6) <sup>b</sup>	1.1	6.0 (13.4) <sup>b</sup>
rCO-HZa	GO chemical reduction using hydrazine hydrate (32 mmol) at 100 °C in water for 24 h	81.4 (82) <sup>b</sup>	0.9	14.8 (15.8) <sup>b</sup>
rCO-ASC	GO chemical reduction using ascorbic acid (32 mmol) at 100 °C in water for 24 h	78.7 (75.2) <sup>b</sup>	1.4	19.9 (24.8) <sup>b</sup>
rCO-T	GO thermal reduction at 200 °C under argon atmosphere	81.1 (74.2) <sup>b</sup>	0.95	17.95 (25.8) <sup>b</sup>

<sup>a</sup> 2.9 wt % of nitrogen has been found in this sample

<sup>b</sup> Values in parentheses indicate C/O wt % from XPS analysis

<sup>1</sup> J.C. Espinosa, M. Álvaro, A. Dhakshinamoorthy, S. Navalón, H. García, ACS Sustainable Chem. Eng. 7 (2019) 15948-15956

## **Chapter 7. *Conclusions***



In view of the results of the present thesis it can be concluded that MOFs and graphene-base materials are excellent candidates to engineer their active sites and develop active solid catalysts to promote condensation and oxidation reactions.

More specifically the conclusions of each chapter are the following:

The development of mixed-metal MIL-101(Cr/Fe) materials results in the formation of stable and reusable heterogeneous catalysts with enhanced catalytic activity for the Prins reactions with respect to the pattern MIL-101(Cr) or the unstable MIL-101(Fe) catalysts. In situ FT-IR spectroscopy using CO and CD<sub>3</sub>CN as probe molecules indicates that the presence of Fe<sup>3+</sup> in the mixed-metal MIL-101(Cr, Fe) and this increases the density and strengthens Lewis acidity with respect to MIL-101(Cr). The presence of Cr(III) ions in the MOF metal node provides stability during the catalytic reaction while the presence of Fe(III) enhances the catalytic activity.

The presence of electron withdrawing (i.e., NO<sub>2</sub> or SO<sub>3</sub>H) or donor (i.e., NH<sub>2</sub>) substituents in the terephthalate organic ligand of MIL-101(Cr) influences the catalytic activity for the synthesis of benzimidazoles using o-phenylenediamine and benzaldehydes. MIL-101(Cr)-NO<sub>2</sub> was the most active catalyst of the series. In situ FT-IR spectroscopy using CD<sub>3</sub>CN reveals that the presence of the NO<sub>2</sub> group in the terephthalate organic ligand of MIL-101(Cr)-NO<sub>2</sub> increases the density and strength of the Lewis acid sites with respect to the MIL-101(Cr) pattern. This material acts as a bifunctional catalyst (acid and redox) facilitating the catalysed condensation and oxidative dehydrogenation during the synthesis of benzimidazoles. The catalytic activity of MIL-101(Cr)-NO<sub>2</sub> slightly decreases during the initial reuses due to the

strong adsorption of the basic nitrogen compounds in the Lewis acid sites of the catalyst during the reaction. The five-times used catalyst retains its crystallinity and morphology as revealed by PXRD and SEM measurements, respectively, and the absence of metal leaching.

The MIL-101(Cr)-NO<sub>2</sub> material is an efficient catalyst for the aerobic oxidation of thiophenols in acetonitrile as a solvent and the oxidative desulfuration of dibenzothiophenes in n-dodecane or commercial diesel. The series of MIL-101(Cr)-X (X: NO<sub>2</sub>, SO<sub>3</sub>H, Cl, NH<sub>2</sub> or CH<sub>3</sub>) prepared a good relationship between the substituent meta Hammet constant on the terephthalate ligand and their redox potential was found for the aerobic oxidation of thiophenol to diphenyl disulphide. Regarding the mechanism, the available data indicates that MIL-101(Cr)-NO<sub>2</sub> is acting as a truly heterogeneous catalyst for the aerobic oxidation of thiophenol, while it acts as an initiator in the aerobic desulfurization of dibenzothiophenes. For both reactions, MIL-101(Cr)-NO<sub>2</sub> is a reusable material without observed deactivation and maintains its crystallinity as revealed by PXRD and with negligible metal leaching.

Hydroquinone is an adequate reagent to promote the reduction of GO to rGO and introduce hydroquinone/quinone-like functional groups that act as active sites for the aerobic oxidation of thiophenol and indane. The preparation of rGO by using hydrazine or ascorbic acid as reducing agents or by thermal methods resulted in samples with relatively low catalytic activity. The reuse experiments using the most active catalyst revealed that most of the initial catalytic activity is retained. Selective radical quenching experiments revealed the generation of hydroperoxyl and hydroperoxyl radicals during the aerobic oxidations as well as carbon-centred radicals in the



case of indane oxidation.



## **Chapter 8. *Abstract of the Thesis***



## 8.1 Abstract

The present doctoral thesis has shown the possibility of engineering the active sites of MOFs and graphene-based materials as catalysts with enhanced activity for oxidation and condensation reactions. Specifically, the development of a mixed-metal MIL-101(Cr, Fe) has resulted in a catalyst with enhanced catalytic activity for the Prins reaction between  $\beta$ -pinene and formaldehyde with respect to the use of MIL-101(Cr) or the unstable MIL-101(Fe) under the studied reaction conditions. The presence of  $\text{Fe}^{3+}$  ions in the metal nodes of the MIL-101(Cr, Fe) increases the density and strength of the Lewis acid sites of the material and the presence of  $\text{Cr}^{3+}$  in the metal nodes provides catalyst stability. Furthermore, this thesis has demonstrated that the presence of  $\text{NO}_2$  groups in the terephthalate organic ligand of MIL-101(Cr) increases the density and strength of Lewis acid sites of the material. Thus, MIL-101(Cr)- $\text{NO}_2$  exhibits a superior catalytic activity for the synthesis of benzimidazoles from o-phenylenediamines and benzaldehyde derivatives, as well as for the aerobic oxidation of thiophenol and the aerobic oxidative desulfuration of dibenzothiophenes. This thesis has also shown that the selection of an appropriate reducing agent (such as hydroquinone) for the preparation of rGO from GO increases the density of active sites and promotes the aerobic oxidations of thiophenol and indane.

## 8.2 Resumen

La presente tesis doctoral ha mostrado la posibilidad de diseñar sitios activos de MOFs y materiales basados en grafeno para ser utilizados como catalizadores con actividad mejorada para reacciones de oxidación y condensación. Específicamente, el desarrollo de una combinación de metales MIL-101(Cr,Fe) ha dado como resultado un catalizador con actividad catalítica mejorada para la reacción de Prins entre  $\beta$ -pineno y formaldehído con respecto al MIL-101(Cr) o el inestable MIL-101(Fe) en las condiciones de reacción estudiadas. La presencia de iones  $\text{Fe}^{3+}$  en los nodos metálicos del MIL-101(Cr, Fe) aumenta la densidad y la fuerza de los sitios ácidos de Lewis del material, mientras que la presencia de  $\text{Cr}^{3+}$  en los nodos metálicos proporciona estabilidad al catalizador. Además, esta Tesis ha demostrado que la presencia de grupos  $\text{NO}_2$  en el ligando orgánico tereftalato de MIL-101(Cr) aumenta la densidad y la fuerza de los sitios ácidos de Lewis del material. Por lo tanto, MIL-101(Cr)- $\text{NO}_2$  exhibe una actividad catalítica superior para la síntesis de bencimidazoles a partir de o-fenilendiaminas y derivados de benzaldehído, así como para la oxidación aeróbica del tiofenol y la desulfuración oxidativa aeróbica de dibenzotiofenos. Esta Tesis también ha demostrado que la selección de un agente reductor apropiado como la hidroquinona para la preparación de rGO a partir de GO aumenta la densidad de los sitios activos para promover las oxidaciones aeróbicas de tiofenol e indano.

### 8.3 Resum

La present Tesi doctoral ha mostrat la possibilitat de dissenyar llocs actius de MOFs i materials basats en grafè per ser utilitzats com a catalitzadors amb activitat millorada per a reaccions d'oxidació i condensació. Específicament, el desenvolupament d'una combinació de metalls MIL-101(Cr,Fe) ha donat com a resultat un catalitzador amb activitat catalítica millorada per a la reacció de Prins entre  $\beta$ -pinè i formaldehíd pel que fa a MIL-101(Cr) o l'íestable MIL-101(Fe) en les condicions de reacció estudiades. La presència de ions  $\text{Fe}^{3+}$  en els nodes metàl·lics de MIL-101(Cr,Fe) augmenta la densitat i la força dels llocs àcids de Lewis del material, mentre que la presència de  $\text{Cr}^{3+}$  en els nodes metàl·lics proporciona estabilitat al catalitzador. A més a més, aquesta Tesi ha demostrat que la presència de grups  $\text{NO}_2$  al lligam orgànic tereftalat de MIL-101(Cr) augmenta la densitat i la força dels llocs àcids de Lewis del material. Per tant, MIL-101(Cr)- $\text{NO}_2$  exhibeix una activitat catalítica superior per a la síntesis de bencimidazols a partir de o-fenilendiamines i derivats de benzaldehid, així com per a l'oxidació aeròbica del tiofenol i la desulfuració oxidativa aeròbica de dibenzotiofens. Aquesta Tesi també ha demostrat que la selecció d'un agent reductor apropiat com la hidroquinona per a la preparació de rGO a partir de GO augmenta la densitat dels llocs actius per a promoure les oxidacions aeròbiques de tiofenol i indano.





## ***Annex I. Publications and conferences***



## Publications derived from the present Thesis

1. **Design of stable mixed metal MIL-101(Cr/Fe) materials with enhanced catalytic for the Prins reaction.**

Cristina Vallés-García,<sup>‡</sup> Effrosyni Gkaniatsou,<sup>‡</sup> Andrea Santiago-Portillo, Mónica Giménez-Marqués, Mercedes Álvaro, Jean-Marc Greneche, Nathalie Steunou, Clémence Sicard,\* Sergio Navalón,\* Christian Serre,\* Hermenegildo García\*, *J Mater Chem A*. 2020, **8**, 17002-17011.

2. **Nitro functionalized chromium terephthalate metal organic framework as multifunctional solid acid for the synthesis of benzimidazoles.**

Cristina Vallés-García, María Cabrero-Antonino, Sergio Navalón,\* Mercedes Álvaro, Amarajothi Dhakshinamoorthy,\* and Hermenegildo García\*, *J. Colloid Interf. Sci.* 2020, **560**, 885-893.

3. **MIL-101(Cr)-NO<sub>2</sub> as efficient catalyst for the aerobic oxidation of thiophenols and the oxidative desulfuration of dibenzothiophenes.**

Cristina Vallés-García, Andrea Santiago-Portillo, Mercedes Álvaro, Sergio Navalón,\* and Hermenegildo García,\* *Appl. Catal. A Gen.* 2020, **590**, 117340.

4. **Tuning the active sites in reduced graphene oxide by hydroquinone functionalization for the aerobic oxidations of thiophenol and indane.**

Cristina Vallés-García, Eva Montero-Lanzuela, Sergio Navalón,\* Mercedes Álvaro, Amarajothi Dhakshinamoorthy\* and Hermenegildo García,\* *Mol. Cat.* 2020, **493**, 111093.

## Other Publications

1. **Plasma-Induced defects enhance the visible-light photocatalytic activity of MIL-125(Ti)-NH<sub>2</sub> for overall water splitting.**

María Cabrero-Antonino, Josep Albero, Cristina Valles-García, Mercedes Álvaro, Sergio Navalón\* and Hermenegildo García\*, *Chem-Eur J.* 2020, 26, 15682-15689.

2. **Bifunctional metal-organic frameworks for the hydrogenation of nitrophenol using methanol as the hydrogen source.**

Arianna Melillo, Cristina Vallés-García, Belén Ferrer, Mercedes Álvaro, Sergio Navalón\* and Hermenegildo García\*, *Org. biomol. Chem.*, 2021, 19, 794-800.

3. **Templateless synthesis of ultra-microporous 3D graphitic carbon from cyclodextrins and their use as selective catalyst for oxygen activation.**

Alejandra Rendón-Patiño, Andrea Santiago-portillo, Cristina Vallés-García, Miguel Palomino, Sergio Navalón, Antonio Franconetti, Ana Primo\* and Hermenegildo García\*, *Small Methods*, 2020, 4, 1900721.

4. **Hybrid sp<sup>2</sup>/sp<sup>3</sup> nanodiamonds as heterogeneous metal-free ozonation catal.**

Francisco Bernat-Quesada, Cristina Vallés-García, Eva Montero-Lanzuela, Antón López-Francés, Belén Ferrer, Herme G. Baldoví\*, Sergio Navalón.\* (Submitted manuscript).

## Conferences

1. **MIL-101(Cr) promotes the efficient aerobic oxidative desulfuration of dibenzothiophenes using O<sub>2</sub> as oxidant.**

Cristina Vallés-García, María Cabrero-Antonino, Arianna Melillo, Andrea Santiago-Portillo, Mercedes Álvaro, Sergio Navalón and Hermenegildo García.

World Congress on Chemistry (WCC-2019). October 2019. Oral communication.

2. **MOFs as heterogeneous catalysts for aerobic oxidative desulfuration of dibenzothiophenes.**

Cristina Vallés-García, María Cabrero-Antonino, Arianna Melillo, Andrea Santiago-Portillo, Mercedes Álvaro, Sergio Navalón and Hermenegildo García.

XVI simposio de jóvenes investigadores de la real Sociedad Española de Química. November 2019. Poster communication.

3. **Tuning the microenvironment of gold nanoparticles encapsulated within MIL-101(Cr) for selective oxidation of alcohol with O<sub>2</sub>: Influence of the amino terephthalate linker.**

Arianna Melillo, Cristina Vallés-García, María Cabrero Antonino, Andrea Santiago Portillo, Mercedes Álvaro, Hermenegildo García, Belén Ferrer.

XVI simposio de jóvenes investigadores de la real Sociedad Española de Química. November 2019. Flash communication.

4. **UIO-67 Rhthenium (II) tris(2',2'-bipyridyl) as photoredox catalyst.**

Arianna Melillo, Cristina Vallés-García, María Cabrero Antonino, Andrea Santiago Portillo, Mercedes Álvaro, Hermenegildo García, Belén Ferrer.

World Congress on Chemistry (WCC-2019). October 2019. Oral communication.

5. **Influence of Co-Catalysts on the Photocatalytic Activity of MIL-125(Ti)-NH<sub>2</sub> in the Overall Water Splitting.**

María Cabrero Antonino, Arianna Melillo, Cristina Vallés García, Mercedes Álvaro, Hermenegildo García, Sergio Navalón.

World Congress on Chemistry (WCC-2019). October 2019. Oral communication.

6. **Bifunctional metal-organic frameworks for the hydrogenation of nitrophenol using methanol as the hydrogen source.**

Celia M<sup>a</sup> Rueda, Arianna Melillo, Cristina Vallés- García, Belén Ferrer, Herme G. Baldoví and Sergio Navalón.

2021 Fall Meeting / EMRS. September 2021.

7. **Plasma-induced defects enhance the visible-light photocatalytic activity of MIL-125(Ti)-NH<sub>2</sub> for overall water splitting.**

Eva Montero-Lanzuela, María Cabrero-Antonino, Josep Albero, Cristina Vallés-García, Herme G. Baldoví and Sergio Navalón.

2021 Fall Meeting / EMRS. July 2021. Poster communication.